STATIC AND DYNAMIC PRE-STRESSING OF METAL DISCS

by

Brian Quartermain, BSc, MSc

A Thesis submitted to
COUNCIL FOR NATIONAL ACADEMIC AWARDS
in partial fulfilment of the
requirements for the
DEGREE OF DOCTOR OF PHILOSOPHY

Sponsoring Establishment : Sheffield City Polytechnic
Department of Mechanical and
Production Engineering
Pond Street
Sheffield S1 1WB

Collaborating Establishment : British Steel Corporation
Sheffield Laboratories
Swinden House
Moorgate
Rotherham S60 3AR

DECEMBER 1985

ABSTRACT

In order to develop a technique of controlled pre-stressing of metal components, mild steel discs were dynamically loaded using explosives. Subsequently, mild steel discs of similar dimensions were loaded statically. The following loading conditions were studied:

(i) at fixed radius and varying load
(ii) at varying radial positions and fixed load
(iii) at constant load and fixed radius but varying outer diameter of disc (dynamic tests only).

For the dynamically loaded discs, residual radial stresses have been obtained by an experimental technique, based on strain gauge readings, which permitted the estimation of the residual stresses at the incremental radius of the successively cut sections of the discs for both outer and inner sections. Further analysis of the experimental results has produced values for the residual radial and hoop stress at radii close to the explosive loading radius. Correlation from results obtained from the statically loaded discs was provided by strain gauges fixed at varying fixed radii on each loaded disc. The experimental analysis for the statically loaded discs was of simpler form than that required for the dynamically loaded discs. In order to establish the validity of the method for estimating the residual radial stresses, certain other experimental measurements have been made viz: plane deformation, hardness, microstructural examination and buckling tests. A theoretical model based on plastic deformation of the loaded annulus has been developed which requires an estimation of the energy transferred from the loading ring or annulus to the surface of the disc. In the majority of cases, agreement between experimental and theoretical values of residual radial and hoop stress have been found in both magnitude and sign. A further theoretical approach was applied using finite element technique to validate the equivalent stress values obtained from the experimental results of the statically loaded discs. Comparison of the results again showed good agreement in magnitude and sign.

ACKNOWLEDGEMENTS

The author wishes to thank Dr M S J Hashmi and Dr T D Campbell for acting as supervisors and for their guidance and helpful comments at all stages of this research. Thanks are also due to K Wright, S Brandon and R Goldthorpe - Technicians, for their help in preparation of tests and specimens. Finally to Miss A Hughes for typing the thesis.

CONTENTS Page

CHAPTER 1 : INTRODUCTION

1.1	Introduction	1
1.2	Literature Survey	5
1.3	Present Work	20

CHAPTER 2 : SPECIMENS AND EXPERIMENTAL TECHNIQUE

2.1	Introduction	26
2.2	Specimen Material Preparation and Dimensions	27
2.3	Stress-Strain Characteristics	47
2.4	Equipment, Testing Procedure and Schedule	50
2.5	Data Recording	71

CHAPTER 3 : EXPERIMENTAL RESULTS

3.1.1	Introduction - Dynamic Loading	96
3.1.2	Strain Gauge Rosette Analysis	96
3.1.3	Method of Assessment and Prediction of Residual Stress at the Outer and Inner Boundaries of the Cut Discs	100
3.1.4	Experimental Results	111
3.1.5	Comments	141
3.2.1	Introduction - Static Loading	148
3.2.2	The Derivation of an Experimental Stress Strain Constitutive Equation	149
3.2.3	Derivation of Elastic-Plastic Constitutive Equation from Results	154
3.2.4	Summary of Method used to obtain Stress Values from Strain Gauge Readings	157
3.2.5	Programme Format for producing Stress Values from Strain Gauge Values	158
3.2.6	Example of Experimental Evaluation Tables	160

		Page
3.2.7	Summary of Experimental Loading Criteria and Disc Parameters	163
3.2.8	Experimental Graphs	165
3.2.9	Appraisal of Results	177
3.2.10	Buckling Tests	179
CHAPTER 4 : THEORETICAL - FINITE ELEMENT ANALYSIS		
4.1	Introduction	192
4.2	Finite Element Method and the PAFEC Programme	192
4.3	The Data Modules	195
4.4	Tables of Results for Predicted and Measured Values of Equivalent Stress	196
4.5	Graphical Comparison	199
4.6	Conclusions	203
CHAPTER 5 : PLASTIC DEFORMATION MODEL		
5.1	Introduction	205
5.2	Assumptions	205
5.3	Nomenclature	207
5.4	Boundary Conditions for the Plastically Deformed Region of the Disc	209
5.5	An Estimate of the Order of Magnitude of the Radial Stress in terms of the Applied Compressive Stress	212
5.6	The Relation between Surface and Edge Deformation of a Plastically Loaded Element of a Metal Annulus	214
5.7	Calculation of Stress Formulae	218
5.8	Energy Transfer	224
5.9	Deformation at Surface of Annulus due to Energy Transferred from Explosive	234
5.10	Table of Theoretical Energy Transferred into Discs	236

		Page
5.11	Example Calculations	237
5.12	Application of Plastic Deformation Model to Statically Loaded Discs	249
5.13	Conclusions	254
CHAPTER 6 : DISCUSSION AND COMMENTARY		
6.1	Introduction	257
6.2	Dynamic Loading Tests (A, B and C Series)	258
6.3	Static Loading (D Series)	265
6.4	Buckling Tests (E Series)	271
6.5	Plane Symmetry, Hardness, Microstructural Analysis	273
6.6	Plastic Deformation Analysis	276
6.7	Finite Element Analysis	278
6.8	Final Comments	279
CHAPTER 7 : CONCLUSIONS AND FURTHER WORK		
7.1	Conclusions	283
7.2	Further Work	286
CHAPTER 8 : REFERENCES		289
APPENDICES		

FIGURES : CHAPTER 2 Page

2.1	Marking of Discs for fixing Strain Gauges	29
2.2	Booster Detonation Arrangements for Plastic Bulk Charges	34
2.3	Booster Detonation Arrangements for Cast Explosive Charges	35
2.4	Methods for Initiating Detonating Cord	36
2.5	Explosive Arrangement on Disc	38
2.6	Explosive Layout	39
2.7	Arrangement of Strain Gauges on Disc C1	44
2.8	Loading of Sample Disc A3	48
2.9	True Stress vs True Strain	49
2.10	Bridge Circuit	52
2.11	Dynamic Loading System for Measurement of Strain Gauge Readings	53
2.12	Circuit for Accuracy Estimation	55
2.13	Disc : Grinding Out : Dynamic Loading	60
2.14	Rear View of Data Logging Equipment	63
2.15	Disc : Press Loading : Static Compression	64
2.16	Disc : in Anvil on Press : Static Loading	65
2.17	Statically loaded Disc : Loading Ring, and Top Plate Strain Gauges	66
2.18	Statically loaded Disc : Loading Ring and Strain Gauge Connections	67
2.19	Statically loaded Disc showing close-up of Loading Ring and Strain Gauges	68
2.20	Schedule for Loading Ring Annuli	69
2.21	Typical Strain Gauge Configuration Pattern	70
2.22	Deformation Measuring Technique	74
2.23	Typical Deformation Profile Disc C1	76

		Page
2.24	Typical Deformation Profile Disc C5	77
2.25	Plan Measurements of Brinell Hardness for Disc C2 showing measurements prior to and after explosive loading	82
2.26	Hardness Changes produced by Detonation of Line Cord in contact with discs for Series A (varying explosive)	84
2.27	Hardness Changes produced by Detonation of Line Cord in contact with discs for Series B (varying radii)	85
2.28	Hardness Changes produced by Detonation of Line Cord in contact with discs for Series C (varying size)	86
2.29	Microstructural Investigation	87
Photomicrographs		92 93 94

FIGURES : CHAPTER 3

		Page
3.1	3 x 45° - Rosette	99
3.2	Experimental Analysis Cutting Parameters	104
3.3	Disc Turning/Boring Sequence	105
3.4	Stresses at Final Cut in A Series	116
3.5a	Stresses at Final Cut in B Series (B3, B5, B6 and B8)	117
3.5b	Stresses at Final Cut in B Series (B3, B5, B6 and B8)	118
3.6	A Series (based on Radial Readings)	121
3.7	A Series (based on Hoop Readings)	122
3.8	B Series (based on Radial Readings)	125
3.9	B Series (based on Hoop Readings)	126
3.10	C Series (based on Radial Readings)	129
3.11	C Series (based on Hoop Readings)	130
3.12	Special Series (based on Radial Readings)	137
3.13	Special Series (based on Hoop Readings)	138
3.14	Comparison of Discs A7, B5, C2 and A3 based on Radial Readings	139
3.15	Comparison of Discs A7, B5, C2 (based on Hoop Readings) and A3 (based on Radial Readings)	140
3.16a	True Stress vs True Strain	152
3.16b	True Stress vs True Strain	153
3.17	Summary - General Shape of Stress vs Distance from Centre of Discs	166
3.18	Loading and Residual Stresses; Static Loading for Disc D1	167
3.19	Loading and Residual Stresses; Static Loading for Disc D2	168
3.20	Loading and Residual Stresses; Static Loading for Disc D3	169
3.21	Loading and Residual Stresses; Static Loading for Disc D4	170

		Page
3.22	Comparison of D1 (1400 kN) with D3 (2000 kN)	172
3.23	Stress vs Load for Disc D1	173
3.24	Stress vs Load for Disc D3	174
3.25	Stress vs Load for Disc D3	175
3.26	Stress vs Load for Disc D4	176
3.27	Arrangements for Buckling Tests	181
3.28	Circular Plate under Compression	185
3.29	K vs $\frac{b}{a}$ simply supported	186
3.30	K vs $\frac{b}{a}$ edge clamped	186
3.31	Ring and Disc Profile after Loading Disc D1 showing dishing	190

FIGURES : CHAPTER 4

		Page
4.1	Division of Disc Section	193
4.2	Division of Sections into Elements	193
4.3	Division of Elements into Nodes	193
4.4	Equivalent Stress Values for Disc D2 (Load 2300 kN and 1850 kN)	200
4.5	Equivalent Stress Values for Disc D2 (Load 1600 kN and 1400 kN)	201
4.6	Equivalent Stress Values for Disc D2 (Load 1150 kN and 920 kN)	202

FIGURES : CHAPTER 5

		Page
5.1	PETN on Disc Surface	205
5.2	Disc Parameters	209
5.3	Three-dimensional stress block	212
5.4	Deformation of Block	214
5.5	Extension Parameters	217
5.6	Displacement after Explosive Loading	218
5.7	Explosive Loading Parameters	226
5.8	Reflection and Transmission through a Plane Boundary	228
5.9	Explosive System	230
5.10	Plastically deformed Region (Energy transfer from explosive)	234
5.11	Graph of Comparative Values of Radial Stress using Theory, Radial and Hoop Readings for A5	241
5.12	Graph of Comparative Values of Radial Stress using Theory, Radial and Hoop Readings for B6	245
5.13	Graph of Comparative Values of Radial Stress using Theory, Radial and Hoop Readings for C2	247

CHAPTER 1

1.1 Introduction

The residual stress distribution can significantly affect the in-service performance of a material so that a design procedure based on expected levels of stresses arising from external sources may be reduced by the presence of undetermined residual stresses. In finished components, micro and macro strains co-exist and influence the properties in different ways. Thus crack nucleation in fatigue, creep and stress corrosion may occur in the vicinity of a micro-strained region, whilst crack propagation, and hence the resultant failure, is markedly influenced by the macro-strains.

The total (material) strength of a piece of metal is altered by the level of residual stress induced in the course of mill processing, heat treatment, fabrication and surface treatment. The nature of the residual stress, tensile or compressive, is characteristic of the integrated effect of all the processing, the part-geometry and any temperature gradient. Since fatigue failures usually start at a surface location under a tensile stress, any treatment that leaves the surface under compression would be beneficial by reducing an applied tension.

Early applications of small controlled permanent deformations were found in the auto-frettage of gun barrels (i.e. a deliberate deformation of part of the wall thickness to give a preferential residual stress pattern

in the gun barrel). In high pressure chemical processes reaction vessels, tubular heat exchangers, pipework, valves, and the like would be much more expensive and inconvenient if designed on classical safety factors.

The concept of controlled plastic deformation in designing high pressure chemical plant, allayed engineer's fear of allowing permanent distortions in highly stressed components. Tubular elements have also been proposed as safety elements in high pressure systems. They can be accurately made and it has been shown that the bursting pressure can be reliably established. The reason why a thick walled tube is particularly suitable for plastic design is that plastic deformation starts at the bore whilst the outer material is still relatively lightly stressed. Thus the work-hardening properties of the tube material and the elastic restraint of the outer containing layers provide a reservoir of strength.

The effects of residual stresses on the performance of a component are often difficult to dissociate from strength modifications inherent in their origin, but an investigation by Osgood[1] concluded that:

(1) Residual stresses have a similar effect on the fatigue behaviour of materials as do mechanically imposed static stresses of the same magnitude.

(2) Thus the significant residual stresses are beneficial if compressive, and detrimental if tensile, particularly in "hard" materials. A "hard" material is one that has been hardened by working or heat

treatment.

It is, however, worth pointing out that tensile residual stresses could be beneficial in a buckling situation.

The major processing factors that affect residual stresses have been traditionally, heat treatment, welding, core hardening, induction hardening, machining, grinding, cold-working and straightening. However, additional processes could be used to deliberately induce residual stresses by causing plastic deformation. These processes could be dynamic, (ie of explosives) or static (ie of presses) provided that the residual stresses could be predicted both in magnitude and nature.

The use of explosives, as opposed to conventional techniques, has the advantage of providing both a cheap and simple source of energy, and of removing the need for a complex tooling system.

The application of explosives produces a non-uniform plastic deformation and can be used to impose a favourable residual stress pattern. Other more traditional examples are surface rolling, or shot peening of fillets and seats for press fits whilst unwanted tensile stresses from cold-straightening represent the opposite situation.

Pre-stressing techniques are already used for the stress relief of components in order to produce a beneficial effect on the fatigue life. Deformation methods currently used to obtain stress relief are surface rolling and shot peening. Residual stresses also occur in welded

structures originating from hot material being cooled at different rates. Pre-heating prior to welding or shot peening after welding reduces the magnitude of the residual stresses.

1.2 Literature Survey

1.2.1 Mathematical Theories of Stress-Strain Relations of Plasticity

1.2.2 Residual Stress Measurement

1.2.3 Stresses in Discs

1.2.4 Explosive Hardening

1.2.5 Sensitivity of Strain-measuring Instruments and Strain Gauge Techniques

1.2.6 Cutting Techniques

1.2.7 Buckling

1.2.1 Mathematical Theories of Stress-Strain Relations of Plasticity

St. Venant[2] founded the mathematical theory of plasticity in his famour "Memoire" published in 1870. His work represents the first attempt at a concise mathematical formulation of the behaviour of materials stressed beyond the elastic region. It is closely linked with the theoretical studies of Levy[3] and the experimental investigation of Tresca.[4]

Theoretical investigations have been, and still are, concerned with two questions of prime importance, namely the choice of the type of stress-strain relation to be employed and the choice of criterion which will determine when a material enters the plastic range. On the basis of his experimental results, Tresca[4] concluded that the shear resistance in a material determines the point of yield. Tresca formulated a yield criterion by stating that yield will occur at a point if the maximum shear stress at that point exceeds a certain value. Geometrically this criterion is represented, for the case of biaxial stress, by a hexagon in the principal stress plane. Von Mises[5] proposed a yield criterion choosing an ellipse which circumscribes the hexagon of Tresca. This octahedral shear stress criterion has been found adequate experimentally for the onset of plastic deformation and for many simple tests. It was used almost exclusively until 1945 although von Mises had long before suggested the third invariant of stress, in the yield criterion.

This modification remedies some of the faults of J2, or octahedral shear stress, hypothesis. The yield curve corresponding to a J_2, J_3) yield criterion is an oval which usually lies between the ellipse of von Mises and the hexagon of Tresca. Prager[6] showed that the (J_2, J_3) criterion is the most general depending on shear stress alone. In order to account for anistropic effects due to straining, such as those found by Bauschinger[7] and Schmidt,[8] yield criteria involving strains as well as stress were considered by von Mises,[9] Odqvist,[10] and Prager[11] and Edelman and Drucker.[12]

There are essentially two fundamental types of theories for continua in the plastic range: incremental or flow theories, of which that by St. Venant is a special case, and total or deformation theories. In incremental or flow theories, strain increments are given in terms of stress increments and the given state of the material. In total deformation theories, strains depend on stresses only and are independent of the manner in which the stresses were obtained. Prandtl[13] and Reuss[14] elaborated on the incremental theory of St. Venant by including elastic strains as well as plastic.

Deformation theories have been, and still are, used extensively because of their simplicity in problems in which the strains are not large. The first deformation theory of plasticity for contained plastic flow of perfectly plastic materials was proposed by Hencky[15] in 1924. Nadai[16] introduced a deformation law for work-hardening materials, otherwise similar to the law of

Hencky. In 1945, Prager[17] proposed a general deformation law for isotropic work-hardening materials. In later papers Prager[18] and Drucker[19] developed a general stress-strain relation of the flow type for work-hardening materials in terms of a loading function which characterises plastic flow. These laws may be initially isotropic but can, by proper choice of the loading function, take account of any anisotropic work-hardening, and of initial anisotropy present in the material. Drucker[18] in deducing the concepts of work-hardening, ideal plasticity and stability of plastic deformation to a mathematical formulation made an assumption for ideal plasticity that a yield or loading function $F(\sigma_{ij})$, a function of stress alone, exists. It exists such that plastic deformation takes place without limit when $F(\sigma_{ij}) = k$, and that the material behaves elastically for $F(\sigma_{ij}) < k$. Symbolically when $F = k$, $dE^{p}_{ij} \neq 0$, $dF = 0$. A particular value of the loading function was proposed by Geiringer[20] in which for an incompressible isotropic material in plane strain a general yield condition can be expressed as function of the single variable $\sigma_1 - \sigma_2$; σ_1 and σ_2 being principal stresses in the plane Z = constant.

Recent years have seen great advances in plasticity theory, the general theoretical work of Hill[21], Prager and Hodge,[22] Drucker[23], being of particular note. On the basis of this work, the solution to particular problems have been found, such as the elastic-plastic analysis for rotating cylinders[24] and strain-hardening solutions to plate problems[25] (though in most cases simplifying

assumptions have had to be made). Some workers have extended the solution to predict the residual stress by completing the elastic-recovery problem.[21,26-28]

Nearly all common materials have elastic as well as plastic components of strain. Hill proposed the Prandl-Reuss stress/strain relationship for the case when the principal axes of stress and strain are coincident and the material exhibits work-hardening. These equations do not lend themselves to analytical solution even when applied to the simple case of the plane-stress bending of a beam. Autofrettage of cylinders, producing an axisymmetric stress distribution, would appear to be, after the bent beam problem, the next simplest.

Prager and Hodge,[22] Hill[21] and Thomas[29] discussed the problem at length but showed that the use of precise criteria produces great intractability which is overcome only by making simplifying assumptions.[30,31] Franklin and Morrison,[27] in particular, made the assumptions that shear stress is proportional to the square of the cylinder radius, and that the Tresca criteria ($\sigma_1 - \sigma_3 = \bar{\sigma}$) described the yield behaviour of the material (2½% nickel-chromium-molybdenum steel). Their justification for this was illustrated by actually measuring the residual stresses in an auto-frettaged cylinder by the Sachs boring technique and comparing with theoretical values. Agreement was within ∿ 5% except for the values of axial stress near the inner surface of the cylinder where the experimental

method seemed to be insufficiently sensitive. This work provides the illustration that accurate prediction of residual stresses can be made, provided that assumptions used to reduce the intractability of the mathematics are carefully selected. Hill[32] produced completed solutions for various elastic-plastic problems. These included the expansion of a spherical shell and of a cylindrical hole in an infinite medium. The solutions were used to exemplify certain features common to all elastic-plastic problems, with a view to introducing valid approximations in more complex cases.

Ramu and Iyengar[33] investigated the dynamic behaviour of a simply supported, orthotropic, circular plate subjected to a strong blast. The blast was assumed to impart an axisymmetric transverse, velocity which has a general Gaussian distribution spatially. It concluded that the rate of growth of plastic regimes and the final plastic deformation were strongly dependent upon the initial Gaussian distribution parameter.

1.2.2 Residual Stress Measurement

The symmetrical simplicity of a uniformly stressed round bar attracted the attentions of early investigators of residual stress. The effect of machining metal from a severely worked or heat-treated specimen in producing a deflection was well-known, so that first attempts at residual-stress determination naturally employed an easily machined symmetrical section. Bauer and Heyn[34] worked

out equations connecting longitudinal residual stress with change in length of the specimen. These were subsequently replaced by the more rigorous equations due to Mesnager[35] which, in turn, were simplified by Sachs.[36] The general technique of boring out a cylinder or tube in stages and measuring the longitudinal and circumferential strains at the outer surface caused by the release of residual stress, is now known as the Sachs method.

The following assumptions are implicit in the method:

(1) The metal is effectively isotropic and has a constant value of Young's modulus and Poisson's ratio.

(2) The residual stresses are distributed with rotational symmetry about the axes of the bar.

(3) The tube formed by boring the bar is circular in section and the inner and outer wall surfaces are concentric.

(4) The specimen is sufficiently long to prevent bending.

The equations derived by Sachs and quoted by others are well-known. They have been further modified for outer layer removal by Bühler[37], Loxley[38] and Sachs and Espey.[39]

1.2.3 Stresses in Discs

The Sachs boring technique can be applied to the measurement of residual stresses in discs, as well as in solid bars, provided that the initial radius is sufficient to allow for boring. For the usual case of the disc being thin enough to assume $\sigma_2 = 0$, Birger[40] has discussed at length the necessary modifications to the usual Sachs expressions. He assumes that σ_2 is absent when the thickness is less than one-fifth of the diameter, though more precisely the lack of axial stress is a function of disc thickness only. The practical optimum is the minimum thickness to accommodate the circumferentially attached strain-gauge.

Kalakutsky[41] first suggested attaching strain-gauges in a circumferential direction and then cutting out the annulus ring containing them. The rings are taken thin enough to assume complete release of both σ_r and σ_θ. Thus the hoop strain is

$$e_\theta(r) = \frac{1}{E}\left[\sigma_\theta - \nu\sigma_r\right]$$

and from equilibrium considerations

$$\frac{d\sigma_r}{dr} = \frac{1}{r}\left[\sigma_\theta - \sigma_r\right]$$

Kalakutsky solved these equations by the method of finite differences taken from section to section, with the transition equations based on those due to Lamé.

Birger[40] gives a simpler solution, thus

$$\sigma_r(r) = \frac{1}{r^{1-\nu}} \int_r^{R_2} \frac{Ee_\theta}{r^\nu} \, dr$$

and $\sigma_\theta(r) = \nu\sigma_r(r) - Ee_\theta(r)$

for the boundary condition $\sigma_r(R_2) = 0$.

The actual method of cutting out thin rings has been applied experimentally by Mach[42] with a certain amount of success.

For thicker rings, where σ_θ does not disappear entirely on cutting out, Davidenkov[43] suggested parting the rings to allow them to bend.

Where no axisymmetry exists in a disc, strain-gauges can be attached in both radial and circumferential directions before cutting out the surrounding segment. Dugdale[44] applied the technique to hammered foil.

Dugdale and Squires[45] used strain energy absorbed and work done by applied forces on a disc gripped at its centre and loaded with radial and transverse loads acting simultaneously at a point of the periphery. The effect of radial load on transverse stiffness was evaluated and the values obtained confirmed experimentally. Quartermain and Blazynski[46] examined the residual stresses resulting from the explosive loading of discs and found an acceptable degree of correlation between the individual

gauge cut-out and the standard Sachs method used to analyse the residual stresses in discs. Abé[47] introduced a finite deformation theory for axially symmetric thin elastic plates based on a consistent approximation from the corresponding three dimensional theory. This theory was then applied to a plate of finite thickness and which appeared to be different from the usual plane stress theory. Finally, the problem of the expansion of a circular hole in an infinite plate was investigated and the effect of the transversely variable stress components studied. He concluded that, with this type of two-dimensional problem of loading circular plate, the thickness plays an important part and the solutions may involve some error in the disc boundary.

1.2.4 Explosive Hardening

Work-hardening of a metal in the region of loading can be expected and also the changes in the engineering properties of the metal will result where an explosive charge is detonated in contact with a metal specimen, or where the specimen is subjected to the impact of an explosively driven object. Among several workers who have investigated work-hardening and property changes are Dieter[48], Minshall[49], Zukas and Fowler[50] and Holtzman and Cowan.[51] Dieter applied high intensity shock waves of increasing pressure to a variety of bcc and fcc metals. He found that iron with an initial hardness of 60 Vickers hardness (1 kg load) strain-hardened to a value of 280 following a

discontinuity in the hardening curve at the pressure of 13 GNm^{-2}. This discontinuity has also been observed by several other workers. Holtzmann and Cowan[51] found that austenitic manganese steel hardened from 210 to 580 Vickers hardness at a shock pressure of 40 GNm^{-2}. The examined crystals showed grain markings but practically no distortion. The major use of explosive hardening has been with austenitic manganese steel (12-14% Mn). This produces unusual properties, as mentioned in the books edited by Shewmon and Zackay[79] and by Rinehart and Pearson.[53]

Commercial explosive hardening is discussed by Jenkins[52], the hardening being accomplished by detonating a thin layer of plastic sheet explosive in contact with the metal surface to be hardened. Also the action of explosive hardening of restricted zones or extensive areas is discussed. Rinehart and Pearson[53] described the explosive hardening effects on rolled manganese steel. For a sample of size (3 x 1.25 x 7.6 cm), the BHN before explosive treatment was 200 and after treatment 370, whilst the yield stresses before was 400 MNm^{-2} and after 865 MNm^{-2}.

Smith and Fowler[54] have described experiments with single crystals of high purity copper subjected to a pressure of 30 GNm^{-2} plane shock in a free surface shot. Metallographic examination showed that mechanical twins had developed in the crystals except for one shocked in the [100] direction. Microhardness tests on the [100] face

of the specimen gave 134 for Vickers hardness (50g load) whilst the unshocked copper was 52 Vickers hardness on a [112] plane. White, Trott and Backhofen[55] in their work on the Physics of Explosion Containment, came to the conclusion that somewhat less than 1% of the energy of explosion is transferred to a material by the air shock wave. The remainder of the explosive energy appears in the high-temperature and high-pressure gases generated.

1.2.5 Sensitivity of Strain-measuring Instruments and Strain-Gauge Techniques

The use of strain-gauges for residual-stress determinations has been discussed by several workers[56-59]. Details given by Bloomfield[60] give some idea of the technique necessary for success. 60Ω foil gauges were attached by Araldite strain-gauge cement, protected by Araldite AY103, and temperature-cycled to stabilise them. The bridge had helical-wound apex units and means of reversing the polarity to eliminate thermo-elastic effects. Silver-plates brass plugs provided an excellent means of disconnecting and reconnecting the leads to the gauges, giving a reproducibility equivalent to $< \pm 1$ microstrain. The temperature of the specimen and dummy was maintained to within ± 0.2°C (Barker and Hardy[57] quote an example of temperature variation in which a difference of 1°C between active and dummy gauges caused an error in the strain measurement of 5×10^{-5}), and the results achieved had a scatter in strain values of only 10^{-5}.

An inaccuracy in the positioning of the gauge relative to the direction of principal stress cause a cosine error in the stress value, e.g. a 3° misalignment leads to a maximum error in the strain of 10^{-5}.

Denton[61] concludes that the Sachs boring method has now been sufficiently developed to justify its application to specimens that exhibit an axisymmetric stress distribution. Strain-gauges have been used with much success, but the precautions necessary in the Sachs boring application, where drift cannot be checked, may deter the adoption of Sachs boring technique. The gauges are capable of measuring stress in a removed layer to $\pm 7.72 \times 10^{6}$ Nm^{-2}.

1.2.6 Cutting Techniques (Machining)

Machining has had many supporters, particularly in the earlier days of the development of residual-stress methods. Leaf[62], however, pointed out that any machining process would upset the existing residual stress to some extent, the degree of disturbance being a function of the method of removal, the material, and the degree of hardness of the material. He recommended careful filing as a means of keeping the stress distortion to a minimum.

Frommer and Lloyd[63] showed that, in general, the coarser the cut, the greater the disturbance of the stress pattern, the worst case being where the tool is enclosed by the material, as in a milling slot.

The tensile residual stresses introduced by grinding have been investigated by Letner[64], Frisch and Thomsen[65] and Leaf.[62] These authors show that the value of stress varies with the type of grinding wheel and specimen material used, but the minimum stress quoted was nevertheless $\lesssim 18$ MNm^{-2} in the outer .005 cm layer. Richards[66] recommended the use of sharp tools, taking small cuts, to minimise the stress introduced from a cutting process. His resulting experimental scatter of only $\pm$ 13.8 MNm^{-2} over a range of 345 MNm^{-2} unfortunately gives no indication of the effect of milling, but serves only to confirm that conditions had been kept constant. Barker and Hardy[57] and Bloomfield[60] in boring out experiments have taken similar precautions including the supply of a liberal quantity of coolant to the cutting surface. Dodd[67] gives the normal percentage for bored out cross-sections for the measurement of strain as 10%.

1.3.7 Buckling

Timoshenko and Gere[68] in their book provide a chapter on elastic stability and give stability equations for a circular plate with concentric hole under uniform radial compression on the outer edge. Two cases may be considered, in the first case the outer edge is simply supported, inner edge being free; and in the second case, the outer edge is clamped, the inner edge being free. The conditions for both cases are similar in form

$$\sigma^1 = K \frac{E}{1 - \nu^2} \left(\frac{t}{a}\right)^2$$

where σ^1 is the critical unit compressive stress.

with K varying for the different support conditions and being dependent on b/a, b = inner radius, a = outer radius and t = thickness.

Many authors[69-71] have concerned themselves with the problems of the stability of a circular plate under the action of axisymmetric in-plane edge loading. The edge of the plate was considered to be either simply supported, elastically restrained or clamped but free to move in the direction of loading. Whereas Hirata and Watanabe[70] and Amon and Widera[71] considered buckling of plates with no hole at the centre, Vijayakumar and Rao[69] considered variational solutions for buckling of annular plates with holes. They concluded that the techniques applied to discs without holes were difficult to employ when the plate has a hole. They also concluded that the spectra of eigenvalues for axisymmetric buckling are identical for free-free, simply supported-free and free-simply supported combinations of edge conditions.

1.3 Present Work

The main purpose of this work has been to ascertain whether loading methods causing plastic deformation could be used to produce ordered pre-stressing of disc-shaped metal components. Initially, dynamic loading was used and subsequently more traditional pre-stressing methods have been applied to components of similar specification in order to compare and contrast the results found for the high energy rate explosive loading method.

In the present work, circular mild steel discs have been used for experimental and theoretical investigations. The advantages of using such a shape can be summarised as follows:

(i) Ease of production of mild steel discs from plate.

(ii) Convenient for annealing and pre-loading preparation and measurement.

(iii) By considering discs with initial diameters at least five times greater than their thickness, the longitudinal axial stresses can be assumed to be zero.

(iv) Allow simple loading parameters to be adopted.

(v) The pre-stressed discs could be loaded to induce a nominal axisymmetric residual stress distribution.

(vi) The discs allow experimental analysis by the turning down and boring out technique.

(vii) The case of plane strain deformation with axisymmetric loading is most readily amenable to treatment in plasticity.

(viii) Finally, the results should be of interest in relation to circular saw blades and turbine rotor discs etc.

The method used to produce pre-stressing in mild steel discs have been:

(i) the detonation of PETN sheathed cordtex in contact with both sides of the discs for dynamic loading, and

(ii) the application of compressive load through metal rings from both sides of the discs by means of a press (static loading).

Analysis of experimental results for each form of loading has been carried out which involved the use of strain gauge techniques. The dynamic loading method involved the application of strain gauges after loading whilst the static loading method allowed the strain gauges to be fixed to the discs before loading. Hence, two different methods of experimental techniques had to be used;

The boring out/turning down method for the dynamically loaded discs, and the continuous monitoring method for

the statically loaded discs.

A theoretical approach which could be applied to both loading methods was developed which depended on the consideration of the plastic deformation of the loaded annulus and the resulting elastic deformation of the surrounding regions of the discs. The plastic deformation of the loaded annulus depended on the amount of energy which can be transferred from the loading medium into an effective loading pressure. In the dynamic case, the loading medium was explosive material whilst in the static case the loading medium was a press via the compression rings. Hence the calculation of energy transfer has been treated separately for each loading method. The theory allowed the radial boundary pressures at the edge of the plastically deformed zones to be calculated. This pressure was taken to be that which causes residual loading in the remaining areas of the discs. Theoretical formulations based on well-known Lamé equations for elastic deformation and the use of calculated loading pressures have made it possible to predict patterns of residual stress in the radial and hoop directions of the disc for the two modes of loading. A further theoretical analysis was undertaken for the statically loaded discs using elastic-plastic finite element techniques. This allowed prediction of theoretical residual stress values for different loading levels up to the experimentally observed maximum residual values of stress. As a result of the choice of 6.25 mm

thick plate, a degree of buckling was evident in both loading methods and therefore a limited exercise for the prediction of buckling via the static loading method was undertaken in order to explain any divergences in the experimental results obtained. In order to establish the extent of plastic deformation created by the dynamic loading method, hardness tests and microstructural examination of the loaded zone were also carried out.

The entire programme of experimental work was designated by a number of series of tests A to E. The details of the test conditions can be found in the following tables:

Table 3.1, p 113 (A, B and C)

Table 3.15, p 163 (D)

Table 3.18, p 183 (E)

The following work comprises eight chapters and appendices. The first two chapters deal with the objectives and preparation of specimens including three special tests on plane deformation, hardness and micro-structural examination. The third chapter deals with the dynamic and static experimental analyses. The fourth and fifth are concerned with theoretical models to validate the experimental results. The sixth and seventh draw the work to a close with discussion, conclusions and further work. The eighth chapter contains 79 references which are discussed in Chapter 1.

CHAPTER 2

PREPARATION OF THE SPECIMENS AND EXPERIMENTAL TECHNIQUE

2.1 Introduction

2.2 Specimen Material Preparation and Dimensions

2.3 Stress-Strain Characteristics

2.4 Equipment, Testing Procedure and Schedule

2.5 Data Recording

2.1 Introduction

With the object of pre-stressing metal discs, two methods of loading have been applied. The first method, designated dynamic, used annular explosive rings attached to both sides of the disc. The second method, designated static, utilised a metal annulus applied to each side of the disc through which a load from a press could be applied. The two methods, because of their inherent differences, demanded different preparation and measurement methods to be adopted. Both loading methods utilised strain gauges to predict the residual strains caused by the applied loads. However, because it was decided to release the applied loads in the dynamic case by the process of turning down, boring out the strain gauges were applied as near as possible to the loaded annulus of the discs. The static loaded discs did not present the same problem since the strain gauges could be attached prior to loading and their readings taken both during loading and unloading of the discs. Consequently, different instrumentation and analysis techniques have been required in each case.

The dynamically loaded discs were processed first and the opportunity taken to obtain three characteristic parameters which could help provide a lead to the method of analysis which should be used for the strain gauge readings. The three characteristic parameters which were measured were plane deformation, hardness and microstructural examination of the loaded zone. The first of these parameters gave an

indication of the degree of bending or buckling produced in the discs whilst the other two gave evidence of the localization of the plastically deformed zone. As a result of the previous three measurements and in view of the similar loading constraints and parameters, it was only deemed necessary to carry out plane deformation measurements on the statically loaded discs.

2.2 Specimen Material Preparation and Dimensions

2.2.1 Dynamic Testing

2.2.1.1 Annealing and Marking of Discs

The heat treatment of the discs was carried out in three separate sessions. The A series being processed first and the B and C series processed in a similar fashion. Before annealing took place the samples of discs were coated in alumina powder and sealed in a stainless steel box which allowed nitrogen gas to be passed over the discs whilst annealing took place. The process for the annealing treatment was as follows:

(i) Heat to 910°C for 1 hour 15 mins

(ii) Soak at 910°C for 1 hour 15 mins

(iii) Furnace switched off and discs allowed to cool to 540°C in 1 hour 30 mins

(iv) Cooled further in the furnace to 360°C in approximately 2 hour

(v) Box containing discs removed from furnace and air cooled.

Items (i) to (iv) constitute a standard form of stress relieving anneal.

In a later section, it will be shown that the effect of annealing was a necessary requirement for the experimental measurements to be produced.

Discs in all series were marked prior to the explosive contact in two ways. The surfaces of the discs were marked on both sides in quadrants and circularly (Figure 2.1). The quadrant marking lines were to fix the angular positions of the strain gauges. The circular marking was to fix a circular cardboard strip and thus fix the position of contact for the cordtex. The circular markings were of fixed radii for the A and C series of discs but of variable radii for the B series. The circular marking was carried out on a lathe in order to achieve concentric equal radial marking on both sides of the discs, thus allowing the loading rings to be concentric on either side of the discs.

2.2.1.2 Explosive Arrangement for Contact Operations

(a) Types of Explosives

Many types of explosives are available which can be used in metal working operations. They come under a large number of different names, possess a wide range of properties, and can be divided into various categories depending on the parameters which are of interest.

The major breakdown on explosive types and the one most important to metal working is into high explosives and low explosives. A high explosive is typified by

Figure 2.1 : Marking of Discs for Fixing of Strain Gauges and Explosive

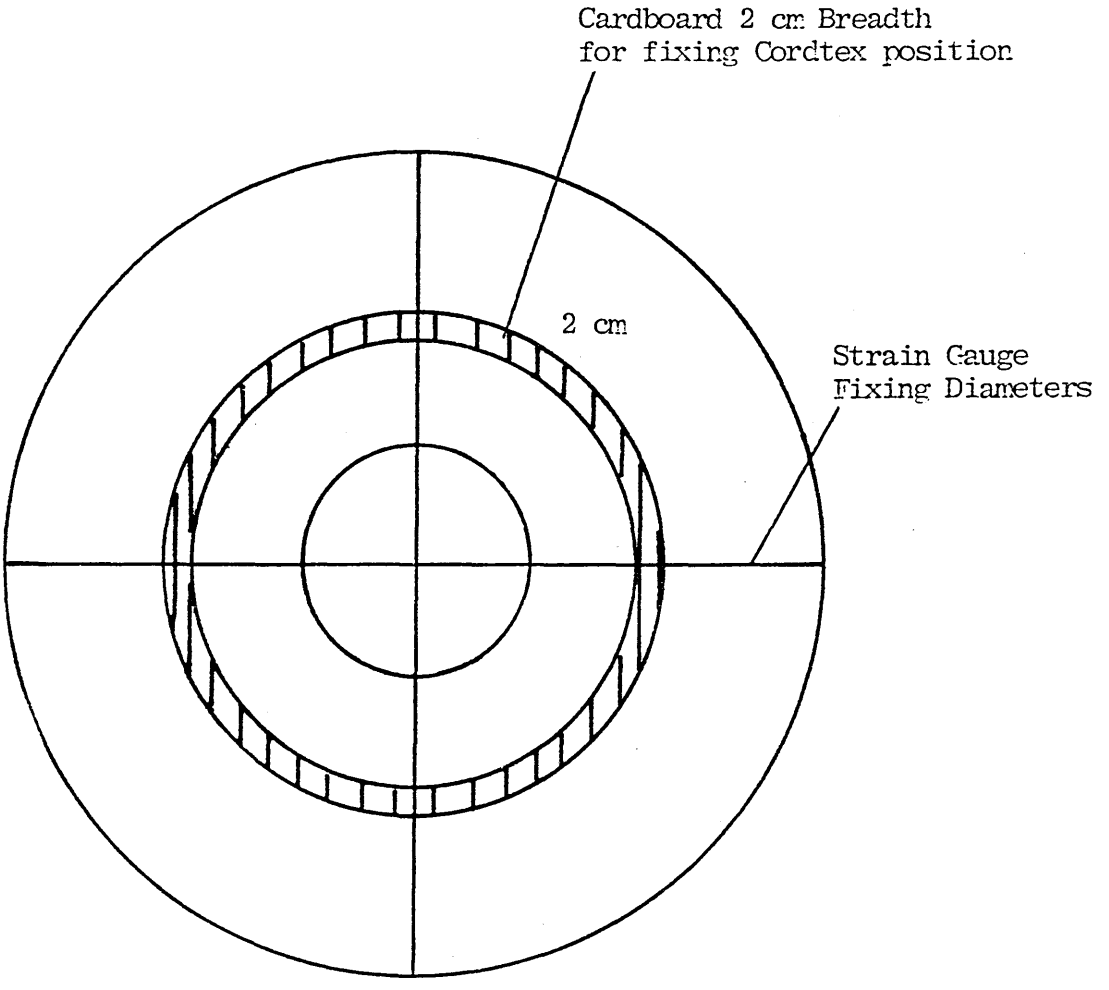

Markings on both sides of disc

TNT, PETN or dynamite. A secondary breakdown for the high explosives is into primary or initiating explosives and secondary or non-initiating explosives, and is based on the sensitivity to detonation of an explosive. A high explosive detonates producing extremely high pressures. The conversion time, i.e. the time required to convert a working amount of high explosive into high pressure gaseous products, is measured in microseconds.

Secondary, or non-initiating, high explosives comprise that class of high explosives which are so insensitive that they require initiation to detonation by another explosive. They are used as booster and bursting charges, for blasting and demolition, and are the high explosives used as energy sources in metal working operations. The conversion time for these operations is measured in μs.

(b) Properties

When comparing the effectiveness of various explosives to do a particular job, two properties are normally considered. These are the BRISANCE and POWER of the explosive. The brisance of an explosive represents its shattering power, as distinguished from its total work capacity. It is of practical value in determining the fragmentation effectiveness of an explosive against a metal. It has been found that there is a general linear relationship between rate of detonation

and brisance. The higher the detonation rate of an explosive, the greater its brisance. This value can be determined by the (i) Sand test, (ii) Plate dent test, (iii) Fragmentation test.

The total work capacity of an explosive is a function of the total available heat liberated at the instant of detonation, while the power of the explosive is determined by the rate at which the heat energy is liberated.

(c) Systems for Operation of Explosive Charges

Secondary high explosives come in a variety of physical forms as follows:

(i) Cast (melt loaded) or pressed to shape
(ii) Plastic sheet
(iii) Plastic bulk
(iv) Powders
(v) Liquids
(vi) Gelatins
(vii) Detonating Cords

Many of these forms have the same basic explosive constituents, with various additives used to provide physical form.

In preparing an explosive charge for an operation, consideration must be given to the most appropriate type to use, and to the manner of shaping the charge to the desired configuration. A brief description

of those methods relevant to contact operations follows:

(1) Plastic sheet explosive comes in rectangular sheets which can be cut into an unlimited variety of flat shapes. A charge of sheet explosive can be built up to a desired thickness through the adhesion of multiple layers. Plastic sheet explosive is normally detonated by special detonators.

(2) Plastic bulk explosive can be hard-moulded into a variety of shapes, hard-packed into variously shaped containers, or rolled into sheets. Bulk amounts of this explosive can be initiated by a special detonation, with the detonation inserted about 1.5 cm into the explosive. For small amounts, or for thin shapes, it is often desirable to place a small tetryl booster at the base of the detonator to insure initiation of the explosive. Figure 2.2 illustrates the manner of detonation for plastic bulk explosive charges. The effect of small explosive charges of plastic bulk is shown in Figures 2.2 and 2.3.

(3) Cast explosives - many of these can be machined to shape after casting. Figure 2.2 illustrates booster-detonator arrangements.

(4) Primacord or Cordtex - a type of linear detonating cord which normally has a PETN base is available in a range of explosive weights per linear metre. It comes in spools and is cut to the desired length for each operation. It is sufficiently flexible that it can be formed into various configurations. Methods for initiating detonating cord are shown in Figure 2.4.

(5) As yet, liquid and granular high explosives have found only limited application in the metal forming field.

2.2.1.3 Adopted System

The system chosen to produce high rates of strain, as required by the experimental section of this work, Chapter 3, has to satisfy the following conditions:

(i) High brisance (see 2.2.1.2 (b))

(ii) High power (see 2.2.1.2 (b))

(iii) Capable of being shaped to the desired configuration (see 2.2.1.2 (c))

(iv) Ease of detonation (see 2.2.1.2 (c))

(v) Relatively cheap and safe

(vi) Produce simultaneous detonations on both sides of the metal disc.

Figure 2.2 : Booster-Detonator Arrangements for Plastic Bulk Explosive Charges

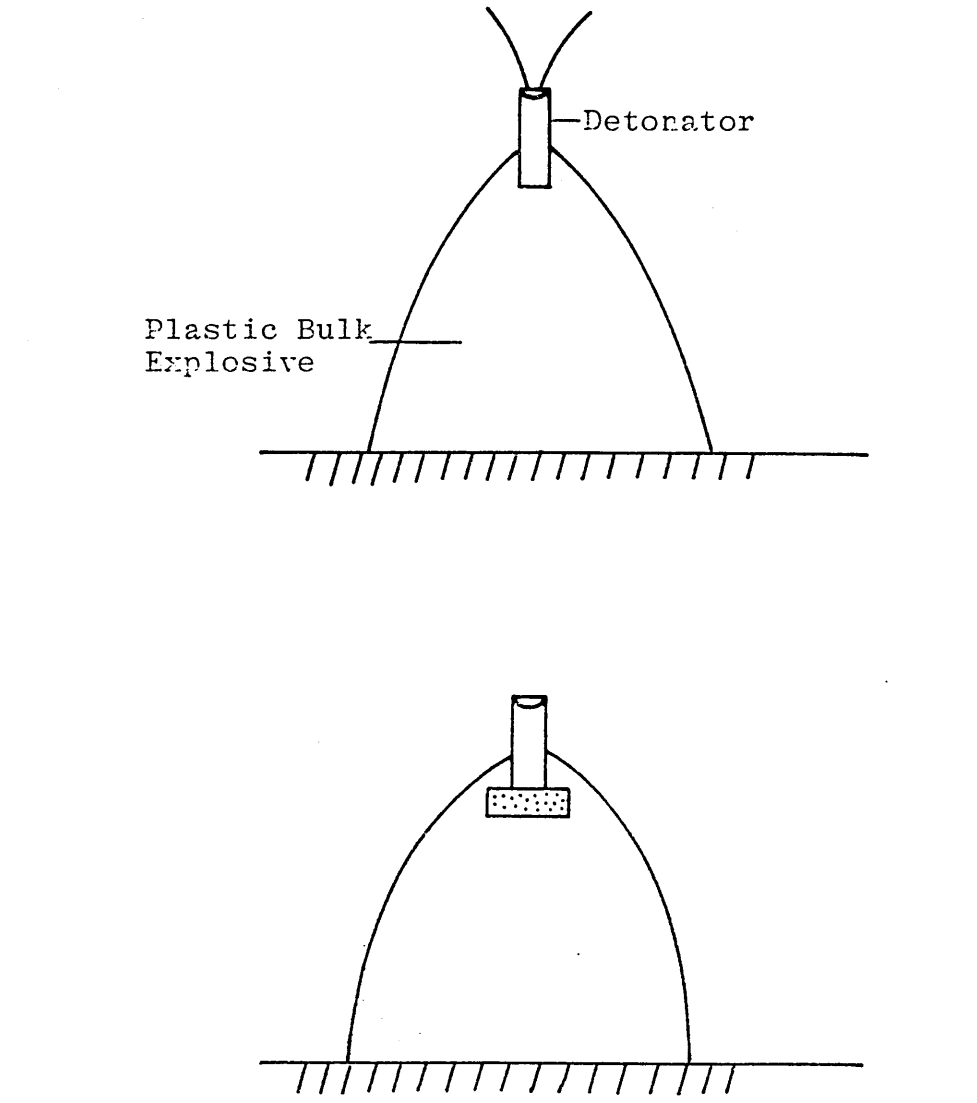

Figure 2.3 : Booster-Detonator Arrangements for Cast Explosive Charges

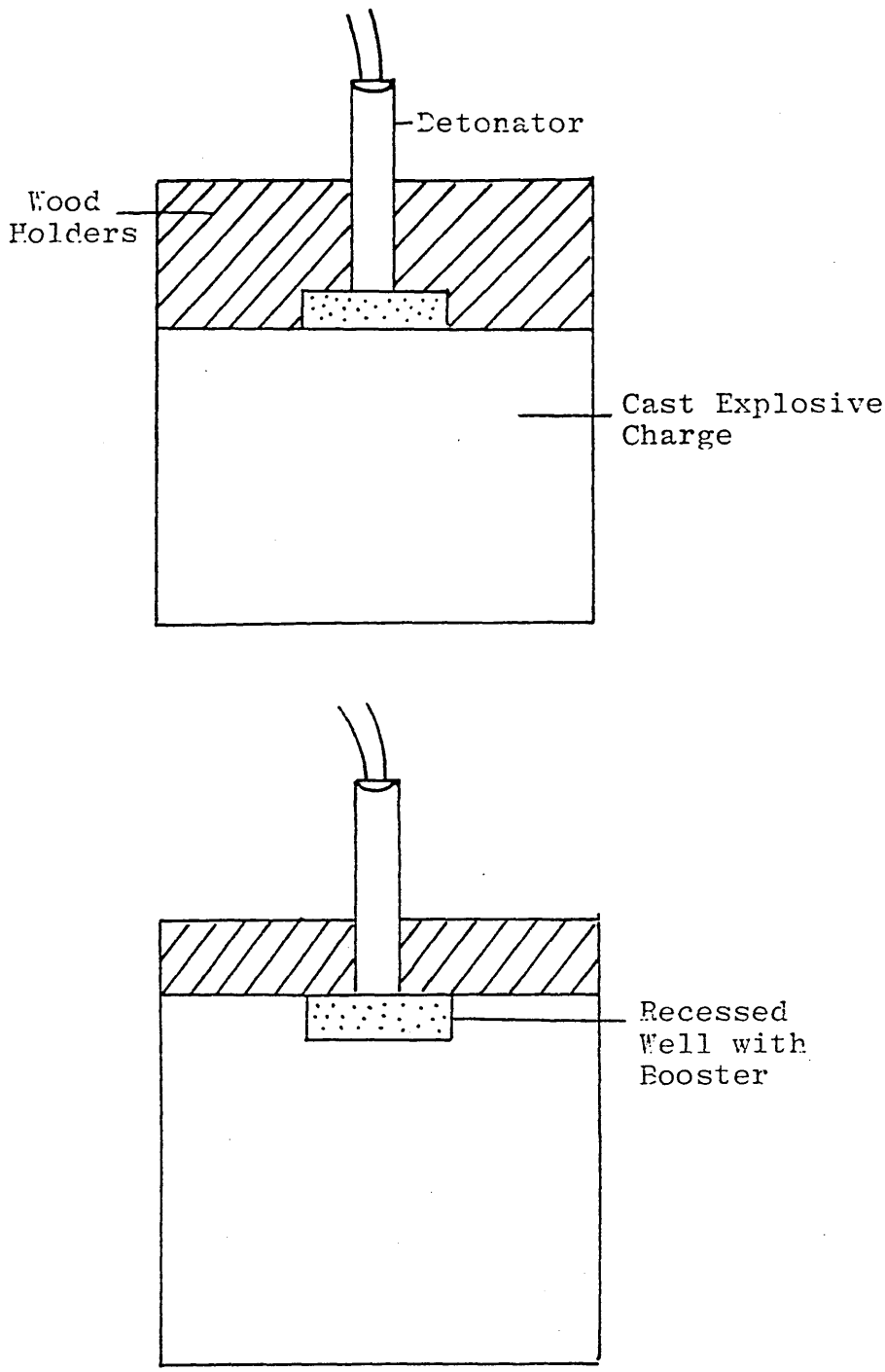

Figure 2.4 : Methods for Initiating Detonating Cord

(a)

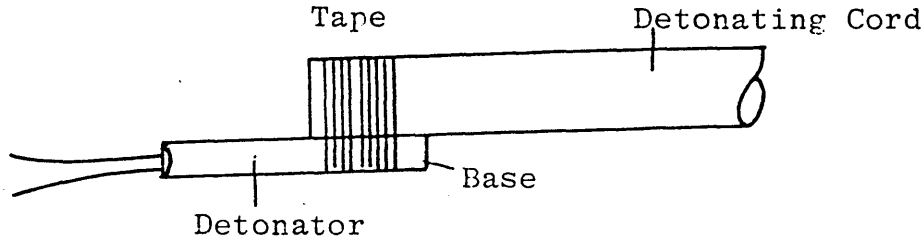

(b)

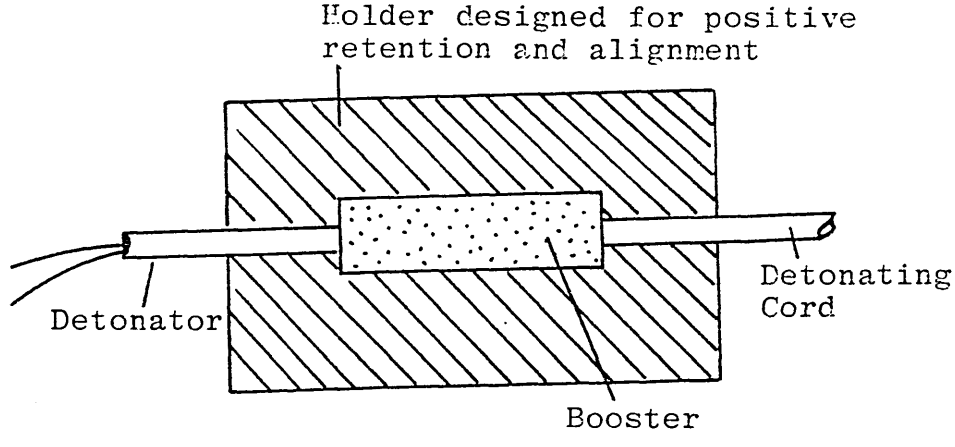

(c)

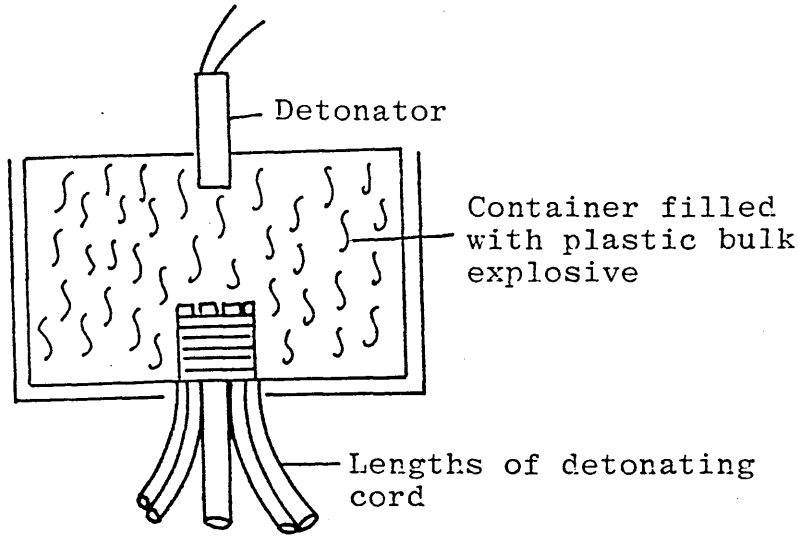

A system which satisfies conditions (i) to (vi) is an electric detonator connected to a detonating cord (see Figure 2.4a) connected to a shaped line cord. The method of connection is shown in Figure 2.4 and 2.5 . The detonating cord consists of a high explosive, usually PETN, contained within a waterproof covering. The type used in this work was called I.C.I. CORDTEX, having an energy content of 4310 Jg^{-1} and packing density of 3.175 gm per foot run. The explosive was initiated with standard I.C.I. No 6 electric detonators.

Detonating cord has been used in two main ways in explosive metal working operations.

(a) First, it has been used an an energy source in the forming and sizing of long tubular parts and flat surfaces. For tubular parts it is usually used as single or multiple strands stretched along the axis of the part. For flat surfaces it is frequently wound into a spiral or used in multiple loops.

(b) Second, it is used as a timing and initiating fuse for some other explosive. Frequently, detonating cord leads are used for the simultaneous initiation of multiple charges. When used as an energy source, detonating cord is usually initiated by placing an electric detonator alongside the initiation end of the fuse and taping the two together. Having decided that the line cord system can satisfy the conditions (i) to (vi) and principally that the fixing of the explosive to the disc will allow equal detonation rates

Figure 2.5 : Explosive Arrangment on the Discs

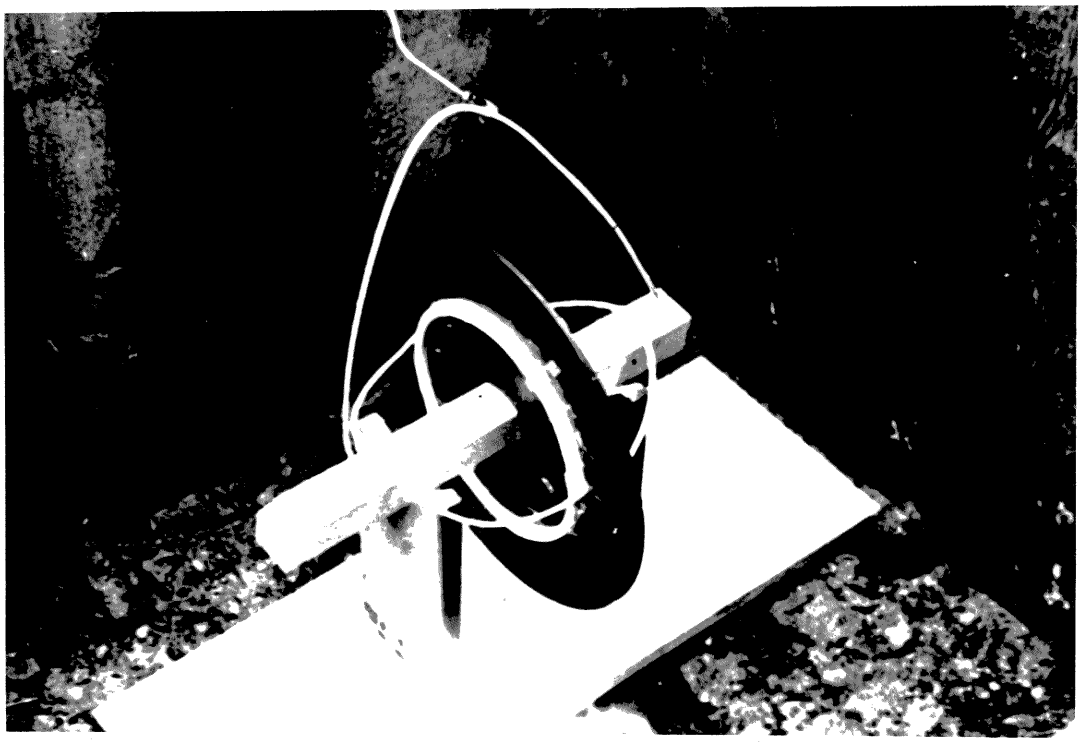

Figure 2.6 : Explosive Layout

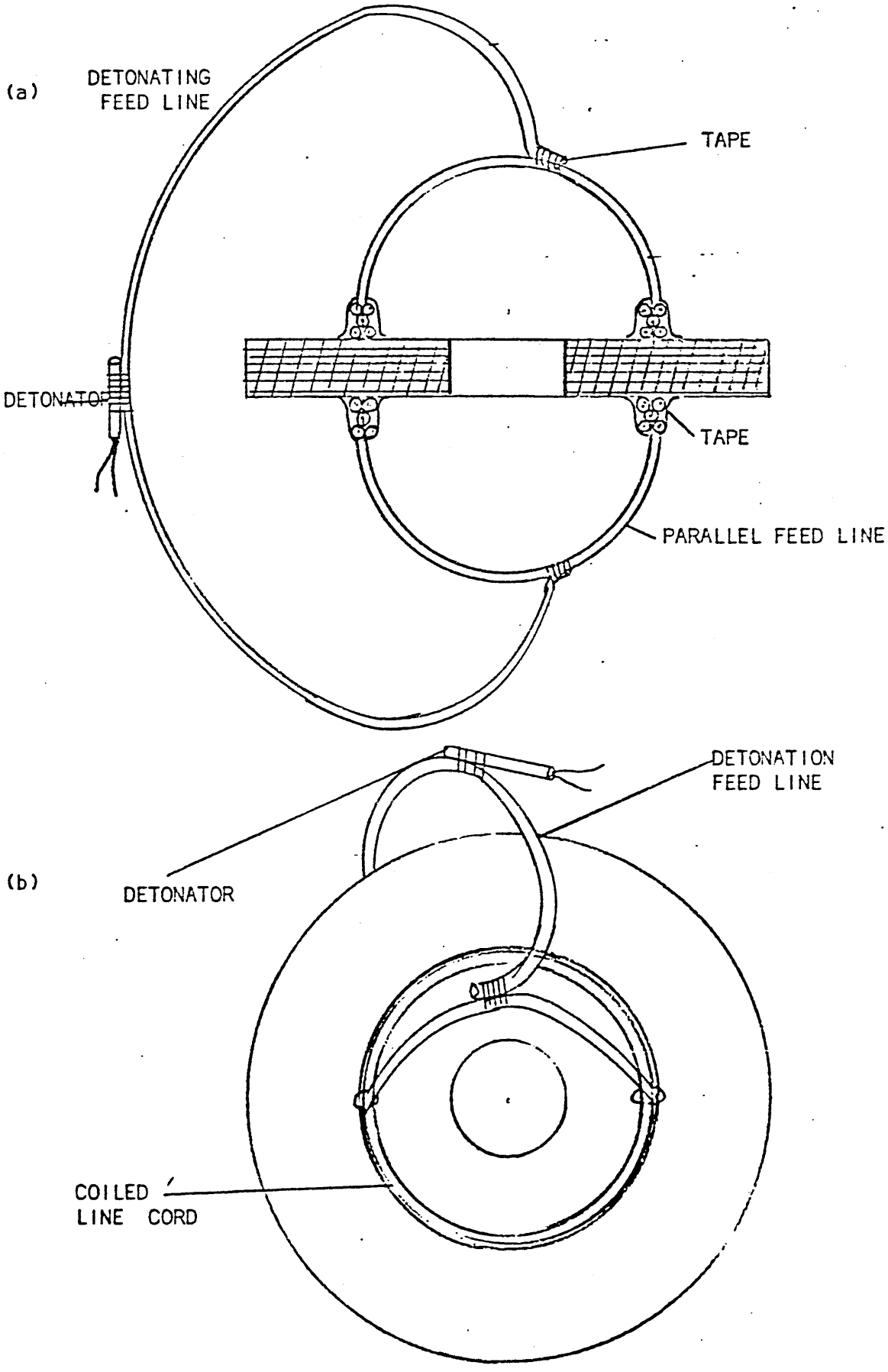

and equal pressure on both sides of the disc, the system was designed as shown in Figures 2.5, 2.6 In order to ensure that the disc explosive loading was axisymmetric, the explosive radii were marked out by using cardboard rings as shown in Figure 2.1.

2.2.1.4 Radial Dimensional Measurements before and after Explosion

The outer and inner diameters of the discs were measured prior to and after the explosive charge. The measurements were taken using an external and internal set of vernier calipers which could read to an accuracy of $\frac{1}{100}$ mm for the outer and for the inner. The measurements thus obtained can give a measured indication of the values of a_0-a and $b-b_0$, which are required in the theoretical calculation of σ_{r_1} and σ_{θ_1}. In practice, the internal and external measurements were taken along the marked axes of the discs and in intermediate quadrants. The four values of diameter then giving a mean value as shown in Tables 2.1, 2.2 and 2.3. The values given in the tables can only be used to indicate the order of magnitude for a_0-a and $b-b_0$ because all the discs were subjected to a degree of buckling after the explosive contact. A measure of the amount of buckling associated with each disc is given in Section 2.5.

a_0 = initial inner radius

a = final inner radius

b_0 = initial outer radius

b = final outer radius

External and Internal Radial Changes

Accuracy of measuring vernier = $\frac{1}{100}$ mm = 1 x 10^{-5} m

Table 2.1

A series (Fixed Position : Variable Quantity of Explosive)

Disc	a_0/cm	a/cm	$(a_0-a)/10^{-5}$ m	b_0/cm	b/cm	$(b-b_0)/10^{-5}$ m
A4	3.815	3.815	0	19.030	19.032	2
A6	3.810	3.810	0	19.000	19.002	2
A5	3.813	3.810	3	19.039	19.042	3
A7	3.808	3.806	2	19.029	19.027	2
A8	3.805	3.802	3	19.030	19.030	0

Table 2.2

B series (Fixed Quantity of Explosive for B1, B2, B3; Variable Position)

Disc	a_0/cm	a/cm	$(a_0-a)/10^{-5}$ m	b_0/cm	b/cm	$(b-b_0)/10^{-5}$ m
B1	3.795	3.790	5	19.035	19.035	0
B2	3.800	3.794	6	19.050	19.050	0
B3	3.801	3.800	1	19.046	19.047	1
B5	3.805	3.803	2	19.035	19.037	2
B6	3.815	3.813	2	19.059	19.064	5

Table 2.3

C series (Fixed Position, Variable Outer Diameter)

Disc	a_0/cm	a/cm	$(a_0-a)/10^{-5}$ m	b_0/cm	b/cm	$(b-b_0)/10^{-5}$ m
C1	3.730	3.728	2	21.522	21.523	1
C2	3.820	3.817	3	19.036	19.040	4
C3	3.793	3.790	3	16.500	16.503	3
C4	3.830	3.825	5	13.986	13.990	4

2.2.1.5 Strain Gauge Fixing Parameters

Method of Fixing Strain Gauges

The system used had azimuthal symmetry and this fact was used when fixing the strain gauges. Four 45° rectangular rosettes were fixed at points diametrically opposite to each other in four quadrants, and on each side of the discs, thus giving the possibility of eight readings. As shown in Table 2.4 the gauges were fixed to the disc at the same radii for the A and C series discs, but varied for the B discs. One arm of the rosette was fixed in the radial direction and the 90° arm in the hoop direction. The e.r.s. gauges used in all the series were TOKYO SOKKI gauges of length 10 mm, gauge resistance 120 ± 0.3Ω and gauge factor 2.07. A typical arrangement is shown in Figure 2.6 in which the gauges are fixed as previously described and inside the explosive ring as indicated by Table 2.4 for the disc illustrated which is C1. The gauge

position in relation to the explosive ring was chosen to maximise the number of cuts from the disc for both outer and inner sections.

Table 2.4

Gauge Parameters

Disc	Radial/(cm) Position of Explosive Ring	Gauge Position/(cm)
A4	11.33	9.75
A6	11.33	9.75
A5	11.33	9.75
A7	11.33	9.75
A8	11.33	9.75
A3	11.33	At 1.5 unit distances from explosive ring
B1	7.62	8.12
B2	8.89	9.89
B3	10.16	11.16
B5	11.43	10.43
B6	12.70	11.70
C1	11.33	9.75
C2	11.33	9.75
C3	11.33	9.75
C4	11.33	9.75
C5	11.33	9.75

Figure 2.7 : Arrangement of Gauges on a Typical Disc - C1

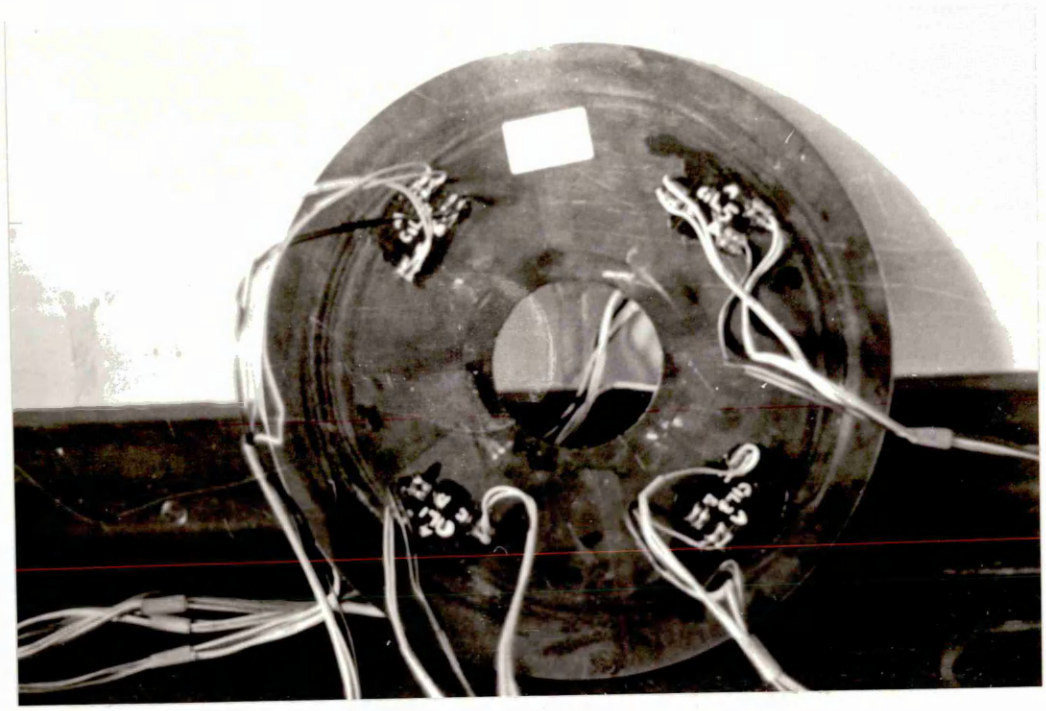

2.2.2 Static Loading (Press)

2.2.2.1 Preparation

The surfaces of the mild steel discs were first lightly abraded with a sanding wheel whereas the areas which were to receive strain gauges were thoroughly cleaned. These were further treated by degreasing with solvent to make them chemically clean.

2.2.2.2 Positioning and Fixing the Hardened Alloy Tool Steel Loading Rings

After experimenting with different methods of fixing the annular rings to the discs, it was found that the best method involved the positioning of the rings by means of three perspex pegs situated around and in contact with the outer circumference of the rings. The perspex pegs were held in position by strain gauge adhesive. The position of the loading rings were thus retained in a central axisymmetrical position with regard to the centre of the disc. The loading rings were laid on a bed of tallow in contact with the disc surface.

The actual fixing and positioning of the loading ring concentrically was achieved with the aid of a micrometer depth gauge with the shoulder held against the plate periphery and the probe onto the ring periphery. Once the ring and plate centres appeared to be coincident, two magnetic blocks were positioned so that the ring could be removed and then wedged between the block edges again. The attached rings were checked for concentricity

by fitting the entire assembly disc plus two annular rings into a three jaw lathe-chuck, spun by hand and eccentrically measured by a dial-test indicator.

2.2.2.3 Preparation and Fixing of the Strain Gauges

Each fixing zone was abraded with a sanding wheel until each surface appeared clean and shiny, taking great care not to overheat the surface. These zones were degreased with solvent. The positions and orientations of the strain gauge rosettes were then marked on the surface of the discs. Each rosette was placed on a strip of MYLER TAPE and affixed to the surface of the disc with the arms of the rosette aligned in the radial and hoop directions of the disc. One end of the rosette was then lifted and removed from the surface. The gauge area was then recleaned first with conditioner and then with a neutralising alkali solution. The under surface of the gauges were then painted with catalyst whilst a spot of adhesive was placed on the predetermined areas of the disc. The gauge was then compressed onto the surface of the disc. Terminal strips were then placed in close location to the gauges.

2.3 Stress-Strain Characteristics

2.3.1 Composition of Mild Steel used in the Sample Discs

Element	%
Carbon	0.17
Manganese	0.74
Silicon	0.05
Sulphur	0.027
Phosphorus	0.020
Nickel	Nil
Chromium	Nil
Molybdenum	0.013

2.3.2 Tensile Test of Sample

A tensile test was carried out on a sample of steel taken from the material of disc A3. The flat specimen of width 1.25 cm, thickness 0.64 cm and gauge length 5.7 cm was loaded at a strain rate of 1.46×10^{-3} sec^{-1}. Readings taken from the Figure 2.8 indicate that 0.5% proof stress for the specimen equals 1.95×10^{8} Nm^{-2} with an ultimate tensile strength of 3.85×10^{8} Nm^{-2}. The final elongation was 41%. Since there is no definite yield point shown on Figure 2.7, the 0.5% proof stress point was used to specify the yield point for the specimens of steels used in the discs A, B and C.

Figure 2.8 : Loading of Steel Sample from Disc A3

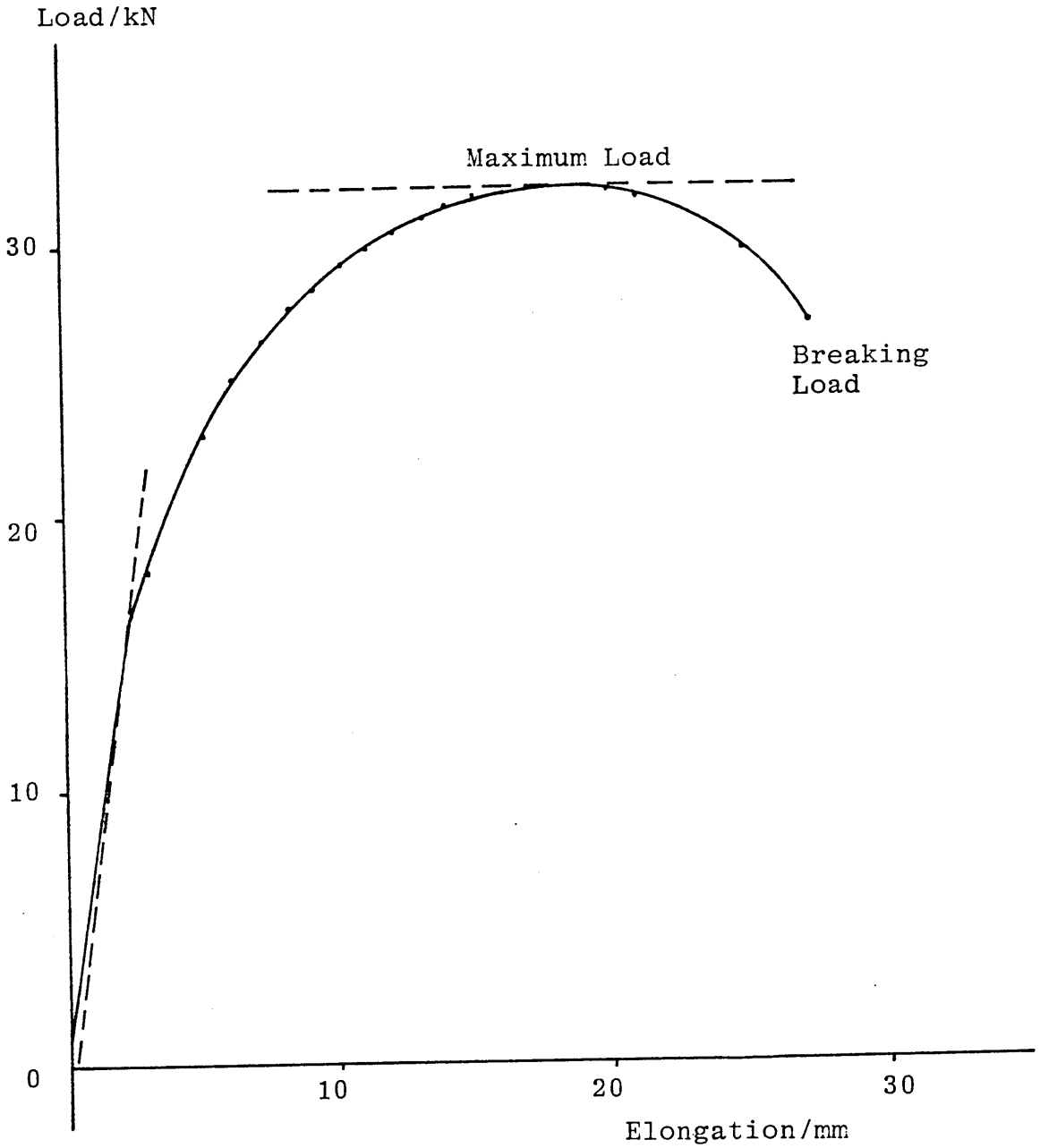

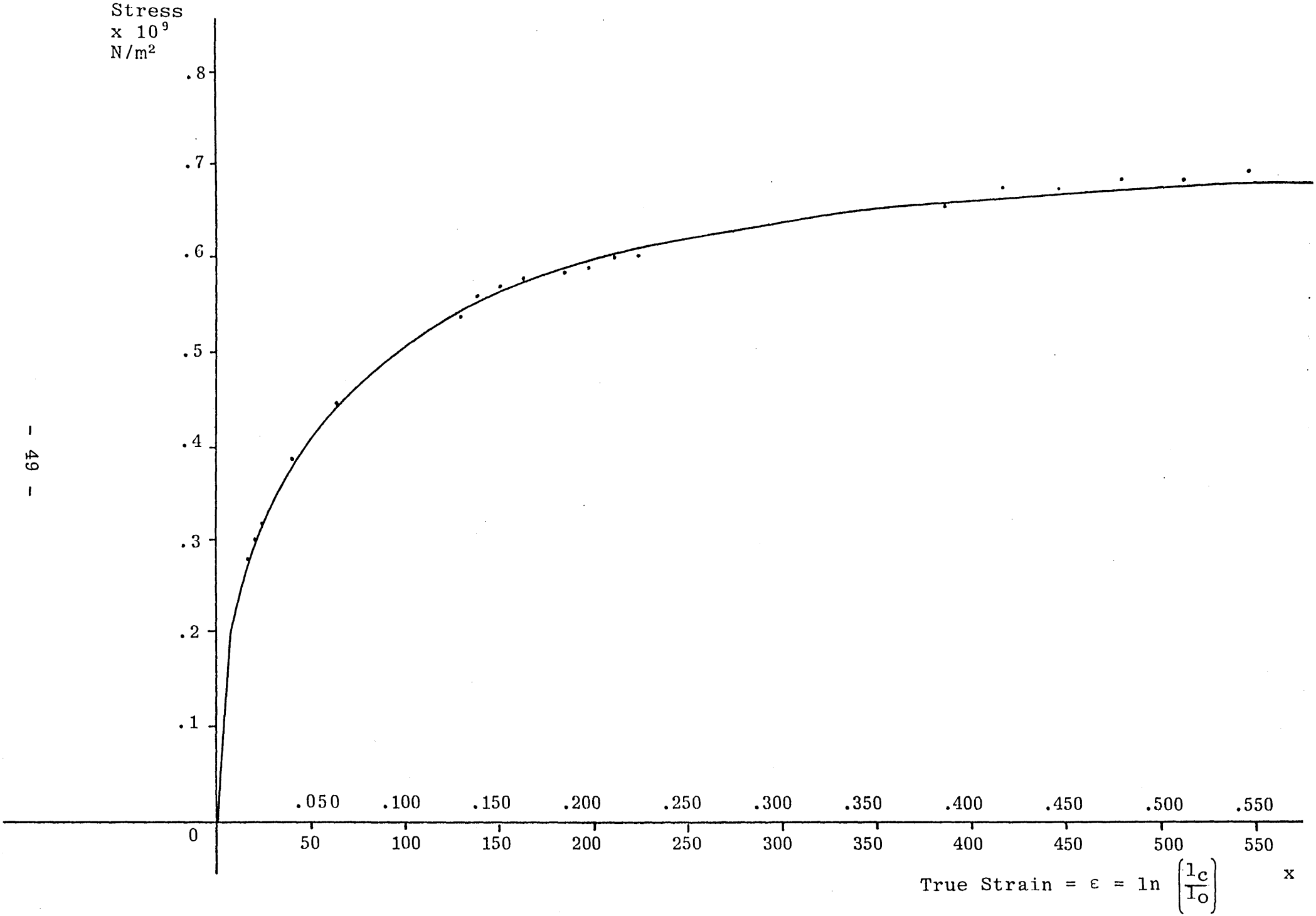
Stress
x 10^9
N/m^2
.8
.7
.6
.5
.4
.3
.2
.1
0
.050
.100
.150
.200
.250
.300
.350
.400
.450
.500
.550
50
100
150
200
250
300
350
400
450
500
550
True Strain = $\varepsilon = \ln\left(\frac{l_c}{l_o}\right)$
x

2.3.3 Compressive Tests

A series of compressive tests were carried out on samples from the discs. The results of these tests were used to produce the constitutive equations required for the plastic-elastic analysis of the statically loaded discs. The results of these tests have therefore been included at the point where the constitutive equations have been derived, i.e. in Chapter 3, Section 3.2.2.

2.4 Equipment, Testing Procedure and Schedule

2.4.1 The essential difference between the explosively (dynamic) and press (static) loaded discs is that in the former the gauges cannot be fixed to the specimen until after loading has taken place whereas in the latter the gauges can be fixed prior to loading. Thus in the dynamic loading the measurements have to be made retrospectively and in the static loading the progressive changes of strain up to maximum loading and then release to zero load can be made in real-time.

2.4.2 Measuring Circuit (Dynamic)

2.4.2.1 Description of Operation

The gauges having been fixed to the disc surface as described in Section 2.2.1.5, the circuit and measuring instruments are then required to provide an indication of the increase or decrease in the resistance of the gauges as the discs are 'turned down'. The circuitry used provided an indication of a voltage change which could then be

converted into strain as shown below.

A standard bridge circuit (Figure 2.10) was used to measure the gauge resistance changes using a digital voltmeter (DVM) capable of reading to an accuracy of 10 μV. A Beckman Helipot was incorporated in the circuit to provide the resistance balance accuracy required to provide a DVM reading to 10 μV. The initial zero load gauge readings were adjusted to give zero readings on the DVM for a set position on the Beckman Helipot, which were recorded for each gauge. In subsequent out of balance readings, the Beckman Helipot was set to the standard zero reading for each gauge and new out of balance readings recorded from the DVM which could thus provide the strain reading for each load.

2.4.2.2 Accuracy

An examination of the formula:

$$\text{Strain} = \frac{\delta R}{R} \times \frac{1}{\text{Gauge Factor}}$$

shows that if the ratio $\delta R/R$ could be measured directly, then absolute values of the initial gauge resistance R ohms and the change in resistance of δR ohms, which is proportional to R, need not be determined.

$$\text{DVM Voltage} = \frac{V}{4} \times \frac{\delta R}{R}$$ (standard formula for one active gauge)

$$\therefore \quad \frac{\delta R}{R} = \frac{4 \times (\text{DVM Voltage})}{\text{Supply Voltage}}$$

Figure 2.10: Bridge Circuit

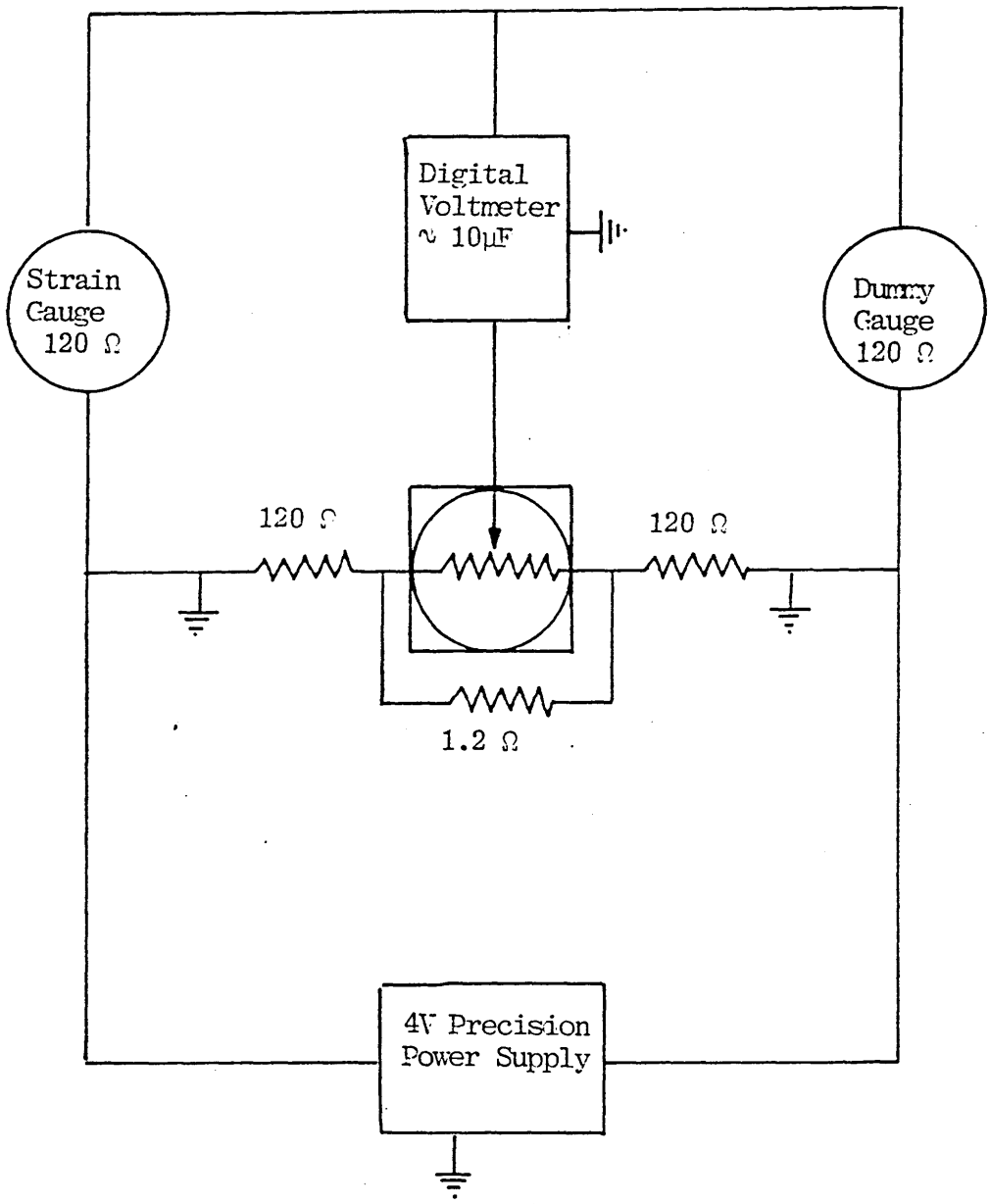

Figure 2.11 : System used for Measurement of Strains for dynamically loaded Discs

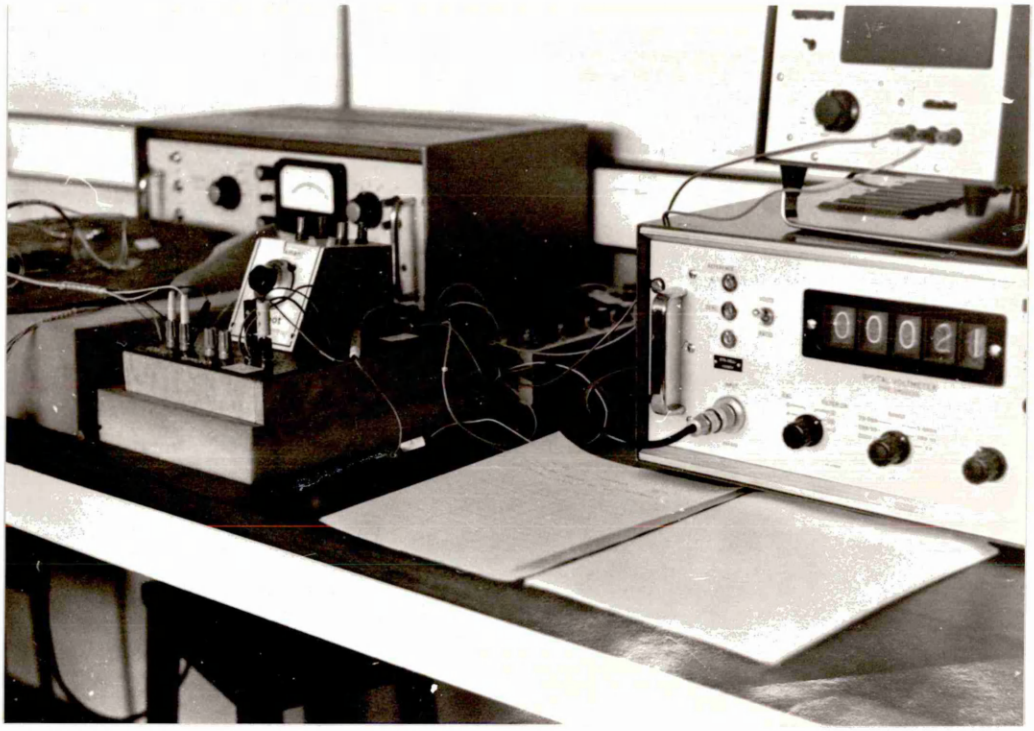

Hence $\text{Strain} = \frac{4 \times (\text{DVM } \mu V)}{4} \times \frac{1}{\text{Gauge Factor}}$

Thus $\text{Strain} = \frac{\text{DVM} \times \mu V \text{ reading}}{\text{Gauge Factor}}$

The circuit necessary to attain the above reading is shown in Figure 2.8a and theoretically in Figure 2.9.

The contact resistance of the Helipot is now in series with the galvanometer and does not introduce error.

By considering Figure 2.12 an estimation of the accuracy obtainable with this system can be made as follows:

At balance T is zero and $\frac{R}{S} = \frac{P}{Q}$

After straining, R changes to R + δR and balance is again obtained by adding T ohms to resistance P and substracting the same amount from resistance Q.

$\therefore \quad \frac{R + \delta R}{S} = \frac{P + T}{Q - T}$

or $\quad \frac{R}{S} + \frac{\delta R}{R} = \frac{P}{Q} \cdot \frac{(1 + T/P)}{(1 - T/Q)}$ and since $\frac{R}{S} = \frac{P}{Q}$

$$\frac{\delta R}{S} = \frac{P}{Q}\left(\frac{1 + T/P}{1 - T/Q} - 1\right)$$

but $\quad \frac{\delta R}{S} = \frac{\delta R}{R} \times \frac{R}{S} = \frac{\delta R}{R} \times \frac{P}{Q}$

Hence $\frac{\delta R}{R} = \frac{1 + T/P}{1 - T/Q} - 1 = \frac{1 + T/P - 1 + T/Q}{1 - T/Q}$

$$= \frac{T/P + T/Q}{(Q - T)/Q} = \frac{QT + PT}{PQ} \cdot \frac{Q}{Q - T}$$

$$= \frac{T}{P}\frac{(P + Q)}{(Q - T)}, \text{ which on dividing out}$$

Figure 2.12: Circuit for Estimation of Accuracy

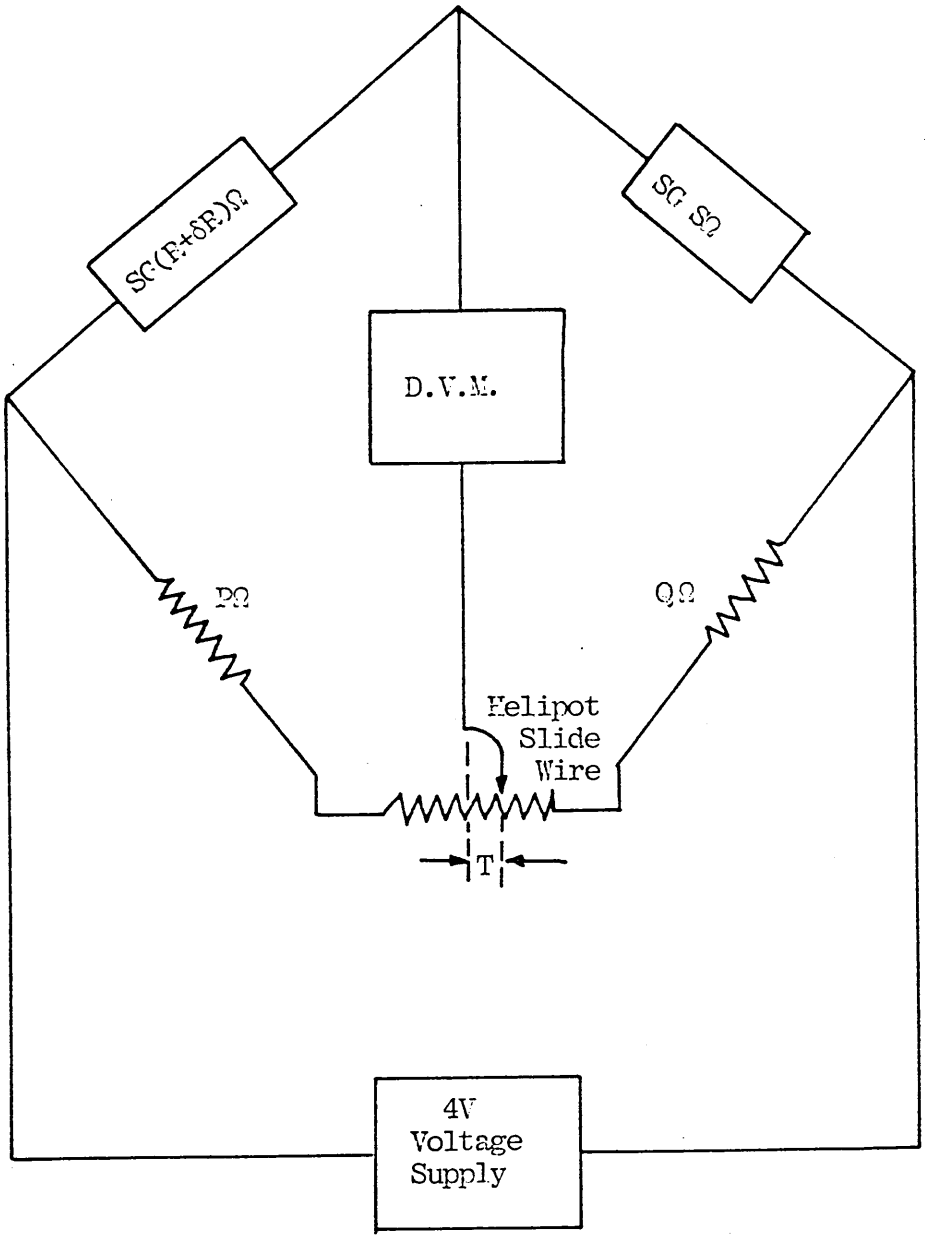

becomes $\frac{\delta R}{R} = \frac{T}{P} + \frac{T}{Q} + \frac{T^2}{PQ} + \frac{T^2}{Q^2} + \ldots.$

If P is made equal to Q, then R must equal S and if T is small compared with P

then $\frac{\delta R}{R} \cong 2\left(\frac{T}{P} + \frac{T^2}{P^2}\right)$

For the circuit shown in Figure 2.12

$$R = S = P = Q = 120\Omega \text{ and } T(MIN) = \pm .005\Omega$$

then $\frac{\delta R}{R} \cong \pm 2 \left(\frac{.005}{120} + \frac{(.005)^2}{(120)^2}\right)$

$$\cong \pm \frac{.01}{120} = \pm .000083$$

$\therefore$ Maximum Strain $= \frac{\delta R}{R} \times \frac{1}{\text{Gauge Factor}} = \pm .000083 \times \frac{1}{2.07}$

$$= \pm .00004$$

For steel inside the limit of proportionality, this strain corresponds to

$$\text{Stress} = E \times \text{Strain} = \pm 1.8 \times 10^{11} \times .00004 \text{ Nm}^{-2}$$

$$= \pm 7.2 \text{ MNm}^{-2} \left(\pm \frac{1}{2} \text{ ton/in}^2\right)$$

2.4.2.3 Measurement Controls

(i) Temperature Compensation

If at balance the strain-gauge attached to the test surface experiences a change in temperature, then the combination of (a) the linear expansion of the test surface, adhesive and paper, and (b) the temperature coefficient of resistance of the strain gauge wire would result in a change of gauge resistance δR^T. This change would unbalance the bridge and be measured as an apparent strain. Temperature effects can be automatically nullified by utilising another strain-gauge, identical to the gauge on the test surface as a "temperature compensation". As shown in Figure 2.10 such a gauge was incorporated in the test circuit in series with the active strain gauge. The 'dummy' gauge was fixed to an unstressed piece of the same material as that under test. In practice, it was fixed to a centre disc taken from one of the discs before stressing and incorporated under the Beckman Helipot stand. Both gauges thus experienced the same temperature changes and in consequence, equal variation in resistance δR^T. Hence unbalance of the bridge did not occur, since the same amount of resistance change due to temperature occurred in each arm of the bridge.

(ii) Zero Drift and Creep

The stability of the circuit was checked for a period of 20 days (5 hours each day). The normal drift in that time was found to be 10-20 μV as indicated on the DVM.

After a bridge has been balanced, it is possible for a slow persistent drift of the DVM from zero to take place. This is generally due to absorption of moisture by the gauge from the atmosphere. The gauges were thus coated with a moisture resistant coating of P2 resin adhesive from Tokyo Sokki, as shown in Figure 2.7. The reproducibility of the readings indicated by the DVM was checked by recording zero balance and the reading on the Helipot noted. The following day the reading of the DVM was checked for the same setting of the Helipot and the same gauge. Over a set of 50 readings the same zero balance was obtained in 47 out of 50 checks. In practice all zeroes for the A, B and C series were checked on three successive days before any cutting took place. Creep is another type of drift which is observed after the gauge has been strained by a fixed amount. The coating of the strain gauges with the P2 adhesive also helped to eliminate this form of creep.

(iii) Cutting of Discs

The cutting of the discs took place on the centre lathe of 11" swing with a face plate of 15" diameter.

Figure 2.13 shows the plate on the lathe chuck. The outside edge cutting speed was 34 rpm and the inside cutting speed was 120 rpm. During cutting the cutting tool was cooled with soluble oil and hence another good reason for the gauges being protected by the resin adhesive.

Prior to machining the discs were tested by loading with a chuck, thus simulating the loading conditions on the lathe. It was found that under maximum loading of the chucks the gauges produced a reading of 40 μV on the DVM. On releasing the load, the readings from the strain gauges returned to zero. Prior to machining the strain gauge leads were removed from the connectors and resoldered after machining in the case of the A and B series. For the C series the leads were left connected and either threaded down the centre of the lathe for outer cutting or taken over the outer rim and fastened to the chuck for the inner cuts.

(iv) Digital Voltmeter Indication of Compression or Tension

The relation between the sign, positive or negative, indicated on the DVM and actual compressive or tension forces on the gauges was tested by:

(i) a linear gauge on a cantilever strip, and
(ii) a cut out sample gauge from a disc.

The item in (i) was tested by bending whilst that

Figure 2.13 : Disc Machining

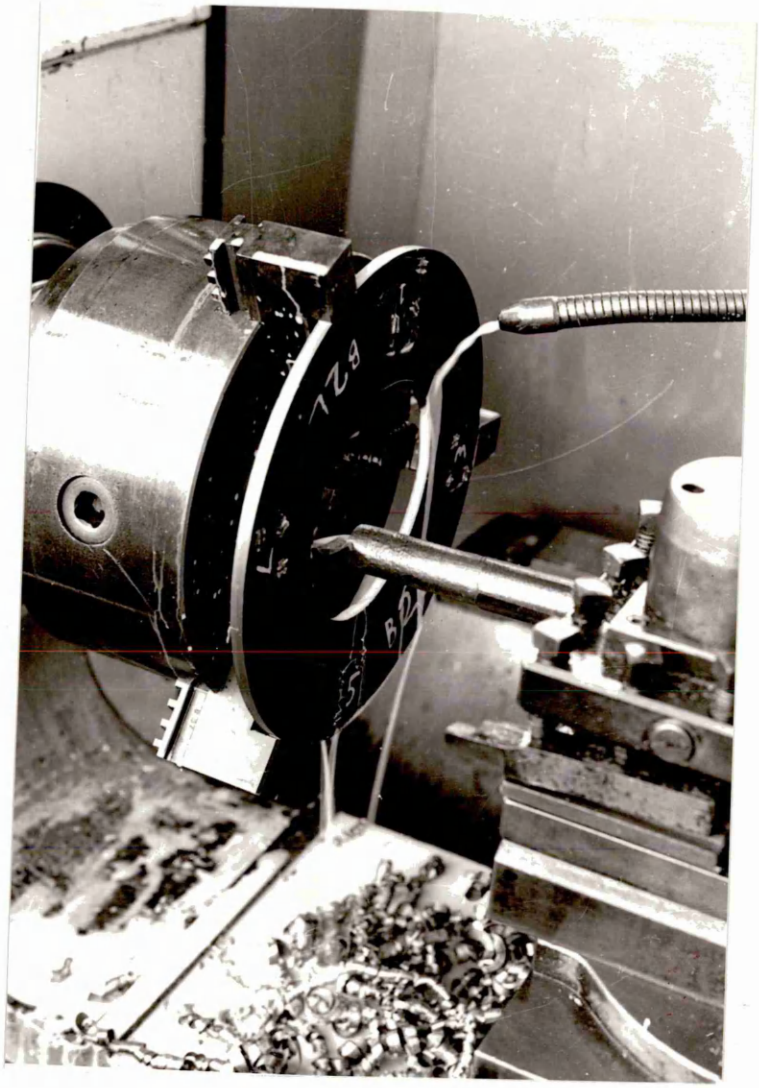

in (ii) was tested by placing the sample in a 'G' clamp.

The result was that a negative sign on the DVM indicated compression and a positive sign indicated tension.

2.4.3 Circuit and Instrumentation (Static)

(See photographs on following pages) Figs 2.14 - 2.19 inclusive

2.4.3.1 The individual strain gauges were wired into a separate channel of a SOLARTRON data logging unit. This consisted of a basic strain gauge bridge power supply unit, an analogue scanner, a digital voltmeter and a print-out facility. The maximum capacity of the system was 80 channels which allowed 26 individual 3 gauge rosettes to be scanned. The print-out gave a mV reading for each gauge and this could be converted to a mV out of balance reading which could later be fed into a programme to calculate Principal Strains and Principal Stresses.

2.4.3.2 Test Procedure

The disc and annular compression rings were sandwiched between two 6.25 mm plates. The connected wires from the gauges fixed inside the loading rings were fed through a hole drilled in the top loading plate.

(See photograph on pages 66/67 Figs 2.17, 2.18)

A zero scan was then taken in order to check that no gauge had been damaged or disconnected. One arm of the balance bridge circuit was then changed from 120Ω to 121Ω for a

check calibration. The compression commenced and an automatic read-out of principal strains and stresses was produced for incremental loading starting from zero load.

Figure 2.14 : Rear View of Data Logging Equipment

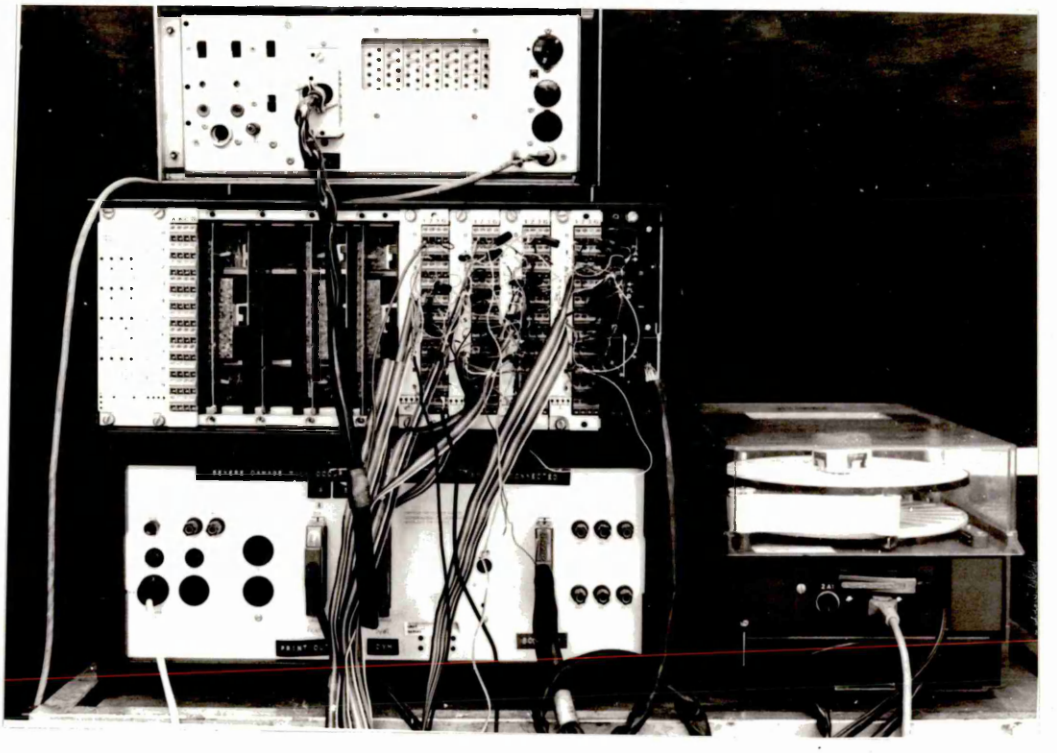

Figure 2.15 : Disc - Press Loading - Static Compression

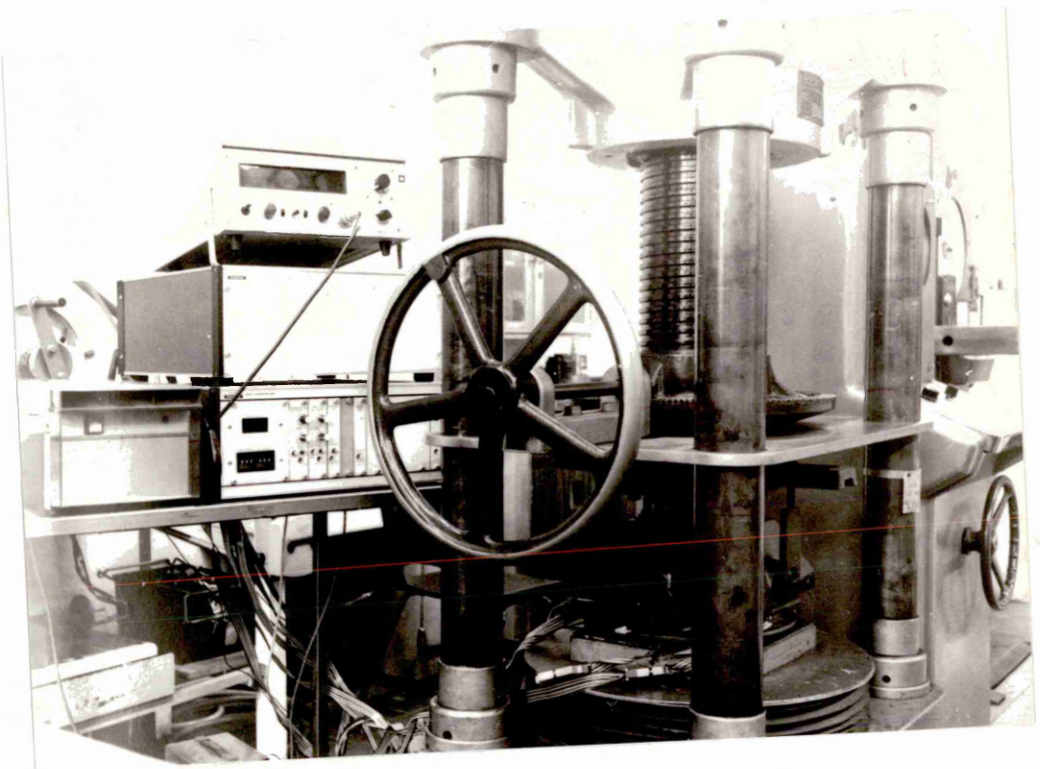

Figure 2.16 : Disc - in Anvil on Press - Static Loading

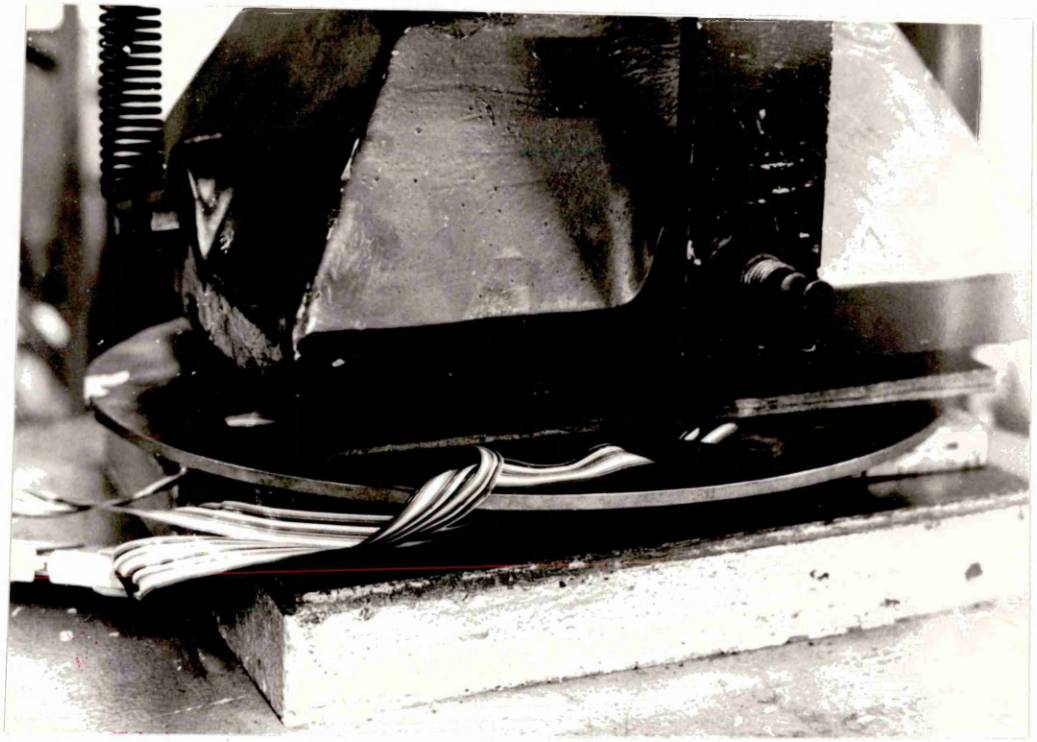

Figure 2.17 : Statically Loaded Disc - Loading Ring, and Top Plate Strain Gauges

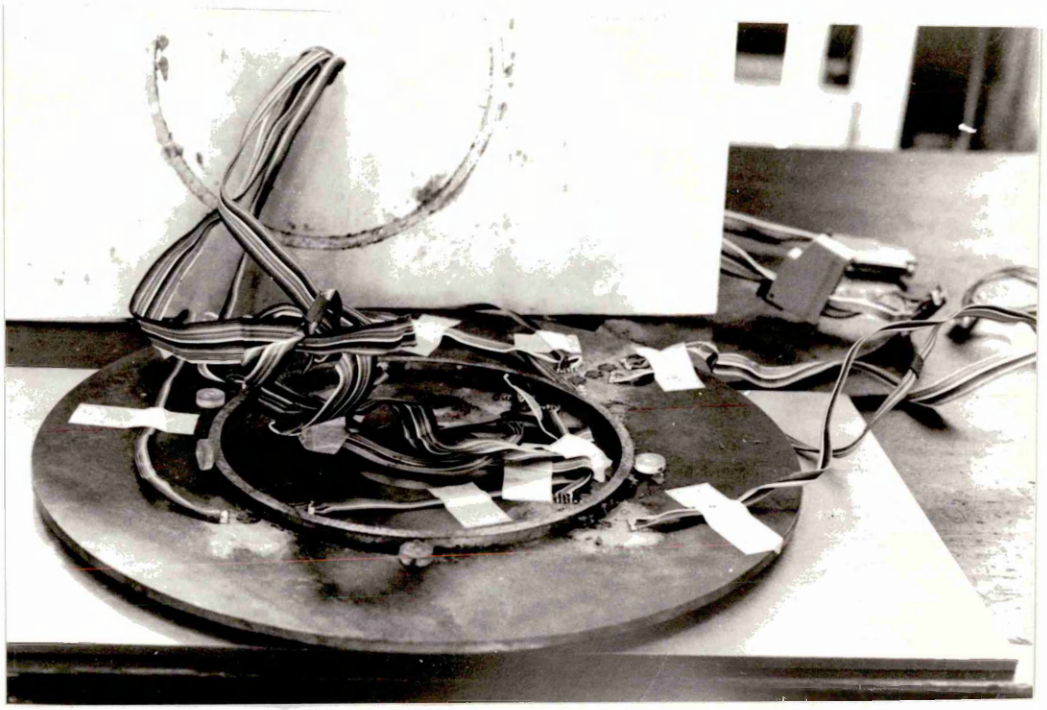

Figure 2.18 : Statically Loaded Disc - Loading Ring and Strain Gauge Connections

Figure 2.19 : Statically Loaded Disc showing close-up of Loading Ring and Strain Gauges

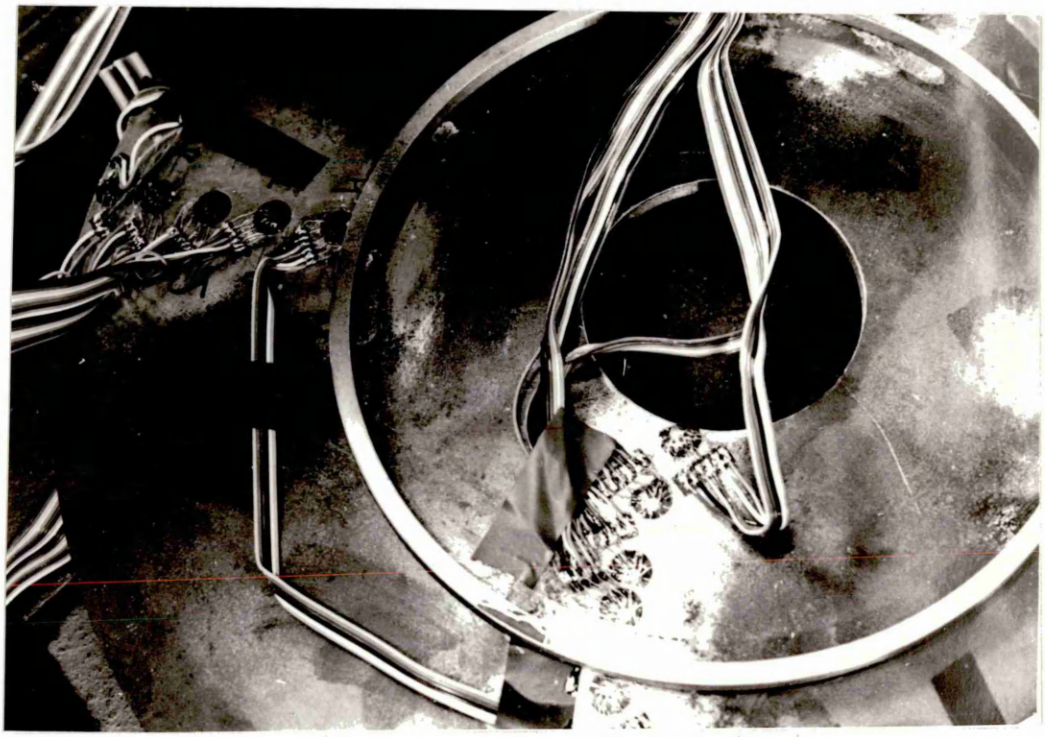

Figure 2.20 : Schedule for Loading Ring Annuli

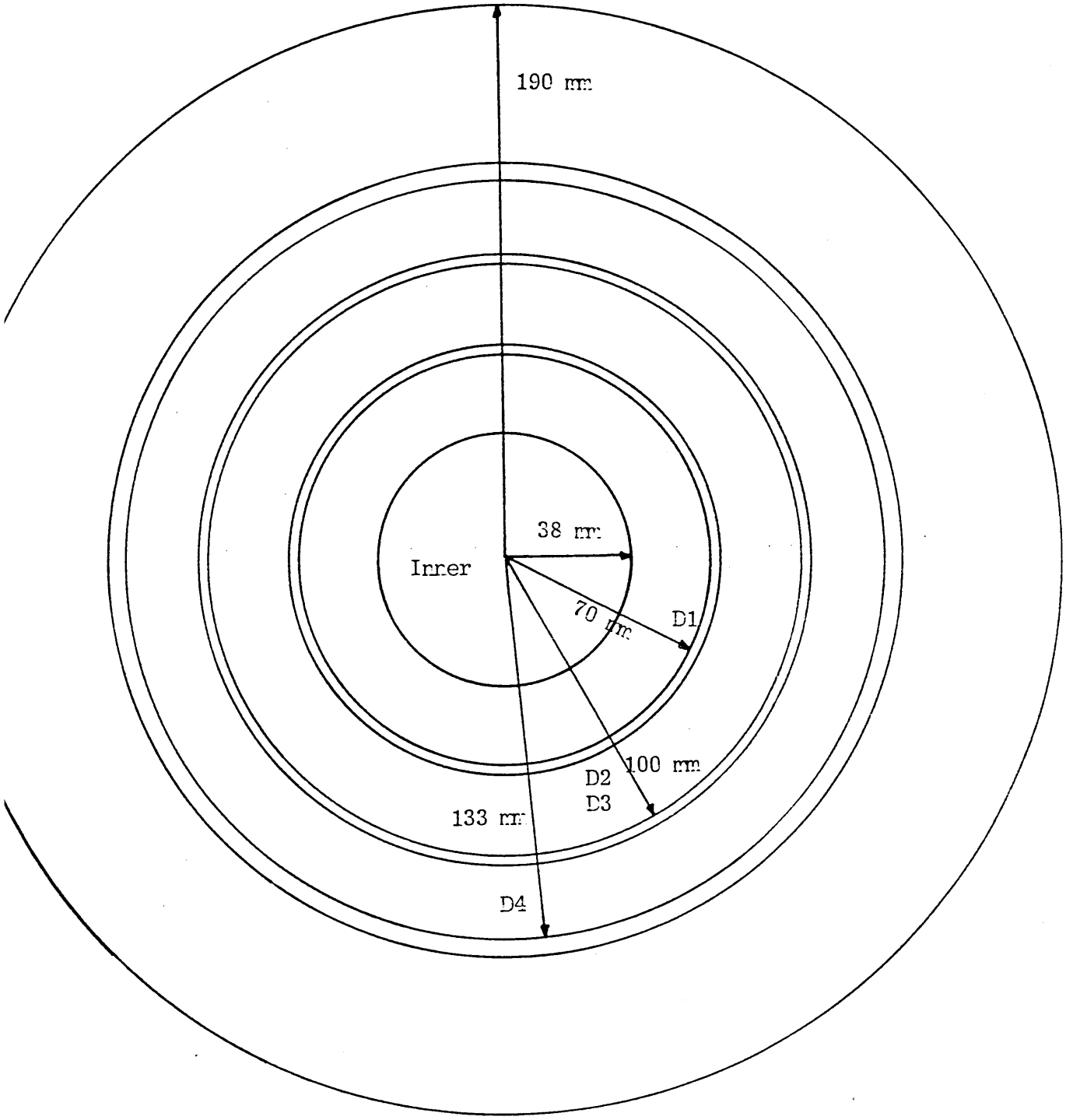

Specification : (a) Disc: O/D = 380 mm
I/D = 76 mm
Thickness = 6.35 mm

(b) Loading Rings: D1 = 140 mm (diam)
D2, D3 = 200 mm (diam)
D4 = 266 mm (diam)

Figure 2.21 : Typical Strain Gauge Configuration Pattern
Loaded Disc D3

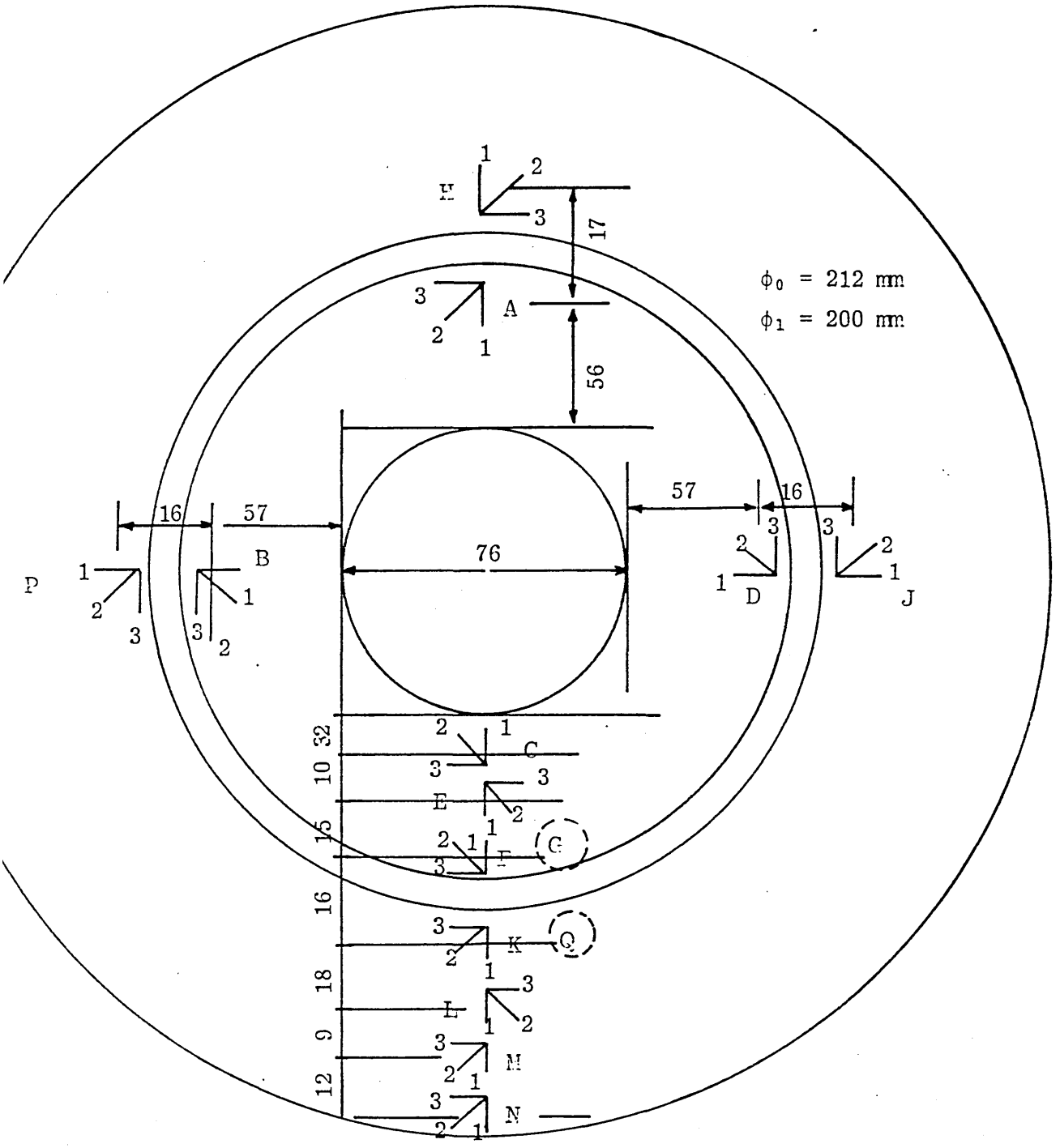

2.5 Data Recording

2.5.1 Dynamic Tests

2.5.1.1 Plane Symmetry Deformation

A time differential in the generation of the explosive shock wave at each surface of the disc could cause the disc to be deformed out of plane section. Accordingly, a method of measuring this deformation was devised.

(a) Method of Measuring Deformation

Each disc was measured before and after the explosive loading on both sides. The measurements obtained were designed to give an average figure for 'out-of-flatness' of the disc which could thus reflect the effectiveness of the explosive loading. Thus the method of loading can be compared for each disc. Also an indication of the energy which had been used in producing a permanent distortion of the discs.

Initially each disc was set up on a flat bed positioned on three ball-bearings. A dial gauge capable of reading to 0.01 mm was then placed on the table and zeroed on position 1, as shown in Figure 2.22 at the explosive radius. The dial readings were then recorded at the 8 explosive radii on each of the diameters. The dial gauge was then moved to radial positions 2 to 8 and zeroed at the explosive radii and subsequently readings were taken at the outer circumference and the inner circumference. After the

explosion had taken place, the same readings were carried out again and recorded in tables. The algebraic differences were recorded for 'before' and 'after' conditions at outer, explosive and inner radial positions. For each position, the maximum range of readings was recorded and finally an average maximum range figure obtained for the complete disc. A table for disc C1 is shown in Table 2.5.

Table 2.5

Calculation of Average Maximum Range of Deformation

DISC C1 : Each unit represents .01 mm
(Upper Surface)

Disc	Diam	Outer Circumference		Explosive Radius		Inner Circumference		Maximum Range		
		Before	After	Before	After	Before	After	Outer	Exp	Inner
C1	1	89	160	0	0	-28	+5	71	0	+33
	2	160	168	+56	65	-80	-42	8	9	+38
	3	35	-10	+62	160	-41	-110	-45	98	-69
	4	-155	-200	+12	194	-12	-110	-45	182	-98
	5	190	200	+154	230	-85	-100	10	76	-15
	6	-52	128	+82	132	-24	-50	180	50	-26
	7	-2	275	+4	-45	+12	-30	277	-49	-42
	8	38	-5	-28	180	4	-138	-43	208	-142
							MAX RANGE	322	257	175

AVERAGE MAX RANGE = $\frac{322 + 257 + 175}{3}$ = 251 units

DISC C5 : (N.B. Not annealed) Each unit represents .01 mm
(Upper Surface)

Disc	Diam	Outer Circumference		Explosive Radius		Inner Circumference		Maximum Range		
		Before	After	Before	After	Before	After	Outer	Exp	Inner
C5	1	8	300	0	0	-7	203	292	0	210
	2	-20	202	-25	-12	9	200	222	13	191
	3	-9	75	-20	53	8	75	84	73	83
	4	21	12	3	84	-9	57	-9	81	63
	5	18	23	10	86	-19	75	5	76	94
	6	18	123	3	86	-10	130	105	83	140
	7	5	200	-10	28	0	260	195	38	260
	8	-12	194	-2	92	-8	92	206	94	100
							MAX RANGE	301	94	260

AVERAGE MAX RANGE = $\frac{301 + 94 + 260}{3}$ = 218

Figure 2.22 : Deformation measuring technique

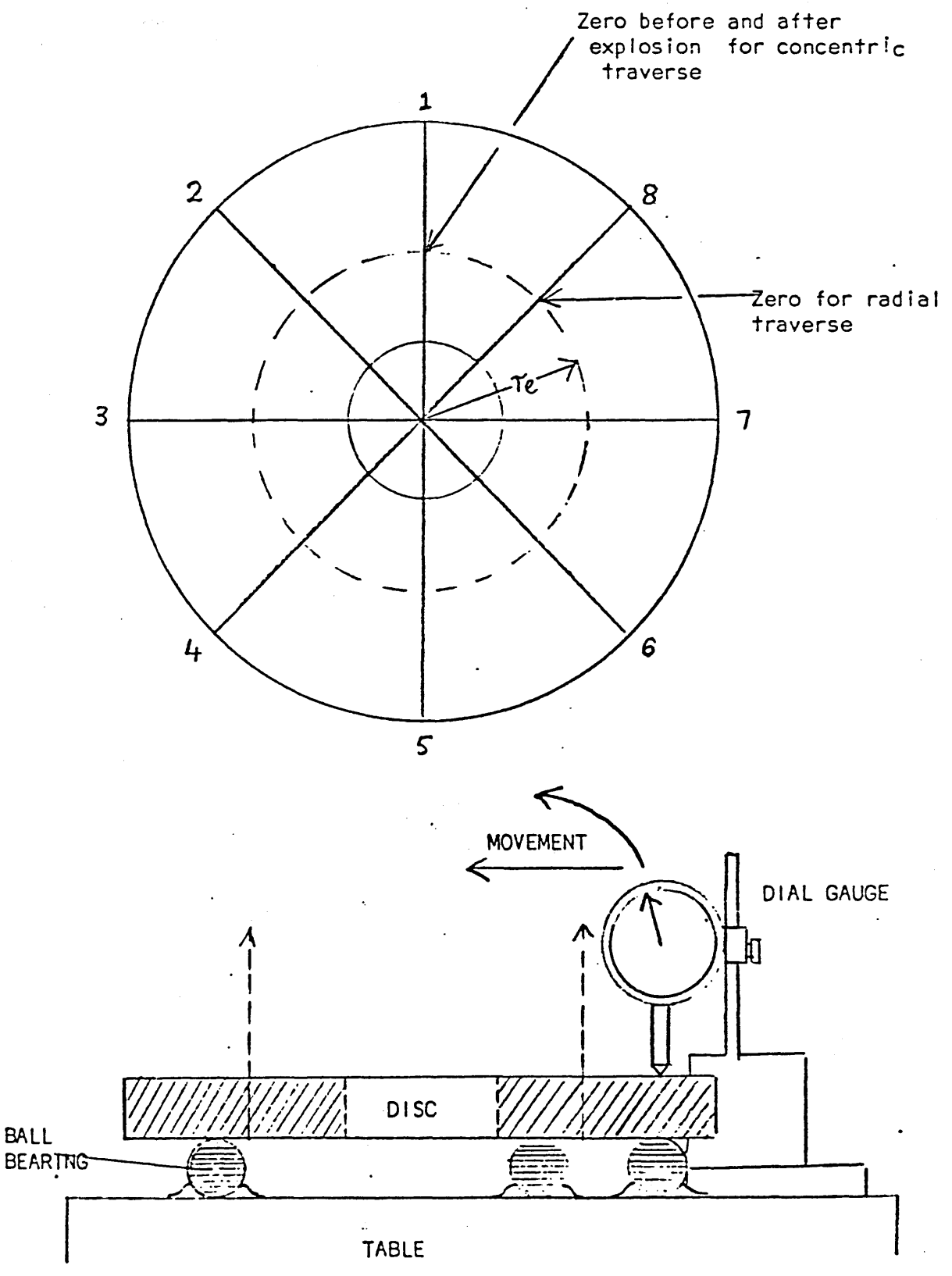

Table 2.6

Summary of Average Maximum Ranges from Plane Symmetry

Disc	Radius of Explosive Ring/cm	Average Maximum Range Deformation (in cm)	Length of Explosive / Explosive Circumference
A4	9.75	0.24	4/1
A6	9.75	0.30	5/1
A5	9.75	0.40	6/1
A7	9.75	0.45	7/1
A8	9.75	0.48	8/1
B1	7.62	0.85	9/1
B2	8.89	0.41	7.6/1
B3	10.16	0.41	6.7/1
B5	11.43	0.35	6.7/1
B6	12.70	0.33	6.7/1
C1	11.33	0.25	6.7/1
C2	11.33	0.20	6.7/1
C3	11.33	0.16	6.7/1
C4	11.33	0.15	6.7/1
C5	11.33	0.22	6.7/1

Figure 2.23 : Typical Deformation Profile C1 (Diameter 2-6)

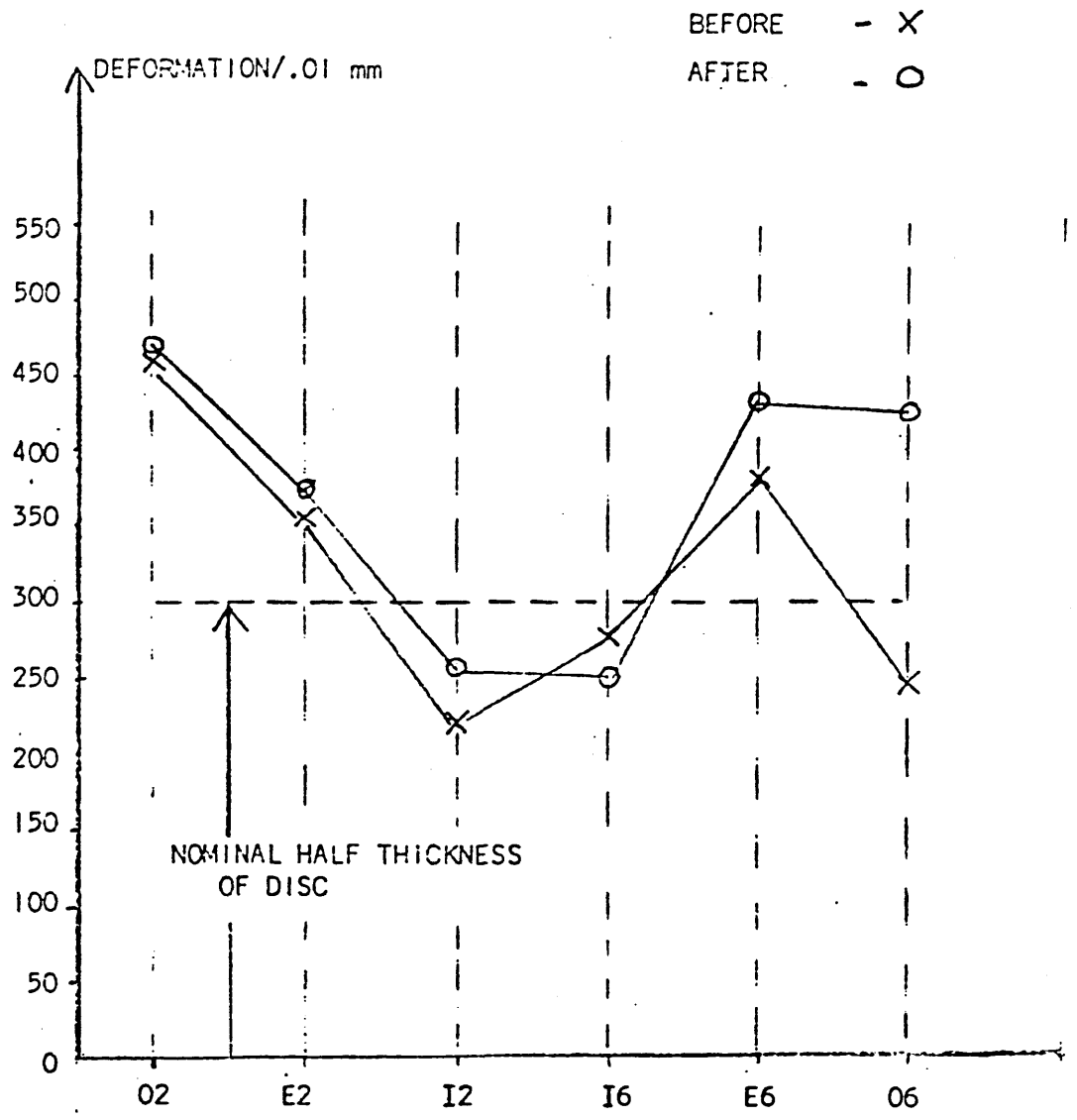

Figure 2.24 : Typical Deformation Profile C5 (Diameter 1-5)

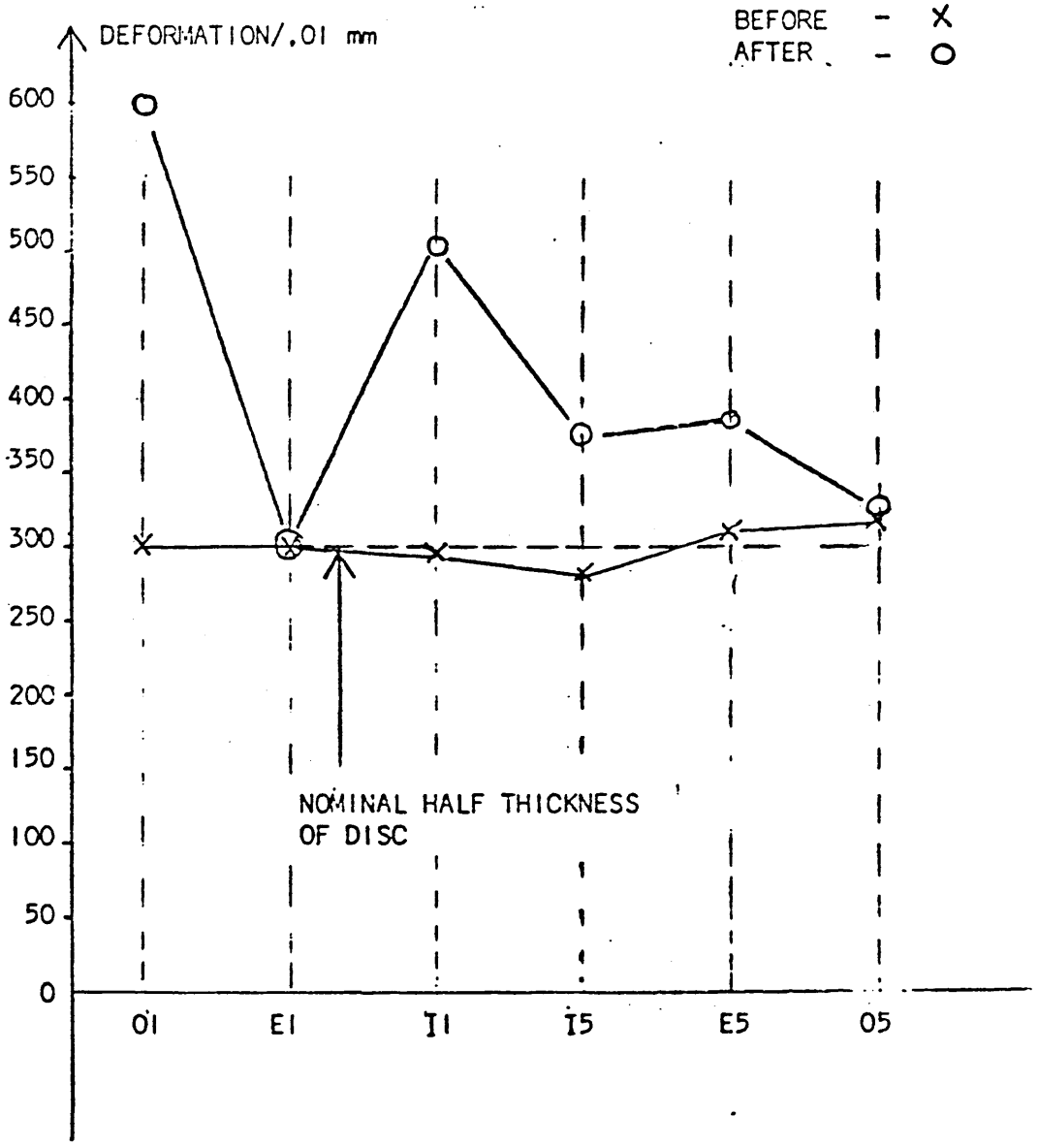

(b) Comments on the Deformation Readings

From the table 2.6 of average maximum ranges from plane symmetry it is possible to make comment on the effect of explosive energy, the radial position of the explosive and the packing arrangement of the explosive on the disc deformation.

(i) The table shows that increasing the amount of explosive energy per unit circumference of the loading ring results in increased deformation to the plane symmetry of the disc.

(ii) There is evidence from the B discs that the radial variation of the explosive ring produces increased plane symmetry deformation with decreasing radius.

(iii) It is possible from the table of results to make a statement with regard to the packing of line cord (Figure 2.4a). An improved system of fixing the line cord to the disc was adopted for the C series. This consisted of two concentric rings of cardboard of 3 cm depth being placed to coincide with the cardboard marker rings (Fig. 2.1).
The line cord could then be dropped into the annulus formed by the cardboard guide rings and so produce a more compact explosive charge than that produced for the loading of rings A and B.

The measurements of deformation for the C discs show an average maximum range deformation lower than comparably loaded discs from the A and B series. This can be seen by comparing discs A7, B5 with any of the C series.

(iv) The effect of the explosive line cord system on the surface of the discs can be seen by reference to Figure 2.7. Here the indentation produced by the explosive contact rings can be clearly seen. The depth of the indentation was variable but an average figure of .1 to .3 mm was recorded for the C series. Table 2.5 indicates that for disc C1, the deformation effect is on average 2.57 mm maximum whereas for disc C5 the deformation is an average maximum range of .94 mm. This is using the change from zero dial gauge reading at the explosive radius after the explosive shock. There was some evidence of intense surface indentation which was localised and could possibly be ascribed to the points where the parallel line feeds made contact with the explosive stack or even to different contact pressure between the explosives and the discs

due to the tape fixing technique. Some indication of this effect can be seen in Figure 2.7 and the intense scars are diametrically opposite. One of the problems produced by the surface indentations was in fixing the strain gauges near to the plastic-worked area of the disc in order to give the maximum number of readings from the inner and outer boundaries of the discs. A further difficulty occurred during the hardness measurements. The portable hardness tester required as far as possible a clear flat surface on which to record readings. So this could account for the variability of the hardness measurements and also perhaps their slightly low values.

(v) The inclusion of measurements of plane deformation for discs C1 and C5 allows a comparison to be made between an annealed disc C1 and a non-annealed disc C5. All the discs in the A series, B series and the C series, with the exception of C5, were annealed as described on page 27 . The stacking of discs in the annealing box can lead to some plane symmetry deformation. Consequently, an indication of this effect is useful in this context. From Table 2.6 it can be seen that the average maximum deformation of C5 and C1

before and after explosive loading are comparable. Thus it can be assumed that the effect of stacking the discs during the annealing process was not significant.

(vi) The figures (2.23 and 2.24) showing typical deformation profiles for discs C1 and C5 indicate that the main deformation from plane occurs at the inner and outer boundaries of the discs, whilst the deformation at the position of the explosive radii are minimal as would be expected with the explosive loading system adopted.

2.5.1.2 Hardness Measurements

(a) Method of Measurement

A portable hardness tester was used to measure the hardness of the discs at varying radii across the inner and outer sections. The use of the portable hardness tester enabled measurements to be taken without the need to take separate metal samples from the discs. The instrument used was the "INSTRUMATIC" universal hardness tester. The application of the Instrumatic hardness tester to a test piece is achieved by depressing the grips with the base of each thumb, the diamond indenter is lowered from its normal (retracted) position and brought into contact with the surface of the disc under test. The operation of the hardness tester required careful constraints and these were carried out and also supplemented by taking four readings

Figure 2.25 Plan measurements of BRINELL HARDNESS for disc C2, showing measurements prior to and after explosive loading

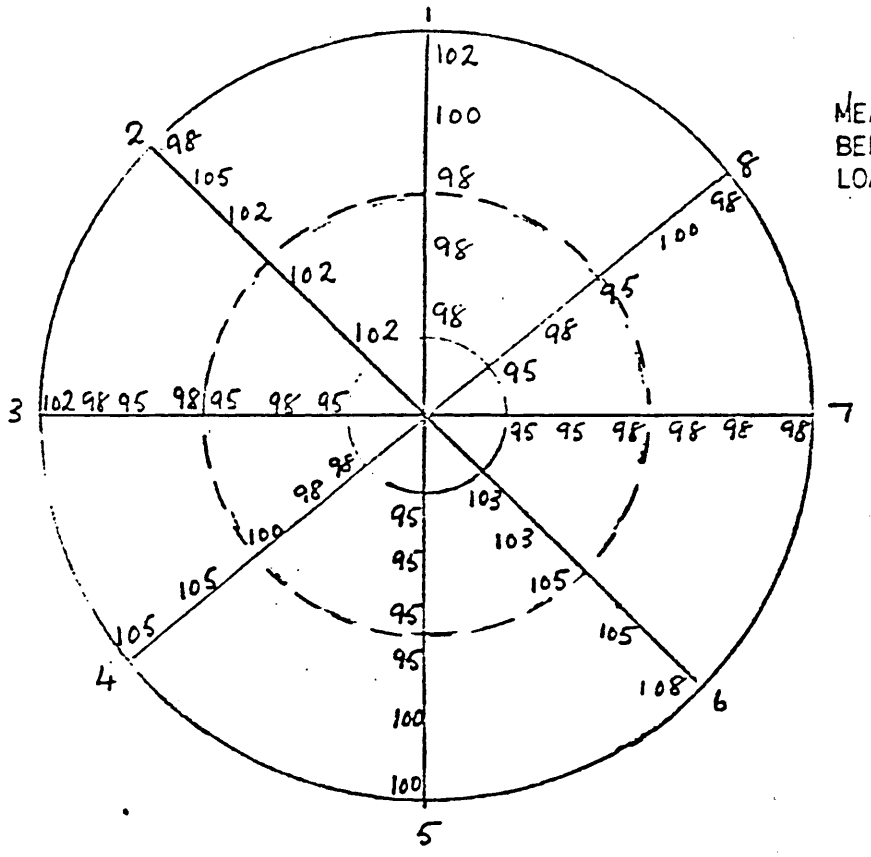

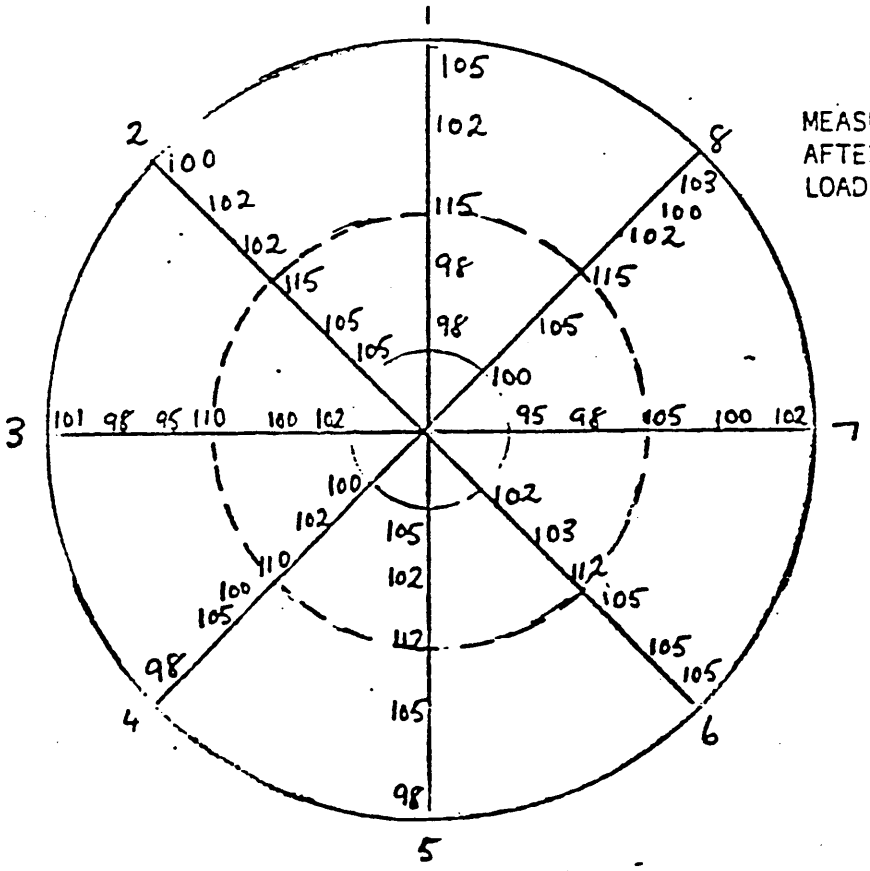

Summary of Hardness Measurements (BRINELL SCALE)

'Standard' refers to Brinell Hardness Readings before explosively loaded

Table 2.7 A Series

DISC	3.8 cm	6.0 cm	r_e = 11.33 cm	16.00 cm	19.00 cm
Standard	96	96	97	96	95
A4	100	100	105	100	97
A6	102	100	106	102	96
A5	97	96	103	98	96
A7	101	104	109	104	99
A8	97	106	115	110	105

Table 2.8 B series

DISC	3.8 cm	5.5 cm	r_e(varying)	16.00 cm	19.00 cm	r_e
Standard	95	98	98	98	95	cm
B1	105	103	111	105	97	7.62
B2	100	102	112	100	98	8.90
B3	100	103	117	102	96	10.16
B5	95	101	113	101	96	11.43
B6	96	103	113	102	98	12.70

Table 2.9 C series

Disc	3.8 cm	5.5 cm	r_e = 11.33 cm	13.00 cm	r_o	r_o
Standard	97	97	98	100	101	cm
C1	99	99	112	102	101	21.5
C2	100	101	111	102	101	19.0
C3	101	101	118	102	102	16.5
C4	107	106	117	104	104	14.0
Standard C5	118	118	118	118	120	19.0
C5	118	120	122	120	122	19.0

Figure 2.26 Hardness Changes produced by detonation of line core in contact with discs for series A (varying explosive)

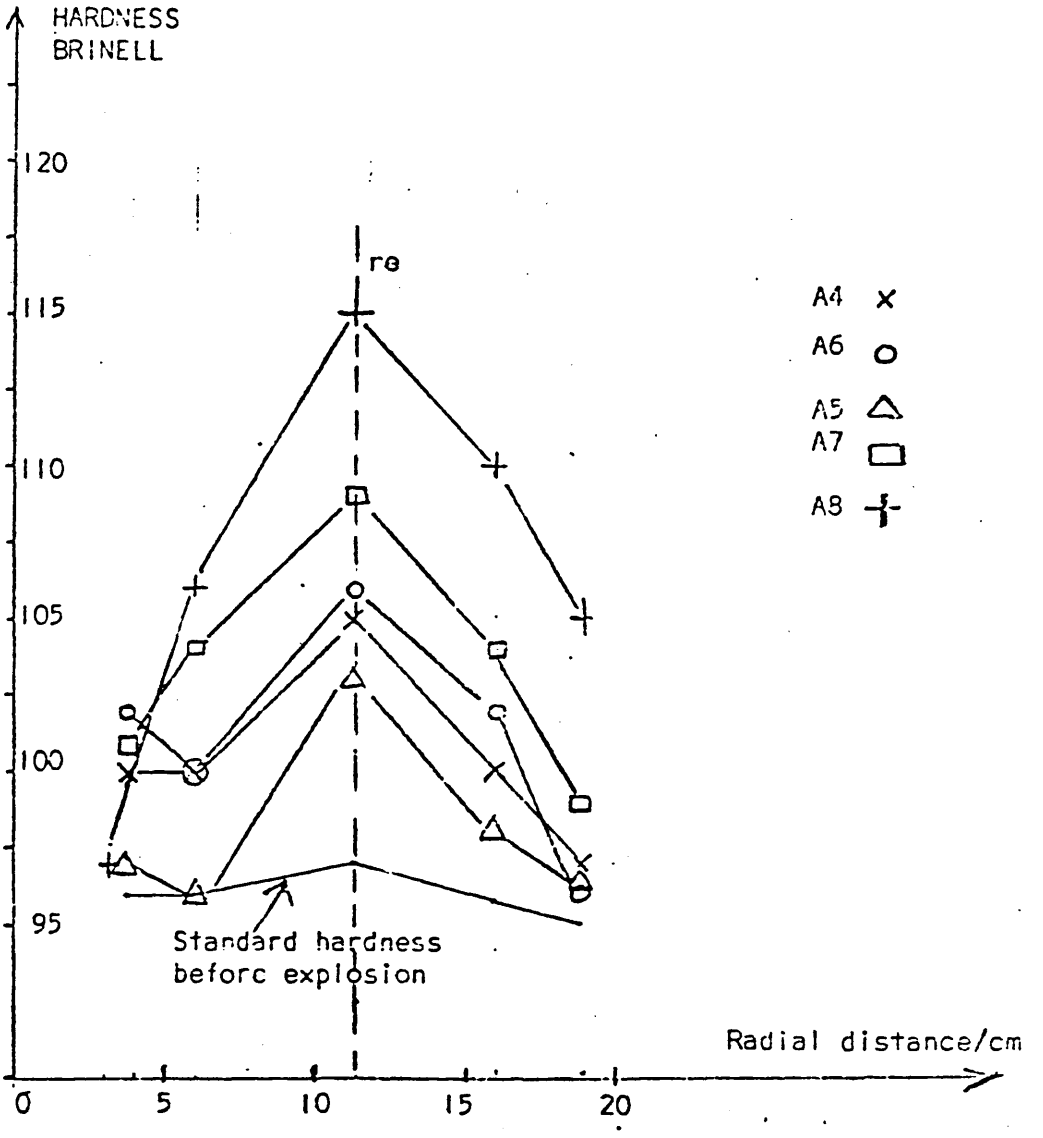

Figure 2.27 Hardness Changes produced by detonation of line cord in contact with discs for Series B (Varying radii)

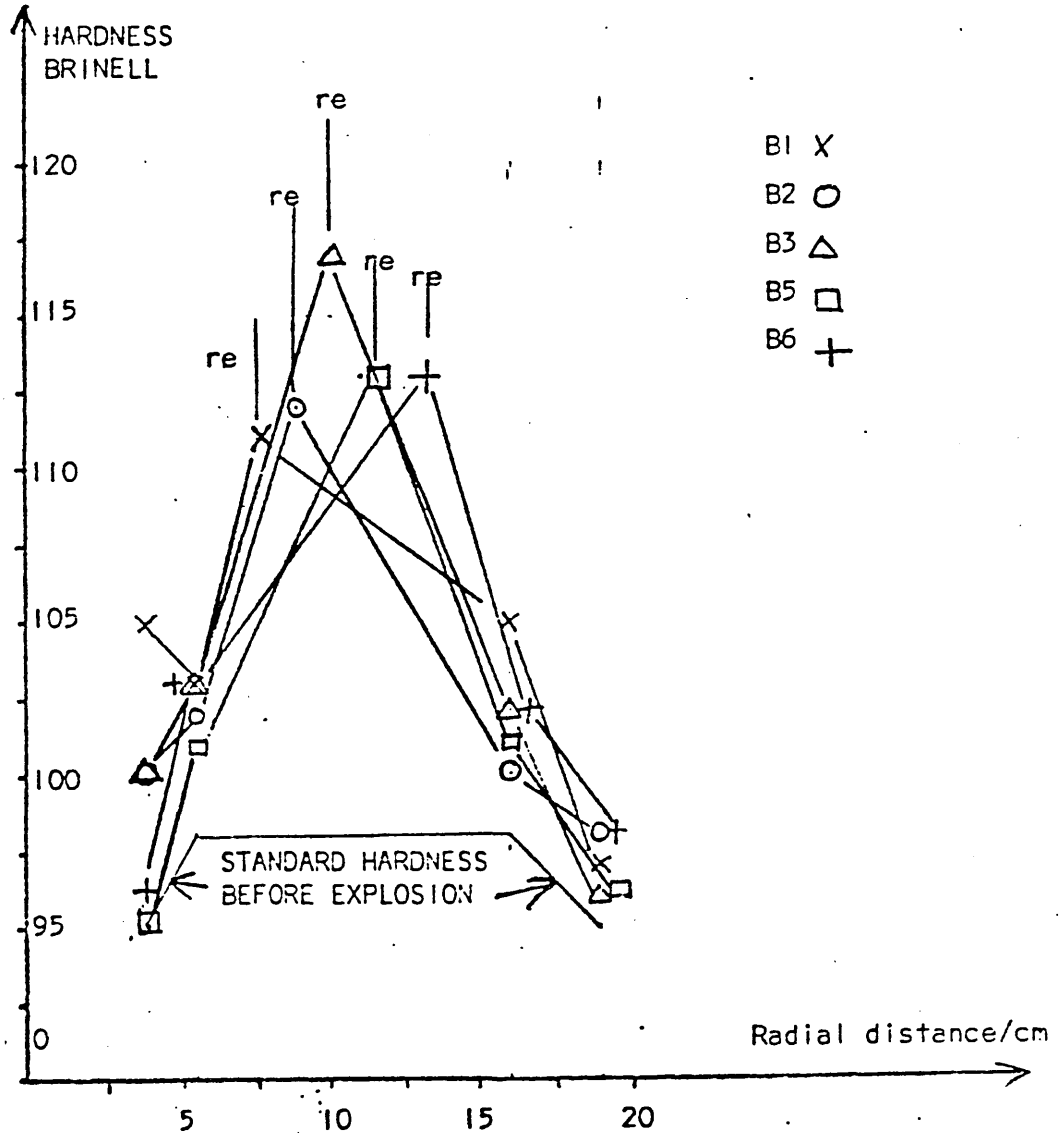

Figure 2.28 Hardness Changes produced by detonation of line cord in contact with discs for series C (varying size)

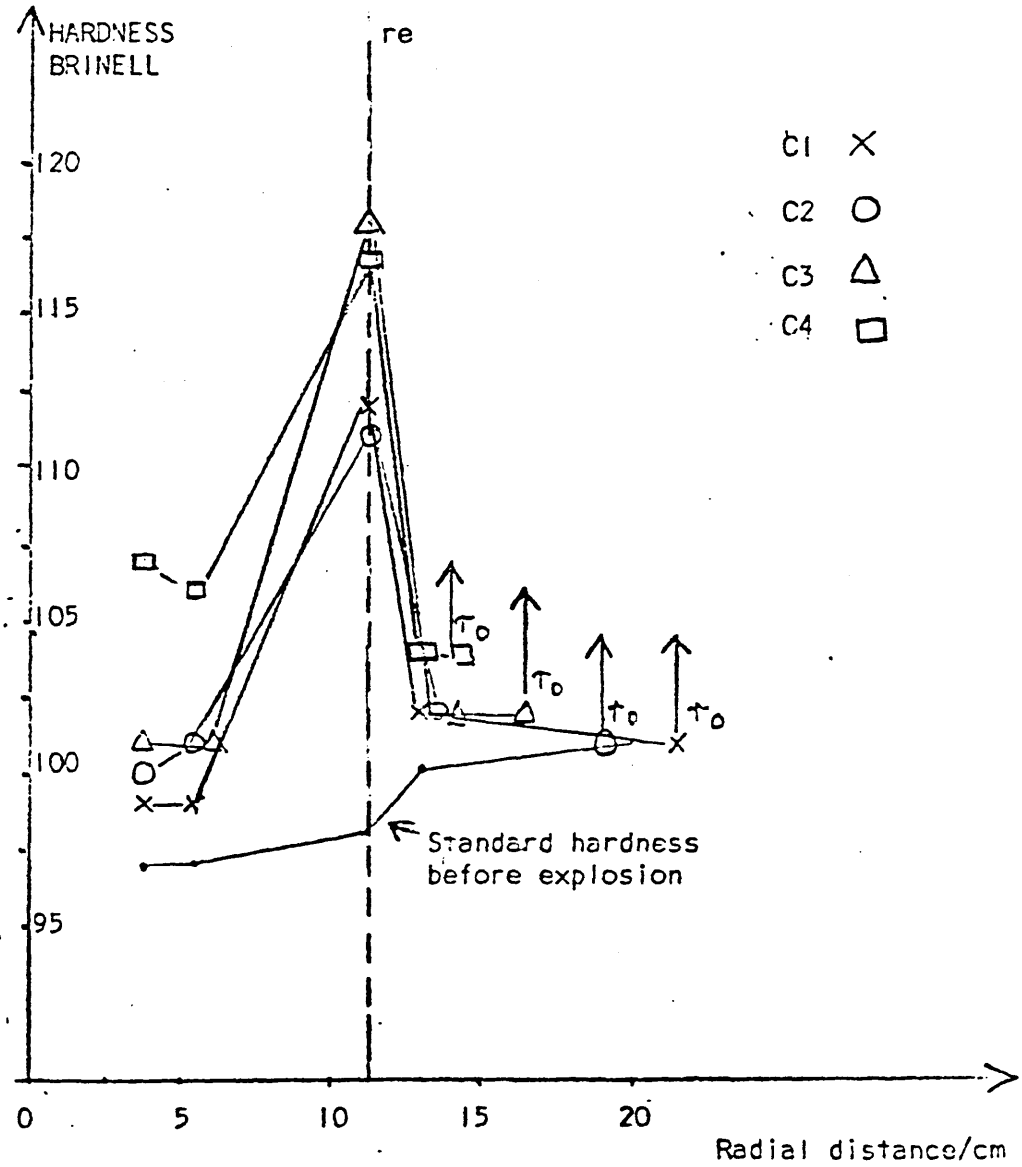

Figure 2.29 : Microstructural Investigation

(a) Plan View - shaded region shows shape of specimen

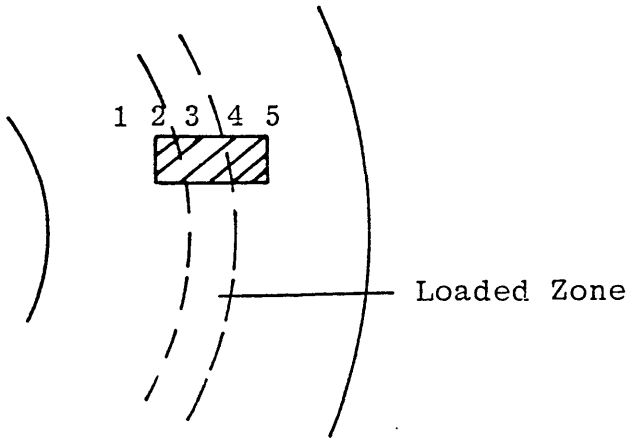

(b) End View - Not to Scale

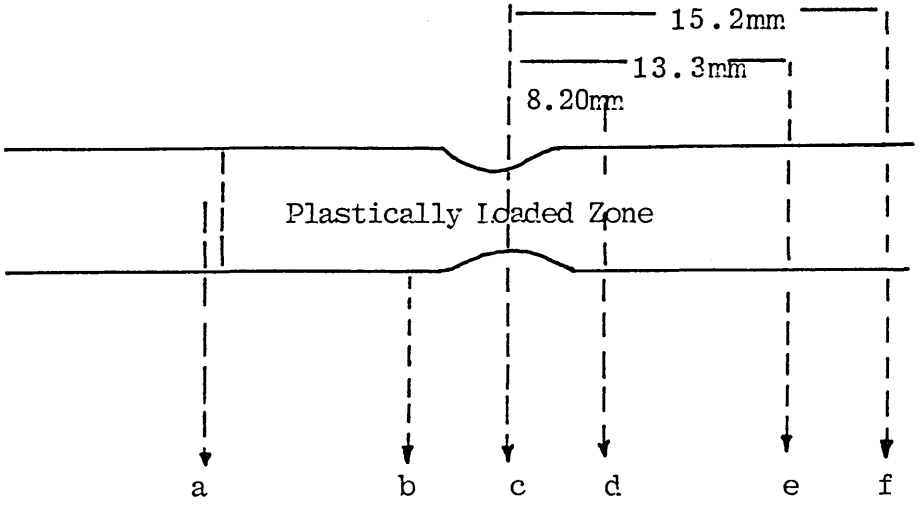

Photomicrographs

at each point. By taking readings at each point of the disc and especially near to the explosively work-hardened areas, a reading of Brinell hardness was obtained. Calibration of the instrument was achieved by using a test block to check the readings on the dial. The instrument requires the test surfaces to be reasonably smooth and free from tool-marks, or other irregularities on the surface, but need not be polished or a mirror finish. Thus limitations on the measurement of hardness for actual discs were encountered at the surfaces of the discs where the indented explosive rings occurred. A further limitation, that of corrosion of the disc surfaces which occurred within 24 hours of the first disc being exploded, was obviated by coating subsequent discs prior to marking out with engineer's blue marking paint. This acted as an inhibitor to corrosion and thus aided hardness measurements by keeping the surface at least reasonably smooth.

Measurement of hardness, using the Brinell scale, was taken along four diameters from the outer boundary to the inner and across to the outer boundary. A typical plot is shown in Figure 2.25. An average figure for hardness was then obtained for the equi-radial positions on each diameter for each disc, and on both sides. Thus each of the readings in Tables 2.7, 2.8 and 2.9 is the average of 64 readings of hardness.

(b) Comments on the Effect of Hardness Changes

The working of metals by rapid transient stress disturbances manifests itself as changes in not only hardness, which is increased, but in changes of tensile strength and yield and plastic flow characteristics. A pronounced effect is the change in hardness produced in explosively attacked mild steel. The salient features of such hardening are a pronounced change in hardness at the boundary between the highly worked region and the region in which working is limited to shock twinning. In the Tables 2.7, 2.8 and 2.9 the following effects are demonstrated (and Figures 2.26, 2.27, 2.28)

(i) the localization of the hardening;

(ii) the effect of producing sustained pressure with increasing explosive (this can be seen in column r_e = 11.33 cm of Table 2.7), Figure 2.26 for the A series;

(iii) the amount of work hardening in the shock twinned region is not especially great, whereas in the heavily worked region, the work hardening figures are quite high;

(iv) a further effect can be seen by reference to Figure 2.28 where the decrease in size of disc and therefore an increase in explosive pressure per unit volume shows an increase in hardness particularly at the inner boundaries;

(v) by reference to the experimental radial residual stress curves (Figures 3.6 to 3.11 inclusive) and a similarity of shape can be seen by comparison with Figures 2.27 and 2.28, indicating that the maximum radial residual stresses occur where there is maximum work hardening. In the A series, not only is there a similarity of shape but a corresponding increase in hardness for increasing radial residual stress (Figure 2.26).

2.5.1.3 Microstructural Investigation

The purpose of this experiment was to provide evidence of the extent of the plastically deformed zone. A section of disc A8 which had been explosively loaded was cut out from the loaded region. An end section was prepared for photomicrographic examination by polishing and etching.

Notes and Comments on the Photomicrographs

The photomicrographs a to f show a progressive transition across the loaded zone which are shown in plan view from 1 to 5 on Figure 2.29.

Photomicrograph

a bands are only visible .06 mm from the left-hand edge of the specimen (magnification 160)

b selective magnification of deformed region showing shock twinning

c centre line micrograph showing highly deformed region (magnification x 80)

d photomicrograph taken 8.20 mm from centre region (as defined by c) still showing bands (magnification x 80)

e photomicrograph taken 13.26 mm from centre region - this is a transition zone (magnification x 80)

f photomicrograph taken 15.19 mm from centre region - no bands visible (magnification x 80).

Conclusion

The photomicrographs show that the region of visible shock twinning is localized and confined to a region ± 13.26 mm of the centre line from the loaded area. Thus the area of plastic deformation is seen to be mainly below the loading zone of the discs.

Photomicrographs

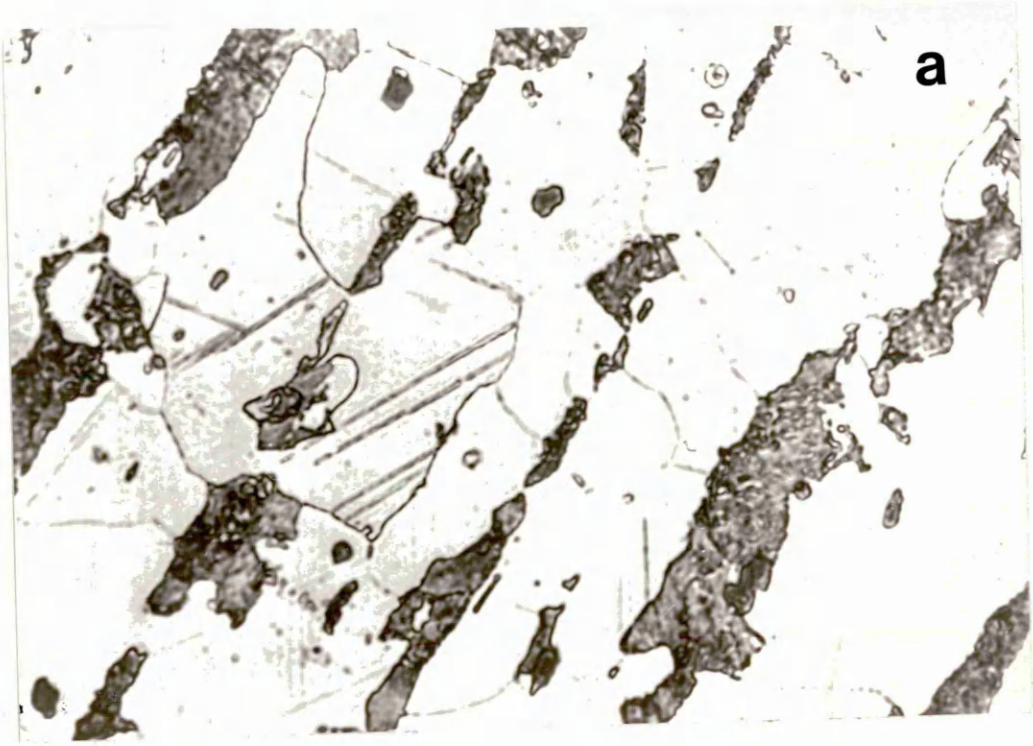

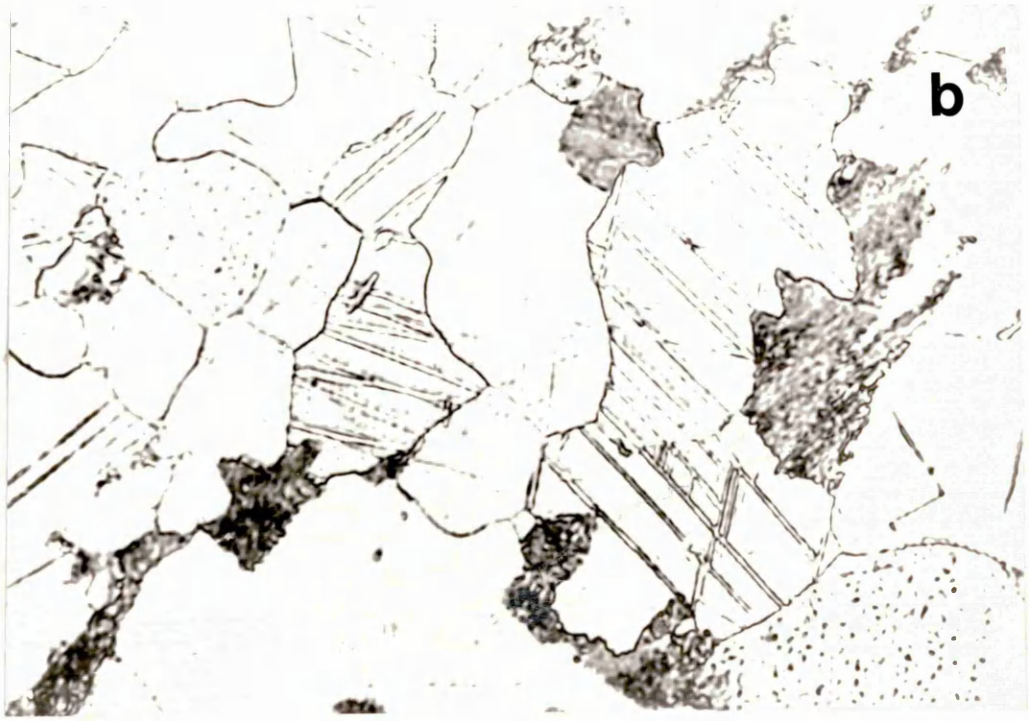

Photomicrographs

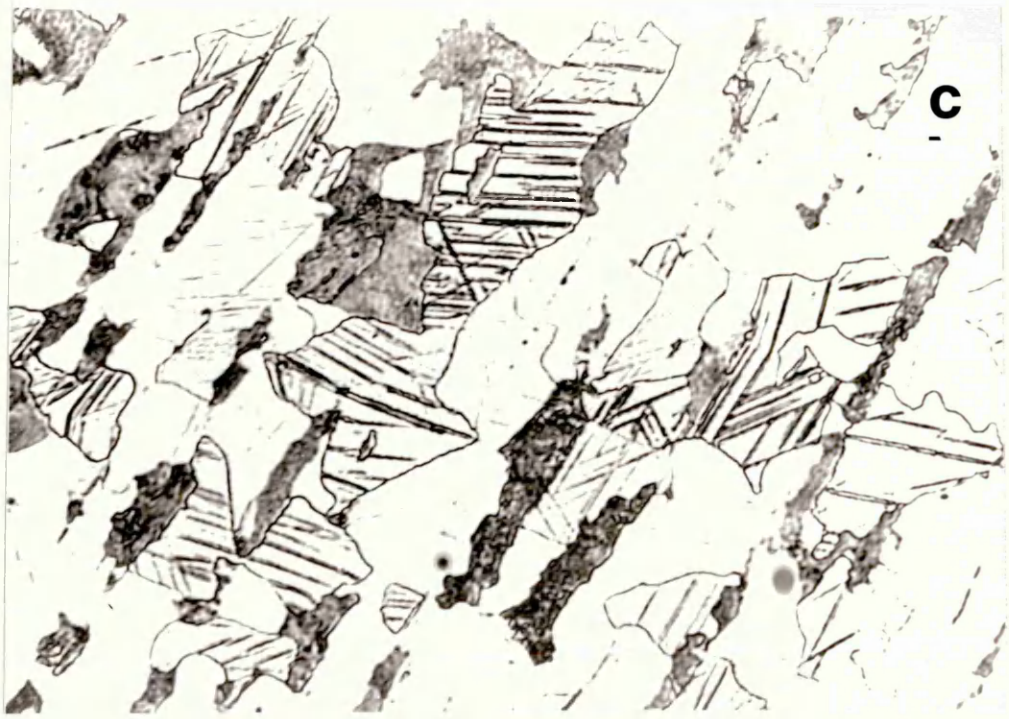

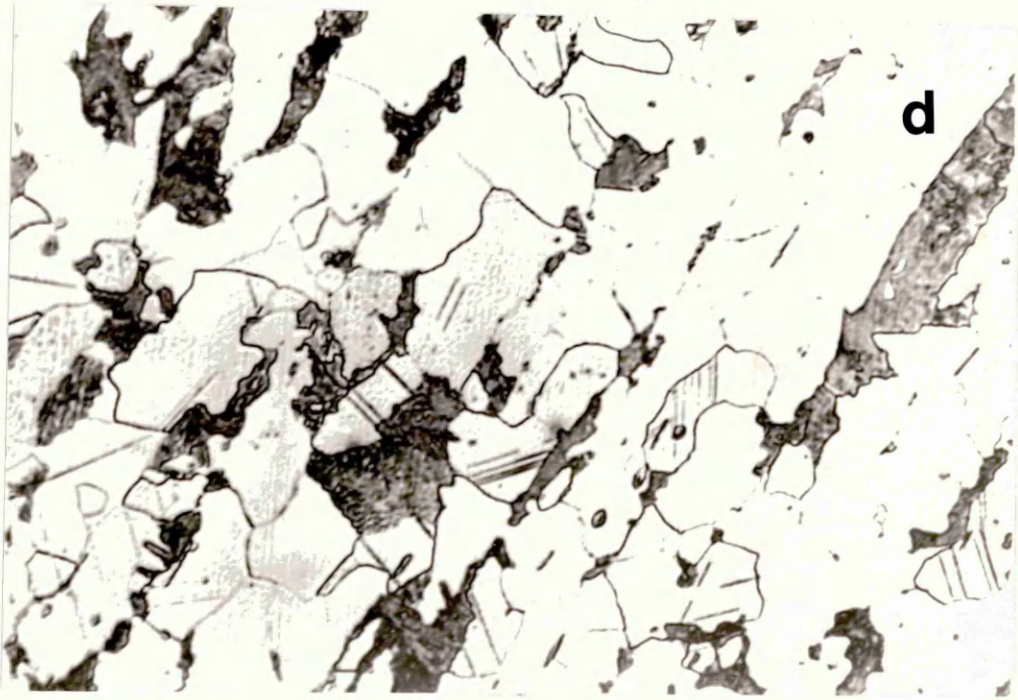

Photomicrographs

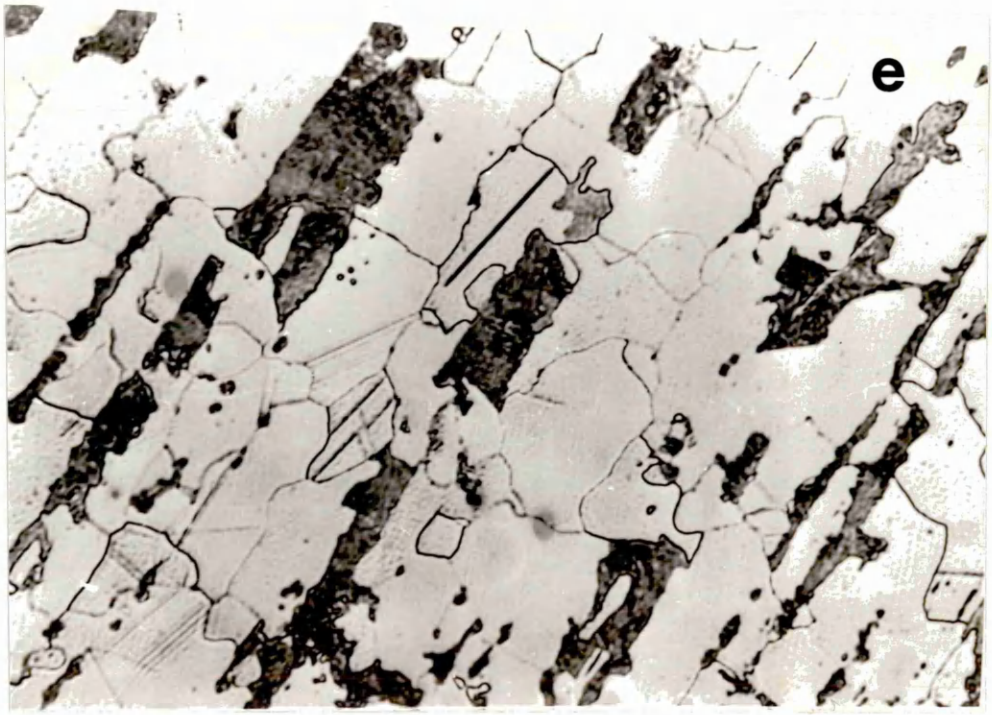

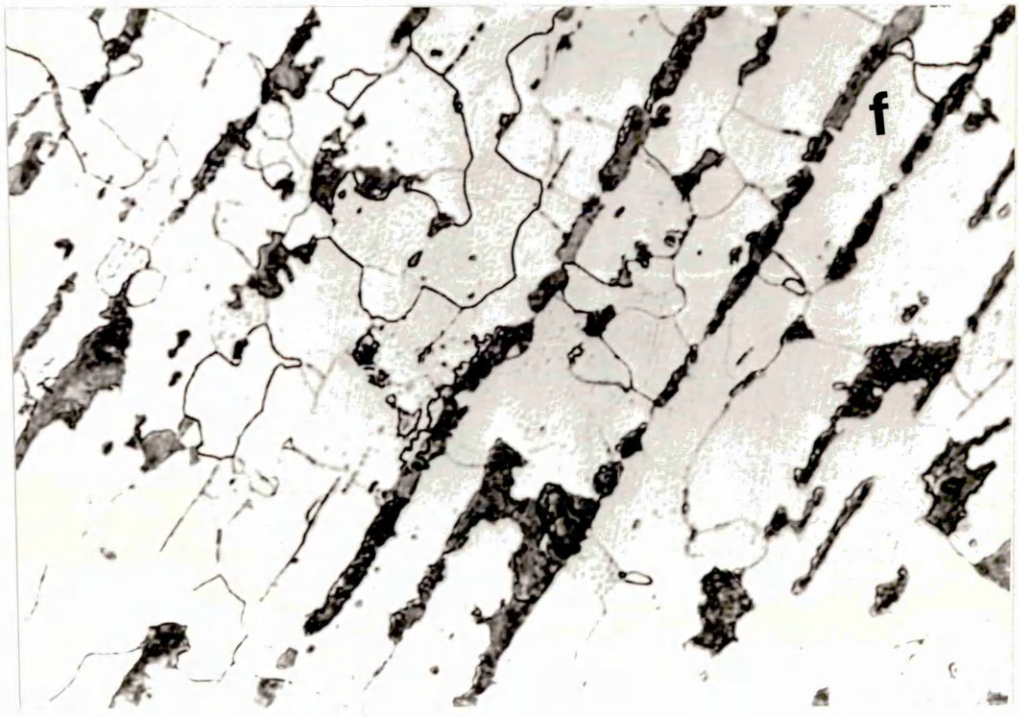

3.1 Analysis of Experimental Results for Dynamically Loaded Discs

3.1.1 Introduction

3.1.2 Strain Gauge Rosette Analysis

3.1.3 Method Prediction of Residual Stress at Outer and Inner Cut Radii of Discs

3.1.4 Experimental Results and Graphs

3.1.4.1 Summary of Disc Loading Parameters

3.1.4.2 Radial and Hoop Stress at Gauge Positions - based on final cuts of inner/outer radii

3.1.4.3 Radial Stress with Radial Position

3.1.4.4 Assessment of Methodology

3.1.5 Comments

3.2 Static Loading Experimental Analysis

3.2.1 Introduction

3.2.2 Derivation of Experimental Stress-Strain Law from Sample of Mild Steel Discs

3.2.3 Application of Elastic-Plastic Law to Experimental Results

3.2.4 Summary of Method used to produce Stress Values from Strain Gauge Readings

3.2.5 Programme Format for producing Stress Values from Strain Gauge Values

3.2.6 Example of Experimental Evaluation Tables used in formulating Results for Graphical Display

3.2.7 Summary of Experimental Loading Criteria and Disc Parameters

3.2.8 Experimental Graphs

3.2.9 Appraisal of Results

3.2.10 Buckling Tests

3.1.1 Introduction

This section describes the analysis and presentation of the experimental results obtained from the dynamic (explosive) annular loading of metal discs. Three series of experiments were carried out, namely the A series in which increasing explosive loads were applied to the discs at a constant radius, the B series in which constant explosive loads were applied at different radial points and lastly the C series in which different size discs were used with constant explosive load applied at constant radii. Sections 3.1.2 and 3.1.3 deal with the manner in which the strain gauge rosette results have been utilised in obtaining the residual stesses at surface points throughout the discs. Section 3.1.4 reproduces the residual stress values calculated from the analysis of Section 3.1.3. In the last part of Section 3.1.4, an attempt is made to assess the accuracy of the adopted methods. The chapter ends with some comments on the results produced but no attempt has been made to draw any conclusions at this stage.

3.1.2 Strain Gauge Rosette Analysis

The method and production of attaching the 3 x 45° strain gauge rosettes has been described in Chapter 2 but a reminder of the arrangement will be useful at this stage. Essentially four 3 x 45° rosettes were attached to the top and to the lower surface of the discs as near to the explosively deformed regions as possible. The alignment of the rosettes was chosen so that the two orthogonal gauges were pointing in the assumed directions of principal

strains, i.e. the radial and hoop directions. It is known that the 3 x 45° rosette gives accurate results if its two orthogonal gauges are pointing approximately in the directions of the principal strains. The decision to place the rosettes either on the inner or outer sides of the deformed region was based on maximising the number of 'cuts' of the disc which could be obtained before the gauges would be damaged.

Reference to Figure 3.1 , shows that the strains from the three gauges are represented by e_α, e_β, e_γ and that the principal strains are represented by e_1 and e_2. Thus e_1 would be indicative of the hoop strain and e_2 of the radial strain in the discs.

A consideration of Mohr's strain circle gives the appropriate values of principal strain as

$$e_1 = A + B \qquad \text{(MAX PRINCIPAL STRAIN)}$$

and $$e_2 = A - B \qquad \text{(MIN PRINCIPAL STRAIN)}$$

where $$A = \frac{1}{2}(e_\alpha + e_\gamma)$$

and $$B = \sqrt{\frac{1}{2}\left\{(e_\alpha - e_\beta)^2 + (e_\beta - e_\gamma)^2\right\}}$$

and $$\tan 2\alpha = (2e_\beta - e_\alpha - e_\gamma)/e_\alpha - e_\gamma$$

The stress distribution, i.e. the magnitudes and directions of the principal stresses σ_1 and σ_2 can be derived from the principal strains:

$$\sigma_1 = \frac{E}{1 - \nu^2} (e_1 + \nu e_2)$$

$$\sigma_2 = \frac{E}{1 - \nu^2} (e_2 + \nu e_1)$$

where E = Young's modulus and ν = Poisson's ratio. For ease of analysis, we substitute here

$$\sigma_1 = C + D$$

$$\sigma_2 = C - D$$

where $C = \frac{AE}{1 - \nu}$ (abscissa of centre of stress circle)

and $D = \frac{BE}{1 + \nu}$ (radius of stress circle)

The complete stress field can thus be determined; the values of A and B are related to the specific rosette configuration, while the directions of the principal stresses are identical with those of the principal strains.

The values of the radial and hoop stresses were computed with the aid of computer software which also gave the angular orientation of the principal strains and stresses with respect to the gauges.

Figure 3.1 : 3 x 45° - Rosette

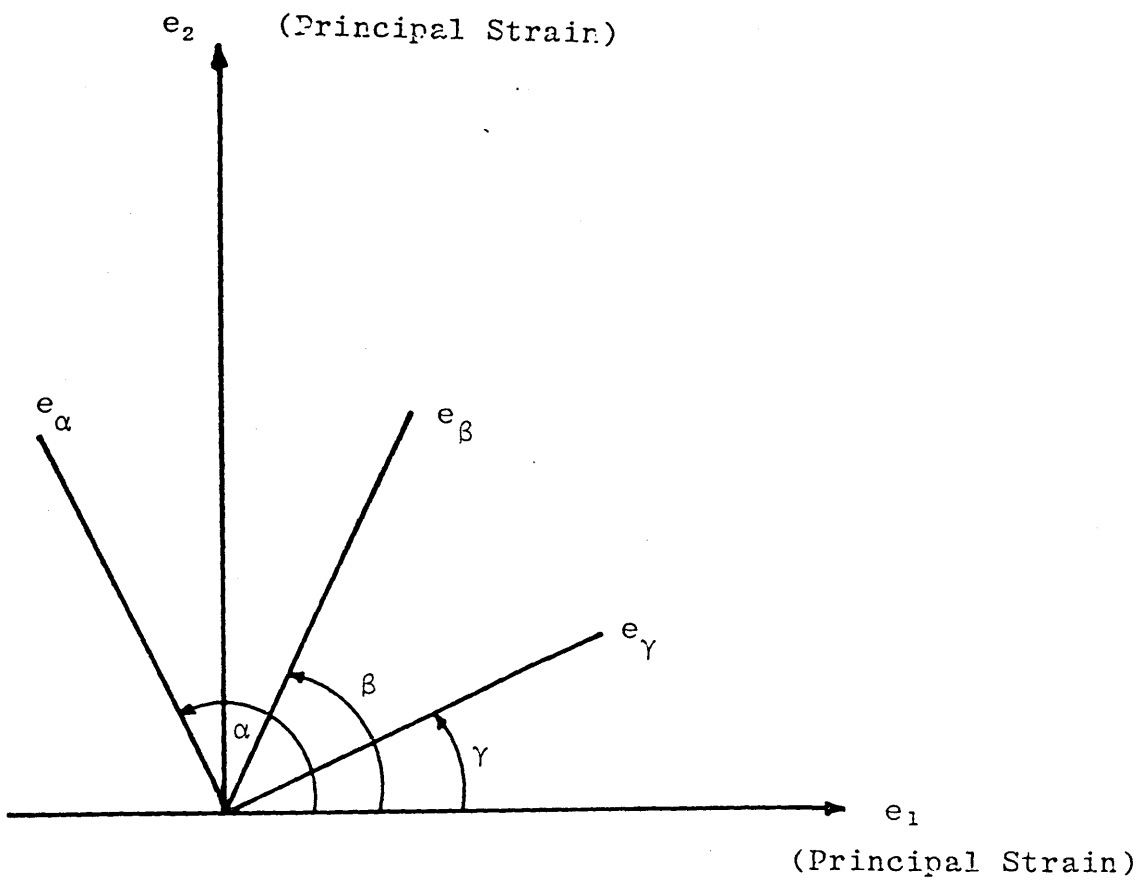

$\alpha - \beta = 45°$

$\alpha - \gamma = 90°$

3.1.3 Method of Assessment and Prediction of Residual Stress at the Outer and Inner Boundaries of the Cut Discs

3.1.3.1 The Strain Gauges rosette analysis of Section 3.1.2 cannot on its own be used directly to obtain strain readings at the cut boundaries of the discs. But the changes in the Strain Gauge readings after each cut may be incorporated in an appropriate analytical model to predict the strain at the boundaries.
Accordingly the following analysis aims to provide a set of working equations which can be used to predict strains at the outer and inner radii of the discs after each cut and which are based on the readings taken from the fixed gauge positions. It should be noted that the effect of turning down and boring out to the new radius of the disc is to release the radial residual stress which existed in the 'removed' metal prior to the cut taking place.

From the nature of the boundary conditions used in the analysis, it is only possible to predict the residual radi al stress values. Thus strain readings for the radial direction and the hoop direction both give a measure of the residual radial stress for individual radii of the disc boundary.

The procedure for taking first outer and then inner cuts of the disc radius is determined by the order which the following experimental analysis was carried out. Thus the outer radii were turned down until the outer perimeter coincided with the outer annulus on which the gauge was positioned. This procedure was followed by boring out the

inner radii until only a thin annulus of the metal disc remained and on which the strain gauge rosette had been originally placed.

3.1.3.2 Relationship between Stresses at a Point and Strain Gauge Readings

The position of an e.r.s. gauge remains constant as the material of the disc is machined off, the magnitude of the actual stress relief, as experienced by the gauge, has to be determined. It is found that, basically, a Lamé system of equations can be used for this purpose. Consider in general a disc of inner and outer radii r_1 and r_2 subjected to inner and outer radial stresses P_1 and P_2 and let σ_r be the radial stress, and σ_θ the hoop stress.

Lamé equations are given by:

$$\sigma_r = A - \frac{B}{x^2} \quad \text{and} \quad \sigma_\theta = A + \frac{B}{x^2}$$

at $x = r_1$, $P = P_1$ and at $x = r_2$, $P = P_2$

Consequently $\sigma_r = P_1 = A - \frac{B}{r_1^2}$ at $x = r_1$

$$\sigma_r = P_2 = A - \frac{B}{r_2^2} \quad \text{at } x = r_2$$

$$\therefore \quad P_1 - P_2 = - B \left(\frac{1}{r_1^2} - \frac{1}{r_2^2} \right) = - B \left[\frac{r_2^2 - r_1^2}{r_1^2 \; r_2^2} \right]$$

$$\therefore \quad B = \frac{(P_2 - P_1) \; r_1^2 \; r_2^2}{r_2^2 - r_1^2}$$

Now $A = P_1 + \frac{B}{r_1^2} = P_1 + \frac{(P_2 - P_1)\, r_2^2}{r_2^2 - r_1^2}$

$$\therefore \quad \sigma_r = A - \frac{B}{x^2} = P_1 + \frac{(P_2 - P_1)\, r_2^2}{r_2^2 - r_1^2} \left[1 - \frac{r_1^2}{x^2}\right]$$

$$\text{i.e. } \sigma_r = P_1 + (P_2 - P_1) \left[\frac{1 - r_1^2/x^2}{1 - r_1^2/r_2^2}\right] \qquad (3.1)$$

Also $\sigma_\theta = A + \frac{B}{x^2}$

$$\text{i.e. } \sigma_\theta = P_1 + \frac{(P_2 - P_1)\, r_2^2}{r_2^2 - r_1^2} + \frac{(P_2 - P_1)\, r_1^2\, r_2^2}{r_2^2 - r_1^2} \cdot \frac{1}{x^2}$$

$$= P_1 + \frac{(P_2 - P_1)\, r_2^2}{r_2^2 - r_1^2} \left[1 + \frac{r_1^2}{x^2}\right]$$

$$\text{or} \quad \sigma_\theta = P_1 + (P_2 - P_1) \left[\frac{1 + r_1^2/x^2}{1 - r_1^2/r_2^2}\right] \qquad (3.2)$$

Consider the case of a gauge mounted at the position $x = r_g$. Radial and hoop stresses felt by the gauge are:

$$\sigma_r = P_1 + (P_2 - P_1) \left[\frac{1 - (r_1/r_g)^2}{1 - (r_1/r_2)^2}\right] \qquad \text{Radial}$$

$$\sigma_\theta = P_1 + (P_2 - P_1) \left[\frac{1 + (r_1/r_g)^2}{1 - (r_1/r_2)^2}\right] \qquad \text{Hoop}$$

Assume standard equations relating stress and strain

$$e_\theta = \frac{1}{E}(\sigma_\theta - \nu\sigma_r)$$

$$\text{i.e. } Ee_\theta = P_1 + (P_2 - P_1)\left[\frac{1 + r_1^2/r_g^2}{1 - r_1^2/r_2^2}\right]$$

$$- \nu \left\{P_1 + (P_2 - P_1)\left[\frac{1 - r_1^2/r_g^2}{1 - r_1^2/r_2^2}\right]\right\}$$

$$= (1 - \nu)\, P_1 + (P_2 - P_1)\left[\frac{(1 - \nu) + (1 + \nu)(r_1/r_g)^2}{1 - (r_1/r_2)^2}\right]$$

(3.3)

A similar expression may be derived for the radial stresses and strains by assuming:

$$e_r = \frac{1}{E}(\sigma_r - \nu\sigma_\theta)$$

$$Ee_r = P_1 + (P_2 - P_1)\left[\frac{1 - (r_1^2/r_g^2)}{1 - r_1^2/r_2^2}\right]$$

$$- \nu \left\{P_1 + (P_2 - P_1)\left[\frac{1 + r_1^2/r_g^2}{1 - r_1^2/r_2^2}\right]\right\}$$

Simplifying:

$$Ee_r = P_1\,(1 - \gamma) + (P_2 - P_1)\left[\frac{(1 - \gamma) - (1 + \gamma)(r_1/r_g)^2}{1 - (r_1/r_2)^2}\right]$$

(3.4)

Figure 3.2 : Experimental Analysis Cutting Parameters

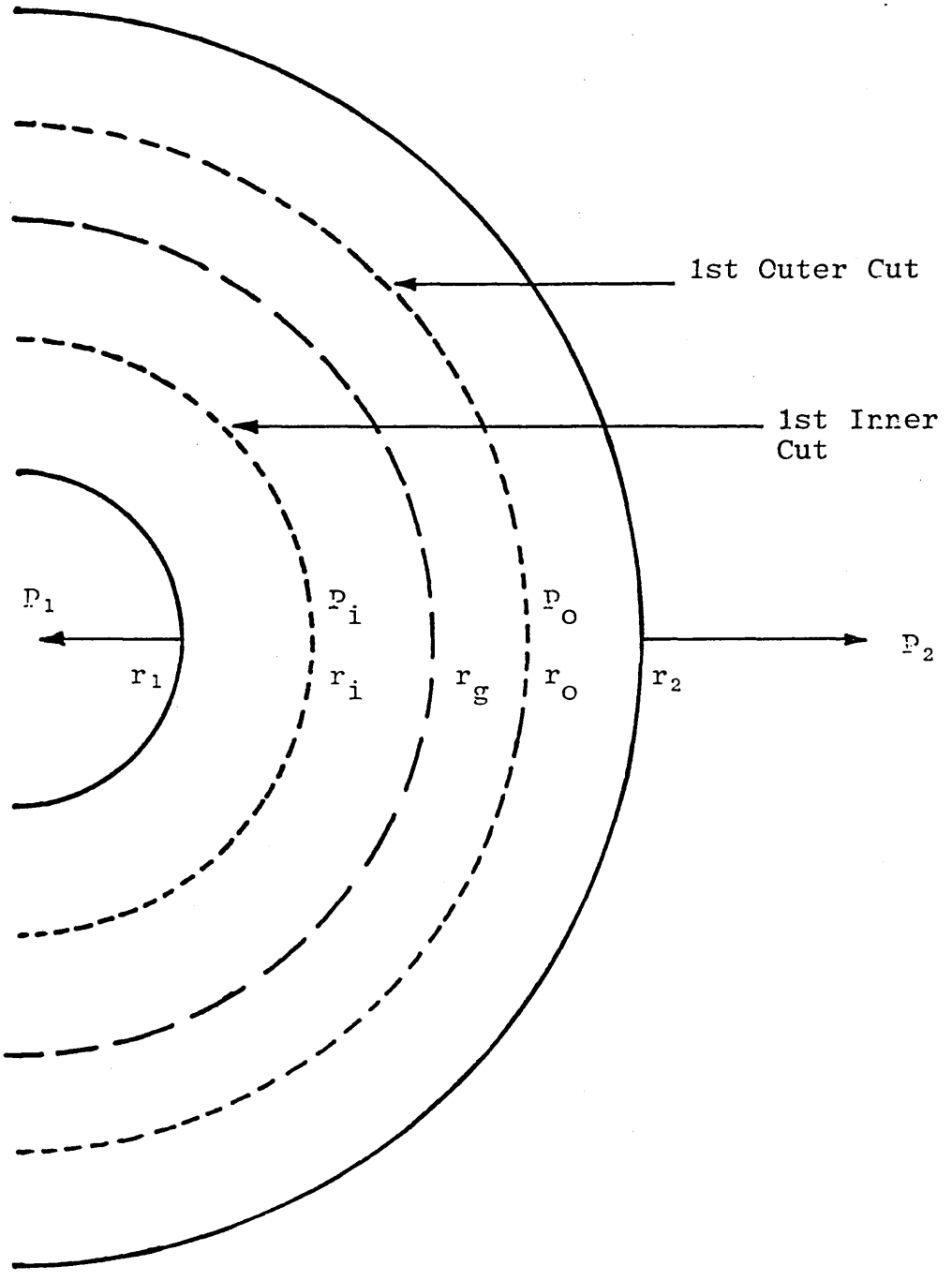

(a) Outer Cuts

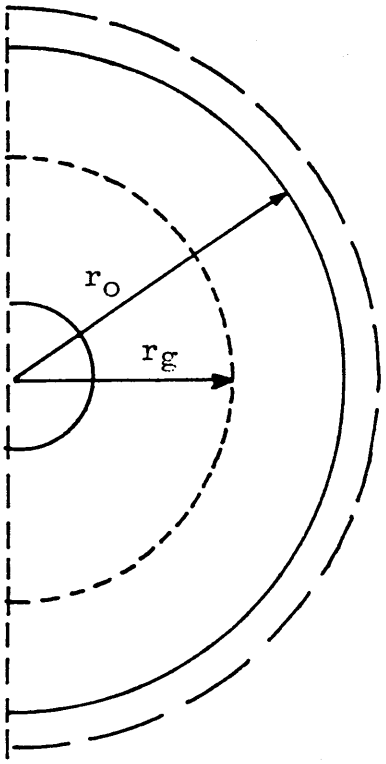

Original Profile of uncut disc

r_o ≡ outer cuts radii

r_g ≡ radius of gauge fixing parameter

(b) Inner Cuts

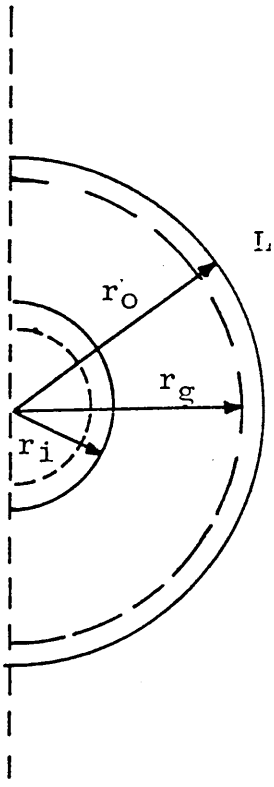

Last Outer Cut

r_i ≡ inner cuts radii

Original Profile of uncut disc

Procedure when disc is turned on the outside radius down to $r_2 - \alpha = r_0$ (see Figure 3.3a)

If required radial stress at r_0 is P_0, then the effect of turning down is to apply $-P_0$ at r_0.

Hence modify previous equations by writing

r_0 for r_2

$-P_0$ for P_2

with the understanding that r_1 stays constant and $P_1 = 0$.

Then considering HOOP direction and substituting in equation

$$Ee_\theta = -P_0 \left[\frac{(1 - \nu) + (1 + \nu)(r_1/r_g)^2}{1 - (r_1/r_0)^2} \right]$$

in which e_θ is understood to be the total strain change at r_g when the radius is turned down to r_0.

Thus $$\frac{Ee_\theta}{P_0} = - \left[\frac{(1 - \nu) + (1 + \nu)(r_1/r_g)^2}{1 - (r_1/r_0)^2} \right]$$

or $$P_0 = \frac{- Ee_\theta}{\left[\frac{(1 - \nu) + (1 + \nu)(r_1/r_g)^2}{1 - (r_1/r_0)^2} \right]} \qquad (3.5)$$

Let $$f = \left[\frac{(1 - \nu) + (1 + \nu)(r_1/r_g)^2}{1 - (r_1/r_0)^2} \right]$$

then $P_0 = -Ee_\theta/f$

Procedure when disc is subsequently bored out to radius $r_1 + \delta = r_i$ (see figure 3.3b)

We now consider, in effect, a disc of outer radius r_0 at which $-P_0$ has been applied, and inner radius r_i at which $-P_i$ has been applied.

Hence modify equation 3.3 by writing

r_i for r_1

$-P_i$ for P_1

r_0 for r_2

$-P_0$ for P_2

$$Ee_\theta = (1 - \nu) - P_i + (P_i - P_0)\left[\frac{(1 - \nu)+(1 + \nu)(r_i/r_g)^2}{1 - (r_i/r_0)^2}\right]$$

in which r_0 is understood to be the last radius uncovered by turning down the outer radius before boring out of the inner radius took place.

In these circumstances P_0 is known from (3.5)

Let $f^1 = \left[\dfrac{(1 - \nu) + (1 + \nu)(r_i/r_g)^2}{1 - (r_i/r_0)^2}\right]$

$\therefore \quad Ee_\theta = -(1 - \nu)P_i + (P_i - P_0)f^1$

$\therefore \quad P_i = \dfrac{Ee_\theta + P_0 f^1}{(\nu-1) + f^1}$ (3.6)

Similarly for radial direction, equation 3.4 is used.

Procedure when disc is turned on outside radius down to

$r_2 - \alpha = r_0$

write r_0 for r_2

$-P_0$ for P_2

with the understanding that r_1 stays constant and $P_1 = 0$, and e_r is understood to represent total strain change at r_g by the time r_0 is reached.

$$\therefore \quad P_0 = \frac{-Ee_r}{\left[\dfrac{(1-\nu) - (1+\nu)(r_1/r_g)^2}{1 - (r_1/r_0)^2}\right]}$$

$$\text{put} \quad g = \left[\frac{(1-\nu) - (1+\nu)(r_1/r_g)^2}{1 - (r_1/r_0)^2}\right]$$

$$\therefore \quad P_0 = -Ee_r/g \qquad (3.7)$$

Procedure when disc is subsequently bored out to radius

$r_1 + \delta = r_i$

write r_i for r_1

$-P_i$ for P_1

r_0 for r_2

$-P_0$ for P_2

In these circumstances P_0 is known from (3.7)

$$\text{and} \quad Ee_r = -P_i(1-\nu) + (P_i - P_0)\left[\frac{(1-\nu) - (1+\nu)(r_i/r_g)^2}{1 - (r_i/r_0)^2}\right]$$

Put $g^1 = \left[\dfrac{(1 - \nu) - (1 + \nu)(r_i/r_g)^2}{1 - (r_i/r_0)^2} \right]$

$\therefore \quad Ee_r = -P_i(1 - \nu) + (P_i - P_0)\, g^1$

$\therefore \quad P_i = \dfrac{Ee_r + P_0 g^1}{(\nu - 1) + g^1}$ (3.8)

Summary

(i) Parameters

r_1 = initial inner radius of disc

r_2 = initial outer radius of disc

r_i = radius of inner after boring out

r_0 = radius of outer after turning down

r_g = radius of gauge position

P_1 = initial inner pressure in radial direction

P_2 = initial outer pressure in radial direction

P_i = inner pressure at point where disc has been bored out to r_i

P_0 = outer pressure at point where disc has been turned down to r_0

(ii) Estimates of Radial Stress based on Hoop Strain Readings

Outer : $P_0 = -Ee_\theta/f$ (Equation 3.5)

Inner : $P_i = \dfrac{Ee_\theta + P_0 f^1}{(\nu-1) + f^1}$ (Equation 3.6 P_0 from 3.5)

(iii) Estimates of Radial Stress based on Radial Strain Readings

Outer : $P_0 = -Ee_r/g$ (Equation 3.7)

Inner : $P_i = \dfrac{Ee_r + P_0 g^1}{(\nu-1) + g^1}$ (Equation 3.8 P_0 from 3.9)

Note $$f = \left[\frac{(1 - \nu) + (1 + \nu)(r_1/r_g)^2}{1 - (r_1/r_0)^2}\right]$$

$$f^1 = \left[\frac{(1 - \nu) + (1 + \nu)(r_i/r_g)^2}{1 - (r_i/r_0)^2}\right]$$

$$g = \left[\frac{(1 - \nu) - (1 + \nu)(r_1/r_g)^2}{1 - (r_1/r_0)^2}\right]$$

$$g^1 = \left[\frac{(1 - \nu) - (1 + \nu)(r_1/r_g)^2}{1 - (r_i/r_0)^2}\right]$$

Interpretation of Equations

Equations 3.1 and 3.2 give the radial and hoop stresses in terms of the initial stresses P_1 and P_2, which are both radial stresses. The remaining equations (3.3 to 3.8 inclusive) are concerned with the prediction of stress at the cut boundaries of the disc in terms of the radial and hoop strains as given by the strain gauge rosettes. Since P_1 and P_2 are both radial stresses and only P_1 and P_2 feature in the equations, hoop stresses cannot be predicted at other than the gauge position. The procedure for

dealing with the progressive radial cuts is governed by the order of the analysis and must be adhered to, i.e. all the outer radii must be turned before the inner radii are bored out.

3.1.4 Experimental Results and Graphs

3.1.4.1 A brief description of the conditions of loading the discs will be given again in order to facilitate the understanding of the experimental results and graphs. The main explosive loading experiments were carried out in three batches. The aim of the experiments was to cover as many variables as possible within the three batches. The three batches were designated A, B and C with the following general designation:

(i) A series; constant radius from explosive ring with increased load (energy) from A4, A6, A5, A7 and A8.

(ii) B series; this series was used to cover two variations in the loading parameters along with increasing radius of explosive ring from B1, B2, B3, B5 and B6. The first three (B1, B2 and B3) had the same load with increasing radii of the explosive ring whereas the last three, B3, B5 and B6, had a constant load per unit length of explosive with an increasing radius of the explosive ring.

(iii) C series; this series was used to investigate the change of residual stress with size of disc, hence the C series had a constant load at a constant

radius but with a decreasing outer diameter of disc from C1, C2, C3, C4.

(iv) A special group of discs were tested at the end of the experiments to compare the effect of annealing and of different strain gauge configuration. Hence A3 was loaded as A7 and strain gauge rosettes placed at individual radii, B8 was annealed but analysed with no load and C5 was loaded as C2 but not annealed.

A summary of the disc loading parameters is as follows:

Disc Loading Parameters

See table overleaf.

TABLE 3.1
DISC LOADING PARAMETERS

Disc	Initial		Radial Position of Explosive r_e/cm	Strain Gauge Rosette Position/cm	Energy Converted /J	Description
	r_i/cm	r_0/cm				
A4	3.8	19.05	11.33	9.75	41.57	Increasing load with constant radius of loading
A6	3.8	19.05	11.33	9.75	51.93	
A5	3.8	19.05	11.33	9.75	62.45	
A7	3.8	19.05	11.33	9.75	72.80	
A8	3.8	19.05	11.33	9.75	83.15	
B1	3.8	19.04	7.62	8.12	62.45	) Constant load.
B2	3.8	19.04	8.89	9.89	62.45	) Increasing radii.
B3	3.8	19.04	10.16	11.16	62.45	)) Energy load/constant
B5	3.8	19.04	11.43	10.43	69.91	) load/m.
B6	3.8	19.04	12.70	11.70	78.06	) Increasing radii.
C1	3.8	21.5	11.33	9.75	69.57	) Constant load.
C2	3.8	19.0	11.33	9.75	69.57	) Decreasing size of
C3	3.8	16.5	11.33	9.75	69.57	) disc.
C4	3.8	14.0	11.33	9.75	69.57	)
A3	3.8	19.0	11.33	Variable	69.57	ANNEALED, LOADED, Different SG constant.
B8	3.8	19.0	-	9.75	-	ANNEALED, NO LOAD
C5	3.8	19.0	11.33	9.75	69.57	Non-annealed.

3.1.4.2 Radial and Hoop stress at fixed gauge positions based on readings taken after the final machining down.

It was pointed out in Section 3.1.3.1 that a limitation of the method adopted was that it only allowed for a prediction of residual radial stress to be made. The only time it is possible to obtain an estimate of the residual radial and hoop stresses is at the point where the machined down part of the disc reaches the strain gauge position. The residual strain results were obtained for the radial and hoop directions after the last machining on the outer part and the last boring of the inner part of the disc.

Values of the residual radial and hoop stresses have been calculated for the A and B series. These results are based on the average of eight strain gauge rosettes, four attached on the upper and four on the lower surface of the disc.

Table 3.2

FINAL CUTS FOR ROSETTE ANALYSIS

A and B Series

Disc	INNER			OUTER		
	Radius cm	σ_{ri} $10^6 Nm^{-2}$	$\sigma_{\theta i}$ $10^6 Nm^{-2}$	Radius cm	σ_{r0} $10^6 Nm^{-2}$	$\sigma_{\theta 0}$ $10^6 Nm^{-2}$
A4	6.4	-40	-30	13.0	-31	+28
A6*	6.3	-38	-21	13.2	-27.5	+23
A5*	6.5	-27	-23	13.2	-16	+14
A7	6.4	- 8	-17	13.5	-23	+15
A8	6.3	- 7	-30	13.5	- 6	+ 2
A3	6.3	-39	-27	13.0	-17	+11.5
B1	5.0	-19	-24	13.0	- 4	+68
B2	6.0	-21	-10	13.0	-10	+11
B3	6.0	-49	- 7	13.0	-16	+11
B5	6.6	-38	-31	13.0	-25	+60
B6	6.7	-73	-70	13.0	-72	+75
B8	6.3	- 2	- 4	14	-10	+ 2

*See Table 3.1 for reason for A6 appearing before A5.

σ_{ri} = radial stress at radius of last inner cut

$\sigma_{\theta i}$ = hoop stress at radius of last inner cut

σ_{r0} = radial stress at radius of last outer cut

$\sigma_{\theta 0}$ = hoop stress at radius of last outer cut

Figure 3.4 : Stresses at Final Cut in A Series

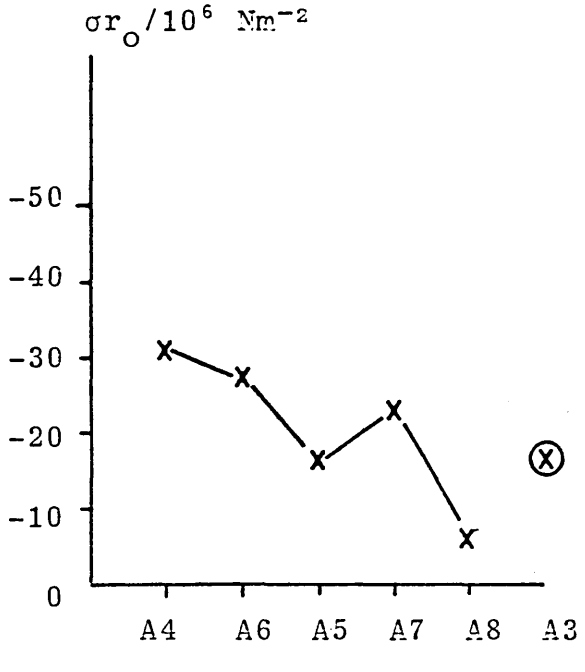

(a) A Series - Radial Outer

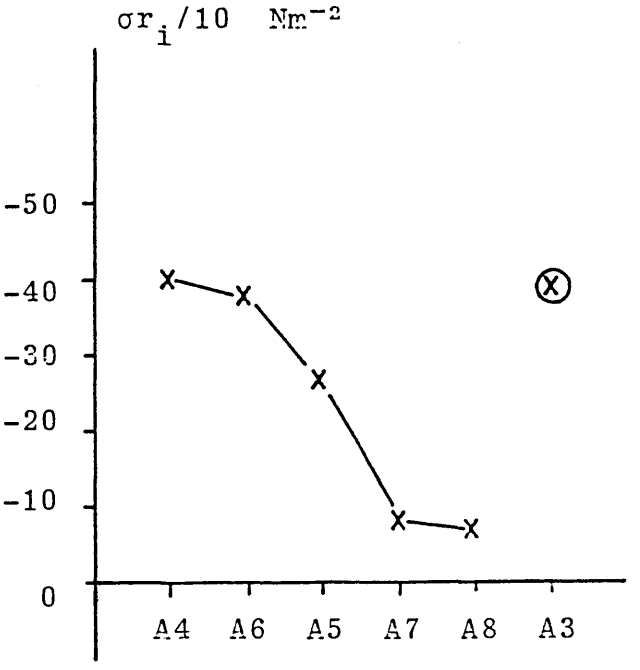

(b) A Series - Radial Inner

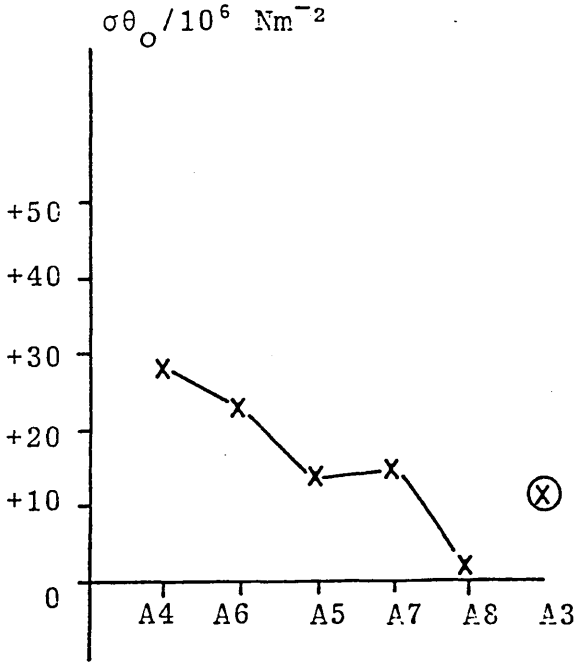

(c) A Series - Hoop Outer

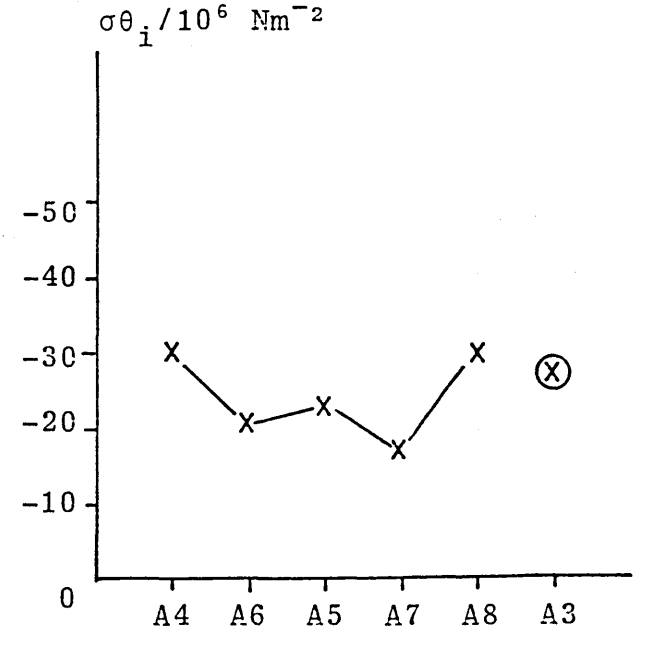

(d) A Series - Hoop Inner

(B1, B2 and B3)

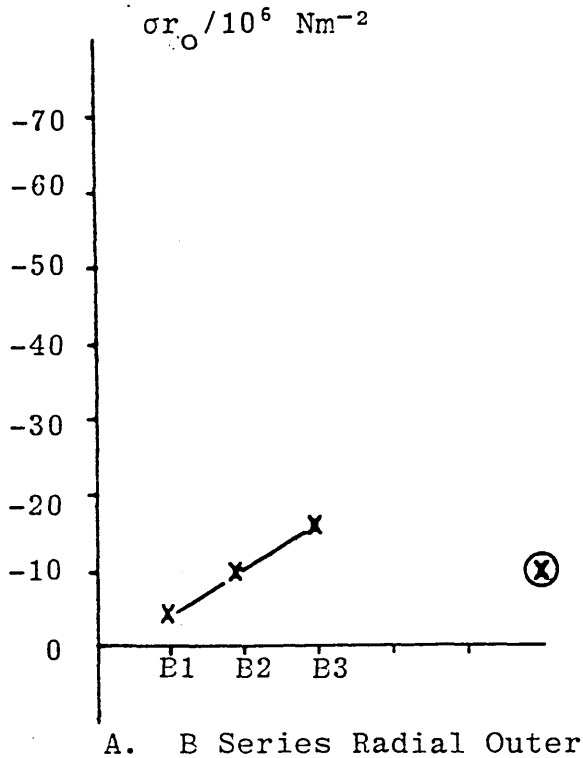

A. B Series Radial Outer

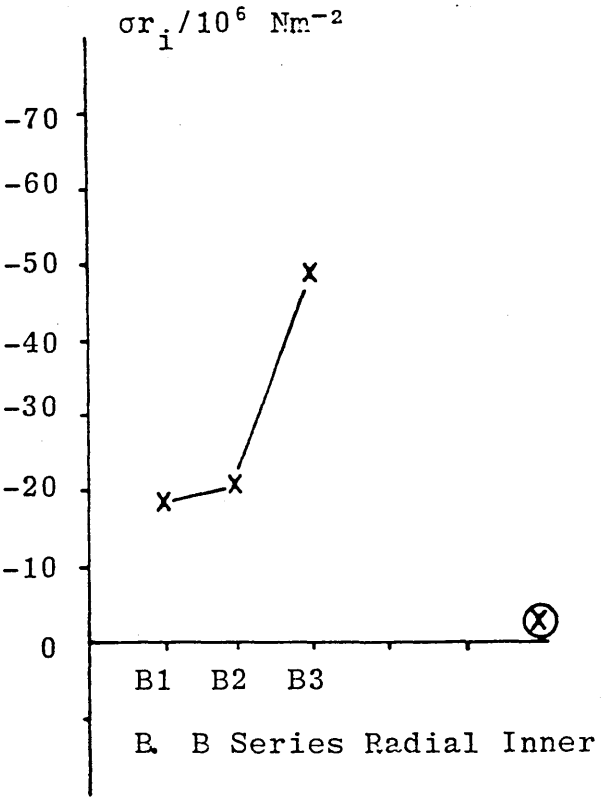

B. B Series Radial Inner

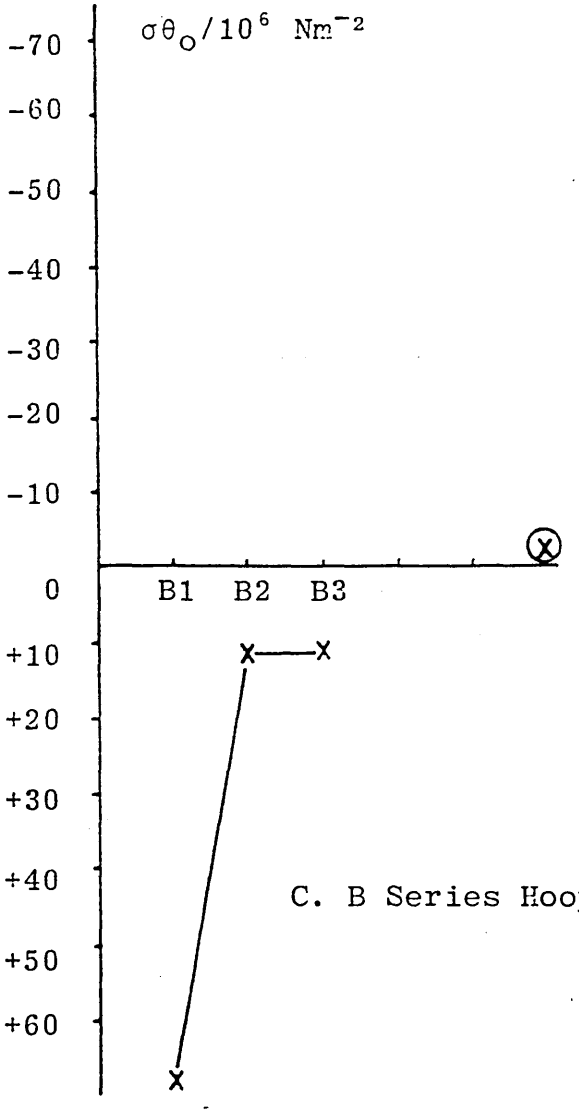

C. B Series Hoop Outer

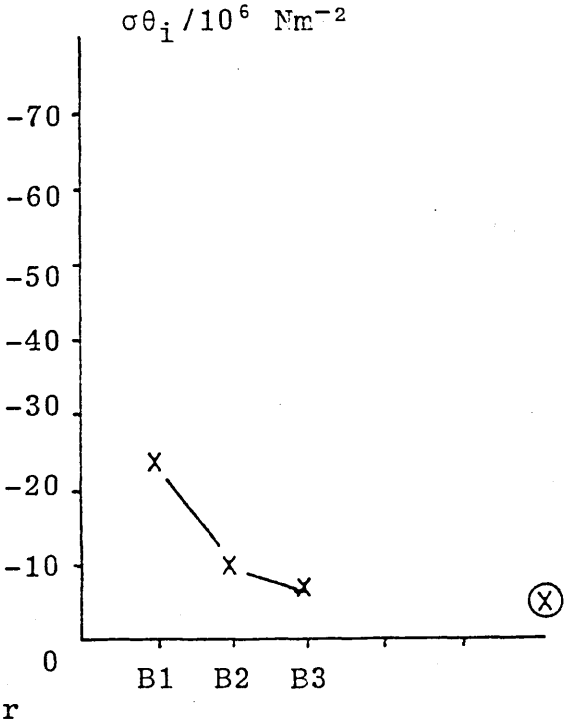

D. B Series Hoop Inner

(B3, B5, B6 and B8)

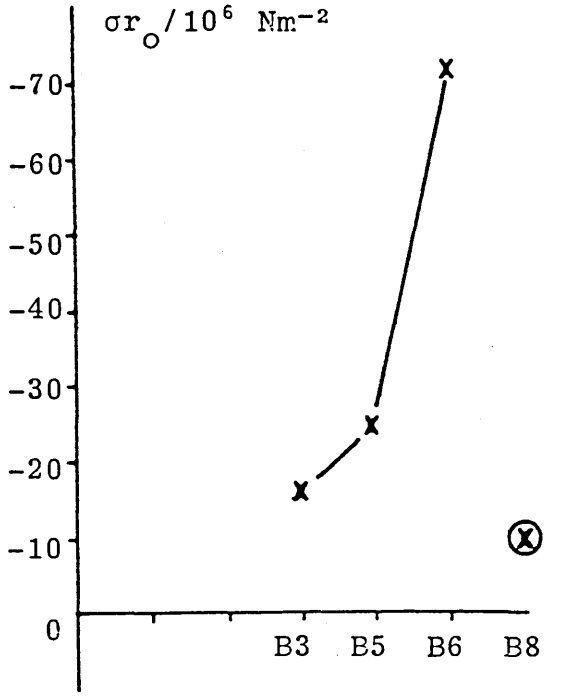

A. B Series Radial Outer

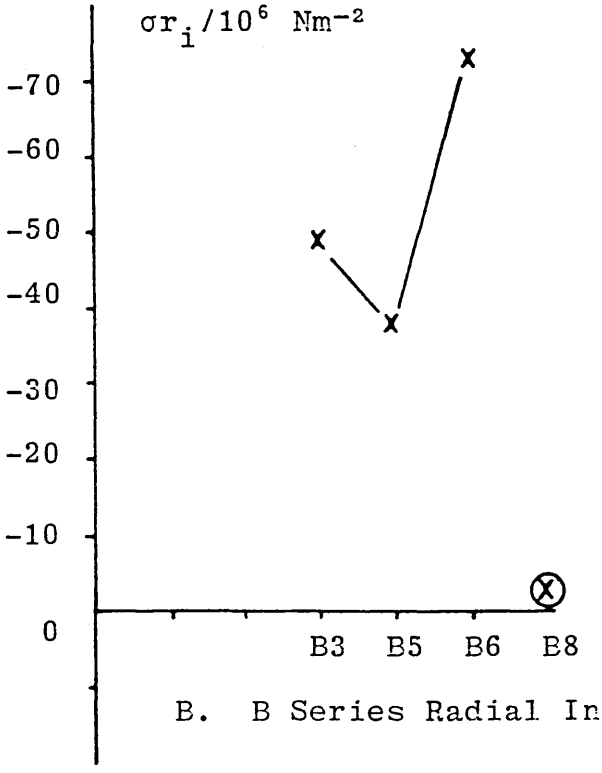

B. B Series Radial Inner

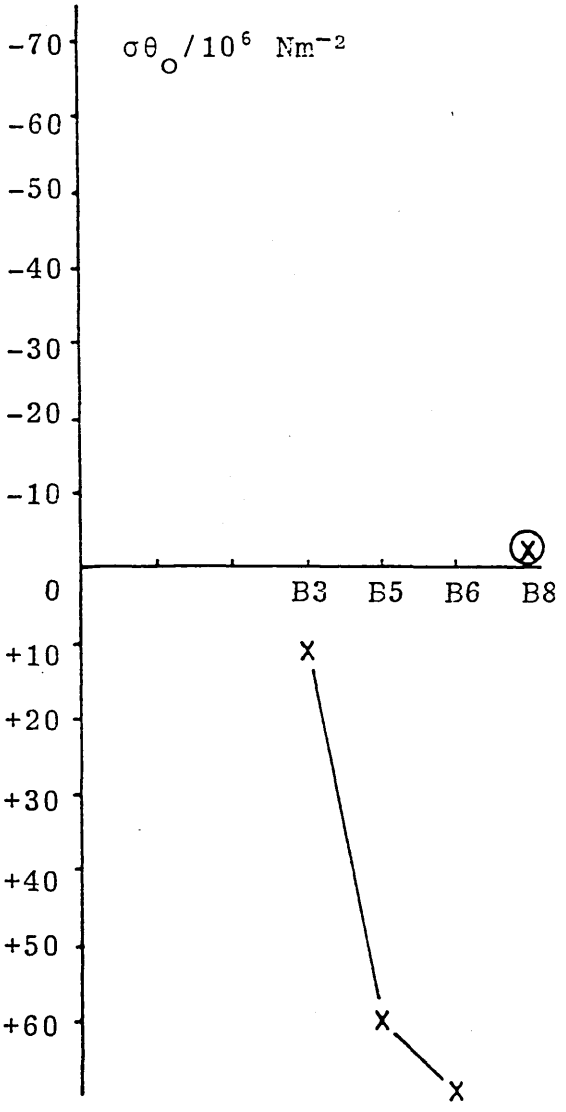

C. B Series Hoop Outer

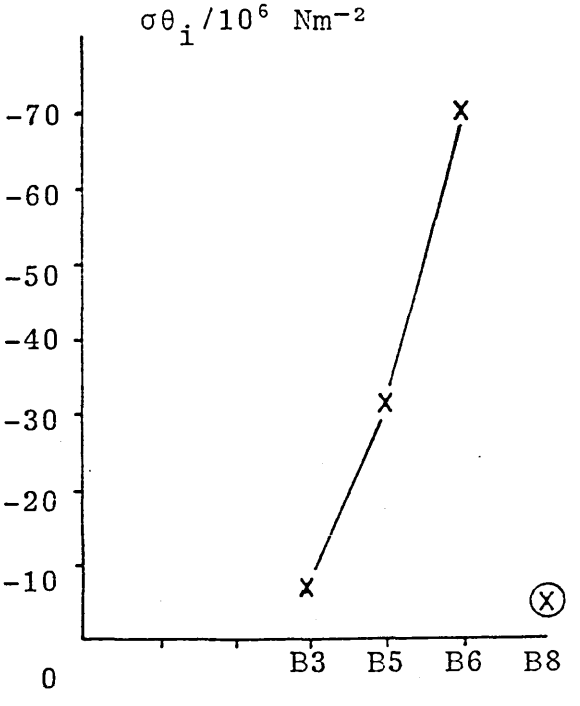

D. B Series Hoop Inner

3.1.4.3 Experimental Results

The following results are based on readings taken from eight rosettes. Four rosettes were positioned on the top surface and four on the bottom. The positions of the rosettes on the top and bottom surfaces was radially and axially symmetric. The tables of results are therefore an average of eight readings.

Note : Negative values represent compression

Positive values represent tension

Table 3.3

A series : σr_i

INNER

Disc	Radius/(cm) INNER	$\sigma r_i / 10^6 Nm^{-2}$ RADIAL	$\sigma r_i / 10^6 Nm^{-2}$ HOOP
A4	5.08 6.4	-12 -29.8	-33.9 -39.5
A6	5.06 6.3	-30.3 - 2	- 9.6 -38.7
A5	4.4 5.65 6.95	-34 -18.1 - 8	-35.8 -27.7 -21.9
A7	5.07 6.34	-4.6 -9.6	-29.6 -29.2
A8	5.04 6.3	-43.3 -19.8	-14.7 -24.2

Table 3.4

A series : σr_0

OUTER

Disc	Radius/(cm) OUTER	$\sigma r_0/10^6 Nm^{-2}$ RADIAL	$\sigma r_0/10^6 Nm^{-2}$ HOOP
A4	18.4	-12.8	- 7.8
	17.2	-28.0	-21.7
	15.9	-23.0	-13.7
	14.6	-22.0	-17.9
	11.8	-28.7	-31.3
A6	17.7	- 3.0	- 3.4
	16.4	- 9.8	- 9.8
	15.1	- 5.1	- 3.2
	13.9	-23.3	-29.4
	12.6	-16.6	-27.5
A5	16.7	-18.8	- .3
	15.4	- 7.2	-10.4
	14.1	-12.4	- 6.7
	12.8	-11.7	-16.0
A7	17.8	-15.3	-11.7
	16.6	-23.9	-13.8
	15.3	-16	- 7.2
	14	-14.7	-13.8
	12.7	- 3.4	-23.7
A8	17.8	-30.3	-14.8
	16.6	-28.6	- 9.9
	15.3	-11.6	- 6.4
	14.1	-12.9	- 3.8
	12.9	-13.6	- 4.1

Figure 3.6 : A Series (based on Radial Readings)

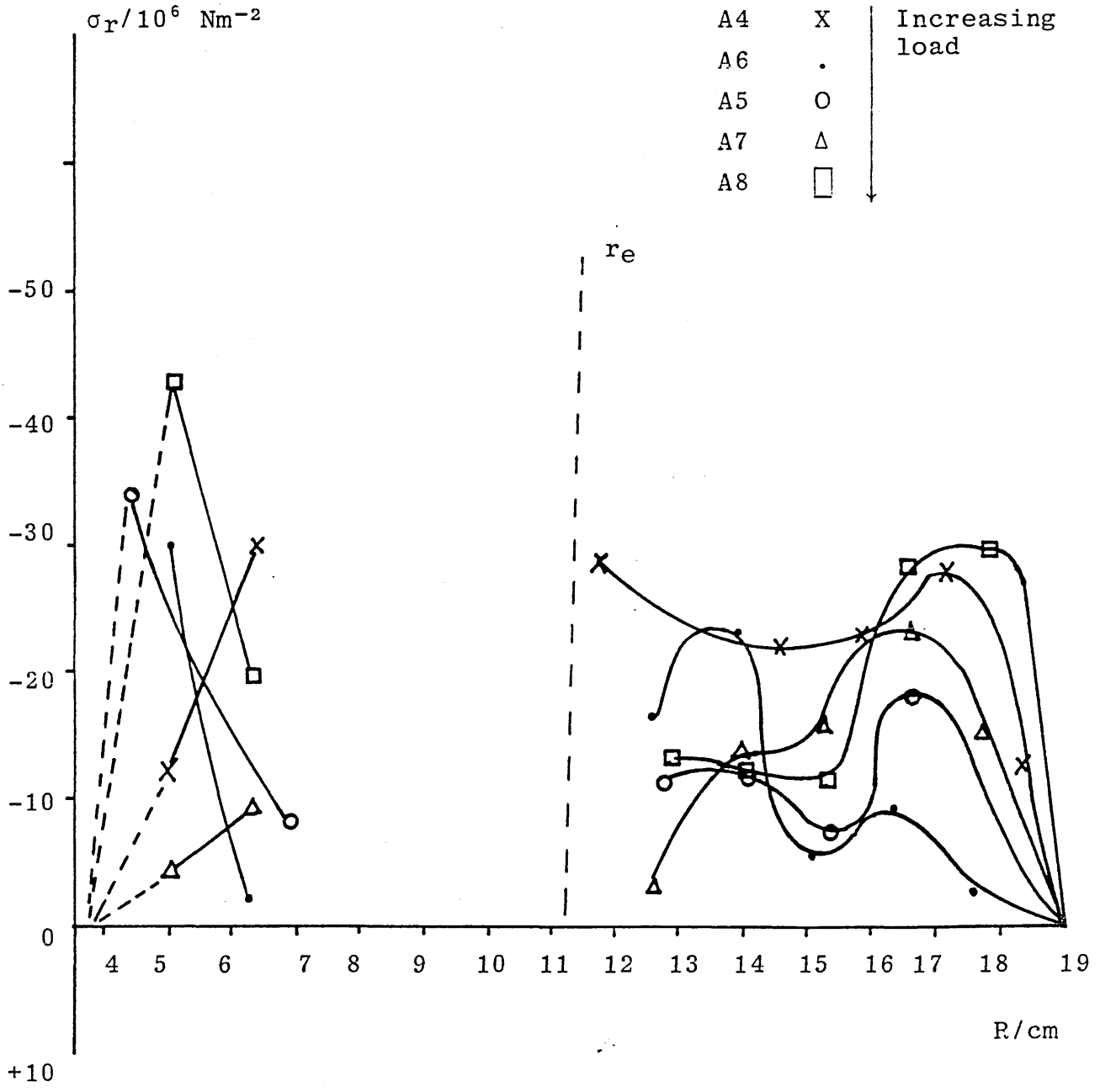

Figure 3.7 : A Series (based on Hoop Readings)

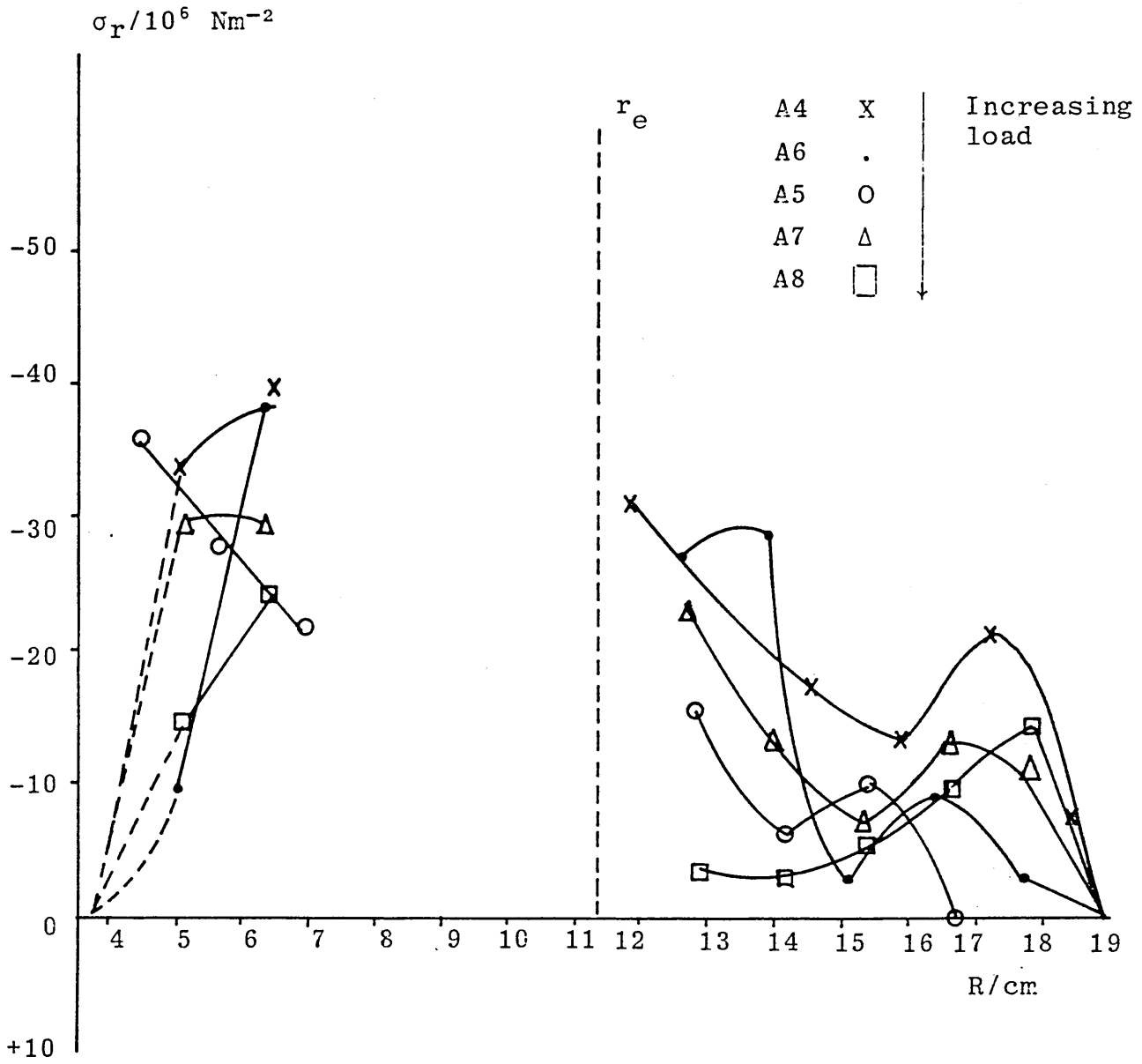

Table 3.5

B series : σr_i

INNER

Disc	Radius/(cm) INNER	$\sigma r_i / 10^6$ Nm^{-2} RADIAL	$\sigma r_i / 10^6$ Nm^{-2} HOOP
B1	5.2	-19.9	-20.5
	6.5	-22.3	-17.0
	7.8	-25.4	- 8.6
B2	5.23	- 9.5	-19.8
	6.43	- 8.4	-19.4
	8.25	-10.4	-18.4
B3	5.11	-42.3	-11.5
	6.45	- 2.3	-46.0
	7.80	- 7.1	-43.3
	9.20	- 8.1	-46.4
	10.10	- 4.4	-40.9
B5	5.54	-33.0	-47.8
	6.56	-42.2	-46.5
B6	5.30	-16.6	-42.8
	6.70	-55.1	-54.0

Table 3.6

B series : σr_0

OUTER

Disc	Radius/(cm) OUTER	$\sigma r_0/10^6$ Nm^{-2} RADIAL	$\sigma r_0/10^6$ Nm^{-2} HOOP
B1	17.8	- 2.5	- 1.3
	16.5	- 8.8	- 2.2
	15.2	-38.4	-14.1
	13.9	-70.0	-32.6
	12.6	-27.1	- 5.3
B2	17.6	- 1.7	- 2.0
	16.2	- 7.0	- 2.3
	14.9	- 2.0	- 7.0
	13.5	-11.7	- 9.3
	12.3	- 7.4	-10.0
B3	17.5	-20.1	-16.1
	16.3	- 1.0	-11.8
	15.0	-11.6	-15.8
B5	17.4	- 5.0	- 1.8
	16.1	- 3.7	- 2.5
	14.9	-13.7	- 1.8
	13.6	-43.6	-14.4
	12.3	-43.6	-28.8
B6	17.8	-14.4	-21.3
	15.3	-22.5	-26.2
	13.9	-42.8	-39.1
	12.6	-56.6	-48.2
	11.42	-56.9	-59.8

Figure 3.8 : B Series (based on Radial Readings)

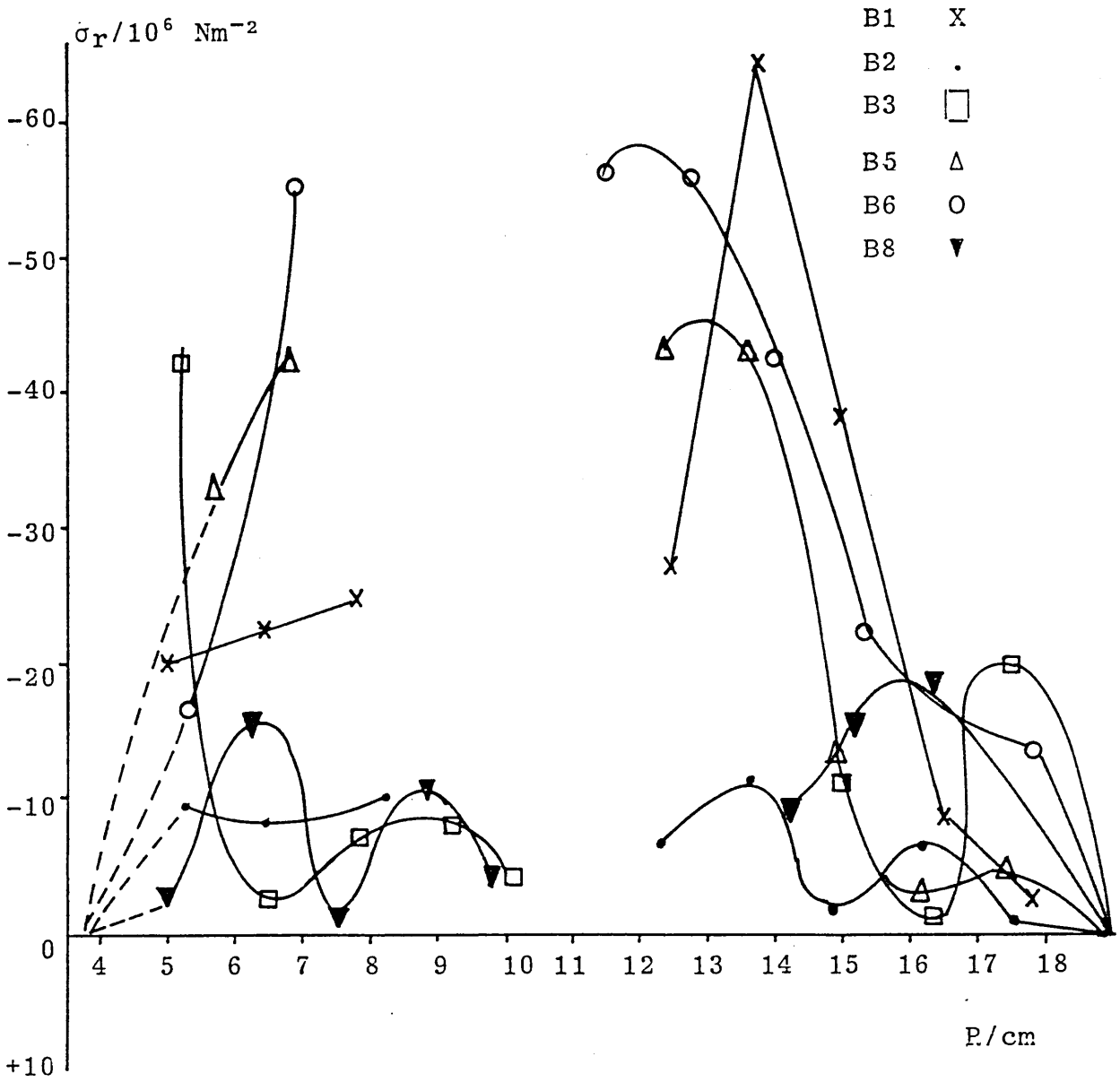

Figure 3.9 : B Series (based on Hoop Readings)

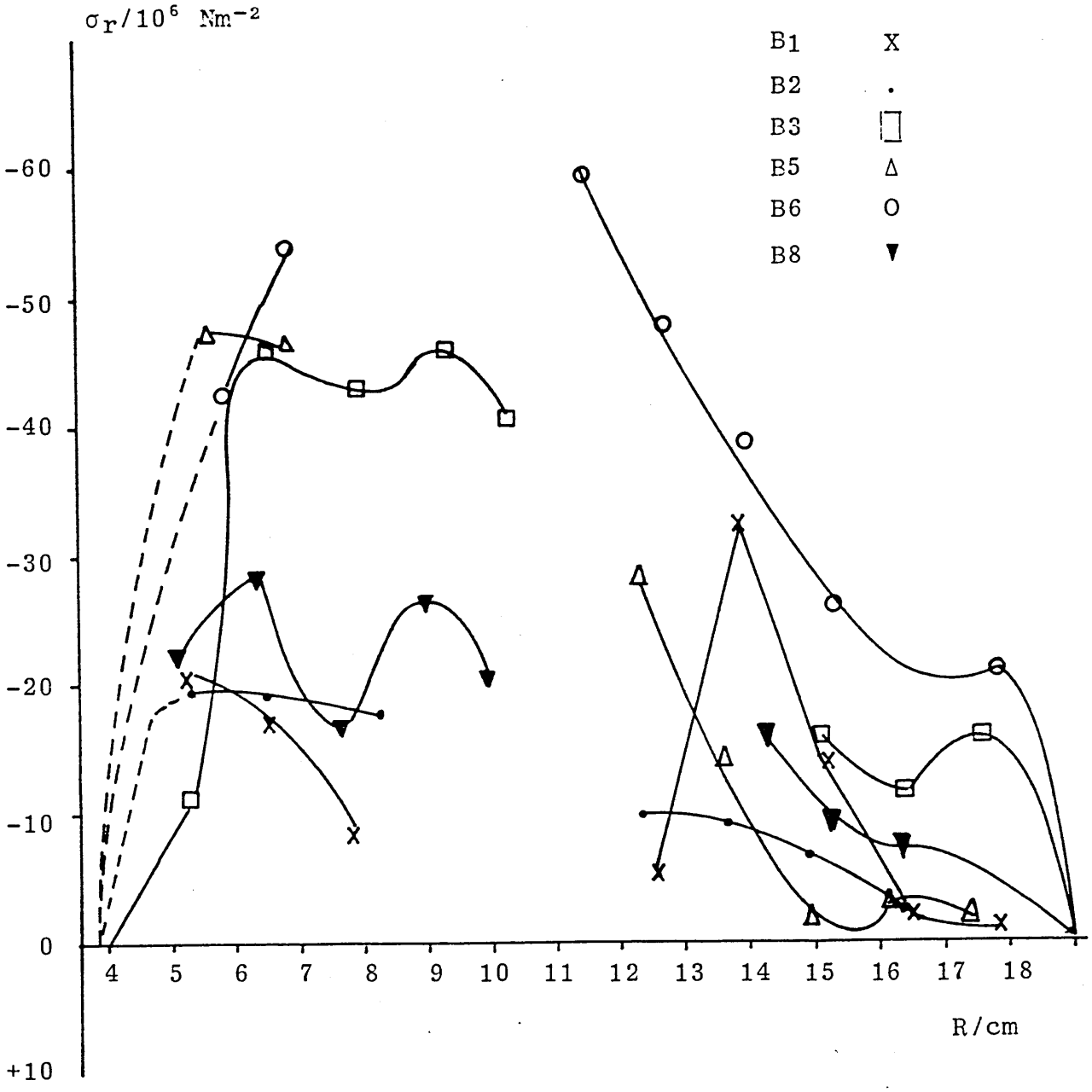

Table 3.7

C series : σr_i

INNER

Disc	Radius/(cm) INNER	$\sigma r_i / 10^6$ Nm^{-2} RADIAL	$\sigma r_i / 10^6$ Nm^{-2} HOOP
C1	4.9	-66.3	-42.4
	6.0	-27.0	-37.6
	7.8	-19.6	-27.9
C2	4.9	- 3.3	-17.7
	6.0	- 9.6	-28.8
	7.1	-14.5	-32.4
	8.2	- 4.2	-37.9
	9.0	-11.0	-36.4
C3	4.9	- 9.0	-17.2
	6.1	-44.9	-24.7
	7.1	-35.9	-26.7
	8.1	-36.4	-28.8
	9.0	-36.0	-26.4
C4	4.9	- 6.6	- 7.9
	6.1	- 7.9	-13.7
	7.2	-13.8	-14.1
	8.2	-18.3	-15.2
	8.8	-24.4	-15.7

Table 3.8

C series : σr_0

OUTER

Disc	Radius/(cm) OUTER	$\sigma r_0 / 10^6$ Nm^{-2} RADIAL	$\sigma r_0 / 10^6$ Nm^{-2} HOOP
C1	20.4	- 2.5	- 1.0
	19.4	- 3.2	- 2.7
	18.2	- 7.0	- 2.7
	17.1	- 5.4	- 3.0
	16.2	- 9.9	- 6.2
	15.1	-18.1	-11.3
	14.1	-19.3	-17.3
	13.1	-19.5	-15.3
	11.9	-28.2	-14.1
	11.0	-31.4	-19.3
C2	18.0	- 3.7	- 4.7
	17.0	- 5.1	- 6.5
	16.0	- 7.3	- 8.6
	15.1	-11.6	-10.8
	14.1	-20.3	-19.4
	13.0	-22.1	-21.1
	12.1	-28.1	-26.6
C3	15.6	- 1.9	- 3.9
	14.5	- 8.0	- 9.0
	13.3	-10.0	-13.8
	12.2	-11.1	-18.3
C4	12.9	- 6.0	- 2.9
	12.1	- 6.4	- 5.3

Figure 3.10 : C Series (based on Radial Readings)

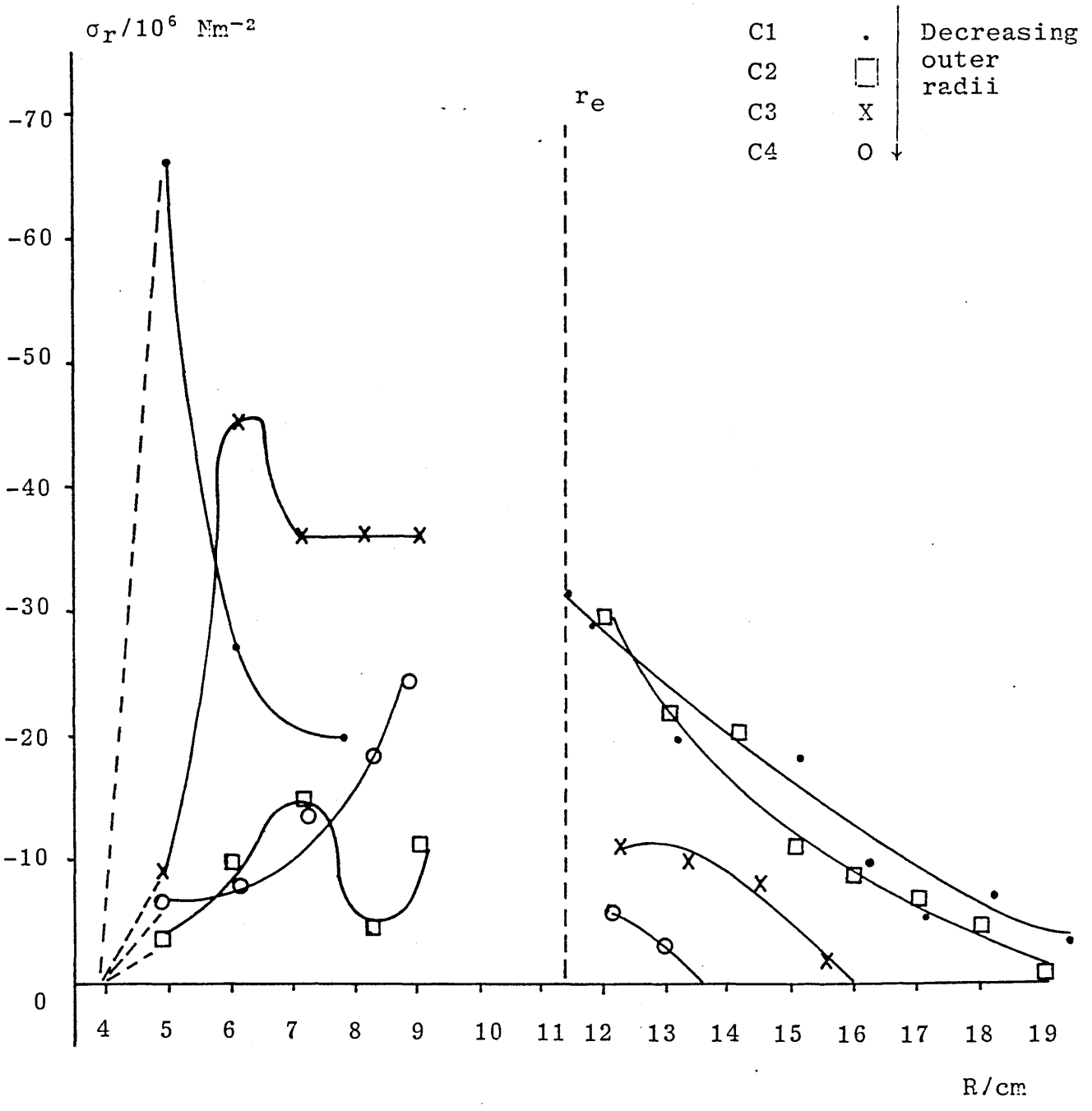

Figure 3.11 : C Series (based on Hoop Readings)

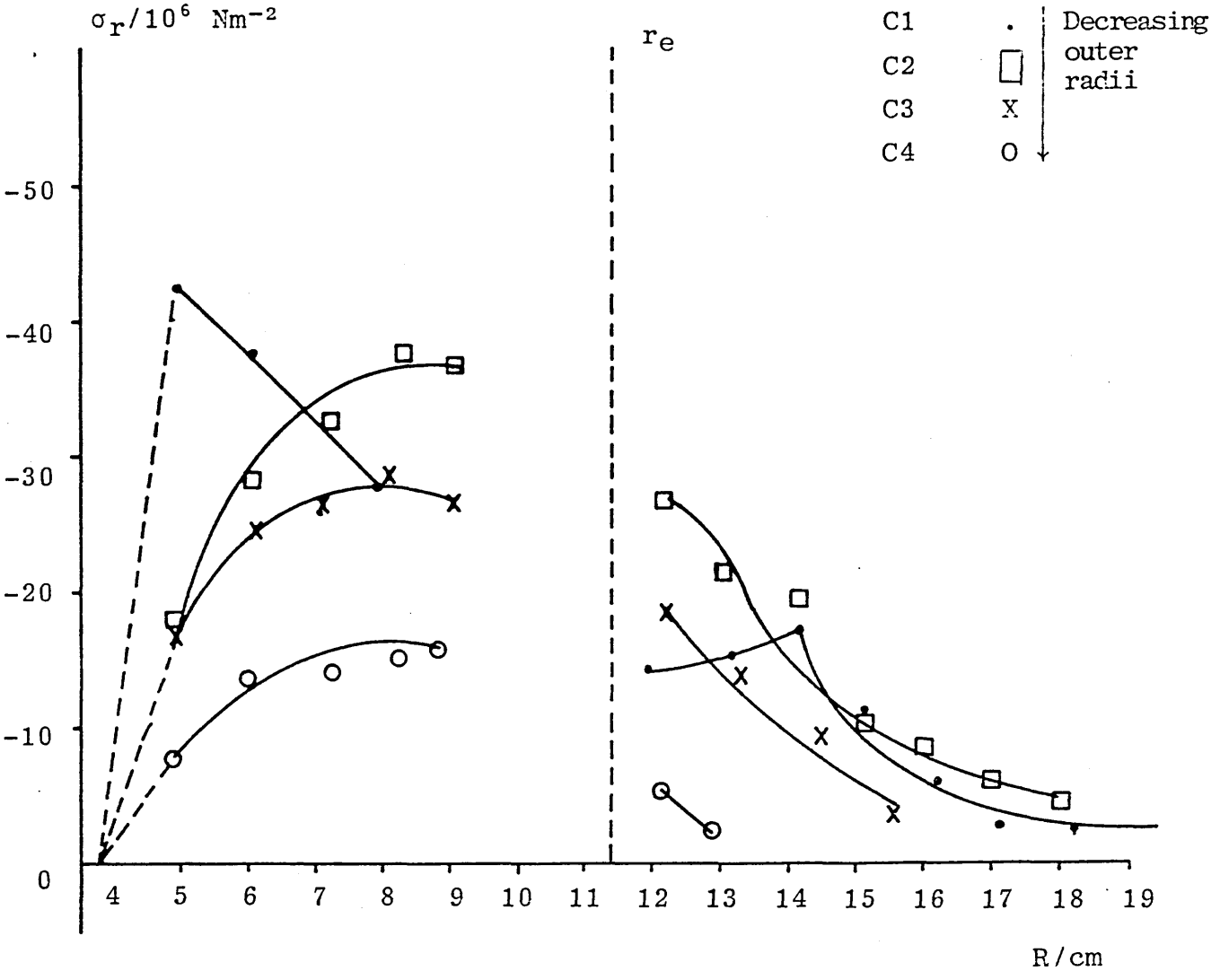

3.1.4.4 Assessment of Methodology

This section consists of three parts which are concerned with the assessment of the procedures adopted in dynamic loading of the discs.

(i) Assessment of repeatability of explosive loading and analysis between A, B and C series

(Figures 3.14, 3.15)

The accuracy of the results obtained for the three different series of discs can be checked by comparing those discs from each series which have similar loading parameters. An inspection of the disc loading summary table, Section 3.1.4.1, shows that discs A7, B5 and C2 have similar loading parameters and can therefore be compared. For convenience, the loading parameters are summarised in the following table: 3.9

Disc	r_0/cm	r_i/cm	r_e/cm	Energy/J
A7	19.0	3.8	11.33	198.7
B5	19.0	3.8	11.43	190.8
C2	19.0	3.8	11.33	190.0

Code for Graphs

A4	X	B1	X	C1	.
A6	.	B2	.	C2	□
A5	0	B3	□	C3	X
A7	Δ	B5	Δ	C4	0
A8	□	B6	0	C5	Δ
		B8	▼		

(ii) Comparison of Methods of obtaining Residual Strains

(Figures 3.14, 3.15)

The method adopted for the dynamic loading work has been that of boring out/turning down with strain gauge rosettes in fixed positions situated as close as possible to the deformed annular loading ring. A more standard method used in other work, and in the static loading work described later, has been to attach strain gauge rosettes at varying radii from the deformed annular loading ring and to release the residual strains by cutting the gauges out from the parent metal.

For comparison purposes the disc A3 was treated in this way and the residual strains obtained from the cut-out pieces at varying radii throughout the surface of the disc. Disc A3 was provided with the same loading parameters as A7, B5 and C2 (see Section 3.1.4.4 (i)).

Disc A3 by having the strain gauge rosettes attached at varying radii and different azimuthal positions on the surface of one side of the disc, provided a measure of radial and hoop residual strains at individual radii throughout the disc surface.

The method of attaching strain gauges at various radii adopted for the disc A3 measures the strain relief at points on the surface of the disc, whereas

the boring out/turning down method predicts the strain relief at a point remote from the position of the strain gauge. Thus a comparison of residual stress levels obtained from disc A3 and those from discs A7, B5 and C2 allows a comparison of the two methods described.

(iii) The Effect of Annealing

(Figures 3.8, 3.9, 3.12, 3.13)

The effect of annealing has been compared by checking the residual stress levels for two similarly loaded discs i.e. C2 and C5. Disc C2 was processed in the way adopted for the three series, A, B and C, whereas C5 was not annealed but received the same loading as C2. A further disc, B8, was annealed with the B series but not loaded before strain gauge rosettes were applied.

Table 3.10

A3 (individual rosettes placed at varying radii in one quadrant of the disc)

Disc	Radius/(cm)	$\sigma r/10^6$ Nm^{-2}	$\sigma_\theta/10^6$ Nm^{-2}
A3 Individual Gauges	16.0	-44	+69
	15.0	-10	+28
	13.0	-23	+57
	12.5	-37	+109
Inside r_e	9.0	-25	-64
	7.5	-20	-38
	4.8	-14	-26

Table 3.11

C5 with C2 (≡ loading)

C2	Radius/cm (inner)	$\sigma r_i / 10^6 Nm^{-2}$ RADIAL	$\sigma r_i / 10^6 Nm^{-2}$ HOOP
Annealed	4.9	- 3.3	-17.7
	6.0	- 9.6	-28.8
	7.1	-14.5	-32.4
	8.2	- 4.2	-37.9
	9.0	-11.0	-36.4
	Radius/cm (outer)		
	18.0	- 3.7	- 4.7
	17.0	- 5.1	- 6.5
	16.0	- 7.3	- 8.6
	15.1	-11.6	-10.8
	14.1	-20.3	-19.4
	13.0	-22.1	-21.1
	12.1	-28.1	-26.6
C5	Radius/cm (inner)		
Non-annealed	4.9	-47.5	-12.8
	6.0	-29.2	-35.8
	7.1	-42.6	-41.6
	8.4	-46.1	-44.4
	9.4	-45.9	-46.0
	Radius/cm (outer)		
	18.0	- 1.5	- 2.0
	16.9	-10.1	- 8.0
	15.9	-11.1	-10.8
	14.8	-19.4	-16.7
	13.9	-25.5	-23.2
	12.9	-36.4	-40.8

B8	Radius/cm (inner)	$\sigma r/10^6 Nm^{-2}$ RADIAL	$\sigma r/10^6 Nm^{-2}$ HOOP
Annealed No LOAD applied	5.0	- 2.9	-22.9
	6.3	-16.1	-28.3
	7.6	- 1.0	-16.9
	8.9	-11.1	-26.8
	9.8	- 4.9	-20.8
	16.3	-19.2	- 7.5
	15.2	-16.0	- 9.6
	14.2	- 9.0	-16.2

Figure 3.12 : Special Series (based on Radial Readings)

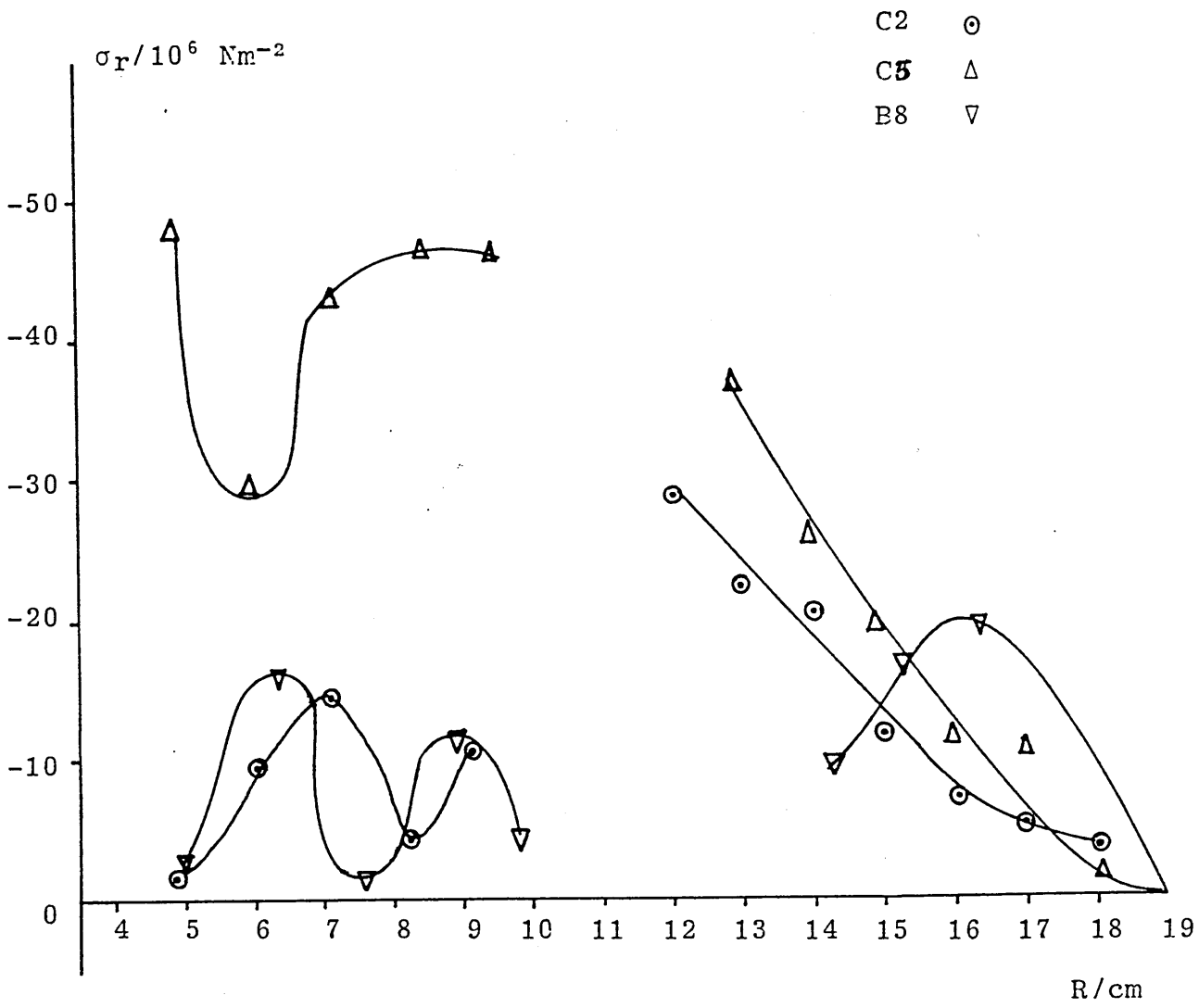

Figure 3.13 : Special Series (based on Hoop Readings)

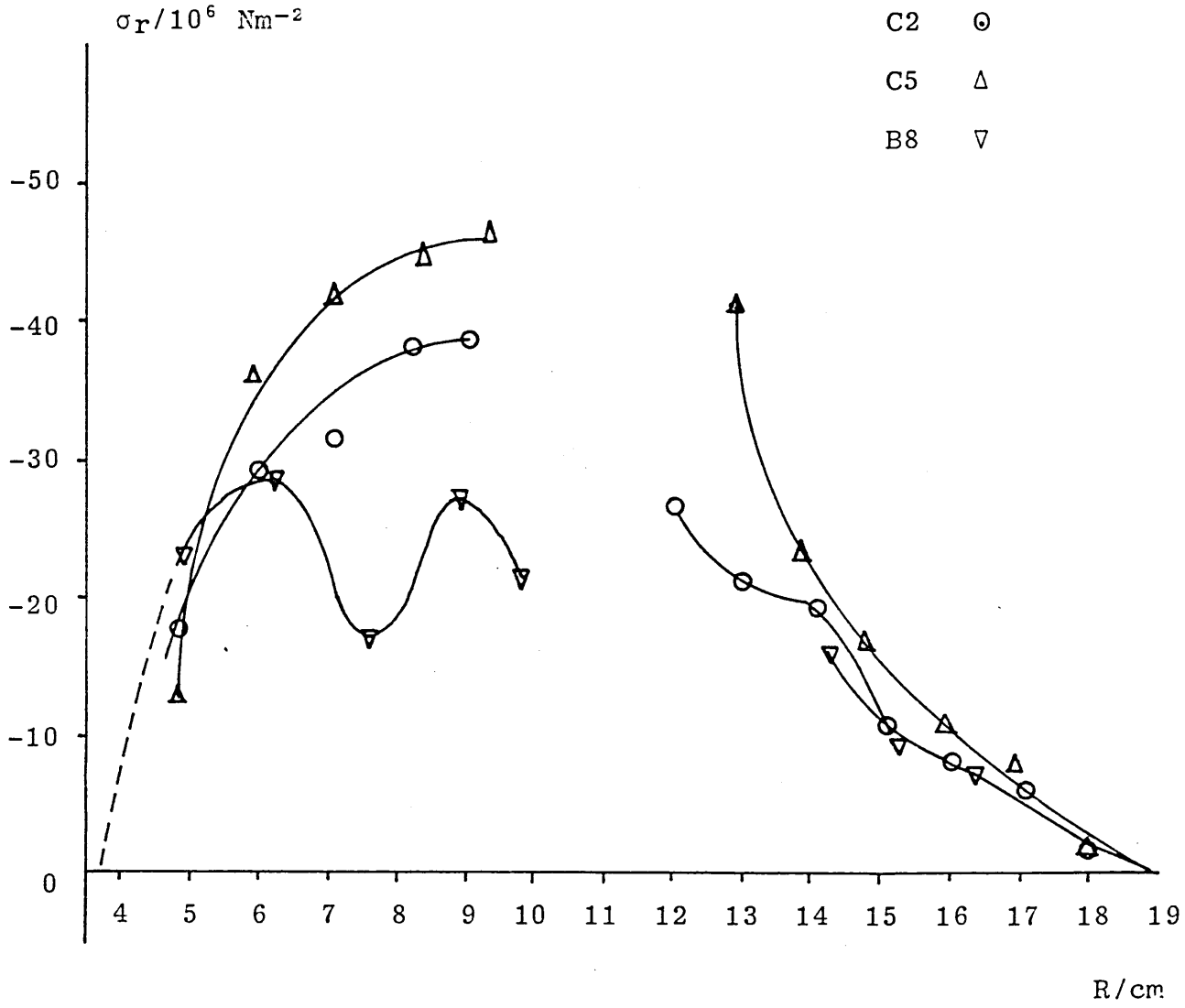

Figure 3.14 Comparison of Discs A7, B5 C2 and A3 based on Radial Readings

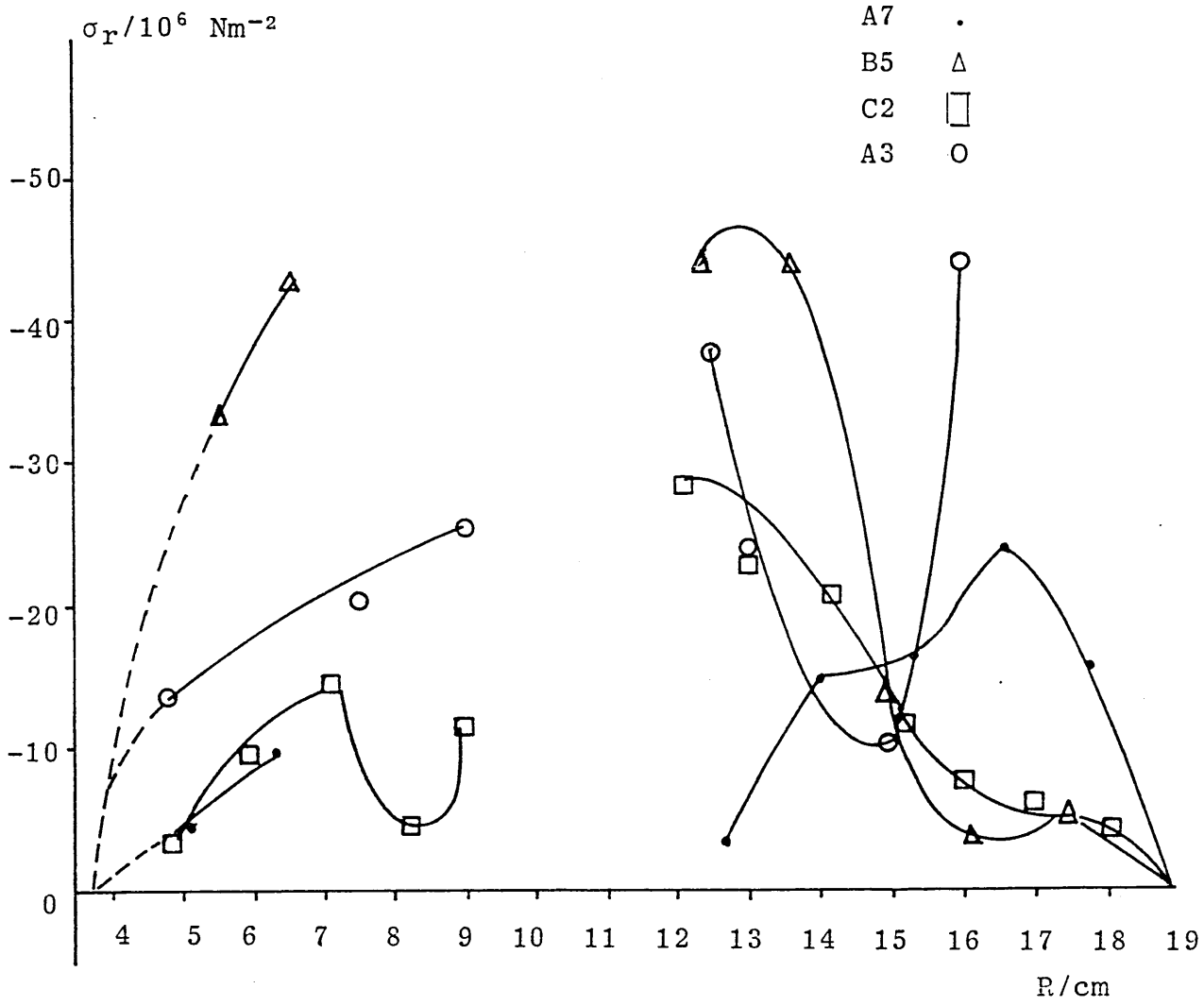

Figure 3.15 : Comparison of Discs A7, B5, C2 (based on Hoop Readings) and A3 (based on Radial Readings)

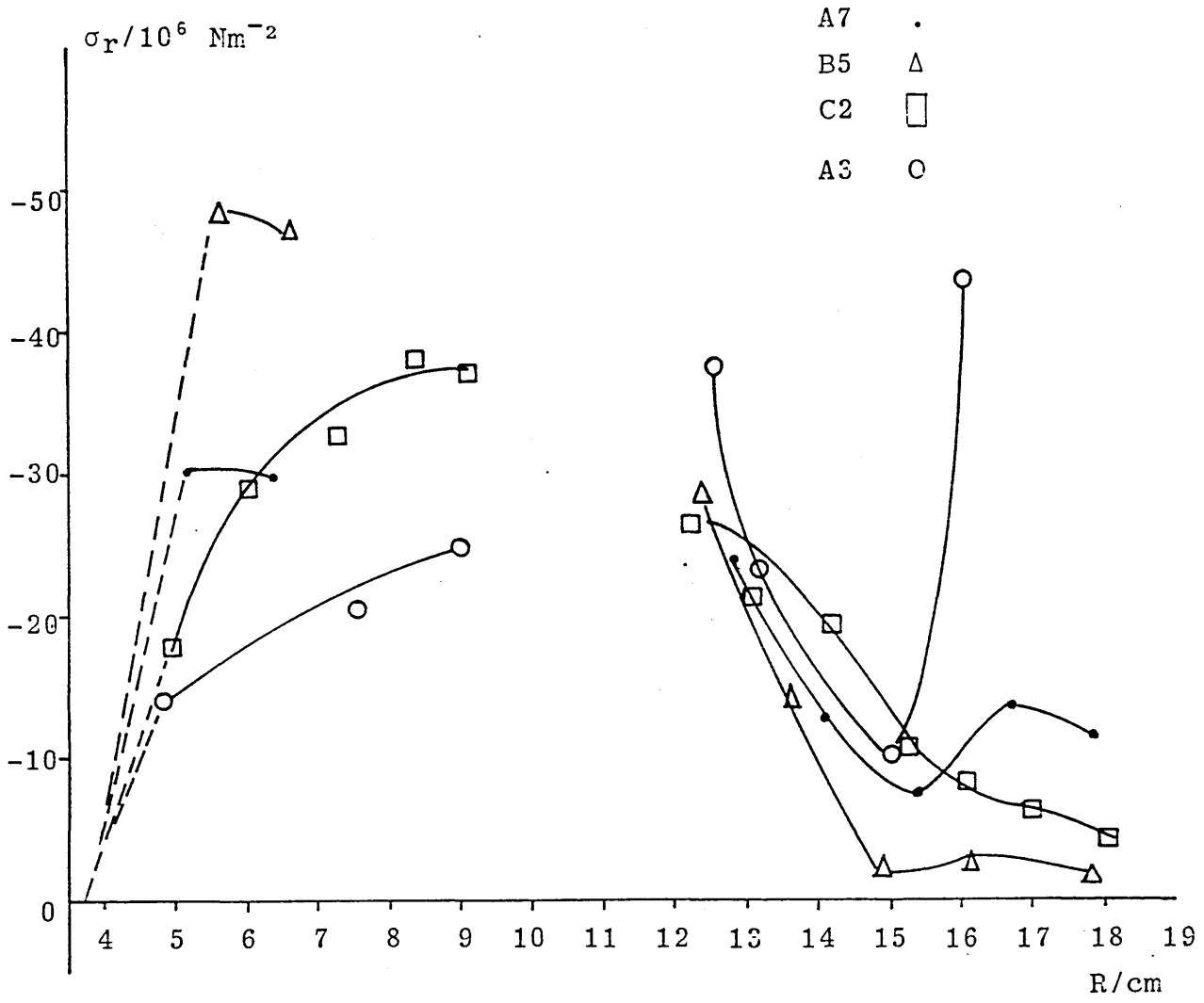

3.1.5 Comments

The following comments relate to the three main sections:

(i) Radial/Hoop residual stress at gauge positions - based on final inner/outer cut of disc (see Section 3.1.4.2).

(ii) Radial residual stress for A, B and C series (see Section 3.1.4.3).

(iii) Assessment of -

(a) the comparative accuracy between batches A, B and C (see Section 3.1.4.4),

(b) the boring out/turning procedure compared with 'cut out' strain gauge method (see Section 3.1.4.4),

(c) the effect of annealing (Section 3.1.4.4).

(i) Radial/Hoop residual stresses predicted by the measurement of strain at the final inner/outer cut of each disc have been plotted in Figures 3.4 and 3.5 for the A and B series.

For A series, the residual compressive radial stresses for both outer and inner zones show a progressive decrease with an increase of loading energy. In general, both the radial and hoop residual stresses are of a similar order of magnitude for each disc. The range of values of residual stress vary from 0 to 40 MN/m^2. The residual radial

stresses for both inner and outer radii are compressive whereas the residual hoop are tensile on the outer radii and compressive on the inner radii.

For B series, with increasing radius of the loading ring and constant load at the loading ring, the radial stress increases but the hoop stresses decrease (B1, B2 and B3). With increasing radius of the loading ring and constant load per unit length, the radial inner and outer stresses continue to increase as well as the hoop inner and outer (B3, B5 and B6). The radial inner and outer radii and the hoop inner are compressive whilst the hoop outer is tensile.

The B series show a range of values from 5 MN/m^2 (B3) to 70 MN/m^2 (B6).

(ii) Radial Residual Stresses predicted by the analysis of Section 3.1.3, and shown in Section 3.1.4.3 Figures 3.6 to 3.11.

A series (Figures 3.6, 3.7)
The two figures should give similar results since they both represent radial residual stresses for the A series of discs.

The radial stresses show two peaks in the outer regions of the discs and no peak at the inner loading boundary but the inner stresses tend to be

higher at the inner radial boundary than the outer loading boundary. The curves in the inner regions are based on a limited number of readings and therefore of reduced value. However, the residual radial stress readings range from 42.5 MN/m^2 to 5 MN/m^2 in the inner region and 30 MN/m^2 to 0 in the outer region. There is some evidence in the outer region of decrease in residual stress with increasing load.

B series (Figures 3.8, 3.9)

The two figures should indicate the same radial residual strains.

Note that B1, B2 and B3 represent radial residual stresses based on increasing loading radius with constant applied energy. B3, B5 and B6 represent radial residual stresses based on increasing loading radius with constant applied energy per unit length of loading circumference.

For B1, B2 and B3

The level of residual stresses in the region inside the loading ring band tend to be higher at the inner disc boundary and show a decrease towards the loading ring radius. In the outer regions, the radial stresses indicate that the main level of residual stress, with the exception of B1, is to be found at the loading ring boundary with a decrease to zero at the outer radius of the disc.

For B3, B5 and B6

The level of residual radial stress increases proportionately to the loaded ring position.

In general, the residual stresses in the inner regions show a maximum value of 55 MN/m^{-2} for B6 and tendency to reduce to 20 MN/m^{-2} at the outer radii of the discs.

C series (Figures 3.10, 3.11)

The residual radial stresses are shown in both figures and show a decrease to zero at the outer boundaries of the discs. The peak values of residual radial stress are to be found located at the boundaries of the loading rings with the exception of disc C1. The overall level of residual radial stress in the discs increases with increasing outer radii ranging from a compressive stress of 5 MNm^{-2} for the smallest outer radii (disc C4) to a compressive stress of 30 MNm^{-2} for the largest outer radii (disc C1). The residual radial stresses in the inner region tend to be higher just at the inner radial boundary of the discs and to show a decrease towards the loading ring boundary. The loading boundary remained constant in this series as well as the level of applied load and yet the inner radial residual stresses increased from compressive stresses of 10 MNm^{-2} to 45 MNm^{-2} with increasing size of disc.

(iii) (a) Assessment of comparative accuracy between batches A, B and C (Section 3.1.4.4) (Figures 3.14, 3.15)

By comparing the loading parameters of discs A7, B5, C2, it can be seen that they were subjected to similar loading conditions. (See Table 3.9 and Summary Table, 3.1)

Hence the residual stress profiles should be similar within the limits of experimental error. The curves show a comparative shape profile and within a range ±20 MN/m^2 a quantitative agreement.

(b) Assessment of boring out/turning down procedure compared with 'cut out' strain gauge method (Section 3.1.4.4) (Figures 3.14, 3.15)

The loading parameters of discs A7, B5, C2 were the same as those applied to disc A3, which received the individual strain gauge cut out procedure as described in Section 3.1.4.4 (ii). That being the case, an inspection of Figures 3.14 and 3.15 shows that there is close agreement between the curves with the exception of the outer radial boundary where the 'cut out' procedure for A3 shows a value of more than 40 MN/m^2 at a radius of 16 cm where the other discs (A7, B5, C2) show a lower value of the order of 10 MN/m^2.

(c) Effect of Annealing (Section 3.1.4.4)
(Figures 3.12, 3.13)
(Figures 3.8, 3.9)

These figures show a comparison between discs C2, C5 and B8, where C2 and C5 had similar loading conditions but C2 was annealed and C5 was not. Disc B8 was simply annealed and strain gauged and analysed with no load having been applied.

Hence, commencing with the unloaded annealed disc B8, it should be expected to produce low residual radial stress values which from the figures can be seen to range from a maximum of 28 MN/m^2 to a minimum of 1 MN/m^2. Disc C2 (annealed and loaded) shows a comparative shape with B8 and at the boundaries of the inner and outer radii a close agreement in magnitude. C5 shows a similar profile to C2 and B8 and with the exception of the inner radial residual stress based on the radial readings when there is a significant divergence of 40 MN/m^2 in places. It can be seen that the two loaded discs C2 and C5 begin to diverge from the unloaded disc when approaching the loading ring radius (11.33 cm). The values of residual radial stress have also been plotted on Figures 3.14 and 3.15 so that a comparison can be made with the other discs from the B series. An indication

from these figures is that the effect of loading on the discs only becomes apparent above a residual stress of 20 MN/m^2 and that the effect of loading is constrained to be within a short range of the loading ring.

3.2.1 Introduction

In this section the results of the quasi-static tests are described. Initial tests were carried out on cylindrical specimens machined from the disc material in order to obtain stress-strain characteristics. The second set of tests are the actual pre-stressing compression tests of the discs. The stress-strain results obtained from the test sample have been used to predict the stresses generated in the loaded discs, especially in the region of the elastic-plastic interface.

When a metal disc is compressed between two ring-shaped indentors under continuously increasing stress, it is first strained elastically, the relationship between stress and strain for radial and hoop components being expressed by the equations based on the theory of elasticity. With an increasing load, the material may be strained beyond the yield limit and permanent plastic strain will take place. The strain in the disc adjacent to the loading ring is then a combination of elastic and plastic components. With the release of the load, the elastic component is reduced to minimise the total stored energy and the material is left with a permanent plastic and residual elastic strain. In the present case where the loading is obtained by means of annular rings on the top and bottom surface of the discs, the amount of deformation in the region adjacent to the loading rings is constrained by a surrounding boundary of elastic material, and the total strain throughout is limited to be of the order of elastic strains.

3.2.2 The Derivation of an Experimental Stress Strain Constitutive Equation

(a) In order that the strain gauge readings from the experiments on the discs could be converted to an elastic-plastic stress behaviour, it was necessary to derive an empirical stress-strain law. This was based on compression tests carried out on cylindrical specimens prepared from the material of the discs. In general the empirical law was derived by considering the following two conditions -

(i) initial loading within elastic limit, and

(ii) plastic straining beyond the yield point.

(b) Compression tests were carried out on three mild steel specimens. The cylindrical specimens were each machined to 5 mm diameter and 5 mm long. They were set up in a 500 kN MAYES testing machine mounted in a special compression tool set. For the purpose of these tests, the maximum load range setting of the machine was restricted to 50 kN since fifty per cent reduction in height was obtained with a load of 25 kN. Two specimens were tested under dry lubrication conditions and the third was tested under lubricated conditions using tallow. The results can be seen from Figure 3.16a which shows that the effect of end lubrication in this case did not cause a significant change in the values of true stress with true strain.

(c) It should be noted that the method of carrying out the loading tests on the cylindrical samples correlated with the method used for loading the discs, i.e. an increasing load was applied to the test piece at a slow straining rate. The results were recorded in Tables, (eg Table 3.12).

Table 3.12

COMPRESSION TESTS ON (5 mm) x 5 mm LENGTH BILLET

(Steel taken from typical disc)

Load/ kN	Comp/ x 10^{-3}	l_f = (5-Comp) x 10^{-3}	$a_f/10^{-6}$	True Stress = Load/a_f x 10^9	l_c/l_f	$\varepsilon = \log_e\left(\frac{l_o}{l_f}\right)$
3.35	0.025	4.975	19.73	.17		5.0 x 10^{-3}
5.645	0.080	4.920	19.95	.28		16 x 10^{-3}
6.045	0.100	4.900	20.03	.30		20 x 10^{-3}
6.545	0.125	4.875	20.14	.32		25.3 x 10^{-3}
7.10	0.150	4.850	20.24	.35		30.4 x 10^{-3}
8.00	0.200	4.800	20.45	.39		40.8 x 10^{-3}
8.745	0.250	4.750	20.67	.42		51.3 x 10^{-3}
9.40	0.300	4.700	20.89	.45		62 x 10^{-3}
9.89	0.350	4.650	21.11	.47		72.5 x 10^{-3}
10.44	0.400	4.600	21.34	.49		83.4 x 10^{-3}
10.84	0.450	4.550	21.58	.50		94.3
11.30	0.500	4.500	21.82	.52		105
11.70	0.550	4.450	22.06	.53		116
12.10	0.600	4.400	22.31	.54		127.8
12.74	0.650	4.350	22.57	.56		139
13.14	0.700	4.300	22.83	.57		150.8
13.35	0.750	4.250	23.10	.58		162.5
13.57	0.800	4.200	23.37	.58		174
13.80	0.850	4.150	23.65	.58		186
14.20	0.900	4.100	23.94	.59		198
14.50	0.950	4.050	24.24	.60		210.7
14.85	1.000	4.00	24.54	.60		223.0
15.60	1.10	3.90	25.17	.62		248
16.30	1.20	3.80	25.83	.63		274
17.00	1.30	3.70	26.53	.64		301
17.75	1.40	3.60	27.27	.65		328.5
18.50	1.50	3.50	28.04	.66		356.7
19.20	1.60	3.40	28.87	.66		385.7
20.30	1.70	3.30	29.75	.68		415.5
21.00	1.80	3.20	30.67	.68		446.2
21.80	1.90	3.10	31.67	.69		478.0
22.60	2.00	3.00	32.74	.69		510.8
26.00	2.20	2.80	35.06	.74		
26.75	2.30	2.70	36.36	.74		
27.30	2.40	2.60	37.76	.72		
28.40	2.50	2.50	39.26	.72		

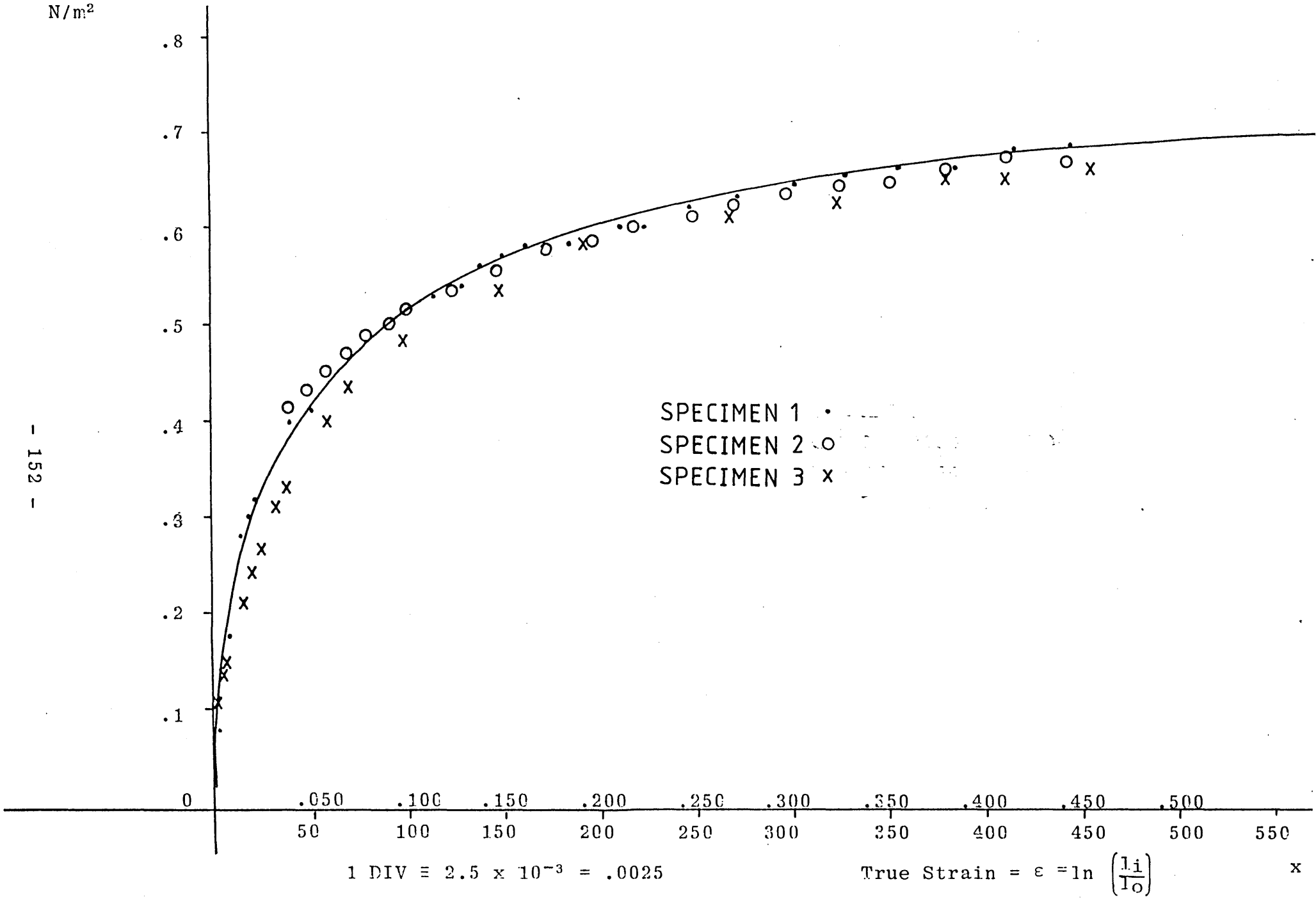
N/m²
.8
.7
.6
.5
.4
.3
.2
.1
0
.050
.100
.150
.200
.250
.300
.350
.400
.450
.500
50
100
150
200
250
300
350
400
450
500
550
x
SPECIMEN 1 •
SPECIMEN 2 o
SPECIMEN 3 x
1 DIV ≡ 2.5 x 10⁻³ = .0025
True Strain = ε = ln (li/lo)

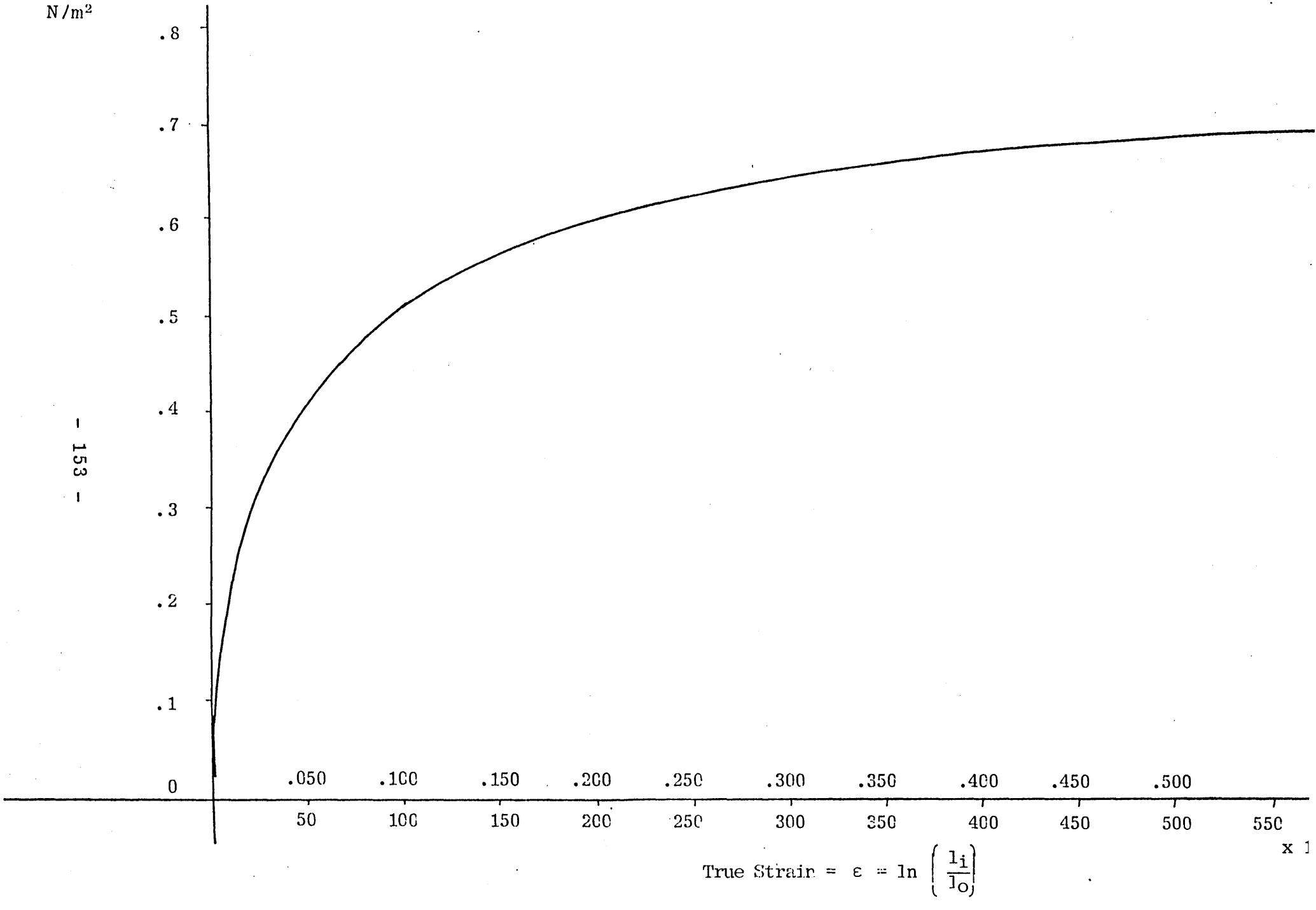
N/m²
.8
.7
.6
.5
.4
.3
.2
.1
0
.050
.100
.150
.200
.250
.300
.350
.400
.450
.500
50
100
150
200
250
300
350
400
450
500
550
x 1
True Strain = ε = ln (li/lo)

3.2.3 Derivation of Elastic-Plastic Constitutive Equation from Results

The true stress vs true strain curve obtained for the disc material could be expressed by means of two constitutive equations to describe the elastic-plastic behaviour.

In the elastic region, the relation between true stress and true strain is linear and of the form $\sigma = E\varepsilon$, where σ = true stress, ε = true strain and E = elastic modulus for the material. From Fig 3.16b obtained from the compression tests, the limit of proportionality and therefore the elastic behaviour was assessed to be 2×10^8 Nm^{-2}. It was decided to use a calculated value of strain of 1×10^{-3} since up to this point the experimental results had proved to be linear.

The value obtained from the graph for the limit of proportionality was thus taken to be the Yield Point of the material tested, i.e. $\sigma_0 = 2 \times 10^8$ Nm^{-2}.

For the plastic region of strain, a constitutive equation of the form $\sigma = \sigma_0 + A\varepsilon^n$ was assumed, where

σ = True stress

σ_0 = Yield stress

ε_p = True strain

A and n are constants

To obtain a good fit for the experimental curve pairs of values of true stress and true strain were used from the experimental graph and the best fit for three ranges of the experimental curve were obtained in the manner described as

follows:

(i) Low strain range : ε from .016 to .025

$$\sigma = 2 \times 10^8 + 32.7 \times 10^8 (\varepsilon)^{.898}$$

(ii) Intermediate strain range : ε from .016 to .210

$$\sigma = 2 \times 10^8 + 10.6 \times 10^8 (\varepsilon)^{.625}$$

(iii) Extended strain range : ε from .020 to .545

$$\sigma = 2 \times 10^8 + 6.7 \times 10^8 (\varepsilon)^{.487}$$

In relation to the range of strain values obtained experimentally from the loaded discs, the best fit is represented by the equation (i) which is valid for strains greater than 1×10^{-3} and less than 25×10^{-3}.

A comparison of experimentally derived stress values and those predicted by the empirical law is shown against strain values in the low range.

$\varepsilon/10^{-3}$	σ derived for low 10^9 Nm^{-2}	σ experiment $/10^9$ Nm^{-2}
5	.22	.17
16	.28	.28
20	.29	.30
30	.34	.35
40	.38	.39
50	.42	.42

Sample Calculation

For relatively low values of strain $\sim 1 \times 10^{-2}$

$$\sigma = \sigma_0 + A(\varepsilon)^n$$

$$2.8 \times 10^8 = 2 \times 10^8 + A(.016)^n$$

$$3.2 \times 10^8 = 2 \times 10^8 + A(.025)^n$$

$$A(.016)^n = .8 \times 10^8$$

$$A(.025)^n = 1.2 \times 10^8$$

$$\log A + n\log(.016) = \log .8 \times 10^8 = 7.903$$

$$\log A + n\log(.025) = \log 1.2 \times 10^8 = 8.079$$

$$n\{\log(.025) - \log(.016)\} = 0.176$$

$$n[-1.60 + 1.795] = 0.176$$

$$n[.196] = 0.176$$

$$n = .898$$

$$\log A = 7.903 - .898\log(.016)$$

$$= 7.903 + 1.612$$

$$= 9.515$$

$$A = 32.7 \times 10^8$$

$$\therefore \text{Law} \quad \sigma = \sigma_0 + 32.7 \times 10^8 \, (\varepsilon)^{.898}$$

3.2.4 Summary of Method used to obtain Stress Values from Strain Gauge Readings

Strain Gauge Measurement from a Rectangular Rosette

The essential parameters are stated without derivation since they are the basis for the programme and the typical test calculations of the conversion of the experimental mV readings to principal strains and stresses. By this means a check on the validity of the calculated stresses and strains produced by the programme has been obtained.

(a) Calculation for one active gauge

(Symbols have usual meanings if not stated)

$$\text{Strain } \varepsilon = \frac{4V}{Ek}$$

where V = voltage obtained from gauge

E = excitation voltage

k = gauge factor

(b) $$\varepsilon_{max} = \frac{\varepsilon_\alpha + \varepsilon_\gamma}{2} + \frac{1}{2}\sqrt{(\varepsilon_\alpha - \varepsilon_\gamma)^2 + [2\varepsilon_\beta - (\varepsilon_\alpha + \varepsilon_\gamma)]^2}$$

(c) $$\varepsilon_{min} = \frac{\varepsilon_\alpha + \varepsilon_\gamma}{2} - \frac{1}{2}\sqrt{(\varepsilon_\alpha - \varepsilon_\gamma)^2 + [2\varepsilon_\beta - (\varepsilon_\alpha + \varepsilon_\gamma)]^2}$$

(d) Angle that principal planes make with gauge 1

N.B. Positive if in direction of numbered gauges

$$\alpha_p = \frac{1}{2} \tan^{-1} \frac{2\varepsilon_\beta - (\varepsilon_\alpha + \varepsilon_\gamma)}{\varepsilon_\alpha - \varepsilon_\gamma}$$

(e) $$\beta_{max} = \sqrt{(\varepsilon_\alpha - \varepsilon_\gamma)^2 + [2\varepsilon_\beta - (\varepsilon_\alpha + \varepsilon_\gamma)]^2}$$

(f) $$\sigma_{max} = \frac{E}{2} \left[\frac{\varepsilon_\alpha + \varepsilon_\gamma}{1 - \nu} + \frac{1}{1 + \nu} \sqrt{(\varepsilon_\alpha - \varepsilon_\gamma)^2 + [2\varepsilon_\beta - (\varepsilon_\alpha + \varepsilon_\gamma)]^2} \right]$$

(g) $$\sigma_{min} = \frac{E}{2} \left[\frac{\varepsilon_\alpha + \varepsilon_\gamma}{1 - \nu} - \frac{1}{1 + \nu} \sqrt{(\varepsilon_\alpha - \varepsilon_\gamma)^2 + [2\varepsilon_\beta - (\varepsilon_\alpha + \varepsilon_\gamma)]^2} \right]$$

(h) $$\tau_{max} = \frac{E}{2(1 + \nu)} \sqrt{(\varepsilon_\alpha - \varepsilon_\gamma)^2 + [2\varepsilon_\beta - (\varepsilon_\alpha + \varepsilon_\gamma)]^2}$$

3.2.5 Programme Format for producing Stress Values from Strain Gauge Values

1. Calculate for elastic conditions ε_{max}, ε_{min}, σ_{max}, σ_{min}.

2. Calculate $\bar{\sigma}_e \equiv$ effective, generalized or equivalent elastic stress $= \sqrt{\sigma_1{}^2{}_e - \sigma_{1e}\sigma_{2e} + \sigma_2{}^2{}_e}$

3. Calculate $\bar{\varepsilon}_e \equiv$ effective strain $= \bar{\sigma}_e / E$

4a. Condition if $\bar{\varepsilon}_e < 1 \times 10^{-3}$ - Print $\bar{\sigma}_e$ from 2.

4b. Condition if $\bar{\varepsilon}_e > 1 \times 10^{-3}$

calculate new $\bar{\sigma}_e = 2 \times 10^8 + 32.7 \times 10^8 \times (\varepsilon_e)^{.898}$

AND PRINT

5. Calculate $\varepsilon_{max} = \frac{\sigma_{max}}{Y}$ and $\varepsilon_{min} = \frac{\sigma_{min}}{Y}$

6. Condition $\varepsilon_{max} > 1 \times 10^{-3}$

   Calculate $\bar{\sigma}_{ep_{max}} = 2 \times 10^{8} + 32.7 \times 10^{8} \times (\varepsilon_{max})^{.898}$

   AND PRINT

   Condition $\varepsilon_{max} < 1 \times 10^{-3}$ then Print $\sigma_{e_{max}}$

7. Condition $\varepsilon_{min} > 1 \times 10^{-3}$

   Calculate $\bar{\sigma}_{ep_{min}} = 2 \times 10^{8} + 32.7 \times 10^{8} \times (\varepsilon_{min})^{.898}$

   AND PRINT

   Condition $\varepsilon_{min} < 1 \times 10^{-3}$ then Print σ_{min}

8. Calculate $\bar{\sigma}_{ep}$ = effective elastic-plastic stress 2

$$= \sqrt{\sigma_1{}^2{}_{ep} - \sigma_{1_{ep}}\sigma_{2_{ep}} + \sigma_2{}^2{}_{ep}}$$

9. A comparison of $\bar{\sigma}_e$ and $\bar{\sigma}_{ep}$ may be made to indicate the reduction produced by the effective stress criterion for plastic deformation compared with the assumption of only elastic deformation.

3.2.6 Example of Experimental Evaluation Tables used in Formulating Results for Graphical Display

1) The strain gauge mV readings were processed for each load value as shown in Table 3.13.

2) The corrected mV readings were then inserted into the programme with format as shown in Section 3.2.7.

3) The extracted results from the programme print-out were tabulated, as shown, again for each load value.

Table 3.13

STRAIN GAUGE EVALUATION

Load = 1500 kN, Load increasing.

Gauge	Radial (G1)			Angle (G2)			Hoop (G3)		
	Zero /mV	Exp /mV	Correct /mV	Zero /mV	Exp /mV	Correct /mV	Zero /mV	Exp /mV	Correct /mV
A	-3.63	-3.30	+ .33	-4.90	-4.36	+ .54	-1.20	- .09	+1.11
B	-1.08	- .72	+ .36	-4.56	-4.16	+ .40	-4.86	-4.58	+ .28
C	-5.20	-5.25	- .05	-3.10	-2.74	+ .36	-4.30	-3.10	+1.20
D	+0.05	+ .69	+ .64	-4.69	-3.78	+ .91	-3.14	-2.18	+ .96
E	-4.09	-4.26	- .17	-4.95	-4.83	+ .12	-3.56	-2.49	+1.07
F	-3.59	-3.78	- .19	-4.57	-4.90	- .33	-4.33	-3.79	+ .54
G(u)	-5.56	-5.07	+ .49	-3.41	-2.12	+1.29	-3.99	-4.15	- .16
H	-5.53	-4.45	+1.08	-2.64	-2.68	- .04	-4.03	-5.39	-1.36
J	-1.73	- .80	+ .93	-2.42	-3.12	- .70	-4.62	-6.56	-1.94
K	-2.18	-1.80	+ .38	-6.20	-6.52	- .32	-4.55	-5.10	- .55
L	-2.63	-2.30	+ .33	-3.76	-3.84	- .08	-3.38	-3.98	- .60
M	-1.54	-1.26	+ .28	-5.61	-5.75	- .14	-0.65	-1.12	- .47
N	-7.06	-6.77	+ .29	+2.00	+1.02	- .98	+1.14	+ .78	- .36
P	+0.68	+1.44	+ .76	-1.19	-1.03	+ .16	-5.45	-6.36	- .91
Q(u)	-1.75	-1.01	+ .74	-1.24	-2.56	-1.32	-1.95	-3.85	-1.90

B.V. = 5.08V

G.F. = 2.11

Ring I/D = 200 mm

Ring O/D = 212 mm

Table 3.14

STRAIN GAUGE EVALUATION

Using Elastic-Plastic Evaluation (Disc D3)

Load 1500 kN, Load increasing.

Gauge	Distance of Gauge from Loading Ring/mm	Angle Max. Strain makes with radial gauge/0	RADIAL	HOOP	RADIAL	HOOP
			ε_{max} 10^{-3}	ε_{min} 10^{-3}	σ_{max} $10^{6}Nm^{-2}$	σ_{min} $10^{6}Nm^{-2}$
A	5.5	12.38	-.507	-.260	-101.42	- 52.10
B	5.0	31.71	-.196	-.144	-39.25	- 28.98
C	30.0	9.49	-.496	-.116	-99.25	- 23.36*
D	5.0	-17.25	-.482	-.370	-96.44	- 74.15
E	20.0	14.01	-.441	-.038	-88.30	- 7.65
F	5.0	27.07	-.272	-.085	-54.43	- 17.11
G(u)	5.0	36.94	-.424	-.248	-84.82	-49.63
H	5.5	2.34	-.276	+.426	-55.35	+ 85.20
J	5.0	-3.86	-.146	+.684	-29.29	+ 136.98
K	5.0	-13.40	-.104	+.194	-20.84	+ 38.97
L	23.0	3.37	-.062	+.206	-12.48	+ 41.27**
M	32.0	-3.42	-.057	+.159	-11.55	+ 31.81
N	44.0	-35.5	-.268	+.305	-53.64	+ 61.10
P	5.0	7.85	-.209	+.288	-41.80	+ 57.79
Q(u)	5.0	-14.63	-.125	+.743	-25.03	+148.72

* Inner ** Outer

Loading Ring Thickness = 6.0 mm

Ring I/D = 200 mm

Ring O/D = 212 mm

Notes

1) Distance of gauge from loading ring refers to mid-point of gauge to ring edge nearest to gauge.
2) Gauges inside ring : A, B, C, D, E, F, G(u)
3) Gauges outside ring : H, J, K, L, M, N, P, Q(u)
4) Note Positive values represent Tensile
   Negative values represent Compressive

3.2.7 Summary of Experimental Loading Criteria and Disc Parameters

The experimental work based on static loading conditions utilised four mild steel discs to which annular rings on the top and bottom surfaces were placed in contact. The annular rings provided the load transmission path between the loading press and the disc surface.

The disc and annular ring dimensions were as follows:

Disc Parameters

All discs are circular with a hole in the centre.

Outer diameter = 380 mm ≡ (a)

Inner diameter = 76 mm ≡ (b)

Thickness = 6.3 mm

Table 3.15

Loading Rings : Breadth = 6.3 mm : Depth = 6.3 mm

(a) D1	Outer diameter = 152.6 mm Inner diameter = 140.6 mm	Outer radius = 76.3 mm Inner radius = 70.3 mm
(b) D2	Outer diameter = 214.6 mm Inner diameter = 202.0 mm	Outer radius = 107.3 mm Inner radius = 101.0 mm
(c) D3	Outer diameter = 212 mm Inner diameter = 200 mm	Outer radius = 106 mm Inner radius = 100 mm
(d) D4	Outer diameter = 273 mm Inner diameter = 261 mm	Outer radius = 136.5 mm Inner radius = 130.5 mm

Table 3.16

Disc	Mean Radius of Loading ring/m	Area of Contact/m^2	Max Load /kN	Min Load /kN	σ_{max}/Nm^{-2} / σ_{min}/Nm^{-2}
D1	73	2.76×10^{-3}	2000	250	$7.2 \rightarrow .9 \times 10^8$
D2	103	3.88×10^{-3}	2500	500	$6.44 \rightarrow 1.28 \times 10^8$
D3	103	3.88×10^{-3}	2300	100	$5.9 \rightarrow .26 \times 10^8$
D4	133	5.03×10^{-3}	2500	250	$4.9 \rightarrow .5 \times 10^8$

Table 3.17 : Showing comparison of discs with equivalent stress at loading surface

Disc	Load/kN	Area/m^2	Stress/Nm^{-2}
D1	1380	2.76×10^{-3}	5×10^8
D2 and D3	1940	3.88×10^{-3}	5×10^8
D4	2500	5.03×10^{-3}	5×10^8
D1	828	2.76×10^{-3}	3×10^8
D2 and D3	1164	3.88×10^{-3}	3×10^8
D4	1509	5.03×10^{-3}	3×10^8
D1	552	2.76×10^{-3}	2×10^8
D2 and D3	776	3.88×10^{-3}	2×10^8
D4	1006	5.03×10^{-3}	2×10^8

3.2.8 Experimental Graphs

The graphs showing the experimental results :

Indicate -

(i) A general shape of stress vs distance from centre of discs.

(ii) Radial and Hoop Stress for discs D1, D2, D3 and D4.

(iii) A comparison of two discs D1 and D3 with equivalent stress for different loads (see Table 3.17)

(iv) Stress vs Load for discs D1, D3 and D4.

Figure 3.17 : Summary - General Shape of Stress vs Distance from Centre of Discs

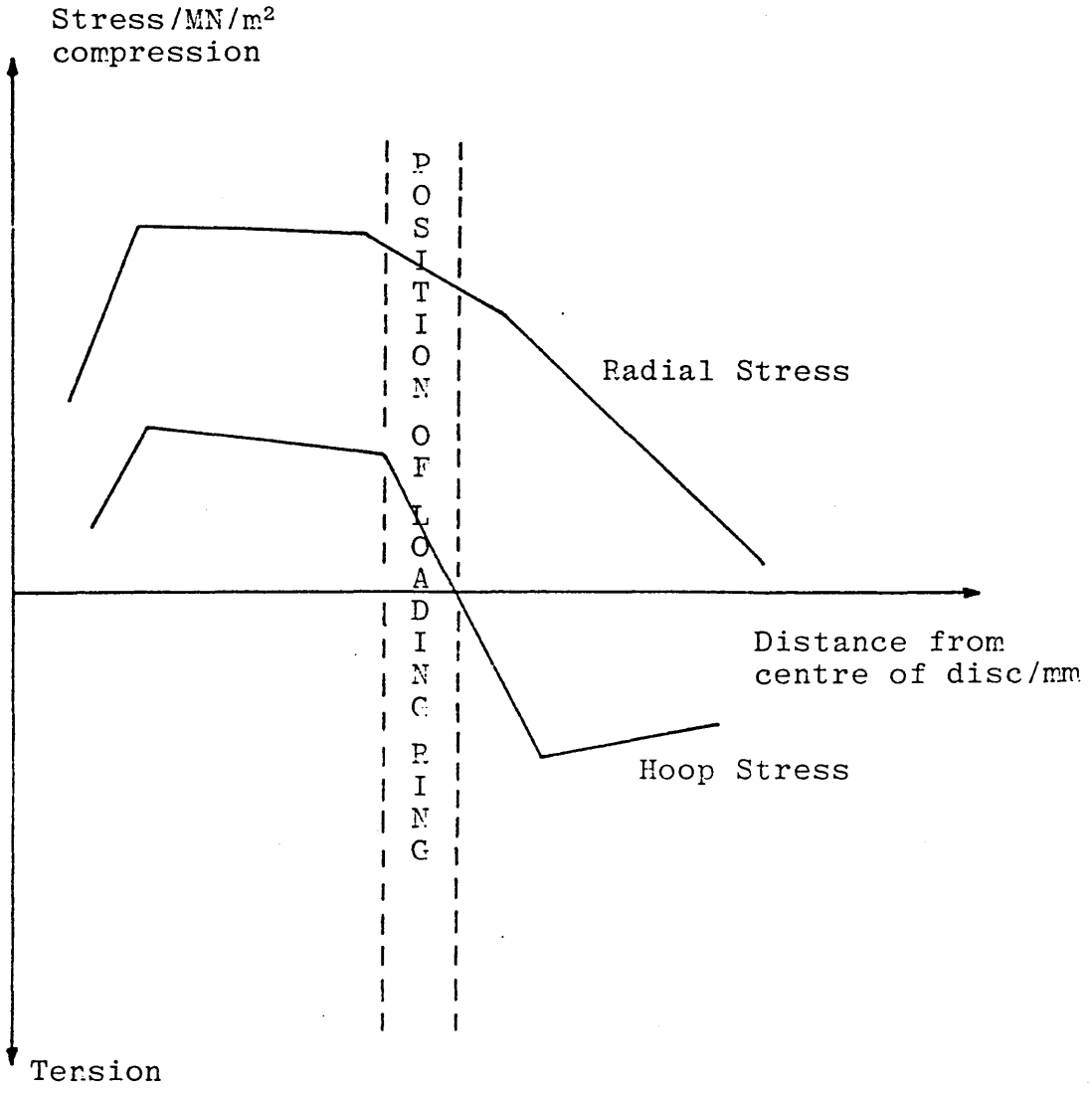

Figure 3.18 : Loading and Residual Stresses for D1

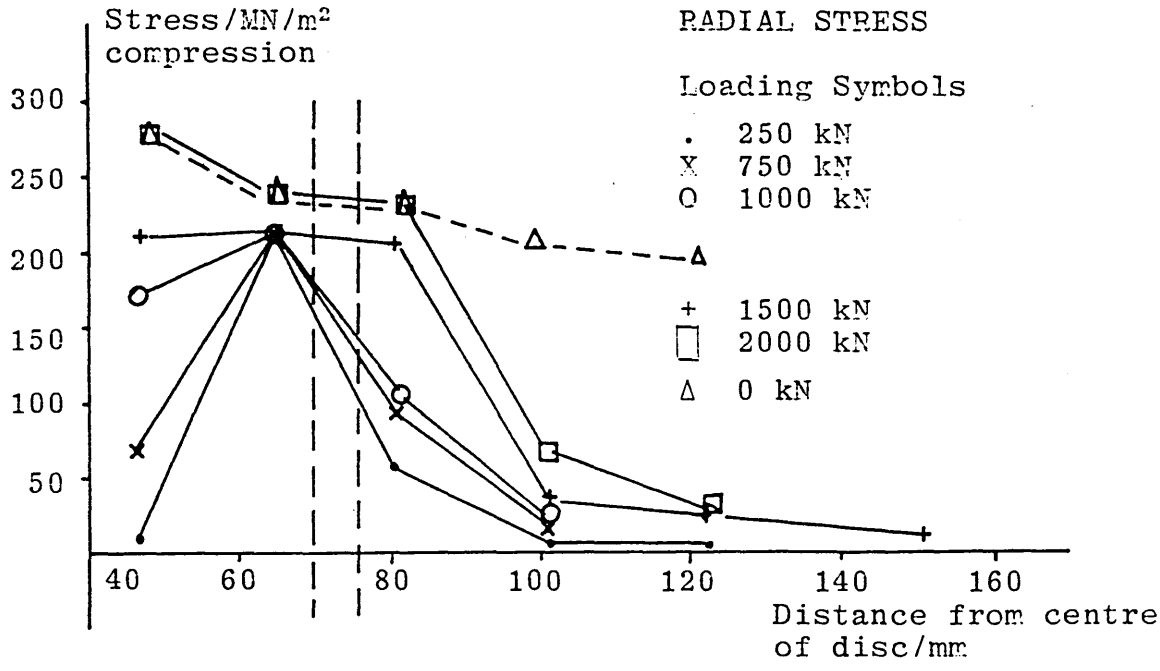

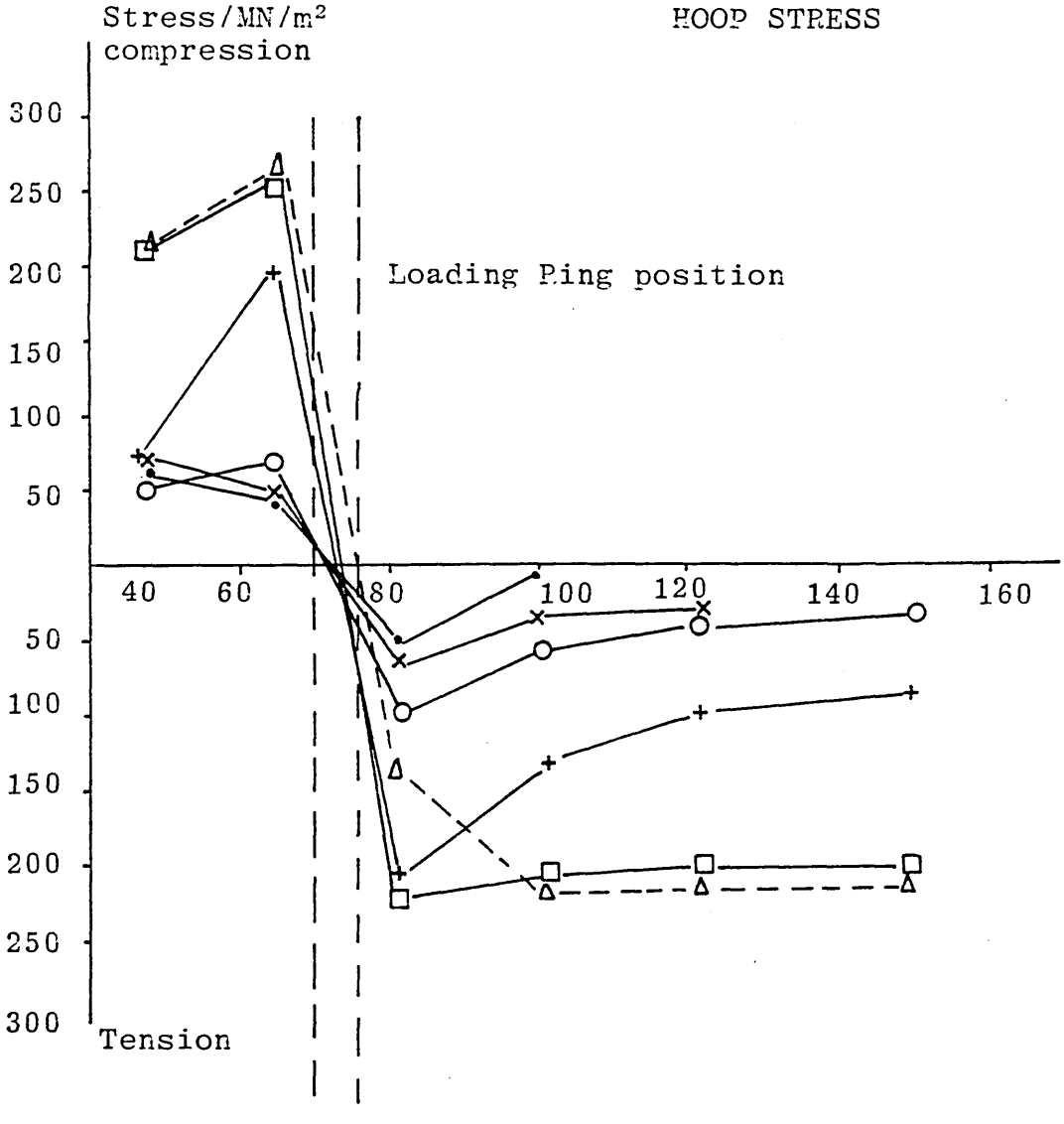

Figure 3.19 : Loading and Residual Stresses for D2

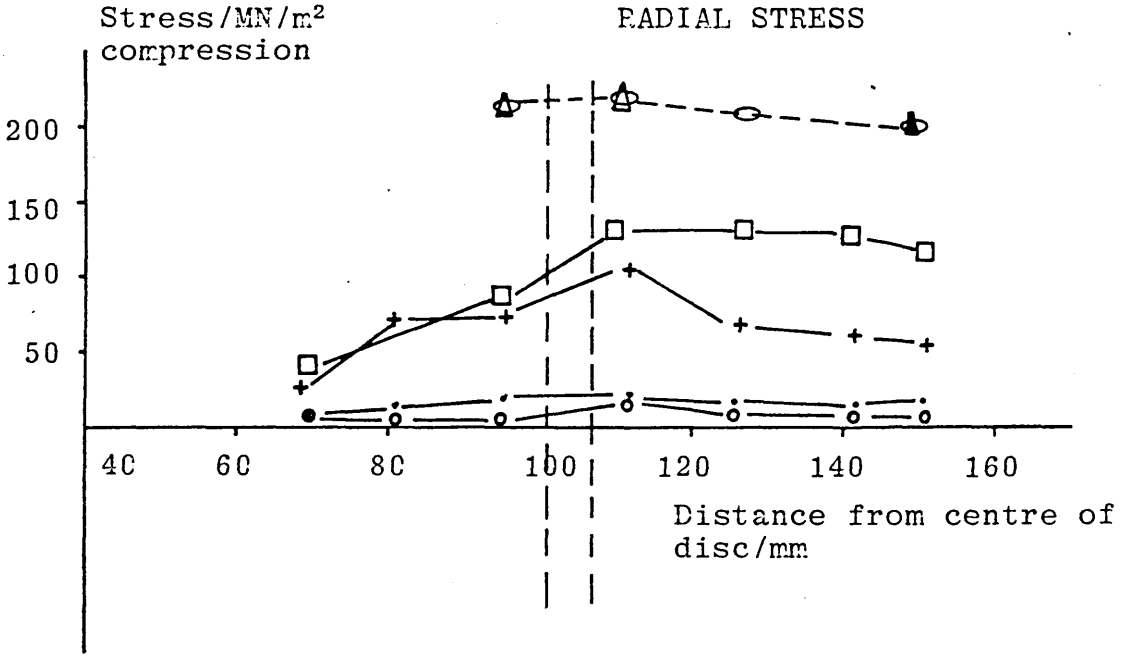

Loading Symbols

.	500 kN	⬭	2500 kN
O	1000 kN	Δ	0 kN
+	1500 kN		
□	2000 kN		

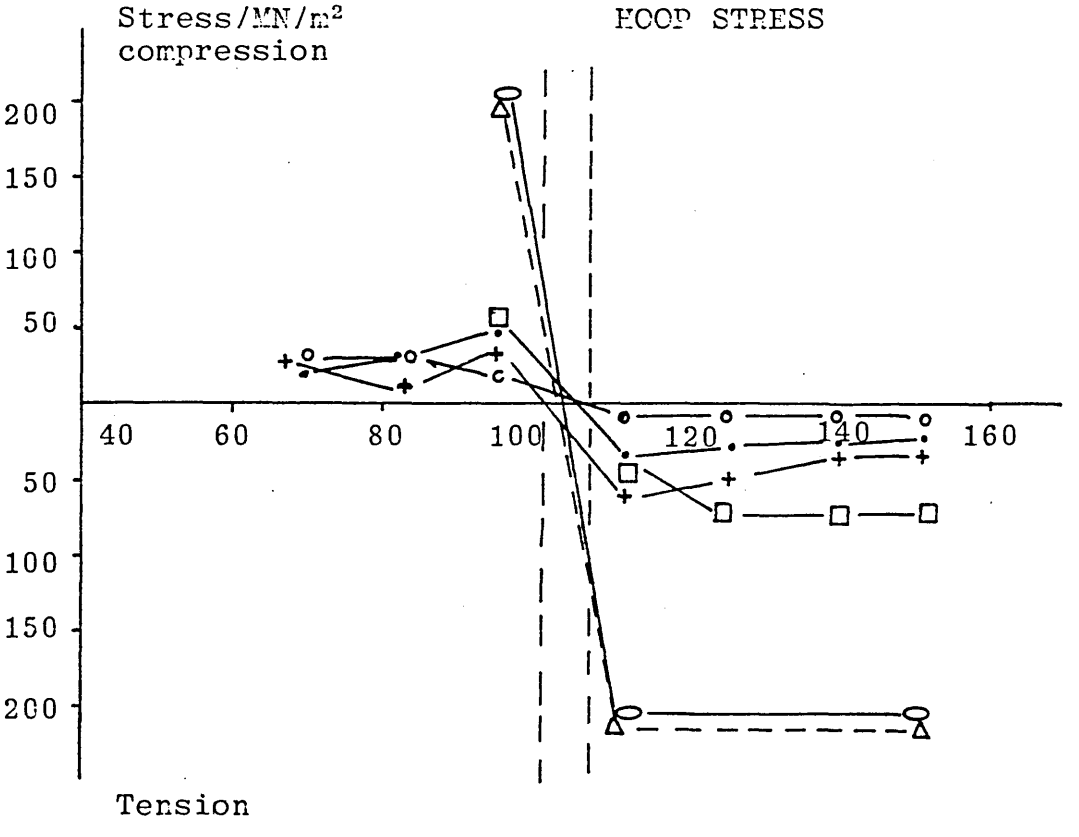

Figure 3.20 : Loading and Residual Stresses for D3

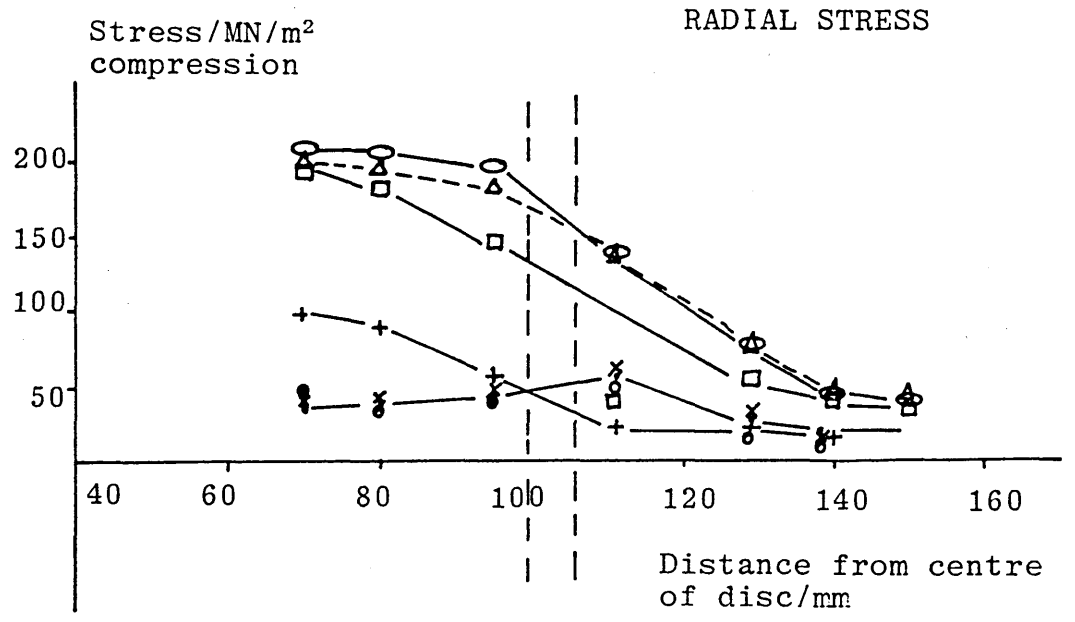

Loading Symbols

.	500 kN	□	2000 kN
X	750 kN	⬭	2300 kN
O	1000 kN		
+	1500 kN	Δ	0 kN

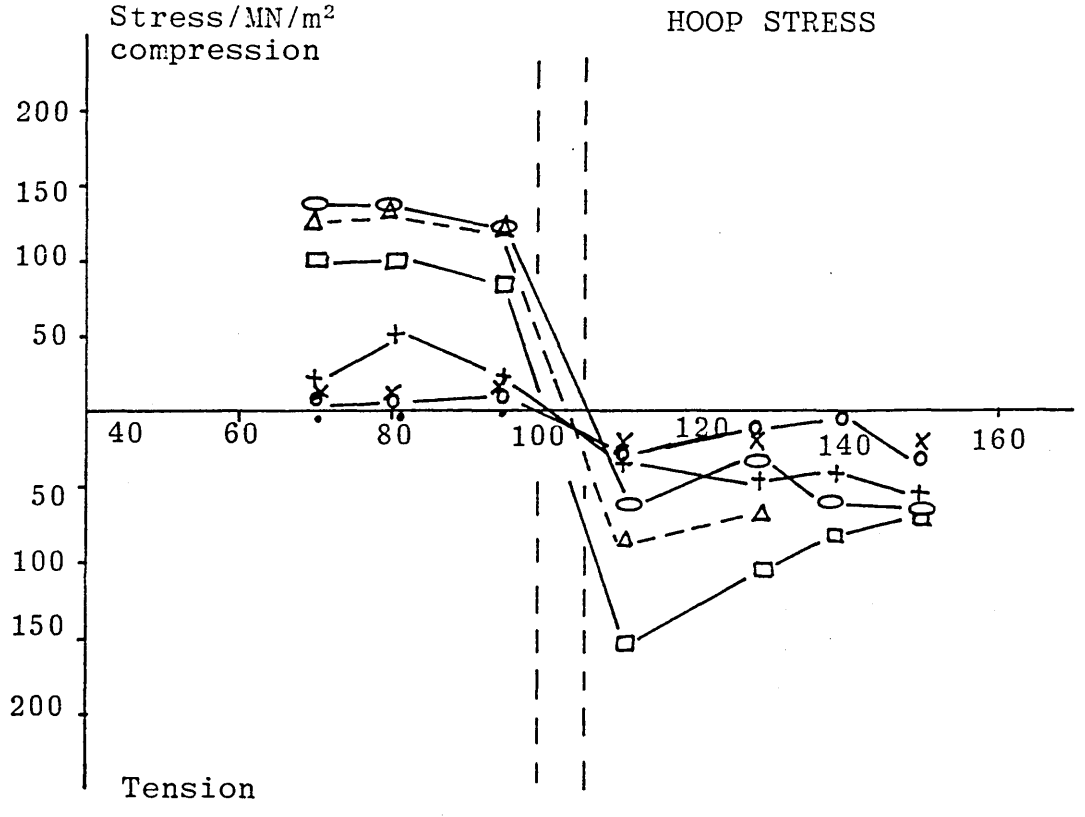

Figure 3.21 : Loading and Residual Stresses for D4

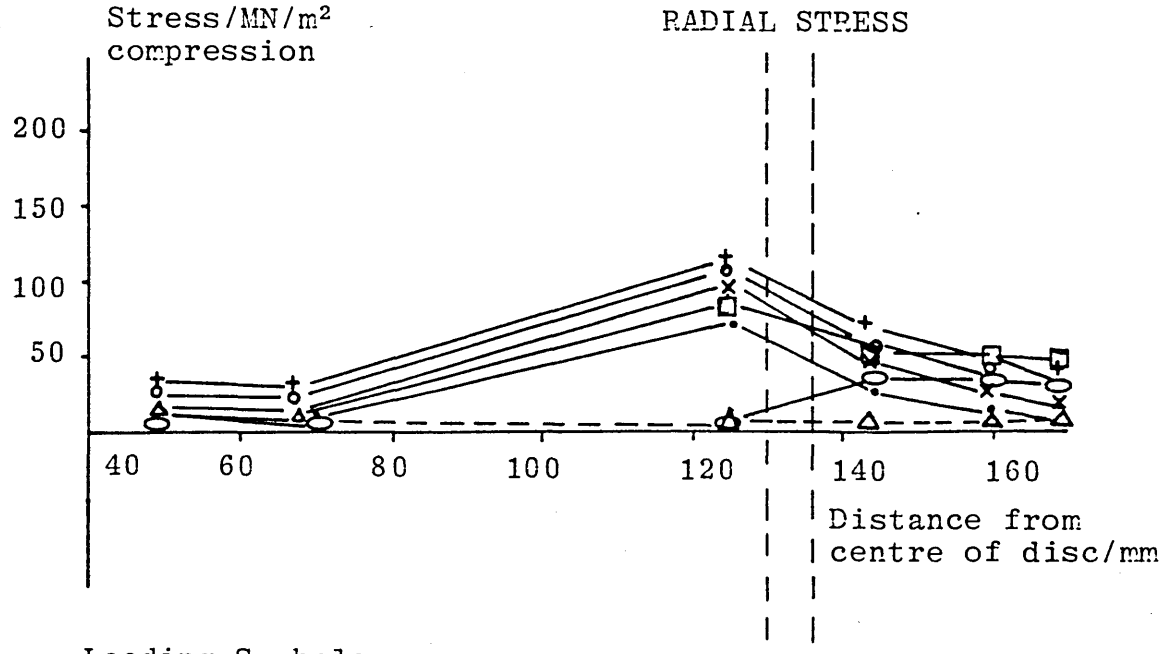

Loading Symbols

.	250 kN	□	2000 kN
X	750 kN		
O	1000 kN	⬭	2500 kn
+	1500 kN	Δ	0 kN

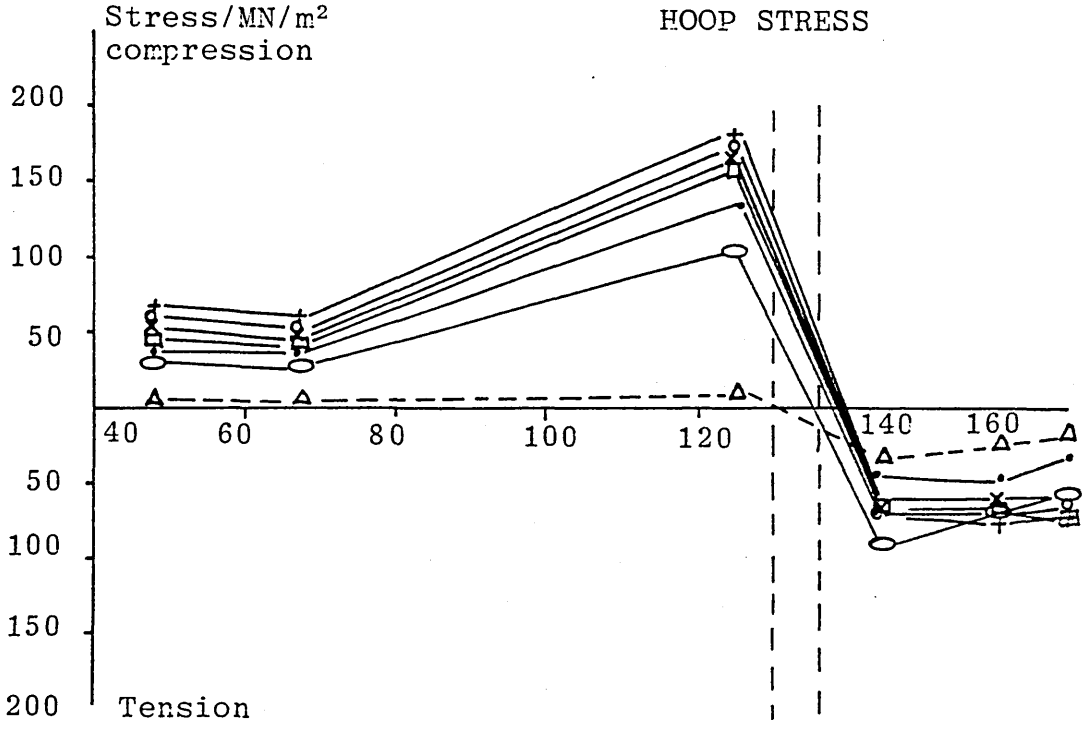

Disc D1 with a load of 1400 kN should give an equivalent stress to disc D3 with a load of 2000 kN (see Table 3.17).

Figure 3.22 : Comparison of D1 (1400 kN) with D3 (2000 kN)

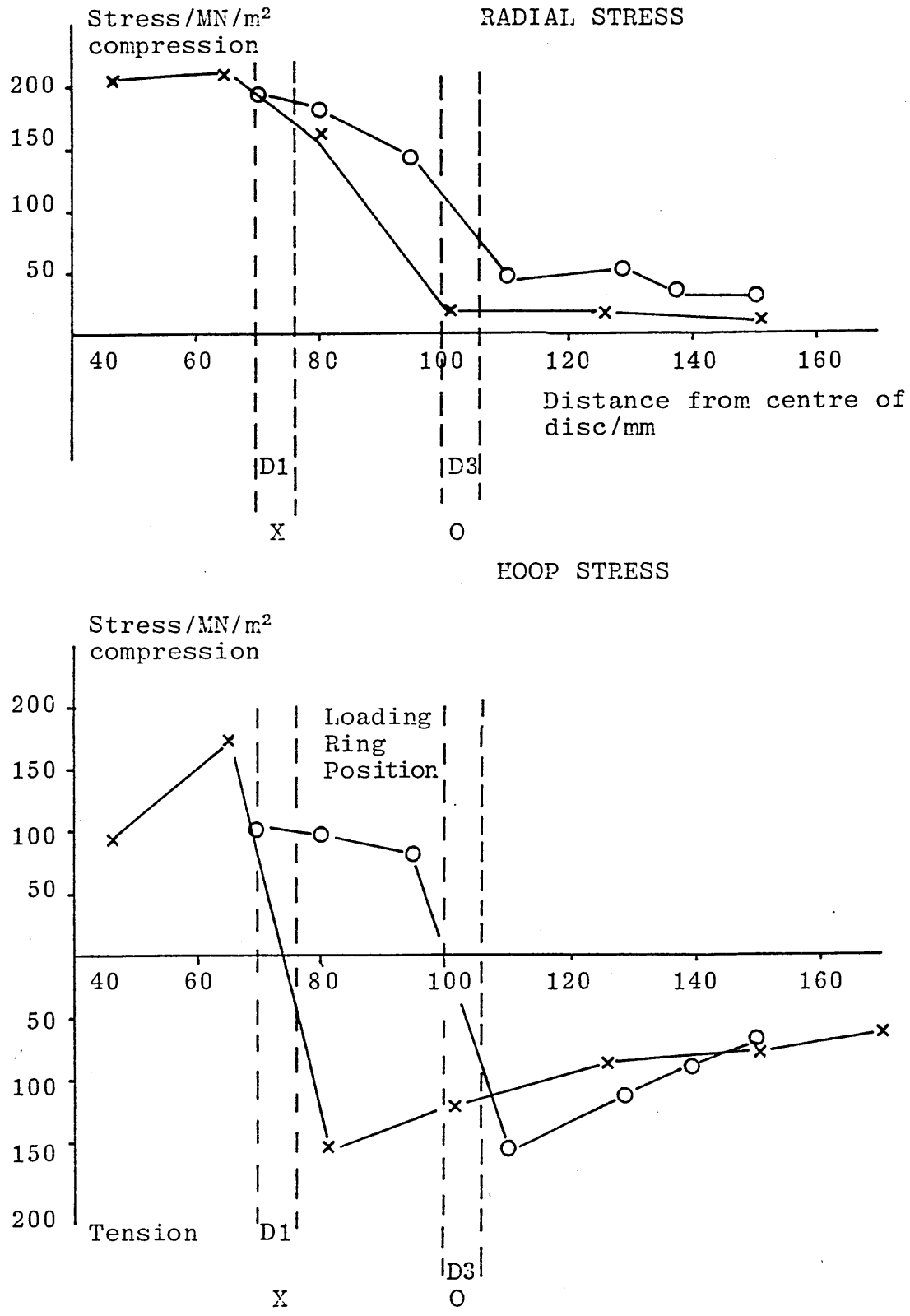

Figure 3.23 : Stress vs Load for Disc D1

Comparison of Gauge Reading Adjacent to Inner and Outer Position at Loading Ring

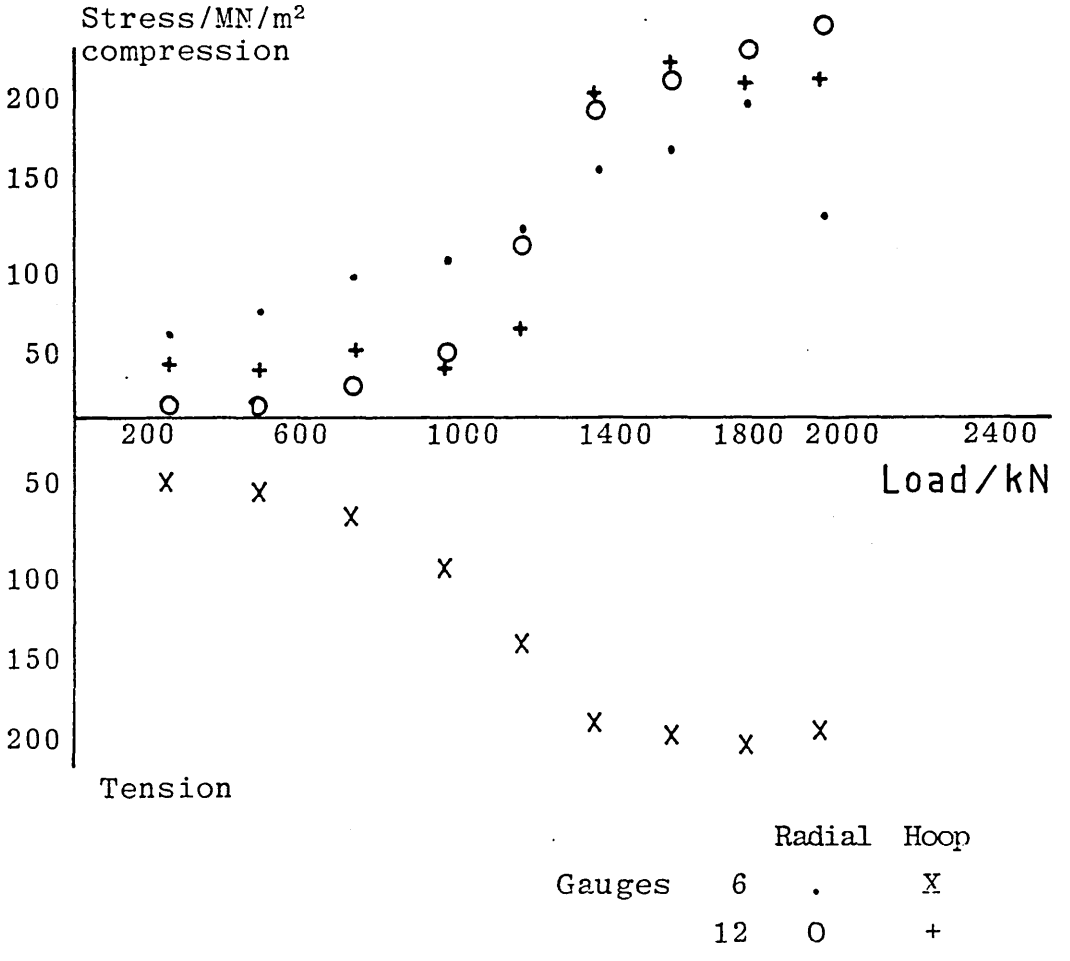

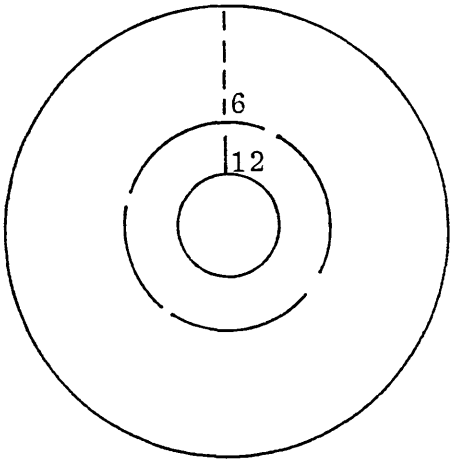

Figure 3.24 : Stress vs Load for Disc D3

Comparison of Gauge Accuracy

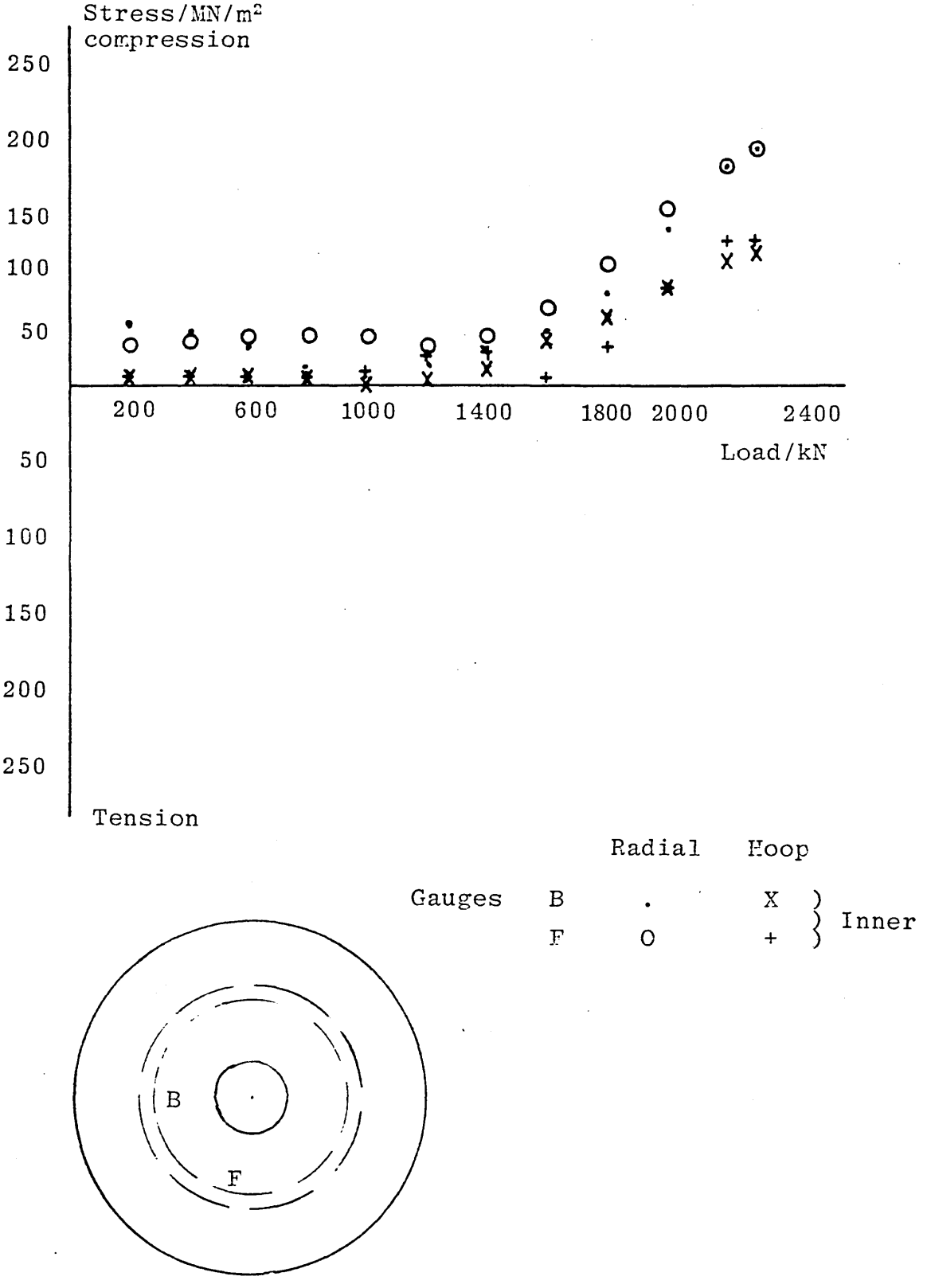

Figure 3.25 : Stress vs Load for Disc D3

Comparison of Gauge Accuracy

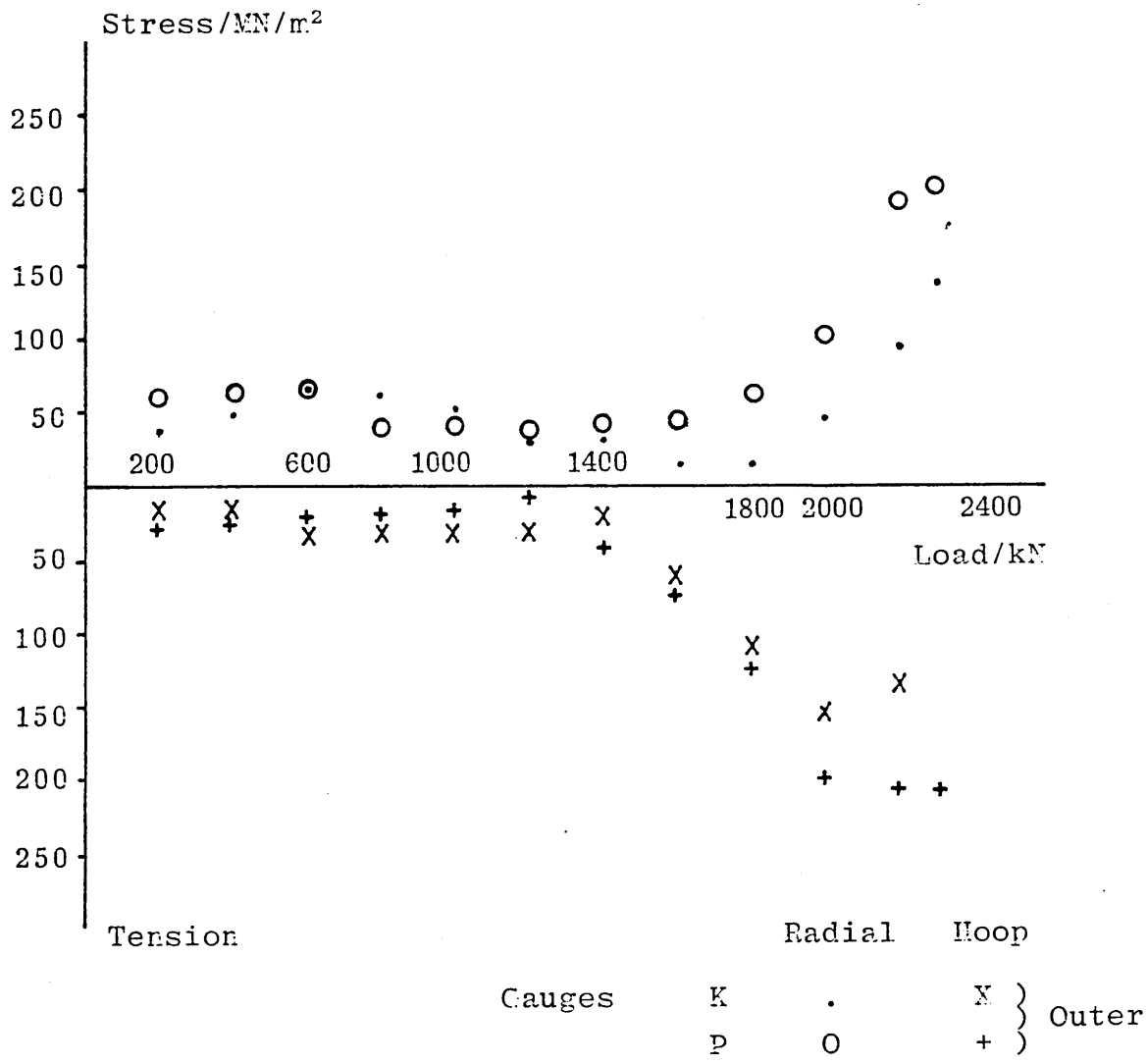

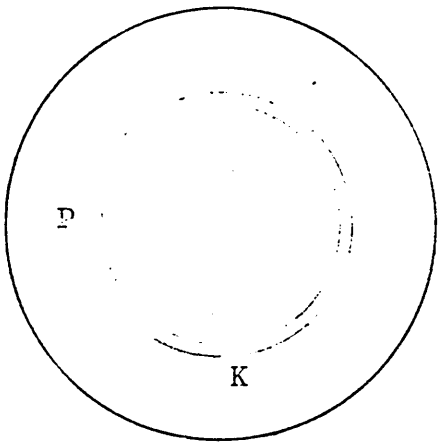

Figure 3.26 : Stress vs Load for Disc D4

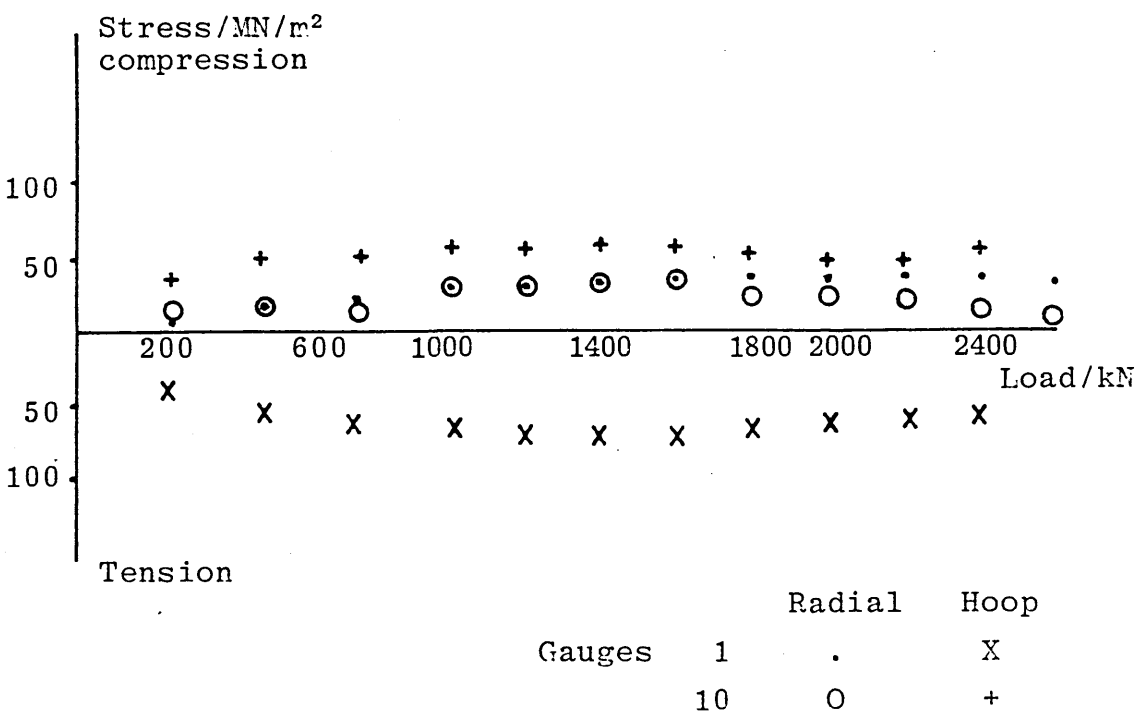

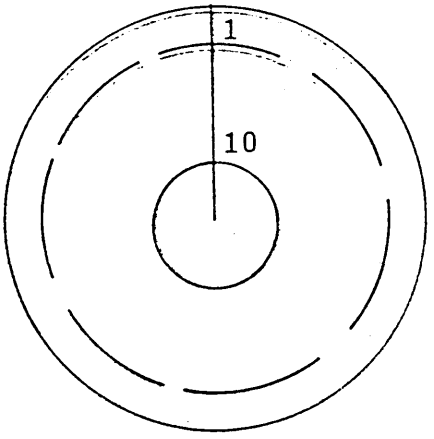

3.2.9 Appraisal of Results

(i) The overall pattern for stress vs distance from centre of disc is shown in Figure 3.17

The radial stress is compressive inside and outside the loading ring whereas the hoop stresses change from compressive inside to tensile outside.

(ii) The maximum values of stress occur in close proximity to the loading ring, indicating the localised effect of the loading on the disc. It can be seen for each of the discs D1, D2, D3 and D4 that the peak stress values follow the increasing diameter of the loading ring.

(iii) The comparative accuracy of the experimentally derived results can be checked by considering equivalent stress values for each disc and looking at the relevant graph for each of the discs, e.g. D1 and D3. A comparative load vs disc table is shown, Table 3.16

(iv) The residual stress values have been obtained for each disc by taking strain gauge readings with zero loading after the discs have been loaded to their maximum values. The relevant graphs, with the exception of D4, show that the residual values are within 10% of the maximum load conditions for each disc.

(v) Until the loads reach values of the order of 1200 kN the graphs show minimal effect of loading.

(vi) The graphs showing stress vs load (comparison of gauge accuracy) for disc D3 are plotted for two gauges which are on radial lines 90° apart as shown on the gauge position diagram. Figure 3.24 shows the results for two gauges placed inside the loading ring whilst Fig 3.25 shows the results for gauges placed outside the loading ring. In each case there is evidence for the onset of buckling at loads of 1400 kN.

3.2.10 Buckling Tests

.2.10.1 Introduction

.2.10.2 Disc Parameters

.2.10.3 Tests on Discs

.2.10.4 Identification of the Onset of Buckling

.2.10.5 Experimental Results and Notes

.2.10.6 Elastic Instability of Flat Plates

.2.10.7 Calculation of Instability Load

.2.10.8 Conclusions

3.2.10 Buckling Tests

3.2.10.1 Introduction

Inspection and measurement indicated that both dynamic and static loading tests on the discs had produced some buckling. Consequently it was decided to investigate the onset of buckling on discs of varying thickness. The tests were carried out on a DENISON 2500 kN press and were designated the E series (E1 - E4). Subsequently, the experimental results were corroborated by inserting the disc parameters and load levels into an instability equation. The use of the instability equation involved the assumption that the position of the loading ring constituted the outer edge of the disc and the inner edge remained free of any load (see Figure 3.28). Thus the instability of that part of the disc inside the loading ring has been investigated and compared with the experimental results.

.2.10.2 Disc Parameters

All Discs	O/D = 381 mm I/D = 75 m
Loading Rings	O/D = 222 mm I/D = 210 mm Breadth = 6.0 mm Depth = 6.3 mm
Thickness	E1 = 6.3 mm E2 = 9.4 mm E3 = 11.3 mm E4 = 14.3 mm

Each disc had four hacksaw blades in quadrature fixed to the upper surface of the disc with double backed adhesive

(Figure 3.27). The discs were placed in the DENISON, 2500 kN maximum load, press. The method of fixing and loading was the same as that described for static loading procedure in Section 2.4.3.2. Four dial gauges were brought into contact with the top surface of the hacksaw blades and zeroed with an indicated load on the machine of 100 kN.

Figure 3.27 : Arrangements for Buckling Tests

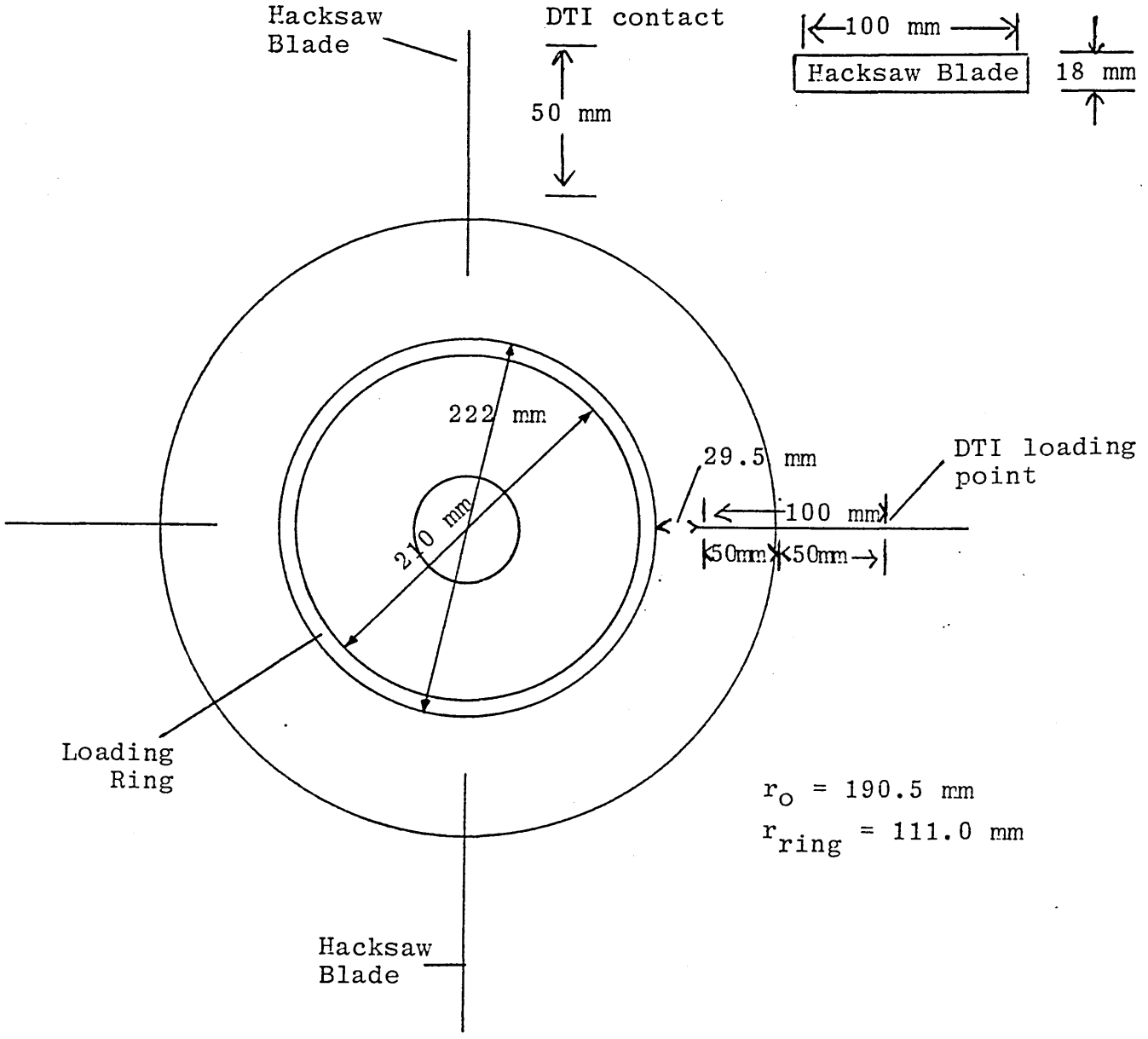

Hacksaw blade fixed with double-sided adhesive to surface of disc.

3.2.10.3 Tests

The following measurements were carried out on the discs:

(a) A profile measurement of the upper surface of each disc was carried out with the aid of the Newall 15-20 profile measuring machine. In effect, a dial gauge traversed across two diagonals and the readings were plotted on a disc diagram. The profile measurements were made before loading and after loading of the discs. This technique was similar to that described in Section 2.5.1.1 and shown in Figure 2.22.

(b) Indentation of the disc surface under the loading ring was measured at the same time as the measurements carried out in (a).

(c) As the loading rings were loaded up to a maximum of 2500 kN, continuous dial gauge readings were recorded for each of the four quadrature positions.

3.2.10.4 Identification of the Onset of Buckling

Each experimental run produced a set of four dial gauge readings which changed with increased loading. As the loading progressed, the readings from the dial gauges changed differentially. However, at a particular load it was possible to see that one or more of the dial gauges started to produce readings in either the opposite direction or a rapid increase. The load at this point was taken to be the indication of the onset of buckling.

.2.10.5 Results

Table 3.18

1	2	3	4	5		6	
Disc	Thickness/ mm	Load at Onset of Buckling/ kN	Indentation at loading ring/mm	Inner Rim		Outer Rim	
				Max/ mm	Min/ mm	Max/ mm	Min/ mm
E1	6.3	900-1000	.07 ∿ .2	3.5	1.3	.97	0
E2	9.4	2100	.08 ∿ .16	.18	.06	.23	0
E3	11.3	>2500	.04 ∿ .17	.19	.02	.24	0
E4	14.3	Not measurable	.2 ∿ .33	*2.53	*1.2	*2.98	*0

Notes

Column 3 — The load at onset of buckling was determined by a reversal or rapid increase of one or more of the dial gauge readings.
E4 - there was no indicated change in the dial gauge readings but the top and bottom loading plates used throughout the series of tests showed bending.

Column 4 — The indentation depth varies around the loading ring and could be ascribed to uneven contact between the loading anvil or the non-symmetric positioning of the upper and lower surface loading rings.

Columns 5 and 6 — These deflections indicate the difference in levels between pre- and post-loading of the discs.

*For disc E4 the large deflections are correct. An inspection of the disc showed that the loading rings had been positioned or slipped into a non-concentric position on the top surface. This has produced a differential loading on the surface and thus an amplified buckling effect has been displayed.

.2.10.6 Elastic Instability of Flat Plates

(a) When dealing with elastic instability, the bending or twisting effect of an applied load is no longer proportional to the deformation it produces. It is possible to obtain formulae for critical load or critical unit stress at which failure occurs. Such formulae can be derived mathematically by integrating the differential equation of the elastic curve* or by equating the strain energy of bending to the work done by the applied load in the corresponding displacement of its point of application, the form of the elastic curve being assumed when unknown. Of all the possible forms of the curve, that which makes the critical load a minimum is the correct one; but almost any reasonable assumption (consistent with the boundary conditions) can be made without gross error resulting, and for this reason the strain-energy method is especially adapted to the approximate solution of difficult cases.

*elastic curve refers to deformed shape of the component

(b) In this particular application, the inner part of the disc, i.e. inside the loading ring, is examined by assuming the loaded annular rings to transmit a loading pressure in the radial direction. A formula (ref 68) can be obtained which predicts the critical compressive stress σ^1 for a circular plate with a concentric hole under uniform radial compression on the outer edge.

Figure 3.28 : Circular Plate under Compression

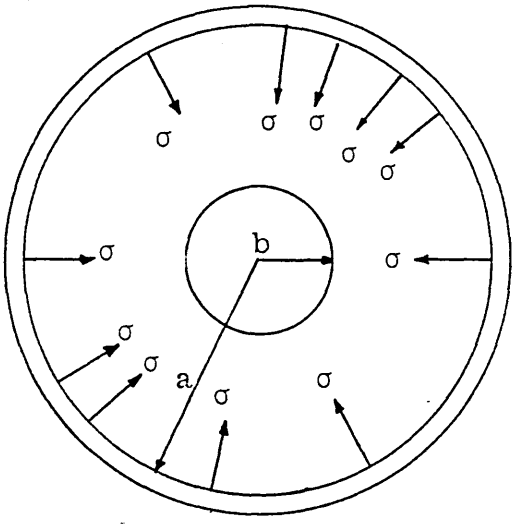

Loading Ring

Circular plate with concentric hole under uniform radial compression on outer edge. The outer edge simply supported, the inner edge free.

$\frac{a}{t} > \pm 0$

Formulae

$$\sigma^1 = K \frac{E}{1 - \nu^2} \left(\frac{t}{a}\right)^2$$

where σ^1 = critical unit compressive stress

E = elastic modulus

ν = Poisson's ratio

t = thickness of plate

a = external radius

b = internal radius

K depends on $\frac{b}{a}$ and is shown approximately on the graph, Figure 3.29 and 3.30.

Figure 3.29 :

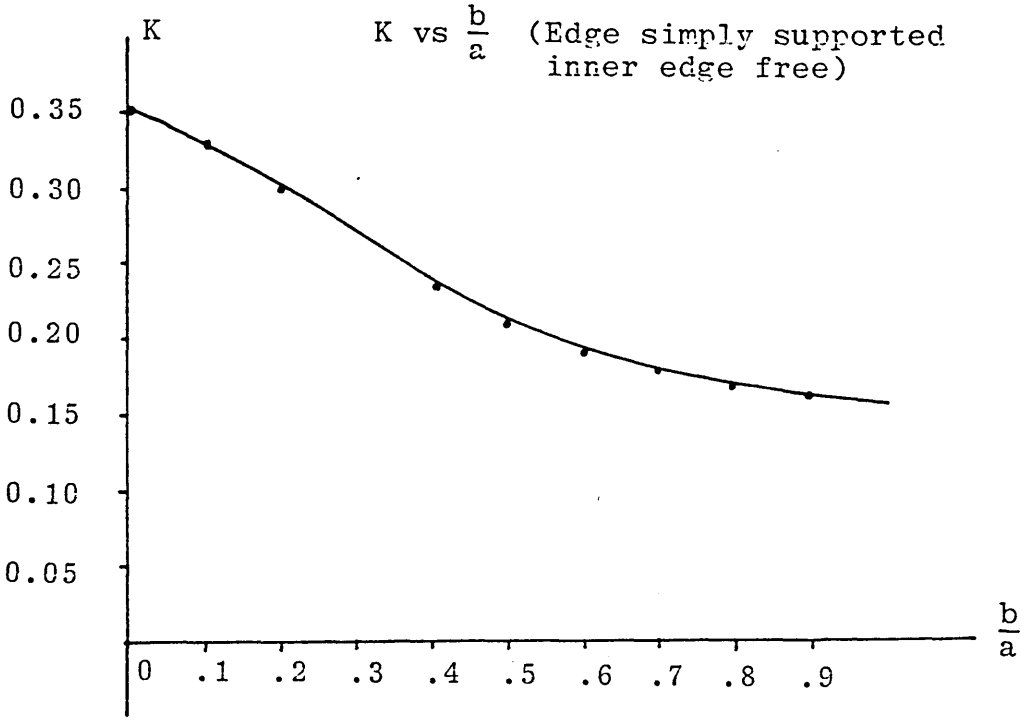

Figure 3.30 :

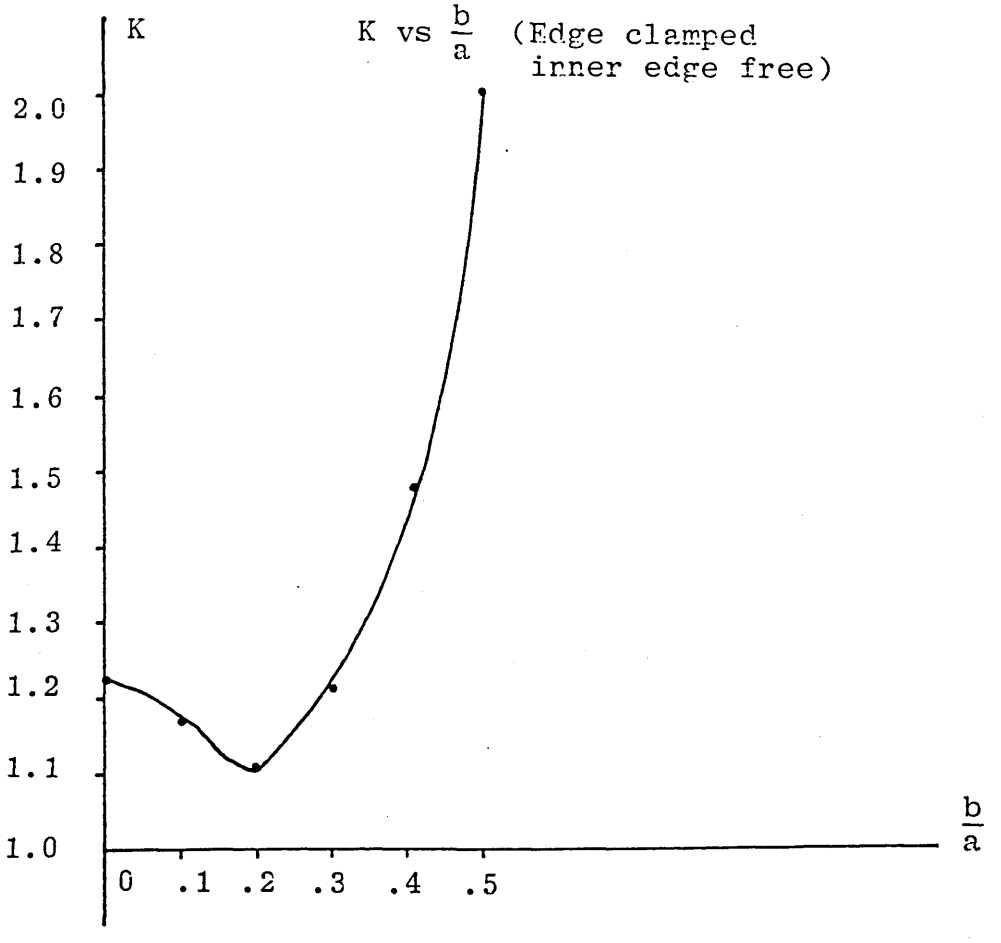

Prediction of compressive stress in radial direction -

$$\sigma = Y = p. \frac{\sqrt{3}}{2}$$

where p = mean pressure over discs

$$\therefore \quad \sigma = p. (.8660)$$

Effective Pressure $p = \frac{L}{area}$, where L = applied load

(1) It will be useful to include here a definition of Simply Supported (Ref 68)

A condition of support at the ends of a beam or column or at the edge of a plate or shell, that prevents transverse displacement of the edge of the neutral surface but permits rotation and longitudinal displacement.

(2) Definition of Clamped -

A condition of support at the ends of a beam or column or at the edges of a plate or shell that prevents rotation and transverse displacement of the edge of the neutral surface but permits longitudinal displacement.

.2.10.7 Calculation of Instability

The critical unit compressive stress, has been found for the discs E1, E2, E3 and E4 in two ways. The first method assumed that the outer edge of the disc was simply supported and the inner edge free whilst the second method assumed that the outer edge was clamped with the inner edge free. The second method, i.e. outer edge clamped, predicted a buckling load far in excess of that indicated experimentally. The first method predicted buckling loads which showed reasonable proximity to the measured values. The method adopted for the prediction of buckling loads was therefore the first, i.e. outer edge simply supported and the inner edge free.

The following table was then obtained which compares predicted and experimental buckling loads.

Disc	$\sigma_1'/10^8 Nm^{-2}$	$p=\sigma_1'/.866$	Load = $\frac{p \times area}{N}$	Predicted Buckling /kN	Experimental Buckling Load from Table 3.18
E1	1.87	2.15	8.75×10^5	875	900 - 1000
E2	4.18	4.83	19.6×10^5	1960	2100
E3	5.99	6.91	28.1×10^5	2810	>2500
E4	9.6	11.1	45×10^5	4500	No buckling obtained

.2.10.8 Conclusions

(a) Disc E1 which was of similar dimensions to those used in the dynamic and static loading tests buckled with load approaching 1000 kN. (See Figure 3.3[illegible])

(b) Disc E2, which was 50% thicker than the original disc, exhibited buckling with loads of approximately 2000 kN.

(c) Discs E3 and E4 did not exhibit any buckling up to the maximum applied load of 2500 kN.

(d) Due to the reasonable agreement between experimental and predicted buckling load, the assumed method of loading with the outer edges simply supported and the inner edges free would appear to be justified. Indeed when a physical appraisal is made of the loading conditions with the relative small area of surface contact between rings and disc surface, the assumption again appears to be reasonable.

(e) In predicting the load required to produce buckling of the whole disc calculations were carried out only on the inner zone, although the detection of buckling was measured at the outer zone of the discs.

Figure 3.31 : Ring and Disc Profile after Loading Disc D1 showing dishing

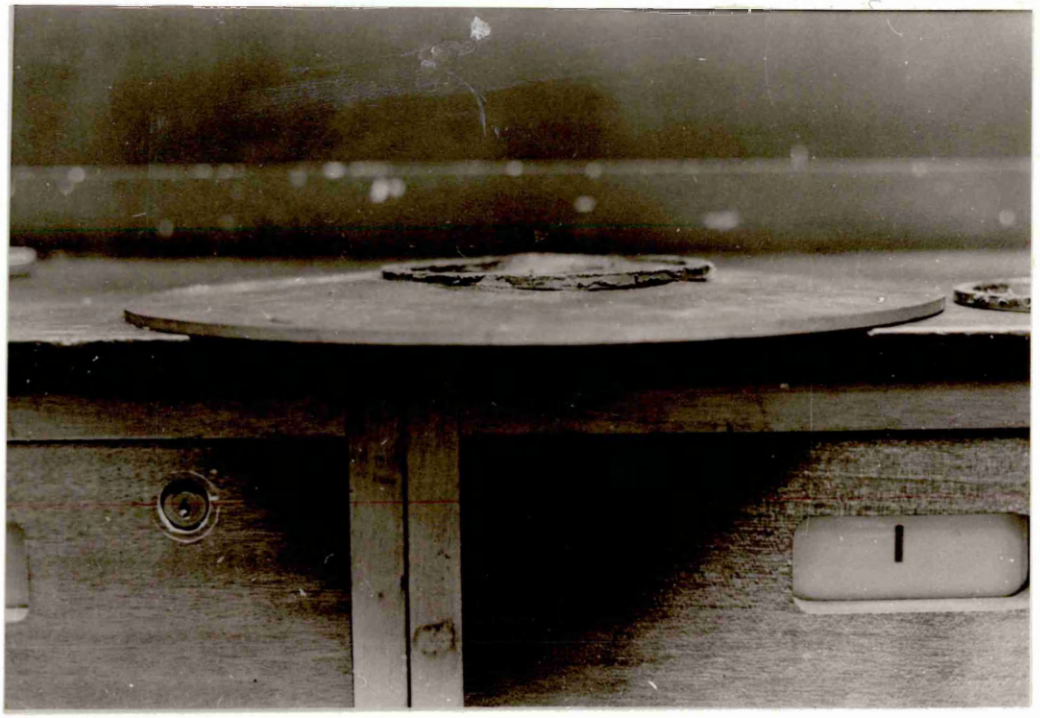

CHAPTER 4

THEORETICAL : FINITE ELEMENT ANALYSIS

4.1 Introduction

4.2 Finite Element Method and PAFEC Programme

4.3 Data Modules

4.4 Tables of Results for Predicted and Measured Values of Equivalent Stress

4.5 Graphical Comparison

4.6 Conclusions

4.1 Introduction

An attempt was made to predict the behaviour of a disc under static loading using the finite element method. In this method, a component is discretized into a number of sub-regions, called elements, which are connected together at points referred to as nodes. A matrix describing the stiffness of each element is formed. These can be merged together to form a global stiffness for the whole component since nodes common to more than one element must have the same displacement.

4.2 Finite Element Method and the PAFEC Programme

The PAFEC finite element package (ref 72,73) was used to perform the elastic-plastic analysis on the geometry used for disc D2. The disc was modelled using eight node quadrilateral axisymmetric isoparametric elements. The mesh was generated using the automatic mesh generation facilities (PAF BLOCK) in the package. As instability effects were not considered, only half the thickness of the plate was modelled, thus taking advantage of the plane of symmetry. The plasticity solution is based on the incremental Prandtl-Reuss equation and it is therefore necessary to apply the final load in a series of load increments. The solution method makes use of the elasticity matrix in conjunction with the initial stress/ initial strain type of approach described by Zienkiewicz (Ref 74).

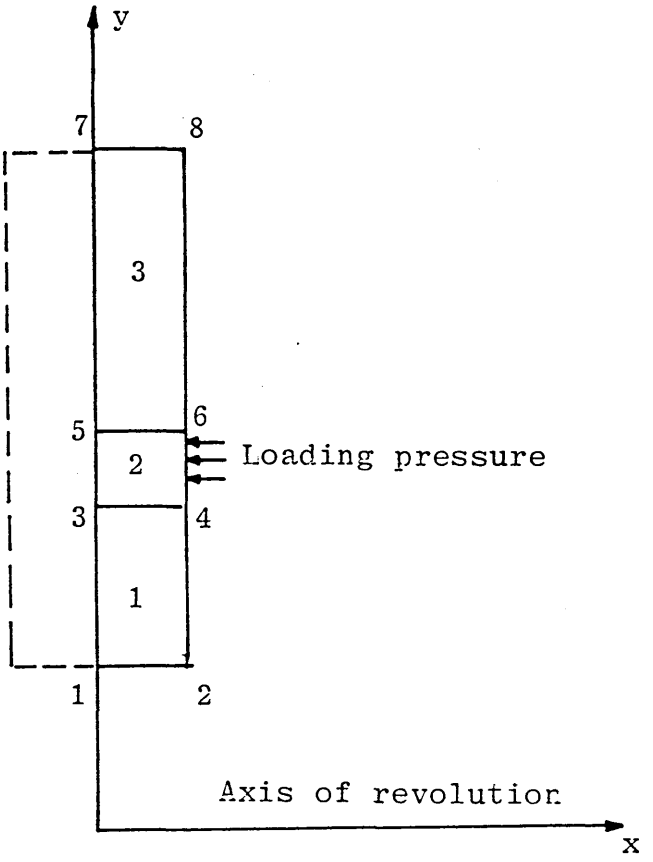

Figure 4.2 : Division of Sections into Elements (Bracketed)

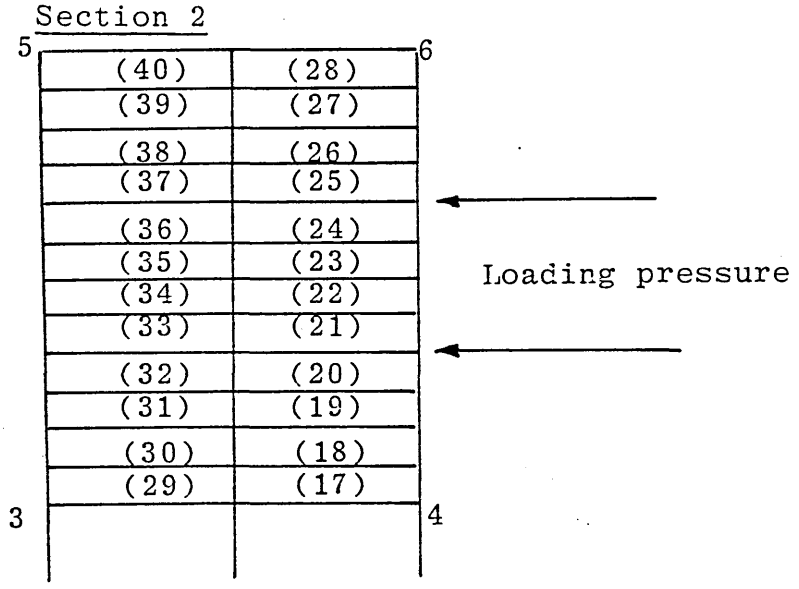

Figure 4.3 : Division of Elements into Nodes

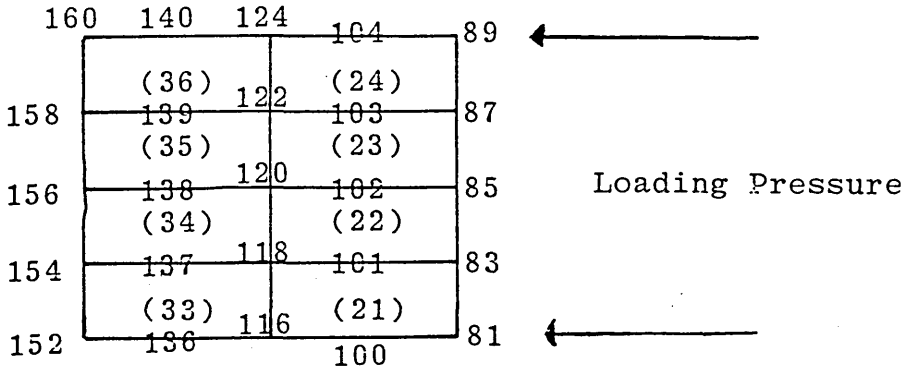

The main features of the model are as follows:

4.2.1 Three PAF BLOCKS were used to model the cross-sections of the disc (Figure 4.1).

4.2.2 The semi-thickness of the disc is modelled using two elements as it was anticipated that there would be little change of stress through the thickness.

4.2.3 PAF BLOCK 2 represents the region of the disc under and adjacent to the loading ring. The number of elements in the radial direction in this region was increased in order to model the anticipated steep stress gradient. The mesh used for this region is shown in Figures 4.2, 4.3.

4.2.4 The nodes on the plane of symmetry coincident with the y axis were restrained from moving in the x direction. The x axis represents the axis of revolution.

4.2.5 The load applied by the rings was modelled by applying a uniform pressure to elements 21 to 24.

4.2.5 The complete model has 64 elements, 261 nodes, and taking into account restrained nodes, 457 degrees of freedom.

The analysis was performed using the Polytechnic IBM 4341 computer facilities.

4.3 The Data Modules

4.3.1 The disc section was divided into three parts, Figure 4.1, numbered 1, 2 and 3. Part 1 representing the disc inside the loading ring, Part 2 representing that part of the disc below and adjacent to the loading ring and Part 3 to that part of the disc outside the loading ring.

4.3.2 Each part was divided into elements, viz:

Part 1 Elements 1, 2 .... 15, 16

Part 2 Elements 17, 18 .... 28, 29 40

Part 3 Elements 41, ... 63, 64

4.3.3 Each element was designated by node numbers.

Part 1 Nodes 1, 2, 3, 4 for the boundaries subdivided into 9, 10 .... 71, 72, 73

Part 2 Nodes 3, 4, 5, 6 for the boundaries subdivided into 71, 72, 73 .... 144, 132, 108

Part 3 Nodes 5, 6, 7, 8 for the boundaries subdivided into 144, 132, 108 .... 259, 260, 261

4.4 Tables of Results for Predicted and Measured Values of Equivalent Stress

4.4.1 The predicted values of σ_{eq} are extracted from computer print-out values produced by the Finite Element Method of stress analysis.

4.4.2 The parameters fed into the Programme were taken from those relevant to disc D2 (see Section 3.2.7 for loading criteria and dimensions) and experimentally measured criteria for stress-strain characteristics (Section 3.2.2).

4.4.3 The measured values of σ_{eq} are taken from those obtained (Section 3.2.4, 2.2.5) and shown graphically (Section 3.2.8).

4.4.4 Six loading results have been compared and the following tables provide the results on which the later graphical comparisons are shown.

σ_{eq} in this section is the same as $\bar{\sigma}_e$ on p 158

Table 4.1 : Data for Disc D2

Load/kN	Radius from Centre of disc/mm	σ_{eq}/MN/m^2	
		Finite Element	Experimental
2300	70	37	183
	80	34	183
	95	172	173
	Load Ring 101-107		
	111	187	185
	129	78	94
	138	71	98
	150	61	93
1850	70	21	141
	80	20	130
	95	134	112
	Load Ring 101-107		
	111	161	185
	129	50	112
	138	42	87
	150	37	73
1600	70	13	104
	80	13	96
	95	135	123
	Load Ring 101-107		
	111	135	133
	129	37	66
	138	31	51
	150	27	49
1400	70	7	76
	80	7	75
	95	116	105
	Load Ring 101-107		
	111	112	101
	129	25	33
	138	21	28
	150	18	37
1150	70	2	44
	80	2	45
	95	77	67
	Load Ring 101-107		
	111	74	65
	129	14	9
	138	12	9
	150	11	11

Load/kN	Radius from Centre of disc/mm	σ_{eq}/MN/m^2	
		Finite Element	Experimental
920	70	1	30
	80	1	35
	95	43	31
	Load Ring 101-107		
	111	41	50
	129	5	18
	138	5	14
	150	4	17

4.5 Graphical Comparison

The following graphs show the comparison of the results tabulated in Table 4.1 for disc D2.

Figs 4.4, 4.5 and 4.6

Note the parameters for disc D2 were as follows:

Outer diameter	380 mm
Inner diameter	76 mm
Thickness	6.3 mm

Loading Rings :

Outer diameter	214.6 mm
Inner diameter	202.0 mm
Breadth	6.3 mm
Depth	6.3 mm

Figure 4.4

Load 2300 kN

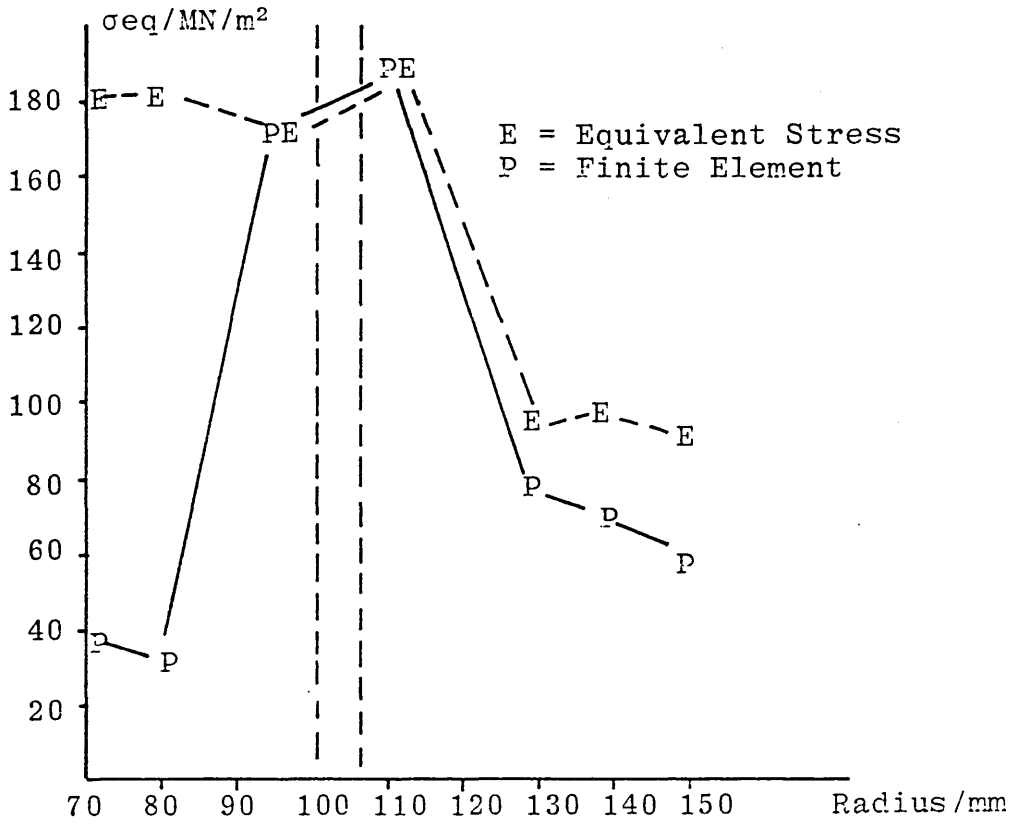

Load 1850 kN

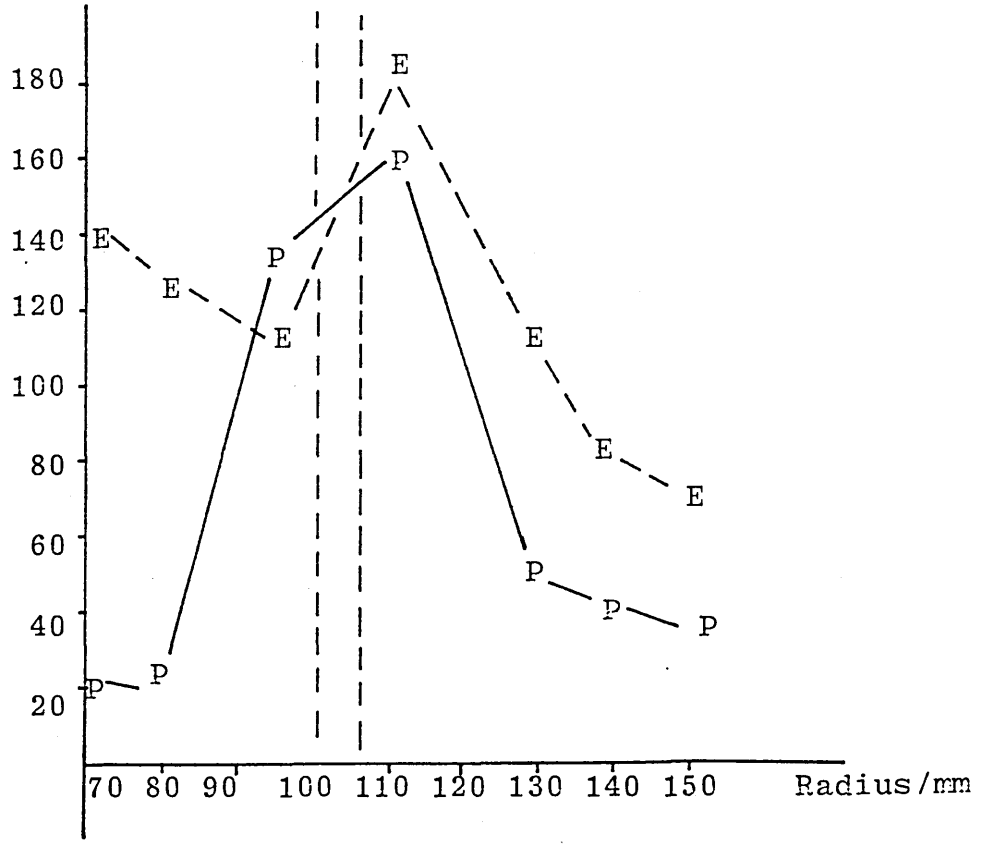

Figure 4.5

Load 1600 kN

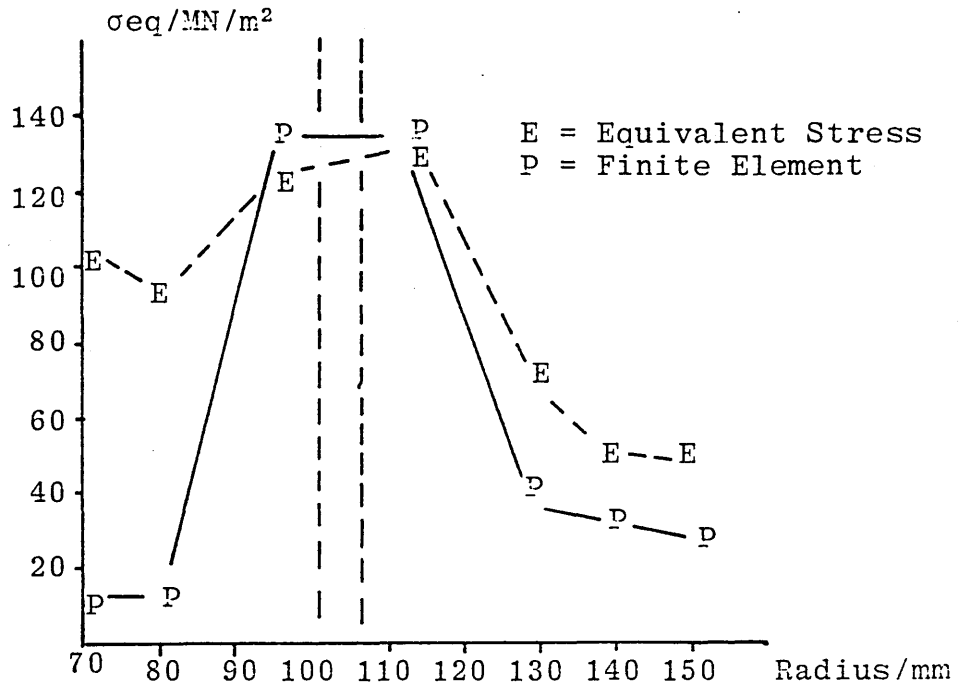

Load 1400 kN

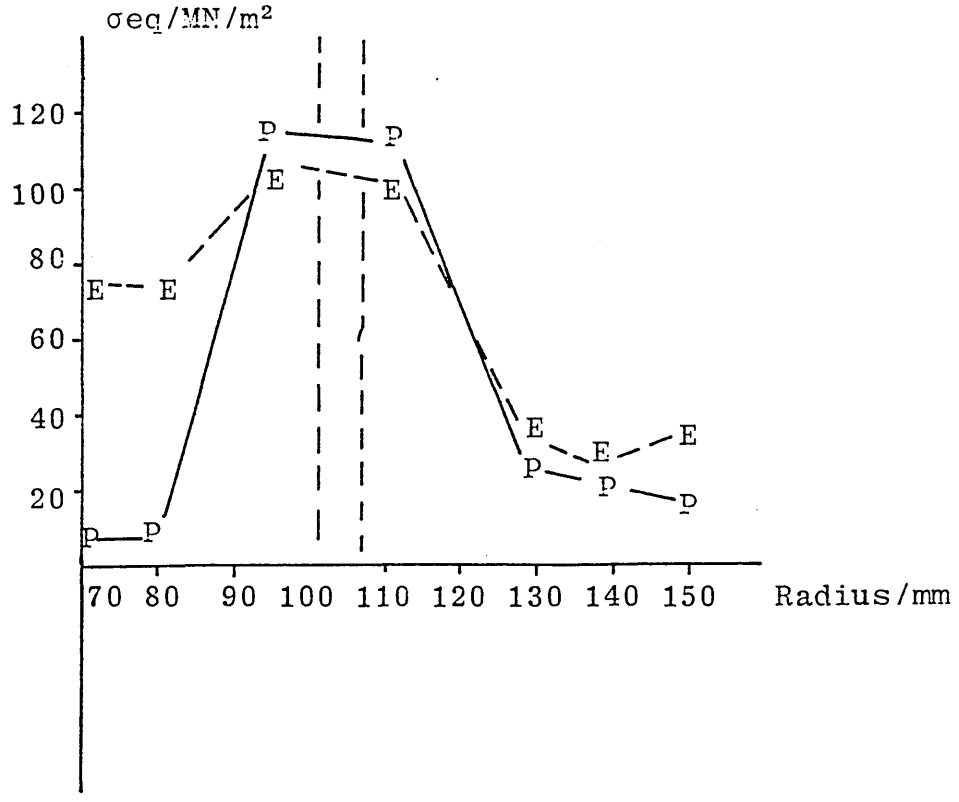

Figure 4.6

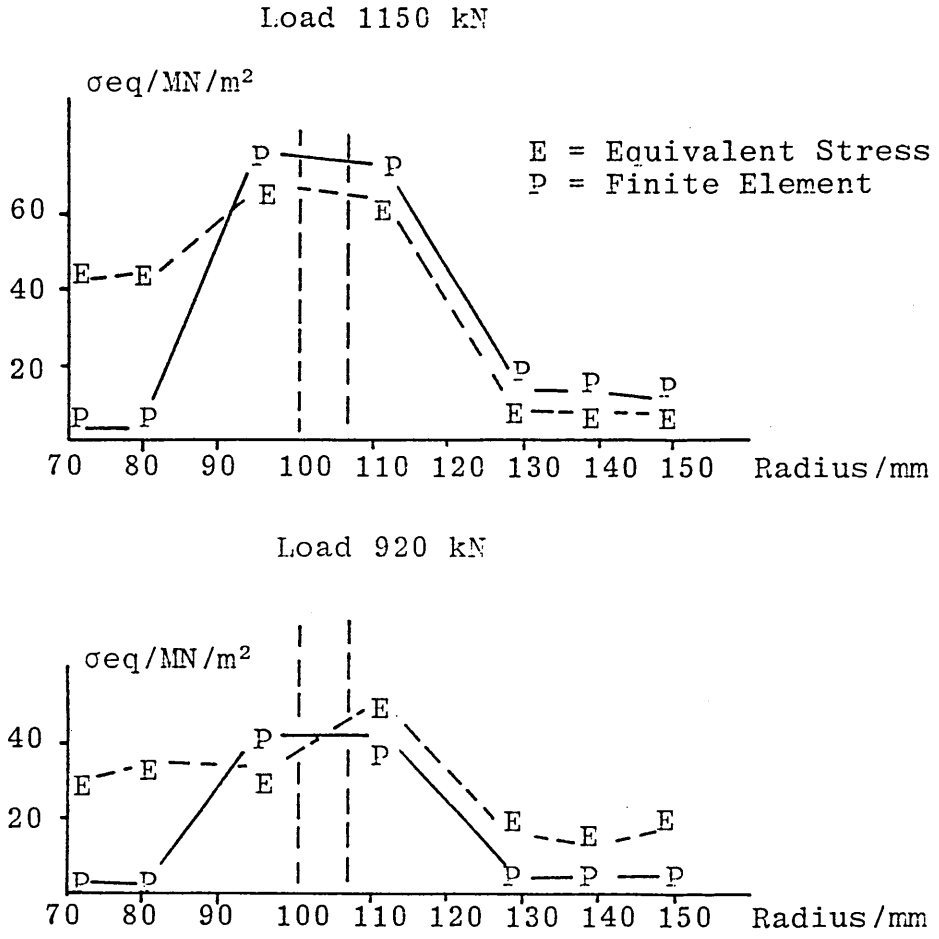
Load 1150 kN
σeq/MN/m²
E = Equivalent Stress
P = Finite Element
60
40
20
70 80 90 100 110 120 130 140 150
Radius/mm
Load 920 kN
σeq/MN/m²
40
20
70 80 90 100 110 120 130 140 150
Radius/mm

4.6 Conclusions

4.6.1 Generally the predicted and experimentally obtained results show the same shape.

4.6.2 At the position of the loading ring, the predicted and experimental values are in close agreement.

4.6.3 The outer values of the predicted results and the experimental results show agreement within the boundaries of experimental error.

4.6.4 There is a divergence of results inside the loading ring. This may be explained by the observation that for the loaded discs the inner section shows a convex dome effect and thus the experimentally derived values reflect this increased curvature whereas the predicted values are based on the disc remaining plane throughout the loading process.

CHAPTER 5

PLASTIC DEFORMATION MODEL

5.1 Introduction

5.2 Assumptions

5.3 Nomenclature

5.4 Boundary Conditions for the Plastically Deformed Region

5.5 A Compressively Loaded Block of Metal

5.6 The Relation between Surface and Edge Deformation of a Plastically Loaded Element of a Metal Annulus

5.7 Calculation of σ_{ri}, σ_{ro}, $\sigma_{\theta i}$, $\sigma_{\theta o}$

5.8 Energy Transfer from Explosive to Discs

5.9 Deformation at Surface due to Transferred Energy

5.10 Tables of Energy Transfer

5.11 Tables of Results (including Example Calculations)

5.12 Application of Method to Statically Loaded Discs

5.13 Conclusions

5.1 Introduction

A theoretical model is described in this chapter for predicting the residual stress levels in metal discs which have been loaded by an annular shaped explosive cord (Figure 5.1). The method has also been applied to the statically loaded discs. The model is deduced from a consideration of the plastic deformation of the loaded annulus and the resultant elastic deformation of the surrounding regions of the discs. The analysis is developed from a consideration of the compression of material in the form of a block, then a section or element of a metal annulus, and finally the effect of the deformation of the element on the surrounding material.

5.2 Assumptions

5.2.1 It will be assumed that the plastically deformed region is confined to the zone of metal immediately below the explosive annulus in contact with the surfaces of the discs. There is experimental evidence to support this assumption in the form of hardness measurements (page 81 microstructural examination (page 90).

Figure 5.1 : PETN on Disc Surface

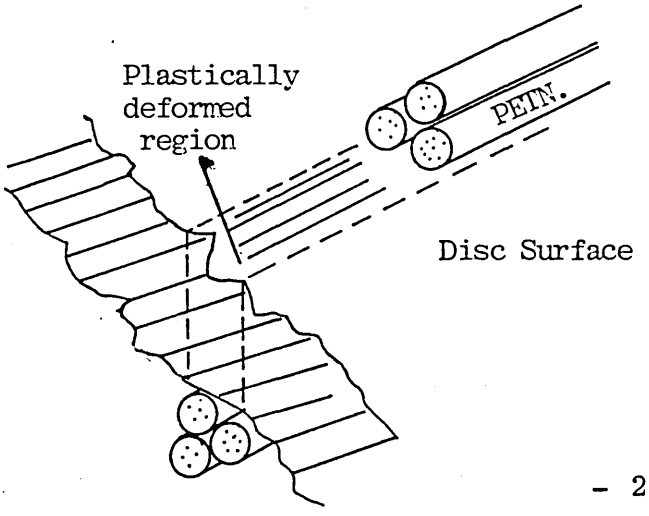

5.2.2 The other assumptions made are as follows:

(i) the material is isotropic,

(ii) the stress-strain property of the material is elastic plastic,

(iii) during plastic deformation the effect of strain rate may be accounted for by the mean rate factor,

(iv) Bauschinger effect is negligible.

5.3 Nomenclature

a	=	inner radius of disc section
b	=	outer radius of disc section
r_e	=	mean radius of explosive annulus
r_i	=	inner radius of explosive annulus
r_o	=	outer radius of explosive annulus
Δd_i	=	displacement at r_i after explosive loading
Δd_o	=	displacement at r_o after explosive loading
d	=	width of explosive annulus = $(r_o - r_i)$
Δd	=	change in width after explosive loading
t	=	undeformed thickness of discs
Δt	=	change in thickness after explosive loading
e_r	=	elastic radial strain with subscripts i and o for inner and outer
e_θ	=	elastic hoop strain with subscripts i and o for inner and outer
e_1^E, e_2^E, e_3^E	=	elastic strain in directions 1, 2 and 3
$\delta\varepsilon_1$, $\delta\varepsilon_2$, $\delta\varepsilon_3$	=	total strain in directions 1, 2 and 3
ε_r	=	plastic radial strain
ε_θ	=	plastic hoop strain
P_1	=	loading pressure on annulus
P_2	=	pressure in radial direction on annulus
P_3	=	pressure in hoop direction on annulus
W	=	work done by explosive on disc surfaces
Y	=	yield stress
P_{1Y}	=	pressure on surface of disc at yield
E_{TOTAL}	=	available explosive energy

E_{STEEL} = W = total effective energy transferred to disc surface

σr_o = residual radial stress in outer region

σr_I = residual radial stress in inner region

$\sigma_{\theta o}$ = residual hoop stress in outer region

$\sigma_{\theta I}$ = residual hoop stress in inner region

Other symbols are explained as they arise or have the usual meaning.

5.4 Boundary Conditions for the Plastically Deformed Region of the Disc

5.4.1 The aim of this exercise is to show that the plastically deformed annulus surrounded by the disc material will strain mainly in the radial direction and be effectively constrained in the hoop direction. This fact is further borne out by experimental evidence. Hence an estimate of the value of the compressive pressure at yield may be obtained by the established procedures given in references 19, 78 and 79.

Figure 5.2 : Disc Parameters

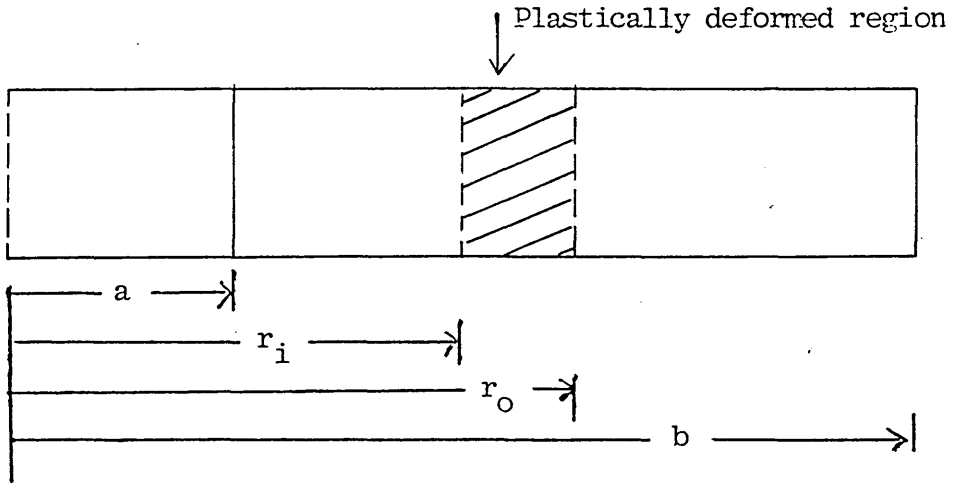

5.4.2 In discussing the boundary conditions in the hoop and radial directions, the problem is to reconcile the existence of plastic deformation in the explosively loaded region $r_i \rightarrow r_o$ with low radial and hoop strains at the boundaries r_i and r_o such that both the inner and outer bulk regions of the disc can remain only in a state of elastic deformation. This apparent anomaly can be explained by considering the fact that a considerable extension of the plastic region between r_i and r_o could take

place in the radial direction without the radial strain at either r_i or r_o becoming appreciable. For example,

let $\varepsilon r_i = \frac{\Delta r_i}{r_i}$ and $\varepsilon r_o = \frac{\Delta r_o}{r_o}$

$$\text{Incremental strain in element} = \frac{\text{Final length - Initial length}}{\text{Initial length}}$$

$$= \frac{[(r_o + \Delta r_o) - (r_i + \Delta r_i)] - [r_o - r_i]}{[r_o - r_i]}$$

$$= \frac{\Delta r_o - \Delta r_i}{r_o - r_i}$$

the extension of the plastic region will be $\Delta r_o - \Delta r_i$, whilst its original length is $r_o - r_i$. Thus the strain along the radial direction in the plastic region will be given by $\Delta r_o - \Delta r_i / r_o - r_i$. In general, for the problem being considered, the strain at the inner boundary r_i will be compressive, i.e. Δr_i will be negative, whilst at the outer boundary r_o the radius will have increased making Δr_o positive. The strain in the plastic region can therefore be rewritten as

$$|\Delta r_o| + |\Delta r_i| / r_o - r_i$$

or $$|\varepsilon r_o| r_o + |\varepsilon r_i| r_i / r_o - r_i$$

and in a case where $\varepsilon r_o \sim \varepsilon r_i$, we could write

$$\varepsilon_p = |\varepsilon r_o| \left[\frac{r_o + r_i}{r_o - r_i} \right]$$

This allows a 'strain multiplication' by a factor of

$$\left[\frac{r_o + r_i}{r_o - r_i}\right]$$

which in a typical case in question of say r_i = 9.5 cm, r_o = 10.5 cm, would correspond to multiplication of 20 times.

In contrast, the hoop strain would not be subject to the same degree of multiplication because it cannot exceed the maximum hoop strain at either boundary and must therefore be elastic and correspondingly small.

Conclusions

In seeking a set of boundary conditions which allow the plastic region to be treated in isolation, it can be seen that the problem would approximate to a rigid boundary in the hoop direction and a deformed boundary in the radial direction. Thus, the analysis may take the form similar to that described in Hill[21] pages 77-79, Hill[32], Ford[75] where in the limit P_1, the compressive pressure approaches a value of 1.155Y

5.5 An Estimate of the Order of Magnitude of the Radial Stress in terms of the Applied Compressive Stress

(Under conditions where the hoop strain is sufficiently small to be neglected.)

Figure 5.3 : Three-dimensional Stress Block

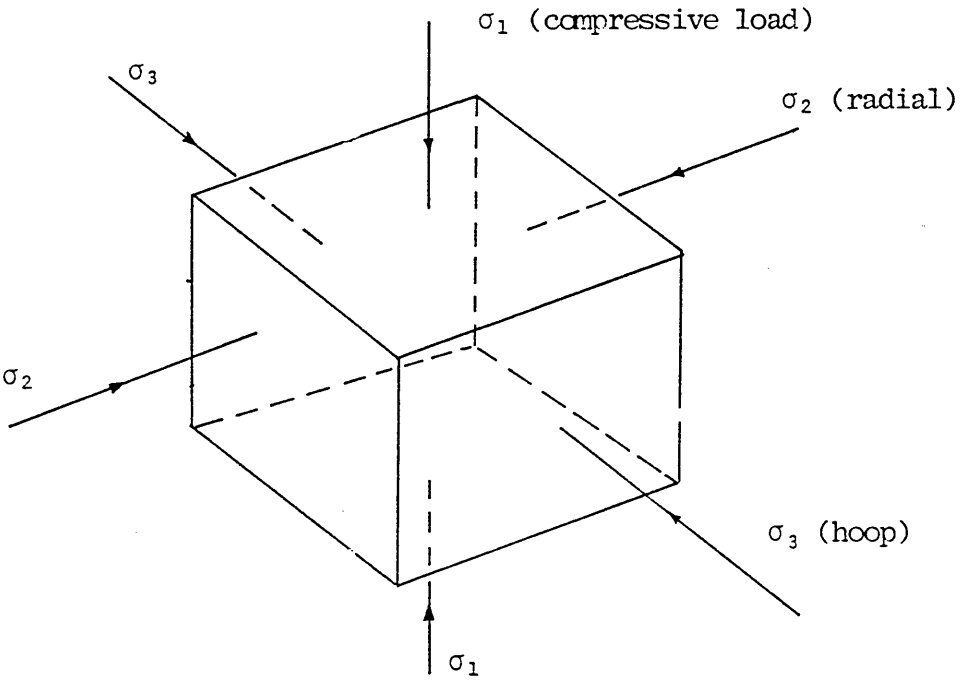

Parameters σ_1 = compressive load $\quad \varepsilon_1$ = plastic strain

σ_2 = radial stress $\quad \varepsilon_2$ = radial strain

σ_3 = hoop stress $\quad \varepsilon_3$ = hoop strain

Consider plastic deformation of a block of metal under plane strain conditions.

Using deviatoric stress-strain relations:

$$\frac{\varepsilon_1}{\sigma_1{}^1} = \frac{\varepsilon_2}{\sigma_2{}^1} = \frac{\varepsilon_3}{\sigma_3{}^1} = C \qquad \text{Levy-Mises Equations}$$

$\sigma_1{}^1$, $\sigma_2{}^1$, $\sigma_3{}^1$ are the reduced or deviatoric components of stress.

Since plastic straining causes no change of plastic volume

$$\varepsilon_1 + \varepsilon_2 + \varepsilon_3 = 0$$

but for plane strain $\varepsilon_3 = 0$

$$\therefore \quad \varepsilon_1 = -\varepsilon_2$$

and from the Levy-Mises Equations

$$\varepsilon_3 = C\sigma_3{}^1 = 0$$

$$\therefore \quad \text{Since } \sigma_3{}^1 = \sigma_3 - \left(\frac{\sigma_1 + \sigma_2 + \sigma_3}{3}\right)$$

$$\sigma_3{}^1 = 0 \quad \therefore \quad \sigma_3 = \frac{1}{2}(\sigma_1 + \sigma_2) \qquad 5.1$$

If Y = stress at yield, then by von Mises criterion

$$(\sigma_1 - \sigma_2)^2 + (\sigma_2 - \sigma_3)^2 + (\sigma_3 - \sigma_1)^2 = 2Y^2 \qquad 5.2$$

Substituting equation 5.1 in 5.2:

$$(\sigma_1 - \sigma_2)^2 + \left(\frac{\sigma_2 - \sigma_1}{2}\right)^2 + \left(\frac{\sigma_2 - \sigma_1}{2}\right)^2 = 2Y^2$$

$$\sigma_1{}^2 - 2\sigma_1\sigma_2 + \sigma_2{}^2 + \frac{1}{2}(\sigma_2{}^2 - 2\sigma_1\sigma_2 + \sigma_1{}^2) = 2Y^2$$

$$3\sigma_1{}^2 - 6\sigma_1\sigma_2 + 3\sigma_2{}^2 = 4Y^2$$

$$(\sigma_1 - \sigma_2)^2 = \frac{4}{3}Y^2$$

$$(\sigma_1 - \sigma_2) = \pm\frac{2}{\sqrt{3}}Y$$

$$\sigma_1 = \sigma_2 + \frac{2}{\sqrt{3}}Y$$

5.6 The Relation between Surface and Edge Deformation of a Plastically Loaded Element of a Metal Annulus

So that the derivation can be usefully applied to the analytical model, it is necessary to assume that the compressive loading and subsequent surface deformation causes a deformation principally in the radial direction of the element. A consequence of this condition is that the dimensions of the element in the hoop direction remain fixed. Thus the two necessary conditions in the following derivation are (a) the volume of the element remains constant, and (b) the value of $r_e \simeq r_e^1$, the radius after deformation.

Figure 5.4 : Deformation of Block

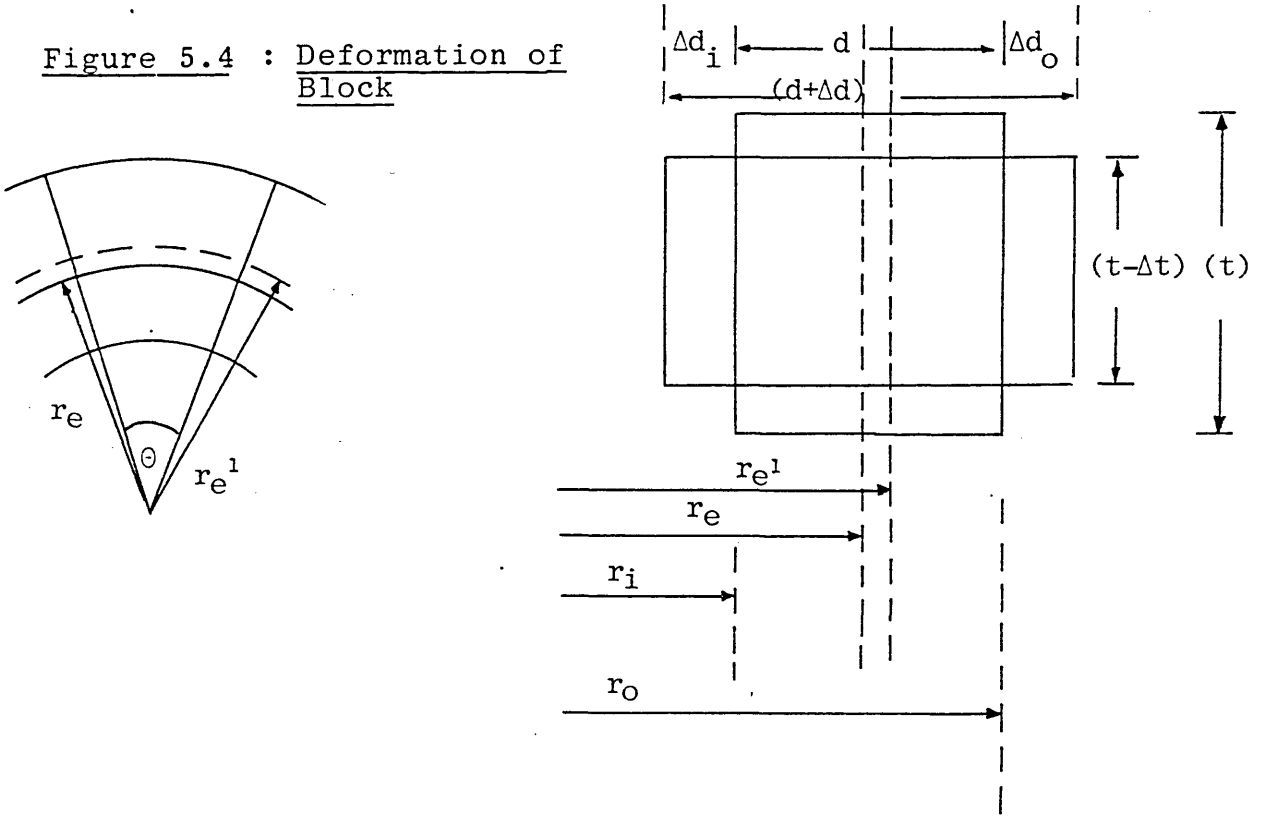

$$r_e = \frac{r_i + r_o}{2}; \qquad r^1_e = \frac{r_i + r_o + \Delta d_o - \Delta d_i}{2}$$

Volume of element before compression = $\theta r_e td$

Volume of element after compression

$$= \theta r_e{}^1(t - \Delta t)[d + \Delta d_i + \Delta d_o]$$

Volume is constant

$$\therefore \quad \theta r_e td = \theta r_e{}^1(t - \Delta t)[d + \Delta d_i + \Delta d_o]$$

Neglecting second order terms in above and substitute for r_e and $r_e{}^1$:

$$(r_i + r_o)td = \{[r_i + r_o + (\Delta d_o - \Delta d_i)]\}\ (t - \Delta t)[d + \Delta d_i + \Delta d_o]$$

$$= \{r_i + r_o + (\Delta d_o - \Delta d_i)\}\ [td + t(\Delta d_i + \Delta d_o) - d\Delta t]$$

$$= (r_i + r_o)td + (r_i + r_o)t(\Delta d_i + \Delta d_o) - (r_i + r_o)d\Delta t + (\Delta d_o - \Delta d_i)td - (\Delta d_o - \Delta d_i)d\Delta t$$

$$\therefore \Delta t\{d(r_i + r_o) + d(\Delta d_o - \Delta d_i)\} = t\{(r_i + r_o)(\Delta d_i + \Delta d_o) + d(\Delta d_o - \Delta d_i)\}$$

$$\therefore \quad \frac{\Delta t}{t} = \frac{\{(r_i + r_o)\Delta d + d(\Delta d_o - \Delta d_i)\}}{\{(r_i + r_o)d + d(\Delta d_o - \Delta d_i)\}}$$

but $(\Delta d_o - \Delta d_i) < \Delta d$ and is small

and $\qquad d << (r_i + r_o)$

$\therefore$ $d(\Delta d_o - \Delta d_i)$ is small in comparison with $(r_i + r_o)d$ and also $(r_i + r_o)\Delta d$

$$\therefore \quad \frac{\Delta t}{t} \cong \frac{\Delta d}{d} \qquad 5.3$$

A numerical example shows that the above relation is accurate to 1% for the type of discs considered.

eg B1 $\quad d = 1.2 \times 10^{-2}$ m, $\Delta d = 10.6 \times 10^{-5}$ m

$r_i = .070$ m, $r_o = .082$ m

Calculation provides $\quad \Delta d_o = e_{\theta o} \times r_o = 6 \times 10^{-5}$

$$\Delta d_i = e_{\theta i} \times r_i = 4.5 \times 10^{-5}$$

$$\therefore \quad \Delta d_o - \Delta d_i = 1.5 \times 10^{-5}$$

$$d(\Delta d_o - \Delta d_i) = 1.8 \times 10^{-7}$$

$$\therefore \quad (r_i + r_o)\Delta d = 1.6 \times 10^{-5}$$

$$(r_i + r_o)d = 1.8 \times 10^{-3}$$

ie $$\frac{d(\Delta d_o - \Delta d_i)}{(r_i + r_o)\Delta d} \cong 10^{-2}$$

and $$\frac{d(\Delta d_o - \Delta d_i)}{(r_i + r_o)d} \cong 10^{-4}$$

Hence using equations:

$$\Delta d = \frac{d}{t} \Delta t \qquad 5.3$$

and $$\Delta t = \frac{W}{2\pi r_e dY} \qquad 5.4$$

See Section 5.9 for derivation of 5.4

We can now calculate Δd, the total displacement at the inner and outer element boundaries remembering that

$$\Delta d = \Delta d_i + \Delta d_o$$

Figure 5.5 : Extension Parameters

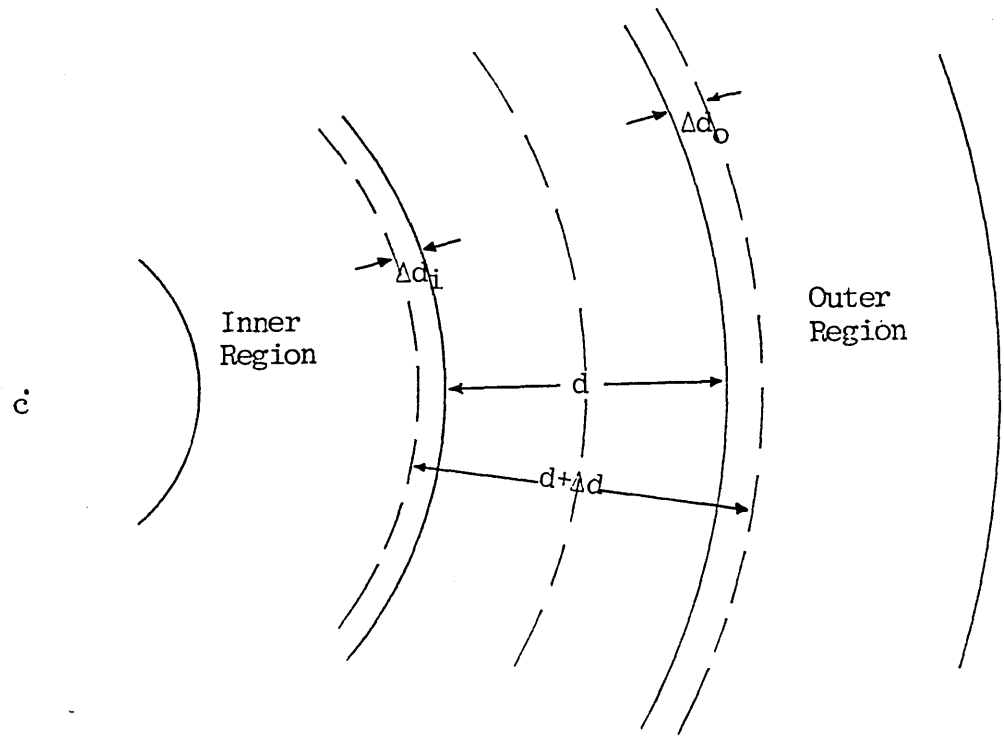

5.7 Calculation of Stress Formulae

The problem now is the apportion the total displacement Δd to the inner and outer regions. It will be assumed that the radial stress or pressure on the inner and outer boundaries of the exploded annulus is the same. (This is the condition for the equilibrium of a thin walled annulus and is a first approximation to this case.)

Model

Assume that Δd_i and Δd_o are known at this stage and use them to calculate the resulting stresses in the inner and outer regions using Lame's equations in terms of Δd_i and Δd_o. The condition that the pressure (radial stress) on either side of the exploded region should be the same can then be used to derive an equation giving Δd_i in terms of Δd_o. Then, because the sum of Δd_o and Δd_i is known, it will be possible to calculate both Δd_i and Δd_o and the resultant stress distribution throughout the disc.

Figure 5.6 : Displacement after Explosive Loading

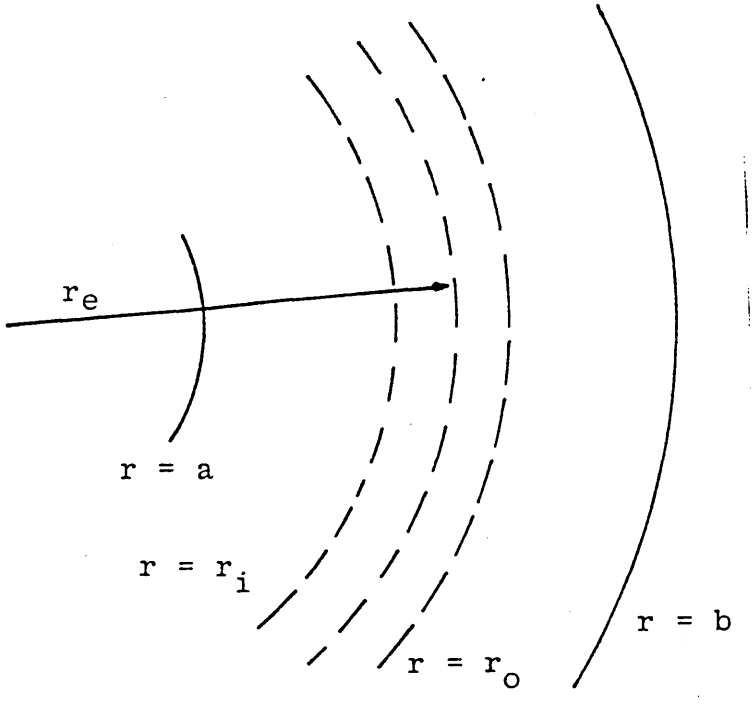

Initially $d = r_o - r_i$

After explosive loading displacement at r_i is Δd_i inwards and at r_o is Δd_o outwards.

The radial strain cannot be calculated from the displacements at r_i and r_o because it will depend on the relative position of the next element of material. But if $r_i \to r_i - \Delta d_i$ then the circumference at this boundary becomes $2\pi(r_i - \Delta d_i)$ and so hoop strain $= \dfrac{2\pi(r_i - \Delta d_i) - 2\pi r_i}{2\pi r_i}$

$$= - \frac{\Delta d_i}{r_i}$$

Similarly, the outer boundary hoop strain $= + \dfrac{\Delta d_o}{r_o}$

NB Designated values of hoop stress $= \sigma_\theta$;
hoop strain e_θ
and radial stress $= \sigma_r$
radial strain e_r

applying the suffix o or i for outer and inner respectively.

eg $e_{\theta o}$ = outer hoop strain

so $e_{\theta o} = \dfrac{\Delta d_o}{r_o}$, $e_{\theta i} = - \dfrac{\Delta d_i}{r_i}$ 5.5

and with E = elastic modulus and ν = Poisson's ratio.

Then $\sigma_{ro} = \dfrac{E}{1 - \nu^2} (e_{ro} + \nu e_{\theta o})$

$\sigma_{\theta o} = \dfrac{E}{1 - \nu^2} (e_{\theta o} + \nu e_{ro})$ } outer

Only $e_{\theta o}$ is known from equation 5.5

$\therefore$ eliminate e_{ro}

$$\nu\sigma r_o = \frac{E}{1 - \nu^2} (\nu e_{ro} + \nu^2 e_{\theta o})$$

or $$\sigma_{\theta o} - \nu\sigma_{ro} = \frac{E}{1 - \nu^2} (e_{\theta o} + \nu e_{ro} - \{\nu e_{ro} + \nu^2 e_{\theta o}\})$$

$$= \frac{(1 - \nu^2) e_{\theta o} E}{(1 - \nu^2)} = E e_{\theta o}$$

From Lamé $$\sigma_{ro} = A_o - \frac{B_o}{r^2}$$

$$\sigma_{\theta o} = A_o + \frac{B_o}{r^2}$$

so $$A_o + \frac{B_o}{r_o^2} - \nu A_o + \nu \frac{B_o}{r_o^2} = E e_{\theta o}$$

(condition applies at $r = r_o$)

Also $\sigma_{ro} = 0$ when $r = b$ (outer boundary)

$$\therefore \quad A_o = \frac{B_o}{b^2}$$

$$\therefore \quad \frac{B_o}{b^2} (1 - \nu) + \frac{B_o}{r_o^2} (1 + \nu) = E e_{\theta o}$$

$$\therefore \quad B_o = \frac{E e_{\theta o} b^2}{(1 - \nu) + \frac{b^2}{r_o^2} (1 + \nu)} \qquad 5.6a$$

$$A_o = \frac{B_o}{b^2} = \frac{E e_{\theta o}}{(1 - \nu) + \frac{b^2}{r_o^2} (1 + \nu)} \qquad 5.6b$$

Now, b, r_o, ν, E are fixed for the outer portion of an exploded disc and so for convenience these can be collected together in the form of a constant ϕ_o,

so that $$\frac{E}{(1-\nu) + \frac{b^2}{r_o^2}(1+\nu)} = \phi_o \qquad 5.7$$

Then $$A_o = \phi_o e_{\theta o}, \quad B_o = b^2 \phi_o e_{\theta o}$$

$$\therefore \quad \sigma r_o = \phi_o e_{\theta o} \left(1 - \frac{b^2}{r^2}\right)$$

But $\sigma_{ro} = P_{2o}$, the pressure at the exploded boundary when $r = r_o$

ie $$P_{2o} = \phi_o e_{\theta o} \left(1 - \frac{b^2}{r_o^2}\right)$$

Similarly for inner

$$P_{2i} = \phi_i e_{\theta i} \left(1 - \frac{a^2}{r_i^2}\right)$$

where $$\phi_i = \frac{E}{(1-\nu) + \frac{a^2}{r_i^2}(1+\nu)} \qquad 5.8$$

But $$P_{2i} = P_{2o}$$

$$\therefore \quad \phi_o e_{\theta o} \left(1 - \frac{b^2}{r_o^2}\right) = \phi_i e_{\theta i} \left(1 - \frac{a^2}{r_i^2}\right)$$

Using equation 5.5

$$\phi_o \frac{\Delta d_o}{r_o} \left(1 - \frac{b^2}{r_o^2}\right) = -\phi_i \frac{\Delta d_i}{r_i} \left(1 - \frac{a^2}{r_i^2}\right)$$

ie $$\Delta d_o = \frac{r_o}{r_i} \cdot \frac{\phi_i}{\phi_o} \frac{(1 - a^2/r_i^2)}{(b^2/r_o^2 - 1)} \cdot \Delta d_i$$

$\therefore$ write $$\Delta d_o = \Omega \Delta d_i \qquad 5.9$$

where Ω is a factor which can now be calculated.

But $$\Delta d_o + \Delta d_i = \Delta d = [(1 + \Omega)\Delta d_i]$$

$\therefore$ $$\Delta d_i = \frac{\Delta d}{1 + \Omega}, \quad \Delta d_o = \Delta d \frac{\Omega}{1 + \Omega}$$

so $$e_{\theta o} = \frac{\Delta d_o}{r_o} = \frac{\Delta d}{r_o} \left(\frac{\Omega}{1 + \Omega}\right)$$

and $$e_{\theta i} = - \frac{\Delta d_i}{r_i} = - \frac{\Delta d}{r_i} \left(\frac{1}{1 + \Omega}\right)$$

Hence for equations 5.7 and 5.8 and similar ones for the inner region A_o, B_o, A_i, B_i can be calculated and thus stress distribution throughout the disc.

Summary - Outer

$$\sigma_{ro} = \phi_o e_{\theta o} \left(1 - \frac{b^2}{r^2}\right)$$

(i) where ϕ_o is given by equation 5.7

(ii) $$e_{\theta o} = \frac{\Delta d}{r_o} \left(\frac{\Omega}{1 + \Omega}\right)$$

(iii) where $$\Omega = \frac{r_o}{r_i} \frac{\phi_i}{\phi_o} \frac{(1 - a^2/r_i^2)}{(b^2/r_o^2 - 1)}$$

(iv) $$\Delta d = \Delta d_o + \Delta d_i = \frac{d}{t} \Delta t \quad \text{where } \Delta t = W/2\pi r_e dkY$$

(v) $$\sigma_{\theta o} = \phi_o e_{\theta o} + \frac{b^2 \phi_o e_{\theta o}}{r^2}$$

$$= \phi_o e_{\theta o} \left[1 + \frac{b^2}{r^2}\right]$$

Summary - Inner

$$\sigma r_i = \phi_i e_{\theta i} \left(1 - \frac{a^2}{r^2}\right)$$

(i) where ϕ_i is given by equation 5.8

(ii) $$e_{\theta i} = - \frac{\Delta d}{r_i} \cdot \frac{1}{(1 + \Omega)}$$

(iii) where $$\Omega = \frac{r_o}{r_i} \frac{\phi_i}{\phi_o} \left(\frac{1 - a^2/r_i^2}{b^2/r_o^2 - 1}\right)$$

(iv) $$\Delta d = \frac{d}{t} \Delta t$$

(v) $$\sigma_{\theta i} = +\phi_i e_{\theta i} \left[1 + \frac{a^2}{r^2}\right]$$

5.8 Energy Transfer

5.8.1 Description of System to be Analysed

In order that the analytical system can be correlated with the experimental system, provision has been made for the analysis to allow variable parameters which correspond to those varied in the experimental arrangements. Thus in the analytical system the three main variable parameters are:

(i) Variations of explosive energy, designated by E_{TOTAL}.

(ii) Variation of radial position of explosive, designated by r_e.

(iii) Variation of the outer radius of the disc, designated by b.

The three variables when considered together with one varying and the other two constant, give the same conditions as those which prevail in the experimental situation. Consequently again there can be three basic series A, B and C and designated as the A series:

E_{TOTAL} varying with r_e and b constant

B series; r_e varying with E_{TOTAL} and b constant

C series; b varying with E_{TOTAL} and r_e constant.

A clearer picture can be obtained by reference to Figures 5.7 a, b and c, which are self-explanatory.

5.8.2 Energy Transferred into Discs

(The calculation of a conversion factor.)

The occurrence of elastic stress waves in solids is the basic process for the transmission of ultrasound. The circumstances leading to the propagation of various types of waves will be considered and refer to the isotropic case appropriate to polycrystalline steel. A transverse or shear wave which has displacements perpendicular to the direction of propagation and proceeds without change in volume and velocity

$$V_s = \left(\frac{\mu}{\rho}\right)^{\frac{1}{2}} \quad \text{or} \quad \left(\frac{G}{\rho}\right)^{\frac{1}{2}} \qquad 5.10$$

A longitudinal or 'irrotational' wave in which the relevant displacements and strains are parallel to the direction of propagation and which travels with velocity

$$V_L = \left(\frac{\lambda + 2\mu}{\rho}\right)^{\frac{1}{2}} = \left(\frac{E(1 - \nu)}{\rho(1 + \nu)(1 - 2\nu)}\right)^{\frac{1}{2}} \qquad 5.11$$

In the general case, displacements and strains may correspond to a combination of these two waves which are in practice usually travelling in different directions. In bounded media, certain other types and velocities may occur.

In the present context, interest attaches to different types of LAMB waves which form in a steel plate or sheet.

In the formulae 5.10 and 5.11 the symbols have the usual

Figure 5.7 : Explosive Loading Parameters

(a) Variable Energy

A Series

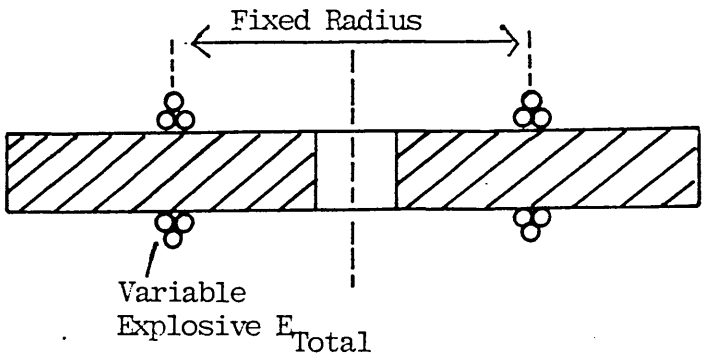

(b) Variable Radius

B Series

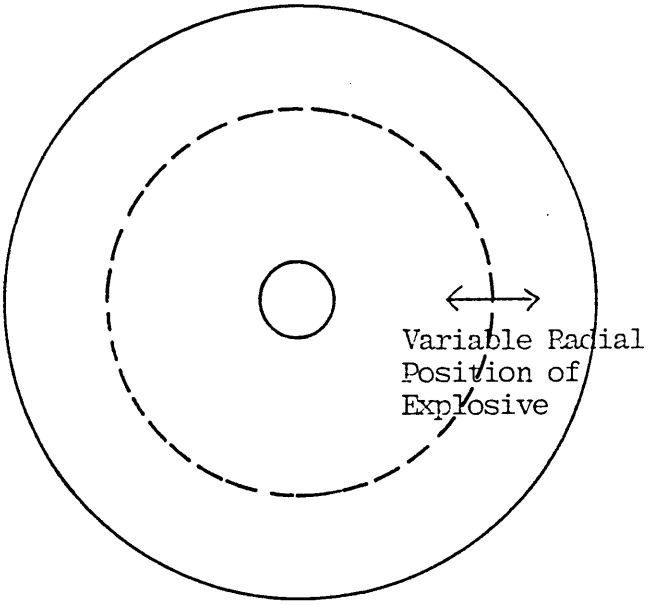

(c) Fixed Radius

C Series

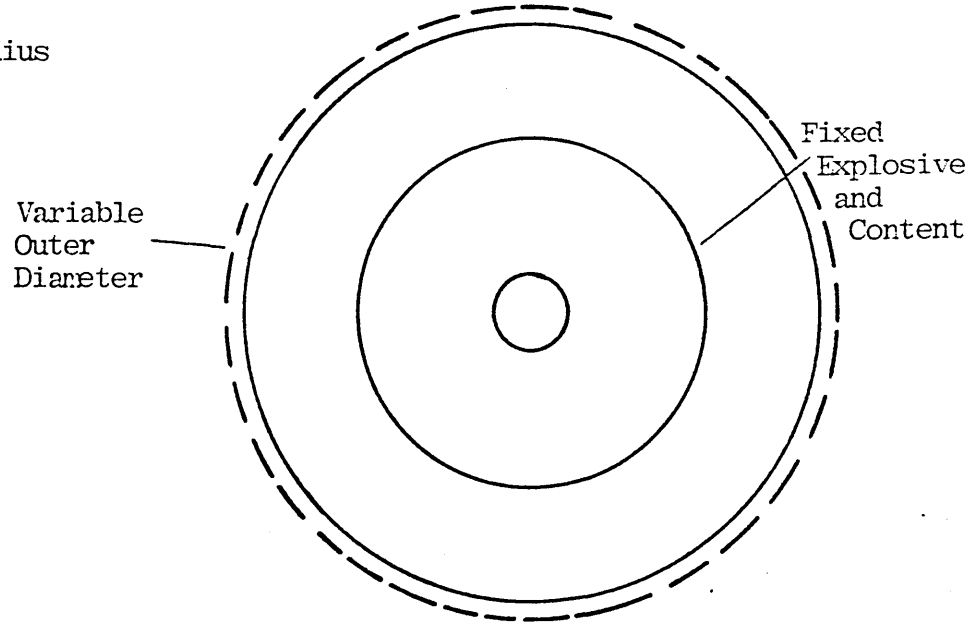

meanings (λ and μ being the Lamé elastic constants, E and G, the engineering moduli, ν is Poisson's ratio and ρ the density.)

Referring to Figure 5.8, the conditions at an interface between two media with an incident longitudinal wave in medium 1 are illustrated.

When there are transmitting media on both sides of the boundary, the relationship between incident and reflected amplitudes at normal incidence is given by

$$\frac{A_r}{A_1} = \frac{\rho_2 v_2 - \rho_1 v_1}{\rho_2 v_2 + \rho_1 v_1} = \frac{z_2 - z_1}{z_2 + z_1} = \frac{1 - n}{1 + n} \qquad 5.12$$

where $z = \rho v$ = characteristic impedance

and $n = z_1/z_2$

The change of phase of π is cancelled if $z_2 < z_1$.

The energy reflection coefficient R is the square of the above quantity.

The transmitted energy fraction $\alpha_E = 1 - R$.

For the more general case of oblique incidence, the partition of energy on the amplitude ratios depend on the resultant impedances which may be real or complex. Equation 5.12 makes it clear that the reflectivity at an interface depends on the difference in characteristic impedances of the two media.

Figure 5.8 : Reflection and Transmission through a Plane Boundary

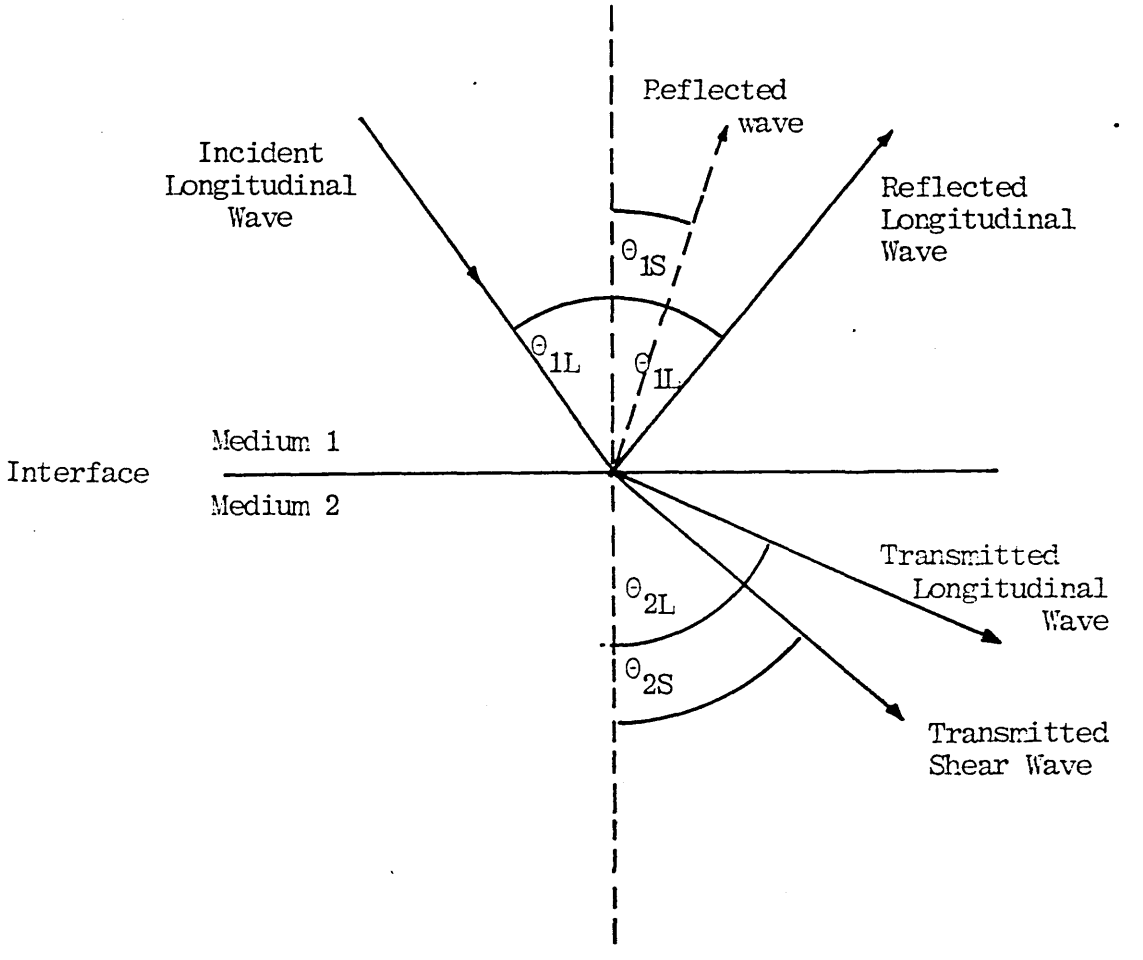

The fraction of energy which is transmitted into the steel discs at the incidence of an explosion is the quantity required by the present consideration. The fraction of the energy which is lost by reflection at an interface can be shown to be

$$\Delta I = 1 - \frac{4z_1z_2}{(z_1 + z_2)^2}$$

where medium 1 has characteristic impedance z_1 and medium 2 has characteristic impedance z_2.

By considering 5.12 which gives reflected amplitude coefficient as $\frac{1 - n}{1 + n}$ and therefore the energy reflection coefficient is

$$\left(\frac{1 - n}{1 + n}\right)^2 = \frac{1 - 2n + n^2}{1 + 2n + n^2} = 1 - \frac{4n}{(1 + n)^2} = 1 - \frac{4z_1z_2}{(z_1 + z_2)^2}$$

Therefore the transmission coefficient = $\alpha_E = 1 - R$

$$= \frac{4z_1z_2}{(z_1 + z_2)^2}$$

The detonation of a chemical high-explosive is accompanied by a high rate of propagation of the detonation wave through the charge, usually of the order of 7000 ms^{-1}. Consequently the physical state of the charge is altered in a very short period of time. A high pressure, high temperature gas bubble is created. The high pressure gives rise to a shock wave which, in turn, is transmitted to the mild steel disc and produces an acoustic wave. This principle is explained in Rinehart and Pearson[53] and Andrews[76].

Figure 5.9 : Explosive System

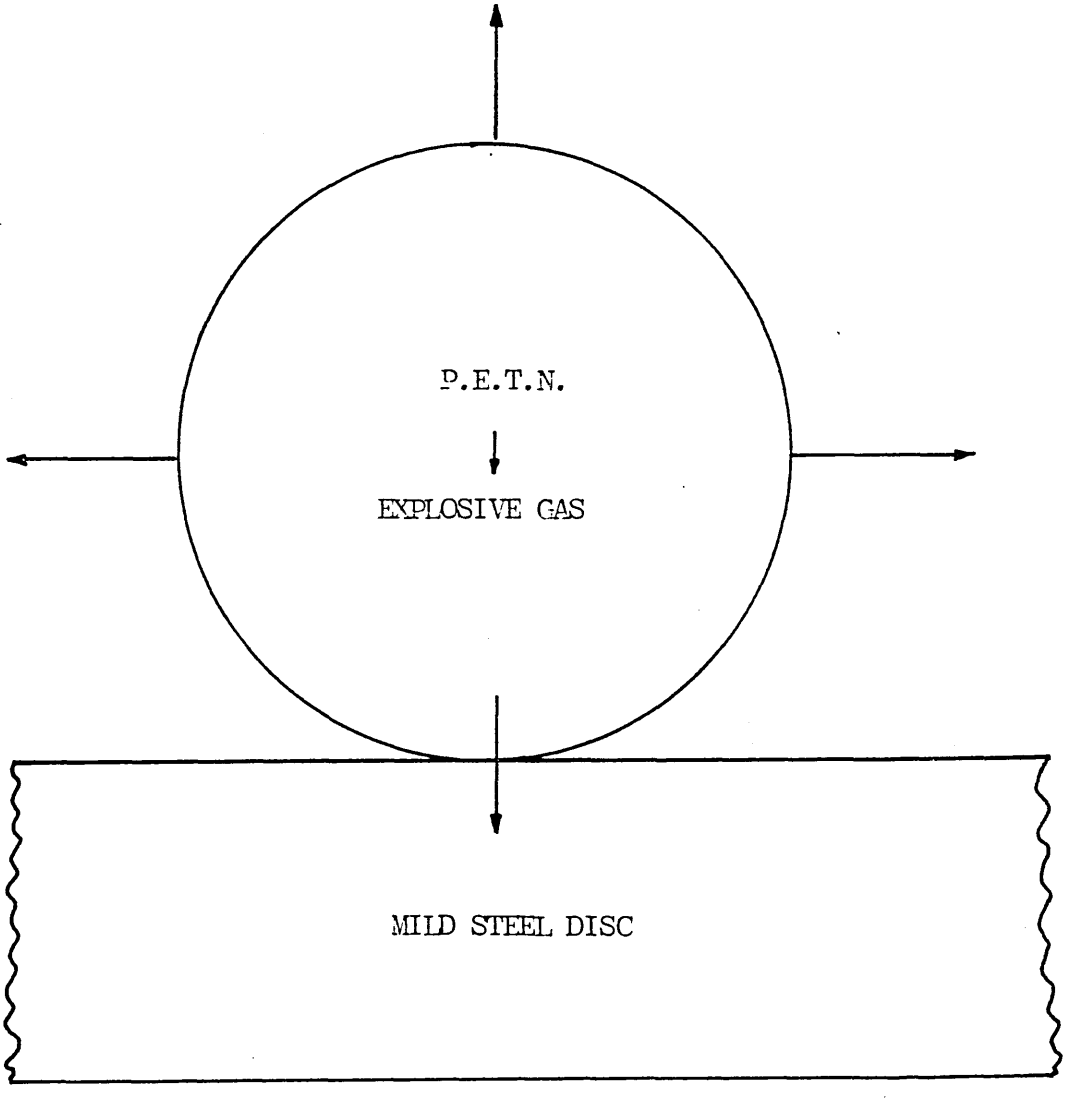

The system used in the present work requires to know the value of the overall transmission coefficient from the exploded PETN gas to steel as shown in Figure 5.9 which further depends on a value of z (characteristic impedance) for the explosive gas.

Hence, a calculation of z for the explosive gas of PETN mixture is calculated using a thermodynamic treatment assuming that

(i) the temperature of PETN at instant of explosion = 5662 K,

(ii) initial pressure is 1 atmosphere,

(iii) initial temperature is 293 K.

Thus pressure change for a fixed mass = $\frac{5662}{293}$ x 1 = 19.32 atmosphere.

Necessary equations:

$$\text{Velocity } v = \sqrt{\frac{\gamma p}{\rho}} \qquad 5.14$$

$$\text{Characteristic impedance } z = \rho v = \sqrt{\gamma \rho p} \qquad 5.15$$

where γ = ratio of principal specific heats

p = pressure of gas

ρ = density

T_K = absolute temperature

For an ideal gas of constant mass

$$p \propto \rho \text{ and } \rho \propto \frac{1}{T_K} \quad \text{ie } \rho \propto \frac{p}{T_K}$$

Thus $z \propto \sqrt{\rho p} \quad \propto \sqrt{\frac{p^2}{T_K}} \quad \propto \frac{p}{\sqrt{T_K}}$ 5.16

Let $z = C \frac{p}{\sqrt{T_K}}$ 5.17

where C = constant of proportionality.

For Air (Beranek[77] p 23) gives z = 406 kg m^{-2} s^{-1} (mks rayls) at a temperature of 293 K

$$C = 406 \times \frac{\sqrt{T_K}}{p} = \frac{406 \times \sqrt{293}}{1} = 6950$$

Therefore $z_{\substack{\text{EXPLOSIVE} \\ \text{GAS}}} = 6950 \times \frac{19.32}{\sqrt{5662}} = 1.78 \times 10^3$ kg m^{-2} s^{-1} 5.18

Now the respective transmission can be calculated for the system as shown in Figure 5.9

Noting that $\alpha_E = \frac{4z_1z_2}{(z_1 + z_2)^2}$ Equation 5.13

Using value of z from equation 5.18

$z_{\text{EXPLOSIVE GAS}} = 1.78 \times 10^3$ rayls

$z_{\text{STEEL}} = 4.196 \times 10^7$ rayls (for a thin plate)

$$\therefore \quad \alpha_{\text{gas-steel}} = \frac{.4 \times 1.78 \times 4.196 \times 10^{10}}{(4.196)^2 \times 10^{14}}$$

$$= \frac{29.875}{17.606} \times 10^{-4} = 1.697 \times 10^{-4}$$

$\therefore$ Transmission Coefficient for exploded gas into steel

$$= 1.697 \times 10^{-4} = \frac{1}{5893}$$

Thus, energy transfer from explosive gas into steel can be expressed as

$$E_{STEEL} = \frac{1}{5893} \quad E_{TOTAL} \qquad 5.19$$

5.9 Deformation at Surface of Annulus due to Energy Transferred from Explosive

5.9.1 Figure 5.10 : Plastically Deformed Region (Energy Transfer from Explosive)

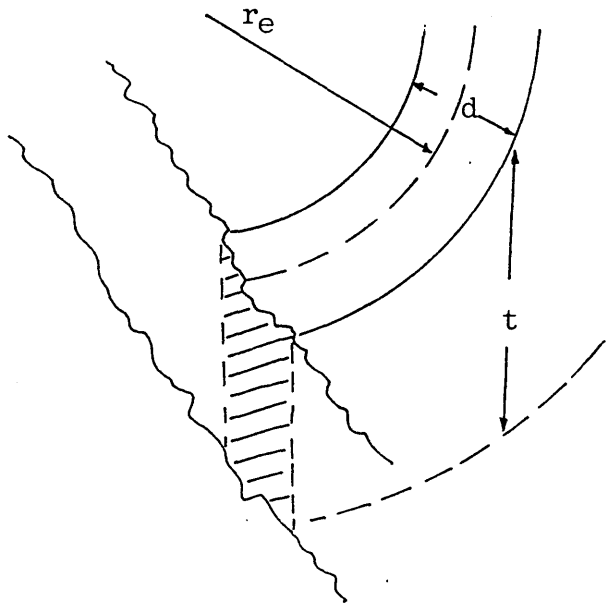

Initially the annulus dimensions will be assumed to be width d, thickness t mean radius r_e.

Let presure on surface of annulus at yield be P_Y.

Area over which P_Y acts is $2\pi r_e d$

$\therefore$ Force acting on top and bottom of annulus

$$= P_Y \cdot 2\pi r_e d$$

$$= fY \cdot 2\pi r_e d$$

where $P_Y = fY$ at yield.

Suppose that the thickness of the annulus, t diminishes by Δt at that point.

Then the work done by the explosive load $= 2\pi r_e dfY\Delta t$

$$= W$$

Values for W have been calculated for varying loads on the basis of impedance matching, Section 5.10

$$\therefore \quad \Delta t = \frac{W}{2\pi r_e dfY} \qquad 5.4$$

5.9.2 A Note on the Value of Y for Mild Steel

For the derivation given in 5.9.1, it has been assumed that the pressure on the surface of the annulus at yield is fY, where Y is the yield stress of the mild steel. An additional consideration in this case is the effect of high strain rate due to explosive loading.

Haque and Hashmi[78] have carried out stress-strain evaluations for mild steel at strain rates up to 10^5 per second and the indications are that yield stress could be 2.5 times as high as static values. It is at points such as this that theories based on high degrees of mathematical exactness are seen to be inappropriate unless the yield stress values are modified. Accordingly, the static experimental stress-strain curve obtained from samples of the disc material was modified to the yield stress corresponding to a mean strain rate prevailing during the compression.

5.10 Table of Theoretical Energy Transferred into Discs

These tables utilised equation 5.19.

The PETN cordtex was assumed to produce energy of 4310 Jg^{-1} and to have a density of .1 g per cm run.

DISC	TOTAL LENGTH OF PETN PER SIDE/cm	$\frac{\text{TOTAL PETN}}{\text{cm}}$	(E_{TOTAL}) TOTAL ENERGY $\frac{\text{AVAILABLE}}{J \times 10^5}$	E_{STEEL} ENERGY $\frac{\text{CONVERTED}}{J}$
A4	284.5	569	2.45	41.57
A6	355.6	711	3.06	51.93
A5	426.7	853.4	3.68	62.45
A7	497.8	995.6	4.29	72.80
A8	569	1138	4.90	83.15
B1	426.7	853.4	3.68	62.45
B2	426.7	853.4	3.68	62.45
B3	426.7	853.4	3.68	62.45
B5	480.1	960.1	4.12	69.91
B6	533.1	1066.8	4.6	78.06
C1	477	954	4.1	69.57
C2	477	954	4.1	69.57
C3	477	954	4.1	69.57
C4	477	954	4.1	69.57
C5	477	954	4.1	69.57

5.11 Example Calculations

In comparing theoretically derived results with experimental results, the following points should be considered:

(i) the results obtained for the third series (C) are based on an improved experimental technique and therefore are expected to be more accurate than those from series A and B;

(ii) the hoop gauge readings give a better resolution than the radial gauges;

(iii) the experimental analysis only gives radial strains from both radial and hoop gauges.

5.11.1 Calculation of $\sigma_{\theta o}$, σ_{ro}, $\sigma_{\theta i}$, σ_{ri} for A6

Data: $Y = 1.95 \times 10^8$ N m^{-2}

$W = E_r = 51.93$ J

$e = 1.2$ cm (2 x diameter of cordtex)

$= 1.2 \times 10^{-2}$ m

$r_o = .1133 + 0.6 \times 10^{-2} = .1193$; $r_o^2 = .0142$

$r_i = .1133 - 0.6 \times 10^{-2} = .1073$; $r_i^2 = .0115$

Calculations:

1. $$\Delta t = \frac{51.93}{2\pi \times .1133 \times 1.2 \times 10^{-2} \times 1.95 \times 10^8}$$

$$= \frac{51.93}{1.6658} \times 10^{-6} = 31.17 \times 10^{-6}$$

2. $$\Delta d = \frac{d}{t} \Delta t = \frac{1.2 \times 10^{-2}}{.635 \times 10^{-2}} \times 31.17 \times 10^{-6} = 5.89 \times 10^{-5} \text{ m}$$

3. $$\phi_o = \frac{1.8 \times 10^{11}}{.69 + \frac{.0363}{.0142}(1.31)} = 4.456 \times 10^{10}$$

4. $$\phi_i = \frac{1.8 \times 10^{11}}{.69 + \frac{.00144}{.0115})1.31)} = 21.077 \times 10^{10}$$

5. $$\Omega = \frac{.1193}{.1073} \cdot \frac{21.077}{4.456} \cdot \left[\frac{1 - \frac{.00144}{.0115}}{.0363/.0142 - 1}\right] = 2.957$$

6. $$e_{\theta o} = \frac{\Delta d}{r_o}\left(\frac{\Omega}{1 + \Omega}\right) = \frac{5.89 \times 10^{-5}}{.1193}\left(\frac{2.957}{3.957}\right) = 36.89 \times 10^{-5}$$

7. $$\sigma_{\theta o} = 4.456 \times 10^{10} \times 36.89 \times 10^{-5}\left[1 + \frac{.0363}{r^2}\right]$$

$$= 16.4 \times 10^{6}\left[1 + \frac{.0363}{r^2}\right]$$

8. $$\sigma_{ro} = 16.4 \times 10^{6}\left[1 - \frac{.0363}{r^2}\right]$$

9. $$e_{\theta i} = -\frac{\Delta d}{r_i}\left(\frac{1}{1 + \Omega}\right)$$

$$= \frac{-5.89 \times 10^{-5}}{.1073}\left(\frac{1}{3.957}\right) = -13.87 \times 10^{-5}$$

10. $$\sigma_{\theta i} = -21.077 \times 10^{10} \times 13.87 \times 10^{-5}\left(1 + \frac{.00144}{r^2}\right)$$

$$= -29.24 \times 10^{6}\left[1 + \frac{.00144}{r^2}\right]$$

11. $$\sigma_{ri} = -29.24 \times 10^{6}\left[1 - \frac{.00144}{r^2}\right]$$

Table 5.1 - Disc A6

r/m	$1-a^2/r^2$	$\sigma_{ri}/10^6 Nm^{-2}$	σ_{ri}(EXP) RG	σ_{ri}(EXP) HG	$1+a^2/r^2$	$\sigma_{\theta i}/10^6 Nm^{-2}$	No exp. results available
.038	0	0	-30		2.00	-58.48	
.05	.44	-12.86		- 9.6	1.56	-45.61	
.06	.61	-17.84	- 2	-38.7	1.39	-40.64	
.07	.72	-21.05			1.28	-37.43	
.08	.78	-22.80			1.22	-35.67	
.09	.83	-24.27			1.17	-34.21	
.10	.86	-25.15			1.14	-33.33	
.11	.88	-25.73			1.12	-32.75	
.1133	.89	-26.0			1.11	-32.45	
	$1-b^2/r^2$	$\sigma_{ro}/10^6 Nm^{-2}$	σ_{ro}(EXP) R		$1+b^2/r^2$	$\sigma_{\theta o}/10^6 Nm^{-2}$	
.1133	-1.84	-30.176			3.84	62.97	
.12	-1.52	-24.93			3.52	57.73	
.13	-1.15	-18.86	-16.6	-27.5	3.15	51.66	
.14	- .85	-13.94	-23.3	-29.4	2.85	46.74	
.15	- .61	-10.00	- 5.1	- 3.2	2.61	42.80	
.16	- .42	- 6.88	- 9.8	- 9.8	2.42	39.68	
.17	- .25	- 4.1			2.25	36.9	
.18	- .12	- 2.0	- 3.0	- 3.4	2.12	34.77	
.19	0	0			2.00	32.8	

5.11.2 Similar calculations to those shown in 5.11.1 will enable tables of comparison between experimental and theoretically predicted results to be produced as follows

Table 5.2 - Disc A5

r/m	$1-a^2/r^2$	$\sigma_{ri}/10^6 Nm^{-2}$	σ_{ri}(EXP)		$1+a^2/r^2$	$\sigma_{\theta i}/10^6 Nm^{-2}$	No exp. results available
			RG	HG			
.038	0	0			2.00	-70.3	
.05	.44	-15.46	-34	-35.8	1.56	-54.84	
			-18.1	-27.7			
.06	.61	-21.44			1.39	-48.86	
.07	.72	-25.31	- 8	-21.9	1.28	-44.98	
.08	.78	-27.42			1.22	-42.88	
.09	.83	-29.17			1.17	-41.12	
.10	.86	-30.23			1.14	-40.07	
.11	.88	-30.93			1.12	-39.37	
.1133	.89	-31.28			1.11	-39.02	
	$1-b^2/r^2$	$\sigma_{ro}/10^6 Nm^{-2}$	σ_{ro}(EXP)		$1+b^2/r^2$	$\sigma_{\theta o}/10^6 Nm^{-2}$	
.1133	-1.84	-36.37			3.84	75.91	
.12	-1.52	-30.05			3.52	69.59	
			-11.7	-16.0			
.13	.1.15	-22.74			3.15	62.27	
.14	- .85	-16.80	-12.4	- 6.0	2.85	56.34	
.15	- .61	-12.06			2.61	51.60	
			-17.2	-10.4			
.16	- .42	- 8.30			2.42	47.84	
.17	- .25	- 4.94			2.25	44.48	
.18	- .12	- 2.37			2.12	41.91	
.19	0	0			2.00	39.54	

Figure 5.11 : Graph of Comparative Values of Radial Stress using Theory, Radial and Hoop Readings for A5

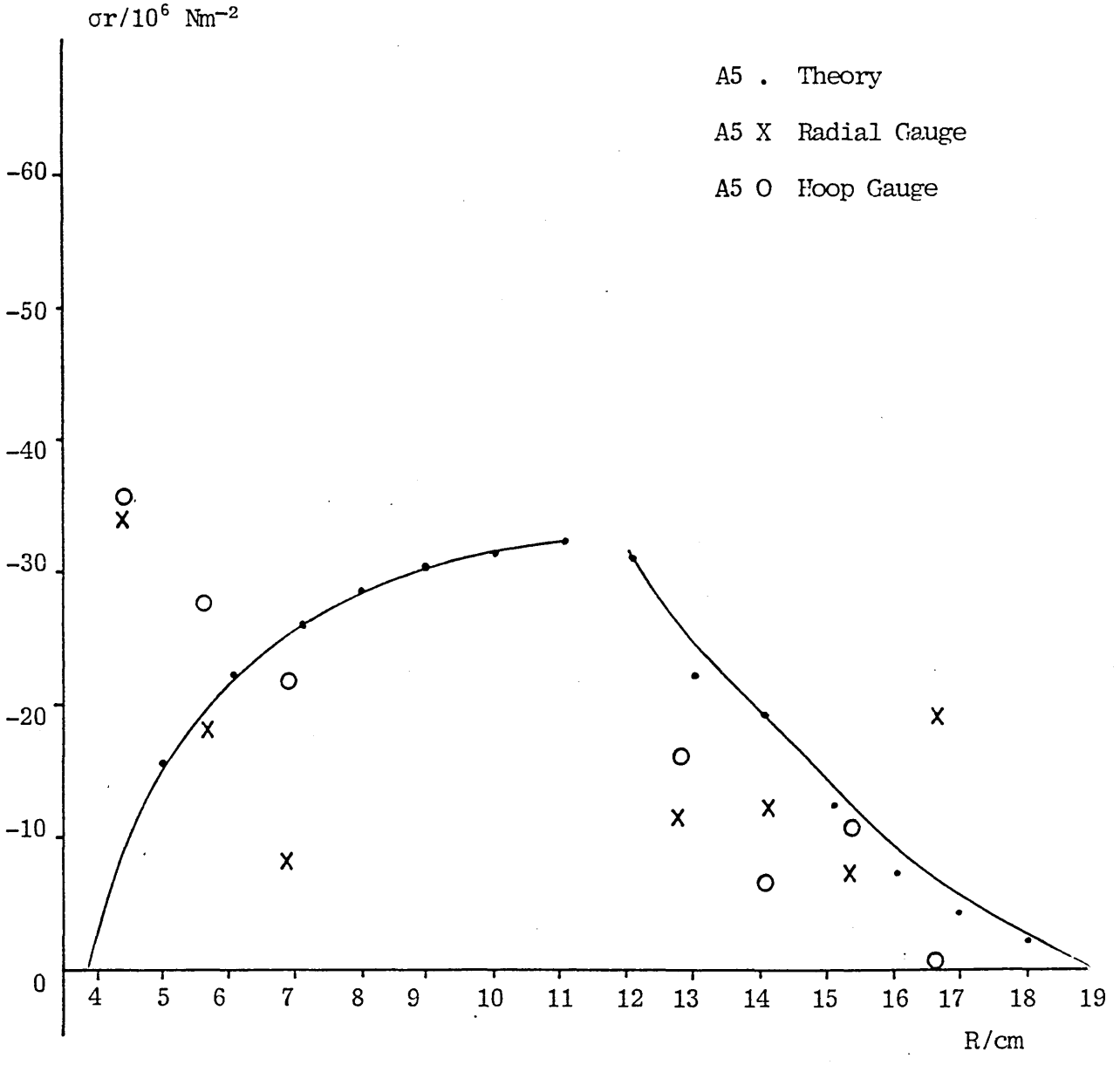

Table 5.3 - Disc B1

r/m	$1-a^2/r^2$	$\sigma_{ri}/10^6 Nm^{-2}$	σ_{ri}(EXP)		$1+a^2/r^2$	$\sigma_{\theta i}/10^6 Nm^{-2}$	No exp. results available
			RG	HG			
.038	0	0			2.0	-214.20	
.05	.44	-47.12	-19.9	-20.5	1.56	-167.08	
.06	.61	-65.33			1.39	-148.87	
			-22.3	-17.0			
.07	.72	-77.11	-25.4	- 8.6	1.28	-137.09	
	$1-b^2/r^2$	$\sigma_{ro}/10^6 Nm^{-2}$	σ_{ro}(EXP)		$1+b^2/r^2$	$\sigma_{\theta o}/10^6 Nm^{-2}$	
.08	-4.67	-79.95			6.67	114.19	
.09	-3.48	-59.57			5.48	93.82	
.10	-2.63	-45.02			4.63	79.26	
.11	-2.00	-34.24			4.00	68.48	
.12	-1.52	-26.02	-27.1	- 5.3	3.52	60.26	
.13	-1.15	-19.69			3.15	53.93	
.14	- .85	-14.55	-70.0	-32.6	2.85	48.79	
.15	- .61	-10.44	-38.4	-14.1	2.61	44.68	
.16	- .42	- 7.19			2.42	41.43	
			- 8.8	- 2.2			
.17	- .25	- 4.28			2.25	38.52	
.18	- .12	- 2.05	- 2.5	- 1.3	2.12	36.29	
.19	0	0			2.0	34.24	

Table 5.4 - Disc B3

r/m	$1-a^2/r^2$	$\sigma_{ri}/10^6 Nm^{-2}$	σ_{ri}(EXP)		$1+a^2/r^2$	$\sigma_{\theta i}/10^6 Nm^{-2}$	No exp. results available
			RG	HG			
.038	0	0			2.0	-98.20	
.05	.44	-21.60	-42.3	-11.5	1.56	-76.60	
.06	.61	-29.95			1.39	-68.25	
			- 2.3	-46.0			
.07	.72	-35.35			1.28	-62.85	
.08	.78	-38.30	- 7.1	-43.3	1.22	-59.90	
.09	.83	-40.70	- 8.1	-46.4	1.17	-57.45	
.10	.86	-42.23	- 4.4*	-40.9	1.14	-55.97	
	$1-b^2/r^2$	$\sigma_{ro}/10^6 Nm^{-2}$	σ_{ro}(EXP)		$1+b^2/r^2$	$\sigma_{\theta o}/10^6 Nm^{-2}$	
.10	-2.63	-50.89			4.63	89.59	
.11	-2.00	-38.70			4.00	77.40	
.12	-1.52	-29.40			3.52	68.11	
.13	-1.15	-22.25			3.15	60.95	
.14	- .85	-16.45			2.85	55.15	
.15	- .61	-11.80	-11.5	-15.8	2.61	50.50	
.16	- .42	- 8.13	- 1.0	-11.8	2.42	46.83	
.17	- .25	- 4.84			2.25	43.54	
			-20.1	-16.1			
.18	- .12	- 2.32			2.12	41.02	
.19	0	0			2.0	38.7	

* radial gauge faulty

Table 5.5 - Disc B6

r/m	$1-a^2/r^2$	$\sigma_{ri}/10^6 Nm^{-2}$	σ_{ri}(EXP)		$1+a^2/r^2$	$\sigma_{\theta i}/10^6 Nm^{-2}$	No exp. results available
			RG	HG			
.038	0	0			2.0	-58.80	
.05	.44	-12.94	-16.6	-42.8	1.56	-45.86	
.06	.61	-17.93			1.39	-40.86	
.07	.72	-21.17	-55.1	-54	1.28	-37.63	
.08	.78	-22.93			1.22	-35.87	
.09	.83	-24.40			1.17	-34.40	
.10	.86	-25.28			1.14	-33.51	
.11	.88	-25.87			1.12	-32.93	
.1133	.89	-26.16			1.11	-32.63	
	$1-b^2/r^2$	$\sigma_{ro}/10^6 Nm^{-2}$	σ_{ro}(EXP)		$1+b^2/r^2$	$\sigma_{\theta o}/10^6 Nm^{-2}$	
.1133	-1.84	-45.43	-56.9	-59.8	3.84	96.38	
.12	-1.52	-38.15	-56.6	-48.2	3.52	88.35	
.13	-1.15	-28.86			3.15	79.06	
.14	- .85	-21.33	-42.8	-39.1	2.85	71.53	
.15	- .61	-15.3	-22.5	-26.2	2.61	65.51	
.16	- .42	-10.54			2.42	60.74	
.17	- .25	- 6.27			2.25	56.47	
.18	- .12	- 3.012	-14.4	-21.3	2.12	53.21	
.19	0	0			2.0	50.2	

Figure 5.12 : Graph of Comparative Values of Radial Stress using Theory, Radial and Hoop Readings for B6

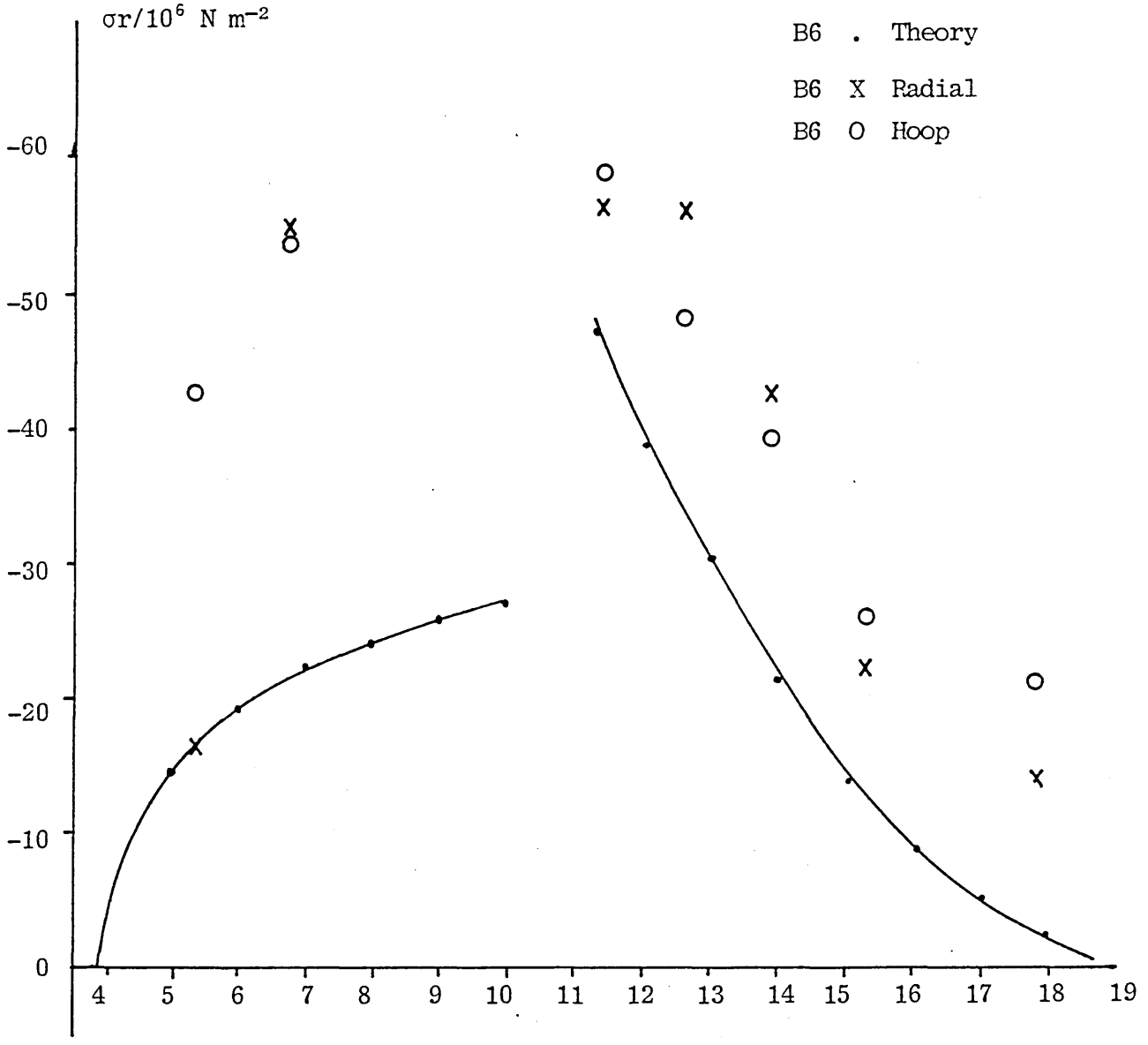

Table 5.6 - Disc C2

r/m	$1-a^2/r^2$	$\sigma_{ri}/10^6 Nm^{-2}$	σ_{ri}(EXP)		$1+a^2/r^2$	$\sigma_{\theta i}/10^6 Nm^{-2}$	No exp. results available
			RG	HG			
.038	0	0			2.0	-76.52	
.05	.44	-16.83	-3.3	-17.7	1.56	-59.68	
.06	.61	-23.34	-9.6	-28.8	1.39	-53.18	
.07	.72	-27.55	-14.5	-32.4	1.28	-48.97	
.08	.78	-29.84	-4.2	-37.9	1.22	-46.67	
.09	.83	-31.75	-11.0	-36.4	1.17	-44.76	
.10	.86	-32.90			1.14	-43.61	
.11	.88	-33.67			1.12	-42.85	
.1133	.89	-34.05			1.11	-42.46	
	$1-b^2/r^2$	$\sigma_{ro}/10\ Nm^{-2}$	σ_{ro}(EXP)		$1+b2/r^2$	$\sigma_{\theta o}/10^6 Nm^{-2}$	
.1133	-1.84	-40.92			3.84	85.40	
.12	-1.52	-33.80	-28.1	-26.6	3.52	78.28	
.13	-1.15	-25.57	-22.1	-21.1	3.15	70.05	
.14	- .85	-18.90	-20.3	-19.4	2.85	63.38	
.15	- .61	-13.56	-11.6	-10.8	2.61	58.05	
.16	- .42	- 9.34	- 7.3	- 8.6	2.42	53.82	
.17	- .25	- 5.56	- 5.1	- 6.5	2.25	50.04	
.18	- .12	- 2.67	- 3.7	- 4.7	2.12	47.15	
.19	0.0	0			2.00	44.48	

Figure 5.13 : Graph of Comparative Values of Radial Stress using Theory Radial and Hoop Readings for C2

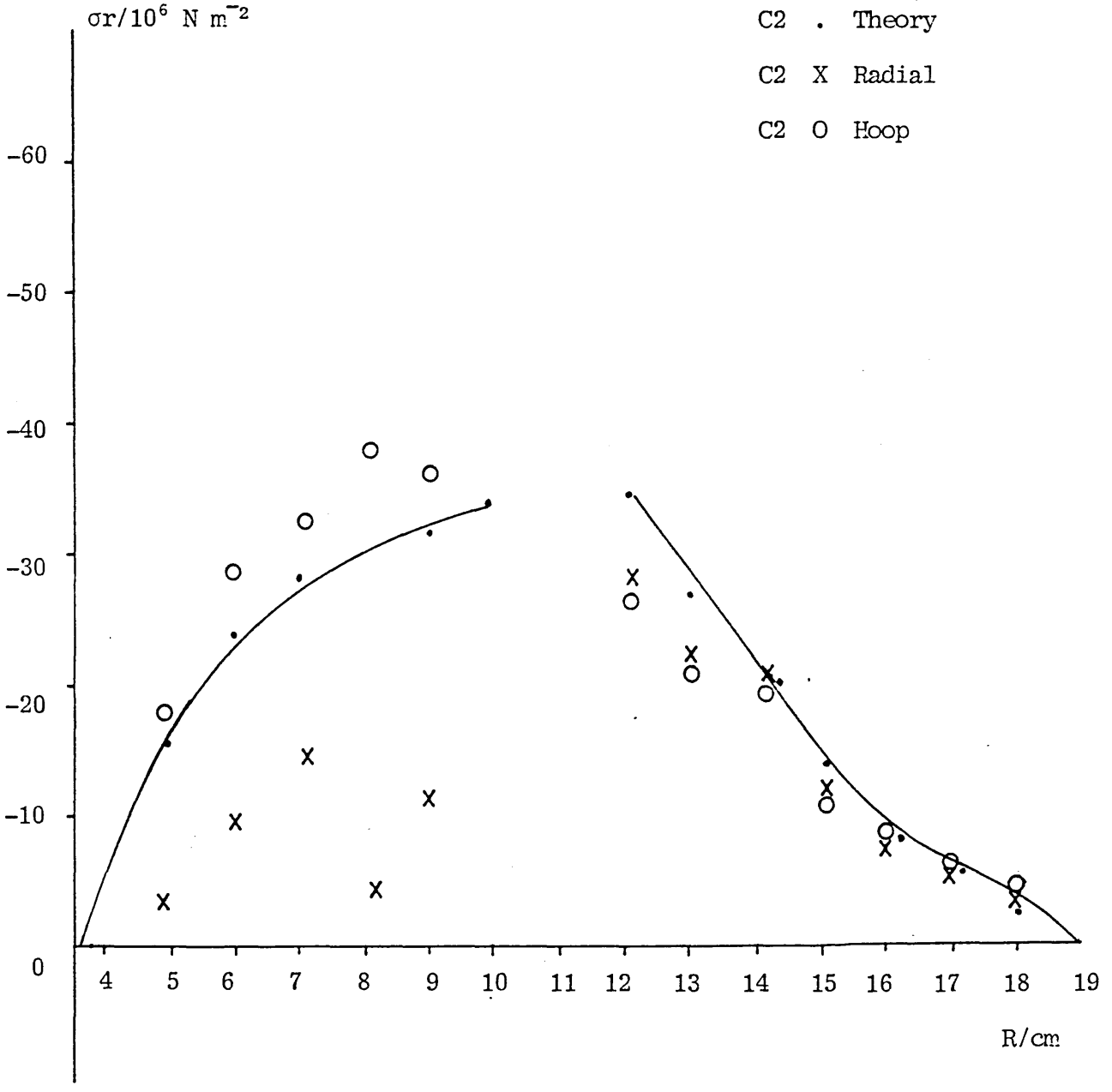

Table 5.7 - Disc C4

r/m	$1-a^2/r^2$	$\sigma_{ri}/10^6 Nm^{-2}$	σ_{ri}(EXP)		$1+a^2/r^2$	$\sigma_{\theta i}/10^6 Nm^{-2}$	No exp. results available
			RG	HG			
.038	0	0			2.0	-34.78	
.05	.44	- 7.65	- 6.6	- 7.9	1.56	-27.12	
.06	.61	-10.61	- 7.9	-13.7	1.39	-24.17	
.07	.72	-12.52	-13.8	-14.1	1.28	-22.26	
.08	.78	-13.56	-18.3	-15.2	1.22	-21.21	
.09	.83	-14.43	-24.4	-15.7	1.17	-20.35	
.10	.86	-14.95			1.14	-19.82	
.11	.88	-15.30			1.11	-19.30	
	$1-b^2/r^2$	$\sigma_{ro}/10^6 Nm^{-2}$	σ_{ro}(EXP)		$1+b^2/r^2$	$\sigma_{\theta o}/10^6 Nm^{-2}$	
.12	- .36	-15.18	- 6.4	- 5.3	2.36	99.56	
.13	- .16	- 6.75	- 6.0	-2.9	2.16	91.13	

5.12 Application of Plastic Deformation Model to Statically Loaded Discs

5.12.1 Calculation of W for Statically Loaded Disc

Measurements taken on the depression caused by the loading ring on the surface of the disc enable a direct calculation of the work done on the surface of the disc to be performed.

For Disc D3, the loading ring radius was 100×10^{-3} m for the inner and 106×10^{-3} m for the outer and the measured depression at 2000 kN load was 1×10^{-4} m. The average measured depression for disc D1 was 1.5×10^{-4} m and for D4 $.75 \times 10^{-4}$ m.

Hence Energy per unit volume = $\frac{1}{2}$ stress x strain

$$= \frac{1}{2} \frac{F}{A} \times \frac{\delta \ell}{e}$$

$\therefore$ Energy available = $\frac{1}{2} F \times \delta \ell$

e.g. for F = 2000 kN and $\delta \ell = 1 \times 10^{-4}$

Energy = 100 J (Disc D3)

A further check using equation 5.4 and assuming

$fY = 1.95 \times 10^{8}$ N m^{-2}

gives the Energy converted as 75 J.

5.12.2 Disc D1

Parameters:

$Y = 1.95 \times 10^{8}$ N m^{-2}

$d = 6.0$ mm $= 6.0 \times 10^{-3}$ m

$r_i = 70.3 \times 10^{-3}$ m; $r_i^2 = 4.9 \times 10^{-3}$

$r_o = 76.3 \times 10^{-3}$ m; $r_o^2 = 5.8 \times 10^{-3}$

$r_e = 73.3 \times 10^{-3}$ m

$a = 38 \times 10^{-3}$ m; $a^2 = 1.44 \times 10^{-3}$

$b = 190 \times 10^{-3}$ m; $b^2 = 36 \times 10^{-3}$

$t = 6.3 \times 10^{-3}$ m

5.12.3 Disc D1 - 2000 kN Load

$$W = \frac{1}{2} (2 \times 10^{6}) \times (1.5 \times 10^{-4}) = 150 \text{ J}$$

$$\Delta t = \frac{1.5 \times 10^{2}}{2\pi(73.3 \times 10^{-3}) \times (6 \times 10^{-3}) \times 1.95 \times 10^{8}}$$

$$= \frac{1.5}{2\pi(73.3)(6)(1.95)} = \frac{1.5}{5388.5} = \boxed{2.78 \times 10^{-4}}$$

$$\Delta d = \left(\frac{6}{6.3}\right) \cdot 2.78 \times 10^{-4} = 2.65 \times 10^{-4}$$

$$\phi_o = 2.26 \times 10^{10}$$

$$\phi_i = 18.7 \times 10^{10}$$

$$\Omega = 1.21$$

$$e_{\theta o} = \frac{2.65 \times 10^{-4}}{76.3 \times 10^{-3}} \left[\frac{1.21}{2.21}\right] = 1.90 \times 10^{-3}$$

$$e_{\theta i} = -\frac{2.65 \times 10^{-4}}{70.3 \times 10^{-3}} \left[\frac{1}{2.21}\right] = -1.70 \times 10^{-3}$$

$$\sigma_{ro} = 2.26 \times 10^{10} \times 1.90 \times 10^{-3} \left[1 - \frac{36 \times 10^{-3}}{r^2}\right]$$

$$= 4.3 \times 10^{7} \left[1 - \frac{36 \times 10^{-3}}{r^2}\right]$$

$$\sigma_{\theta o} = 4.3 \times 10^{7} \left[1 + \frac{36 \times 10^{-3}}{r^2}\right]$$

$$\sigma_{ri} = 18.7 \times 10^{10} \left[-1.70 \times 10^{-3}\right] \left[1 - \frac{1.44 \times 10^{-3}}{r^2}\right]$$

$$= -31.8 \times 10^{7} \left[1 - \frac{1.44 \times 10^{-3}}{r^2}\right]$$

$$\sigma_{\theta i} = 31.8 \times 10^{7} \left[1 - \frac{1.44 \times 10^{-3}}{r^2}\right]$$

Table 5.8 - Disc D1

r/m x 10^{-3}	EXP	THEORY	EXP	THEORY
	$\sigma_r/10^6 Nm^{-2}$	$\sigma_r/10^6 Nm^{-2}$	$\sigma_\theta/10^6 Nm^{-2}$	$\sigma_\theta/10^6 Nm^{-2}$
47	-288	-111	-215	-525
66	-237	-213	-251	-423
81	-225	-193	+225	+279
101	- 70	-108	+208	+195
106	- 16	- 92	+206	+181

Table 5.9 - Disc D3 - 2000 kN

r/mm	EXP	THEORY	EXP	THEORY
	$\sigma_r/10^6 Nm^2$	$\sigma_r/10^6 Nm^{-2}$	$\sigma_\theta/10^6 Nm^{-2}$	$\sigma_\theta/10^6 Nm^{-2}$
70	-200	- 61	-100	-111
80	-175	- 67	-100	-106
95	-150	- 72	- 75	-100
	σ_{ro}		$\Theta_{\theta o}$	
110	-100	- 67	+150	+133
130	- 50	- 38	+100	+105
140	- 45	- 28	+81.5	+ 95
150	- 27	- 20	+ 71	+ 87

Table 5.10 - Disc D4 - 2000 kN (Load)

	EXP	THEORY	EXP	THEORY
$r/m \times 10^{-3}$	$\sigma_r/10^6 Nm^{-2}$	$\sigma_r/10^6 Nm^{-2}$	$\sigma_\theta/10^6 Nm^{-2}$	$\sigma_\theta/10^6 Nm^{-2}$
48	- 12	- 10	- 45	- 45
67	- 15	- 18	- 40	- 36
123	- 70	- 25	-160	- 30
144	- 55	- 20	+ 70	+ 73
160	- 46	- 11	+ 69	+ 64
176	- 34	- 4	+ 62	+ 57

5.13 Conclusions

Beginning with the assumptions in Section 5.2, the work then goes on to analyse the boundary conditions for the plastic region, the magnitude of the radial stress in terms of the explosive compressive stress, the edge and surface deformation of a plastically loaded disc (including the error of such an analysis) and the calculation of the derivation of the stress formulae. The energy transfer from the explosive to the disc and the surface deformation of the annulus of the disc due to explosive loading has then been considered. Examples of calculations of the stresses for various discs have then been calculated and compared with experimental values. In the examples related to the explosively loaded discs, the correlation between theoretical model and experimental results is close but it should be noted that since the experimental values do not approach the exploded ring radius within ± 35 mm (maximum) and ± 15 mm (minimum) the values close to the deformed area are not correlated. A similar conclusion may be made in relation to the statically loaded discs where in this case it has been possible to extend the comparison between experimental and theoretical results to the deformed ring area. There is evidence of a divergence of predicted and theoretical results in the cases of D3 and D4 with the results close to the deformed area. However, in general the plastic deformation model gives a close prediction of the residual loading stresses of the metal discs. The

exceptions may be ascribed to the buckling of the plate which produces differential stress levels especially at the loaded annulus. Finally, it may be concluded that, due to the agreement between experimental and theoretical values, the assumptions made at the beginning are in fair accord with the practical situation encountered in both the dynamic and static loading tests. The correlation between experimental and theoretical values also indicate that the key factor of energy transfer in the case of the dynamically loaded discs and the measured loading ring depression in the case of the statically loaded discs have been calculated and measured respectively to be of the right order of magnitude.

6. DISCUSSION AND COMMENTARY

6.1 Introduction

6.2 Dynamic Loading Tests (A, B and C Series)

6.3 Static Loading Tests (D Series)

6.4 Buckling Tests (E Series)

6.5 Special Measurements : Hardness, Plane Symmetry, Microstructure

6.6 Plastic Deformation : Theoretical Analysis

6.7 Finite Element Analysis

6.8 Final Comments

6. DISCUSSION

6.1 Introduction

The main objective of the work has been to ascertain if residual stress could be induced into metal discs by static and dynamic compression so as to increase the service life of engineering components of similar size and shape, ie disc-shaped circular saws, turbine rotors etc.

With these objectives in mind, an elaborate test programme was undertaken, the results of which will be discussed in this chapter. The application of explosive charge to the disc surface for dynamic pre-stressing governed the technique which was adopted to record and analyse the results especially the fact that only post-operative methods could be used.

The static pre-stressing tests, however, allowed a more controlled approach for recording and analysing the experimental results.

Having analysed the experimental results for both dynamic (explosive) and static (press) loading, a mathematical model was established. This model has been formulated using the plastic deformation characteristics applied to both cases. Finally an elastic-plastic finite element method was applied to the static loading case only.

Hence, it has been possible to compare the results from the dynamically loaded discs with similar discs loaded statically (both theoretical and experimental).

6.2 Dynamic Loading Tests (A, B and C Series)

These series of tests were designed to determine the effect of i) magnitude of load (A series), (ii) position of load (B series) and (iii) changes in outer diameter of disc (C series).

The results have been described in Section 3.1. Apart from the changes in loading parameters, the opportunity was taken to look for consistency between the results from A, B and C series of tests. For the A, B and C series of tests, the strain gauge data produced two sets of results:

(i) a general boring out/turning down technique which could only produce radial measurements of residual stress (Section 3.1.3.1); and

(ii) a final cut technique (Section 3.1.4.2) which enabled estimation of both radial and hoop residual stress to be found in close proximity to the loaded annular zone.

Considering, first the boring out/turning down exercise [Section 3.1.3.2 explains the adopted method], it should be noted that in all cases there is a zone of annulus of approximately 50 mm wide extending between the position of the strain gauge rosette and the loaded annulus where

no machining could be carried out. The strain gauge rosette itself measured 25 mm square and the deformation zone spread over 20 mm (see Figure 2.1). This remaining annulus fixed the radii for the final inner and outer cuts taken from the disc material. Hence from the dynamic tests it has not been possible to obtain values of residual stress close to the loading zone annulus. However, some general characteristics were observed as follows:

A series : for the inner section of the disc, the residual radial compressive stresses show an average level ranging between 2 and 40 MN m^{-2} with no clearly definable trend with loading level. On the other hand, the outer annulus indicates a definite correlation between the applied load and the level of residual stress. As the applied loads increased the level of residual stress near the loaded zone decreased, the values of residual radial stress ranging from 28 MN m^{-2} for the disc A4 to 13 MN m^{-2} for the disc A8 (see Figures 3.6 and 3.7).

The results for the inner section of the discs were based on two strain gauge readings per disc but no clearly definable trend could be observed. However, at the outer sections the decrease in residual stress with increasing energy may be explained by suggesting that, with increasing plastic deformation at the loading zone, less energy was available for elastic strain.

B series : it should be noted that the B series incorporated two patterns of loading, in that discs B1, B2 and B3 represented the same amount of applied explosive energy with increasing ring radius and discs B3, B5 and B6 represented tests with constant explosive charge per unit circumferential length (charge ratio) at increasing radius.

Table 6.1 gives the relevant details.

Table 6.1

Disc	r_e/mm	r_g/mm	Length of Explosive per side/m	Charge Ratio
B1	76	81	4.26	9
B2	89	94	4.26	7.6
B3	101	106	4.26	6.7
B5	114	109	4.80	6.7
B6	127	109	5.33	6.7

As is evident from Figures 3.8 and 3.9 in Section 3.1, the first series of tests B1, B2 and B3 do not show any predictable pattern for the inner radial residual stress except a generally expected decrease of stress level with increase of the radius of the loading zone. The outer radial residual stresses show a significantly higher level (65 MN m^{-2}) near the loading zone radius for disc B1 than those observed in discs B2 and B3, indicating that the decreased charge ratio has produced influence on the level of residual stress.

In considering the B3, B5 and B6 discs, the radial residual stress levels show higher values towards the inner radius of the discs.

eg B3 42.3 MN m^{-2} at 5.1 cm radius

B5 33.0 MN m^{-2} at 5.5 cm radius

B6 16.0 MN m^{-2} at 5.3 cm radius

whereas the radial residual stress values based on the hoop gauges show an overall level of approximately 46.0 MN m^{-2} for the inner zone of the discs (see Table 3.5). For the region of the discs outside the loading zone, results from B3, B5 and B6 tests show a definite trend with increasing load radius of increasing radial residual stress levels (see Table 3.6),

eg B3 11.6 MN m^{-2}

B5 43.6 MN m^{-2}

B6 56.9 MN m^{-2}

Here, it should be noted, however, that in the case of B5 and B6 the strain gauges were fixed inside the loading annulus and therefore the radial residual stress values quoted above for B5 and B6 represent those at locations much closer to the actual loading zone than has been the case with the other B series readings. Nevertheless, the increasing radius of the loading annulus has produced an increase of radial residual stress in the outer zone which represents an increase, for constant charge ratio, which can be related to the decreasing area of the outer zone of disc at a larger radius available for pre-stressing.

C series : the four discs C1, C2, C3 and C4 were made with decreasing outer diameters ranging from 430 mm to 280 mm respectively. The position of the explosive ring remained constant at 227 mm diameter in all four cases and the explosive charge ratio at 6.7 for each side. As can be seen from Figures 3.10 and 3.11, the measured radial residual stress values throughout the inner zone of the discs indicate, on average, a decrease in residual stress level with decreasing size of disc (ie outer diameter). The outer zones indicate a strong correlation with the radial residual stress, the magnitudes of which decrease as the outer radius of the disc is reduced. Thus, for constant energy at a fixed radius, the greater the volume of metal available the higher the residual stress values.

Now, considering the values obtained from the final cuts technique for the discs in the A and B series of tests where it has been possible to obtain both radial and hoop residual stresses, it is possible to make a more definitive statement with regard to the radial and hoop residual stress values in the parts of the disc in close proximity to the plastically deformed loading zone.

A series : from Figure 3.4 in Section 3.1, it is evident that for the inner regions the compressive radial residual stresses at the same radial positions (see Table 3.1) show a decrease from 40 MN m^{-2} in disc A4 to about 8 MN m^{-2} in discs A7 and A8 with increasing load

whereas the compressive hoop residual stresses indicate relatively less variation of between 30 and 20 MN m^{-2}. Again, referring to Figure 3.4, the radial and hoop residual stresses on the outer zone indicate a decrease from -30 and +28 MN m^{-2} respectively in disc A4 to -6 and +2 MN m^{-2} respectively in disc A8. It should be noted that these results are consistent with those described for the A series in the earlier part of this section.

B series : the two series, B1, B2 and B3, and B3, B5 and B6, represent two forms of loading and will therefore again be discussed separately.

(a) B1, B2 and B3 [constant total energy with increasing radius] Referring to Table 3.2 and Figure 3.5a, the inner regions show that the compressive radial residual stress levels increase from 19 MN m^{-2} in disc B1 to 49 MN m^{-2} in disc B3 for increasing radius of loading zone whereas the compressive hoop residual stress shows a decrease from 24 MN m^{-2} to 7 MN m^{-2}. On the other hand, the outer regions show an increase of compressive residual stress from 4 MN m^{-2} in disc B1 to 16 MN m^{-2} in disc B3 for increasing radius of loading zone, whereas the tensile hoop residual stress values decrease with increasing radius of the loading zone from 68 MN m^{-2} to 11 MN m^{-2}. In general then the residual radial stresses increase with increase of radius for both inner and outer zones and the residual hoop stresses decrease with

increase of radius for both inner and outer zones.

It would be difficult to ascribe reasons for this behaviour without reference to the plane symmetry deformation measurements given in Table 2.6, Chapter 2. The table indicates that plane symmetry deformation was greatest for disc B1 and less for discs B2 and B3 so it may be concluded that when less energy goes into buckling the greater the residual radial stress and also the residual hoop stress values are greater with the greater degree of plane symmetry deformation.

(b) B3, B5 and B6 [constant explosive charge ratio with increasing radius of explosive] Referring to Table 3.2 and Figure 3.6b, the inner parts show increasing values of compressive residual stress for both radial and hoop stress with increasing radius of loading zone. The radial residual stress at the inner zone is varying from -49 MN m^{-2} in disc B3 to -73 MN m^{-2} in disc B6 and the hoop inner from -7 MN m^{-2} in disc B3 to -70 in disc B6.

The outer regions also show a significant increase in both radial and hoop residual stress values with increasing radius of loading zone. The radial residual stress at the outer zone is found to be varying from -16 MN m^{-2} in disc B3 to -72 MN m^{-2} in disc B6 and the hoop residual stress is seen to be varying from +11 MN m^{-2} in disc B3 to 75 MN m^{-2} in

disc B6. In this series (B3, B5 and B6), the degree of plane symmetry deformation (Table 2.6) is reduced compared with that for the B1, B2 and B3 series and so the residual stress values tend to follow the expected pattern of increasing with increased amount of explosive loading energy (see Table 3.1) and with increasing radius of loading zone.

6.3 Static Loading (D Series)

The experimental results in terms of residual stress values for the D series of tests are given in Section 3.2.8, Figures 3.17 to 3.21.

The D series of tests were carried out subsequent to the dynamic tests in order to use a different approach to the experimental technique used for the dynamic tests. Apart from the benefits afforded by the static loading in terms of incremental method and a more precisely defined and controlled loading of the discs, it was also possible to improve the strain resolution by using reduced size of strain gauge elements from 10 mm to 3 mm. Thus, it was possible to obtain residual stress values in very close proximity to the loaded zone.

With these tests, the strain gauges were attached prior to loading at fixed radii and therefore the estimation of residual stress at fixed radii over the whole surface of the disc requires a much simpler technique. In this series of tests, the discs, D1, D2, D3 and D4 (see

Figure 2.22) were loaded by means of rings of increasing radii from 73 mm radius for disc D1 to 133 mm radius for disc D4. A consistent overall stress pattern was produced for the four discs, as shown schematically in Figure 3.17, with residual radial and hoop compressive stress near to yield for maximum 2000 kN loads for the zones inside the loading annulus. The residual hoop stress changed from compressive in the inner zone to tensile for the zones outside the loading rings. This pattern fits the physical model whereby the inner zone of the disc is under compression from the loading ring annulus and consequentially both the radial and hoop residual stresses are in a state of compression whereas for the outer zones of the disc the loading ring is trying to expand the zone and thereby produces compressive radial stresses but tensile hoop stresses.

The appraisal of the results given in Section 3.2.9 indicates that in this series of tests the levels of residual radial and hoop stresses are of the same order of the yield stress of the material ($\cong$ 200 MN m^{-2}) in the annuli up to the loaded zone. This observation can be explained by noting that residual stresses refer to a system of stresses that exist in a body free from external force or restraint. As a result of loading, each position of the body must accommodate itself into a compatible shape through mutual reaction with its partners. This accommodation is accomplished by strain and this strain

induces the stress system which is called residual stress. The relationship between the stresses and strains is elastic, for if at any point the body were plastic, it would yield to the extent that the stress-strain relationship at that point would subside into the elastic range. Thus the plastically deformed zone can be seen to be inducing residual stress values of the order of the elastic yield stress in the adjoining regions.

The different radii of the loading rings for disc D1, D2, D3 and D4 has moved the position of the peak residual stress from 73 mm mean radius in the case of D1 to 103 mm mean radius for D2 and D3 and 133 mm mean radius for disc D4. The maximum residual stress induced in the inner zone of disc D1 is recorded as 275 MN m^{-2} for the radial residual stress and 250 MN m^{-2} for the hoop residual stress. As the radius of the loading ring increases, the maximum value of radial residual stress in the inner zone has been reduced to 175 MN m^{-2} for disc D3. The residual hoop stresses for the inner zones showing a similar reduction from 250 MN m^{-2} for disc D1 to 125 MN m^{-2} in the disc D3. The residual stress values found in the outer zones for discs D1, D2 and D3 indicate that the levels of residual stress found in the inner zones are transferred across the loading ring boundary to the outer zone. Hence the value of the residual radial stress in the outer zone for disc D1 is 225 MN m^{-2} and 140 MN m^{-2} for D3 with residual hoop stress being 150 MN m^{-2} for disc D1 and 80 MN m^{-2} for disc D3. The residual stress values for

disc D4 indicate a complete reduction to approximately zero. It should be noted that, if the stress values for the loading value of 1500 kN are considered, it can be seen that in the inner zone the radial stress reached a value of 100 MN m^{-2} and the hoop stress 175 MN m^{-2} with similar values for the outer zone adjacent to the loading ring. However, when the compressive load was increased beyond 1500 kN, the stress values started to decrease with increasing loads to 2500 kN. The reason for this trend may be attributed to the onset of buckling of the disc thus relieving both the hoop and radial stresses. The onset of buckling at 1500 kN has indeed been confirmed as indicated in Section 3.2.10. It should be noted that the position of the loading ring for disc D4 was of radius 133 mm compared with 103 mm for disc D2 and D3 and 73 mm for disc D1. This might have made buckling as the preferred mode for failure at small load intensity. The D series of tests enabled a comparison to be made with similar loading conditions for the A and B series (the C series involved varying size of disc and therefore only C2 is of comparable size). Comparisons may also be made for similar loading levels and variable radii, eg D1 with B1, D2 with B3 and D4 with B6. A typical comparison is shown in Table 6.3 based on extracts from Tables 3.1, 3.5, 3.6 and Figure 3.19, which compares radial residual stress values.

Table 6.3 : Comparing radial residual stress values for Discs D2 and B3

B3 : r_e = 10.2 cm, Load = 62.4 J

D2 : r_e = 10.3 cm, Load = 624 kN (≡ 62.4 J)

B3		D2	
r/cm	$\sigma r/10^6$ N m^{-2}	r/cm	$\sigma r/10^6$ N m^{-2}
7.80	- 7.1	7.0	- 10
9.20	- 8.1	9.0	- 10
15.0	-11.6	15.0	- 15

The comparison of results is limited by the number of results available for disc B3 and probably shows evidence of presence of some pre-stressing in the discs before loading. A further comparison can be shown between discs D3 (static) loading curve for 750 kN (≡ 75 J) and disc A7 (dynamic) loading 73 J. Both discs have similar dimensions and loading parameters. The results for comparison can be obtained from Tables 3.3 and 3.4 and Figure 3.20 and are shown in Table 6.4.

Table 6.4

	A7	D3
r/cm	$\sigma r/10^6$ N m^{-2} (Based on Hoop Gauge)	$\sigma r/10^6$ N m^{-2}
5.0	- 29.6	-
6.3	- 29.2	- 30
130	- 23.7	- 25
140	- 13.8	- 20
153	- 7.2	- 10

The agreement is close and provides evidence that the dynamic and static loading methods produce comparable results. However, the dynamic method adopted in these tests only provides a limited maximum load for producing residual stress patterns as can be seen when comparing the effective load for dynamic loading of 75 J compared with static loading which can provide 200 J.

6.4 Buckling Tests (E Series)

6.4.1 This series of tests was carried out as a result of detecting buckling in both the dynamic tests and the subsequent static tests. With the dynamic tests, it was not possible to detect at what load the onset of buckling took place, indeed some of the buckling could well be ascribed to the loading method [see Section 2.2.1.3]. For if the detonation pulse arrived at one side of the disc before the other, a differential shock would have been produced. Also non-axisymmetric positioning of the loading rings could produce different effects. Inspite of adopting a system to minimise these two effects, some evidence of buckling and differential application of load was detected [see 6.5].

6.4.2 For the static tests, the conclusions given in Section 3.2.10.8 indicate that the onset of buckling commenced with a load approaching 1000 kN for disc E1. Disc E1 had the same dimensional and loading parameters as B3, B5, C2, D2 and D3. But the more important point in these tests is the agreement between the experimental observations and the results from the predictive method used for the onset of buckling. Thus, by considering Figures 3.24, Figure 3.25 for disc D3 and remembering that the loading conditions for discs E1 and D3 were very similar, it can be seen that the prediction for the onset of buckling at loads greater than 1000 kN shows good agreement between experiment and predictions.

In disc E4 in which there was no evidence of buckling, the effect of non-concentric top and bottom loading rings was detected [Section 3.2.10.5]. Hence a comparison could be made with non-concentric positioning of the explosive rings in the dynamic case. The implication of these tests is that with the dynamic tests the transferred energy ranged from 40 to 83 J whereas in static test, E7, the transferred energy at the onset of buckling (at 1000 kN) can be calculated to be 75 J, as demonstrated in Section 5.12.1. Thus the deformation modes in the A, B and C series of tests which were subjected to less than 75 J may be partly attributed to non-concentric loading with a contribution from loading level.

6.5 Plane Symmetry, Hardness, Microstructural Analysis

6.5.1 Plane Symmetry Measurement

Plane symmetry measurements were carried out for the dynamically loaded discs (A, B and C series) and for the discs tested statically for buckling (series E). No plane symmetry tests were carried out on the D series since the loading parameters and dimensions for discs D2 and D3 were identical to those of disc E1. A further comparison can then be made in terms of transferred energy for the dynamic tests (A, B and C series) with the static tests E1 (≡ D2/D3) at the onset of buckling.

Table 6.2 shows that the plane symmetry deformation level is comparable for similarly loaded discs in both the static and dynamic mode.

Table 6.2

Disc	Loading Ring Radius/mm	Load/kN	Energy Transfer/J
B3	102	1000 (MAX)	63
B5	114	1000 (MAX)	70
C2	113	1000 (MAX)	70
D2/3	104	1000	75
E1	108	1000*	75

* Onset of buckling

6.5.2 Hardness Tests

The hardness tests were carried out to establish the localized nature of the plastically deformed annulus. The tests which are described in Section 2.5.1.2 were carried out with the aid of a portable hardness tester thus avoiding the need to take specimen samples from the disc. The hardness measurements were taken pre- and post-dynamic loading. Summary tables 2.7, 2.8 and 2.9 show that for the A series the Brinell hardness at the loaded zone increased from 97 to 105 for A4 and a maximum recorded hardness for A8 of 115, for the B series the Brinell hardness at the loaded zone increased from 98 to 111 for B1 and 117 for B3, dropping back to 113 for B5 and B6, and for the C series the Brinell hardness at the loaded zone increased from 98 to 112 for C1 and a maximum 117 for C4.

As can be seen from Figures 2.23 (A series), 2.24 (B series) and 2.25 (C series) the post-experimental hardness measurements remained close to the pre-experimental hardness measurements at the inner and outer boundary radii of the discs. It is interesting to note from Table 2.9 that the non-annealed disc C5 did not show the same changes in hardness measurement for pre- and post-experimental loading. At the loading zone, the Brinell hardness changed from 118 to 122 with no change at the inner radial boundary and a change from 120 to 122 at the outer radial boundary.

6.5.3 Microstructural Investigation

As described in Section 2.5.1.3, microstructural tests were carried out on a section of disc A8 taken from the loaded region. Six positions were photographed ranging from the centre of the loaded zone to 15 mm distance in the inner and outer directions, as shown in Figure 2.24. An investigation of the photomicrographs indicate that evidence for shock twinning, indicating plastic deformation, only extended from the centre of the loaded zone to a region 13 mm either side of the centre.

6.6 Plastic Deformation Analysis

The plastic deformation analysis has been applied to both the dynamic and statically loaded discs. The dynamic loading model relies on an estimation of the amount of energy transferred to the disc from the explosive ring and it has been shown that the transfer factor is 1/5893 (see Section 5.8.2) which is a very small fraction of the energy supplied. However, the results in Tables 5.1 - 5.7 produced by the model when compared with the experimental results show close agreement and therefore may be said to validate the transfer factor deduced. The plastic deformation model for the statically loaded discs required an assessment of the work done by the loading ring at the disc surface which in turn required the depth of indentation. This was obtained by a series of surface measurements and the results are given in Section 5.12.1. For the statically loaded discs, the transferred energy was twice the level of the dynamic energy transferred from the explosive charge. The consequent higher values of residual stress produced in the discs still showed reasonably good agreement with those given by the mathematical model (Tables 5.8, 5.9 and 5.10). However, there is some divergence between the inner radial predictions from theory and those obtained from experimental measurements. The reason for this divergence could again be attributed to the inner zones of the disc exhibiting buckling at the loads tabulated. An example of this is shown in Table 5.8 for disc D1 where the radial residual stress values given by the experimental predictions

records -288 N m^{-2} at 47 mm radius and the theoretical value estimates that the value should be -111 N m^{-2}. For disc D3 at inner radius 70 mm, the experimental prediction of residual radial stress records -200 N m^{-2} whilst the theory only predicts -61 N m^{-2}.

6.7 Finite Element Analysis

The finite element analysis showed very close agreement between experimental and theoretical results, for example see Figures 4.4, 4.5 and 4.6.
There was one exception, that being the part of the disc on the inner side of the loading ring. Here the finite element analysis indicated a rapid fall of predicted stress with decreasing radius but the experimental values showed a high level of residual stress. An explanation of this disparity was given in Section 4.7.4 but in short could be ascribed to the difference between the idealised theoretical analysis and the actual experimental results where in the inner region a degree of dishing occurred.

Reference to the previous Section 6.6 indicates that both the finite element analysis and the Plastic Deformation analysis are in accord in predicting a rapid fall in radial residual stress values for the inner zones of the discs, whilst the measured results indicate a significantly higher level.

6.8 Final Comments

In many applications the plastic strain is very much larger than the elastic component, and it is permissible to neglect the latter in analysing the deformation. In this case, however, the amount of deformation in the plastic region is constrained by a surrounding boundary of elastic material, and the total strain throughout is limited to be of the order of elastic strain.

In the A, B and C series, the results indicated that zones outside the loading ring annulus were elastic in nature. The D series indicated residual stress levels close to yield and possibly due to the higher loads, an extension of the higher levels of stress to increasing radial positions. Where comparative accuracy checks have been made between similarly loaded discs, a good agreement has been shown which indicates a reasonably consistent level of experimental work.

The comparison between experimental results for all series and the two mathematical models indicate a fair agreement within the limits of experimental error and lead to possible conclusions that the plastic deformation model can be applied to both dynamic and statically loaded discs and the finite element with the statically loaded discs.

The observed patterns of residual radial stresses show a degree of variability for the A and B series which is less evident in the C series. A possible explanation for these variations may be found in the modified experimental

techniques adopted for the series [Section 2.4.2.3(iii)] whereby the strain gauge leads were left connected during the boring out/turning down process and thereby produced a more reproducible set of strain gauge signals throughout the test.

A further reason for the more pronounced shape profile of the C series [see Figures 3.10 and 3.11] as compared to those from the A and B series [see Figures 3.6 to 3.9] is the fact that the C series were based on an increased number of experimental values which were available because of the increased number of boring out/turning down cuts taken for each disc. The pronounced double peak effect of the A series [see Figures 3.6 and 3.7] especially in the outer zone where more recorded results were available, is not so evident in the B series [see Figures 3.8 and 3.9] and even less in the C series [see Figures 3.10 and 3.11]. It may be concluded from this evidence that the double peak effect, as seen in the A series, could be due to strain gauge error (estimated at $\pm$ 10 MN m^{-2} in Section 2.4.2.2) or to the initial heat treatment having produced localised stress relief. As a result of the indications from the A and B series of test results where twelve discs were stacked together for heat treatment it was decided to only treat five discs which subsequently were used for the C series of tests. Evidence of the beneficial effects of this can be seen from the measurements of plane symmetry shown in Table 2.6 where it can be seen that the C series average maximum range deformation was

.19 cm whilst the A series average maximum range deformation was .37 cm and the B series was .47 cm.

Comparisons made between the experimental and theoretical results shows no evidence of the double peak effect in the theoretical results and thus it may be assumed that the experimental deviations have been produced as a result of the preparation of the discs or of the experimental techniques adopted. The D series of discs were not pre-heat treated since the level of residual stress values expected were well in excess of the residual local stress in the discs.

With respect to the practical applications of residual and especially compressive surface stresses, in components of radial symmetry, the following comments can be made:

1) In turbine discs, surface compressive stresses are likely to help against premature crack initiation and growth.

2) With respect to Linear Accelerator Targets, ability to induce a desired stress distribution by pre-stressing may be beneficial in reducing distortion and cracking.

3) Gears provide a fatigue situation and are usually axi-symmetric components. Normal heat treatment gives tensile stresses near the surface which are detrimental. Therefore, the introduction of compressive

stresses by mechanical means at the surfaces may be beneficial.

4) Shafts and cranks, which are similar cases as gears are all improved - fatigue wise - by surface compressive stresses.

5) Spherical pressure vessels, boilers, nuclear containment vessels; compressive residual stresses are beneficial which may be induced by mechanical working.

6) Life of welded components become enhanced if compressive stresses are induced into weld roots by shot peening which prevents crack growth. This may also be achieved by mechanical working.

7. CONCLUSIONS AND FURTHER WORK

7.1 Conclusions

In this work it has been possible to relate the expended energy due to explosive contact on metal discs to the consequent residual radial and hoop stresses produced in the discs. It has also been possible to carry out a similar exercise with static loading method. Two different theoretical methods have been used in order that the validity of the experimental work may be checked and also to extend the possible range of prediction and design criteria which could emanate from the work.

In the main, the correlation between experimental and theoretical results has been within the limits of experimental error. Where there have been divergences from close agreement, the principal cause can be attributed to buckling or distortion of the disc profiles during the loading process.

More specifically, the following points may be stated:

(i) The use of explosive as a loading agent produces localised residual stress which is constrained to be of an elastic nature.

(ii) A static loading method is a more efficient method of transferring load into the discs but involves a more time-consuming process.

(iii) The finite element method of appraisal produces an idealised solution of the correct order of magnitude.

(iv) The plastic deformation model whilst predicting the order of magnitude of the residual stresses outside the loading area also provides an estimate of the amount of energy it is possible to transfer into the discs by the explosive method. The proportion of explosive energy transferred into the disc appears to be very low - less than 0.02%.

(v) The residual radial stresses are compressive in the inner and outer sections of the discs; the residual hoop stresses are compressive in the inner section and tensile in the outer section.

(vi) The thickness of discs used (6 mm) is prone to produce buckling at loads above 1000 kN and therefore affect the values of the residual stress predictions at the higher loads.

(vii) It has been possible to compare the experimental method of boring out/turning down with the cut out method applied to disc A3 and described in Section 3.1.4.4(ii). The comparison can be made by considering similarly loaded discs, i.e A7, B5 and C2 and shown in Figures 3.14 and 3.15. With the exception of one reading for the A3 disc at the outer radius of 16 cm, the measured residual stress values are comparable to ± 5 MN m^{-2} on average.

(viii) In both the dynamic and static experimental tests, it has been difficult to obtain results in the inner section of the loaded discs where evidence of buckling has been seen in both dynamic and static methods of loading. It can also be stated that Franklin and Morrison (25) when testing their theory by measuring residual stresses in an autofrettaged cylinder using the Sachs boring technique found good agreement between theory and experiment with the exception of those inner surfaces of the cylinder where experimental technique seemed to be insufficiently sensitive.

7.2 Further Work

7.2.1 Experimental

(i) The type and method of using high explosives could be considered. There are two areas which could usefully be developed, one in relation to type of explosive and the other to application.

Pentaerythritoltetranitrate (PETN) is classed as an initiating explosive and develops an intense local high pressure and is found usually in the form of a detonator or detonating fuse. If an explosive in a different form, for example sheet, could be used in connection with the PETN as a detonator then a more precise loading zone could be produced. Also the problem of timing of the detonation to both sides of the disc could be improved (see Figure 2.5). The velocity of detonation for the 'Cordtex' or PETN is 6500 ms^{-1}

and when the effective run length per side is considered the time for complete detonation will be of the order of 26 μs which in normal contact operations using increasing strain rate is relatively high. Apart from the axial fixing of the explosive cord, the timing function is probably responsible for a degree of bending initiated in the disc by the explosive.

(ii) The static tests could be developed for thicker discs but the method and fixing of the loading rings would require further development so that precise axisymmetry could be guaranteed before loading commences.

(iii) A natural extension of the present work would be to try to produce concentric loading bands in the discs by having two, three or more, dependent on size, loading rings attached to the surface of the discs. This technique could be applied to both dynamic and static conditions. However, in the dynamic case (7.2.1 (i)) would need developing first.

(iv) Another development could be to analyse different materials and shapes thus making the methods employed more useful in potential applications.

(v) The tests carried out on buckling and bending of the discs could provide a useful basis for further tests. It has already been shown that buckling is an important factor in the limitation of the validity of the experimental results.

7.2.2 Theory

(i) The finite element theory with capability to incorporate work hardening could provide a better insight into the mechanics of deformation of the discs under different conditions.

(ii) The plastic deformation model depends in the dynamic case on the estimation of energy transfer from explosive cord to disc surface and in the static case to the measured depth of deformation under the loading ring. Both these areas of work could be further developed to provide not only accurate information on residual stress levels in the discs but also on the physical transfer parameters.

(iii) The plastic deformation in the discs could possibly be better understood if an analogous physical model could be considered. For example, the mechanism by which residual stresses are formed may be illustrated by the case of an assembly in which the outer sleeve is shrunk on to an inner shaft. Here, if the assembly is regarded as a solid continuum it can be readily appreciated that it is accomplished by a mutual adjustment in sizes of the oversize shaft when pressed into the undersize sleeve. These changes in dimension induce residual stresses in the assembly creating tensile hoop stresses in the sleeve and compressive hoop stresses in the shaft. Finally, a section taken out of the stressed assembly would produce a similar model to an annular loaded disc.

CHAPTER 8 : REFERENCES

1. OSGOOD, C.C., Fatigue Design, 1970, Wiley-Interscience, New York, p.485.

2. de St. VENANT, B., C.R. Acad. Sci., Paris, v.70 (1870), pp. 473-480 and v.74 (1872), pp. 1009-1017, 1083-1087.

3. LEVY, M., C.R. Acad. Sci., Paris, v.70 (1870), pp. 1323-1325, and v.73 (1871), pp. 1098-1102.

4. TRESCA, H., "Memoires Presentes Par Divers Savants", v.18 (1868), pp. 733-799.

5. v.MISES, R., Göttinger Nachr (1913), p.582.

6. PRAGER, W., J. of Appl. Physics, v.16 (1945), pp. 837-840.

7. BAUSCHINGER, J., Mtt der K. Polytech. Schule, München, v.2 (1886).

8. SCHMIDT, R., Ing. Arch., v.3 (1932), pp. 215-235.

9. v.MISES, R., Zamm, v.8 (1928), pp. 161-185.

10. ODQVIST, F.K.G., Zamm, v.13 (1933), pp. 360-363.

11. PRAGER, W., Zamm, v.15 (1935), pp. 76-80.

12. EDELMAN, F., and DRUCKER, D.C., Report A1L-46 to Office of Naval Research and Bureau of Ships, Brown University, Providence, R.I. (1950) (Published in Franklin Inst. Journal).

13. PRANDTL, L., Proc. 1st Int. Congr. Appl. Mech., Delft (1924), pp. 43-54.

14. REUSS, A., Zamm, v.10 (1930), pp. 266-274.

15. HENCKY, H., Zamm, v.4 (1924), pp. 323-334.

16. NADAI, A., Plasticity, McGraw-Hill Book Co. Inc., New York, 1931.

17. PRAGER, W., J. of Appl. Phys. v.16 (1945), pp. 837-840.

18. PRAGER, W., J. of Appl. Phys. v.18 (1946), pp. 375-383 and Trans. Asme, J. of Appl. Mech. v.15 (1948), pp. 226-233.

19. DRUCKER, D.C., J. of Colloid Sci., v.4 (1949), pp. 299-311 and Quart of Appl. Math. v.7 (1950), pp. 411-418.

20. GEIRINGER, H., Encyclopaedia of Physics, edited by S. FLÜGGE, Springer, Berlin, Germany, vol. 6, 1958, section 63.

21. HILL, R., "Mathematical Theory of Plasticity", (1950), Oxford (Clarendon Press).

22. PRAGER, W., and HODGE, P.G., "Theory of Perfectly Plastic Solids", (1951), London (Chapman and Hall).

23. DRUCKER, D.C., U.S. Office of Naval Research, Rep (NR-041-32), (1950).

24. HODGE, P.G., and BALABAN, M., Illinois Inst. Technol., Dept. Mech. Eng., Rep., (1-15), (1962).

25. PERRONE, N. and HODGE, P.G., J. Appl. Mech., 1959, 26, 276.

26. ALEXANDER, J.M., Proc. Inst. Mech. Eng., 1959, 173, 73.

27. FRANKLIN, G.J. and MORRISON, J.L.M., ibid, 1960, 174, 947.

28. SCHAFFER, B.W., and UNGAR, E.E., J. Appl. Mech. 1960, 27, 34.

29. THOMAS, D.G.B., J. Mechanics, Physics Solids, 1953, 1, 124.

30. "Symposium on Internal Stresses in Metals and Alloys", 1948: London (Inst. of Metals).

31. McGREGOR, C.W., COFFIN, L.F., FISHER, J.C., J. Franklin Inst. 1948, 245, 135.

32. HILL, R., General Features of Plastic-Elastic Problems as exemplified by some Particular Solutions, J. Appl. Mech., Proc. of Appl. Mech. Division, N.Y. September 1949, p. 295-300.

33. RAMU, S.A. and IYENGAR, K.J., Plastic Response of Orthotropic Circular Plates under Blast Loading, J. of Solids & Structures, 1976, Vol 12, pp. 125-133, Pergamon Press.

34. BAUER, O., HEYN, E., Internat. Z. Metallographie, 1911, 1, 16.

35. MESNAGER, M., Compt. Rend., 1919, 169, 1391.

36. SACHS, G., Z. Metallkunde, 1927, 19, 352.

37. BÜHLER, H., "Residual Stresses in Metals and Metal Construction", (Edited by W.R. Osgood), 1954: New York (Reinhold): London (Chapman and Hall), p. 305.

38. LOXLEY, E.M., Brit. Iron and Steel Research Assoc. Rep. (MW/E/53/53).

39. SACHS, G., ESPEY, G., Iron Age, 1941, 148, (12), 63 (13), 36.

40. BIRGER, I.A., Indust. Lab., 1963, 28, 859.

41. KALAKUTSKY, M., "Mashinostroenie", Vol. 3, p.65, 1947: Moscow (Mashgiz).

42. MACH, D.R., Proc. Soc. Exper. Stress Anal., 1963, 19(1), 155.

43. DAVIDENKOV, N.N., Zavod, Lab. 1950, 16(2), 188.

44. DUGDALE, D.S., Internat. J. Eng. Sci., 1963, 1, 383.

45. DUGDALE, D.S., and SQUIRES B.A., J. Mech. Phys. Solids, 1965, v.13, pp. 237-245.

46. QUARTERMAIN, B., and BLAZYNSKI, T.Z., Residual Stress in Explosively Pre-stressed Steel Discs, Internat. Conf. on the Use of High-energy Rate Methods for Forming, Welding and Compaction, University of Leeds, March 1973, paper 7.

47. ABÉ, H., The Expansion of a Hole in an Elastic-Plastic Thin Plate of Finite Thickness, J. of Solids & Structures, 1975, Vol. 11, p. 999-1010, Pergamon Press.

48. DIETER, G.E., Metallurgical Effects of High-Intensity Shock Waves in Metals, in Response of Metals to High Velocity Deformation, Interscience, New York, p. 409, (1961).

49. MINSHALL, F.S., The Dynamic Response of Iron and Iron Alloys to Shock Waves, in Response of Metals to High Velocity Deformation, Interscience, New York, p. 249 (1961).

50. ZUKAS, E.G. and FOWLER, C.M., The Behaviour of Iron and Steel Under Impulsive Loading, in Response of Metals to High Velocity Deformation, Interscience, New York, p. 343 (1961).

51. HOLTZMAN, A.H., and COWAN, G.R., The Strengthening of Austenitic Manganese Steel by Plane Shock Waves, in Response of Metals to High Velocity Deformation, Interscience, New York, p. 447 (1961).

52. JENKINS, S.S., Explosive Impact Hardening of Manganese Steel, Pacific Northwest Metals and Minerals Conf., American Institute of Mining, Metallurgical and Petroleum Engineers, Portland (April 1968).

53. Explosive Working of Metals, Rinehart and Pearson, Pergamon Press, 1963.

54. SMITH, C.S., and FOWLER, C.M, Response of Metals to High Velocity Deformation, New York, (1961), p. 309.

55. WHITE, J.J., TROTT, BACKHOFEN, J.E., The Physics of Explosion Containment, Physics in Technology, May 1977.

56. LOXLEY, E.M., Brit. Iron Steel Research Assoc. Rep. (MW/E/53/53).

57. BARKER, A., HARDY, E.H., Proc. Inst. Mech. Eng., 1957, 171, 581.

58. KOCH, J.J. et al., "Dehnungsuresstreiken-Messtechnik", 1952: Eindhoven (Philips Library): Houston, Texas (Elsevier).

59. BÜHLER, H., Giessereian Techn.-Wiss, Beihefte, 1952, (5), 297.

60. BLOOMFIELD, B.S., (R.A.R.D.E., Fort Halstead),

61. DENTON, A.A., Determination of Residual Stresses, J. Inst. of Metals, 1966, v.11, 101, p.9.

62. LEAF, W., Proc. Soc. Exper. Stress Anal., 1952, 9, (2), 133.

63. FROMMER, L., and LLOYD, E.H., J. Inst. of Metals, 1944, 70, 91.

64. LETNER, H.R., Proc. Soc. Exper. Stress Anal., 1953, 10, (2), 23.

65. FRISCH, J. and THOMSEN, E.G., Trans American Soc. of Mech. Eng., 1951, 73, 337.

66. RICHARDS, D.G., J. Inst. of Metals, 1945, 2 (1), 40.

67. DODD, R.A., Metallurgia, March 1952, p.111.

68. TIMOSHENKO, S., and GERE, J.M., Theory of Elastic Stability, Engineering Societies Monograph, McGraw Hill, 1st Edition 1936, 2nd Edition 1961, Ch. 9.9.

69. VIJAYAKUMAR, K. and JOGA RAO, C.V., Buckling of Polar Orthotropic Annular Plates, Journal of Engineering Mechanics Division, Proc Am Soc of Eng., June 1971, Em3, p. 701-708.

70. HIRATA, T., WATANABE, M. and MIYAGAWA, M., Initiation of Elastic Instability of the Laterally Loaded Circular Plates, Bulletin of the JSME, Vol. 19, No. 138, Dec 1976.

71. AMON, R. and WIDERA, O.E., Stability of Edge Reinforced Circular Plate, Journal of Engineering Mechanics Division, Proc of Am Soc of Civil Engs., Vol. 97, No EM5, October 1971.

72. PAFEC 75, Theory and Results Manual.

73. PAFEC 75, Data Preparation Manual

74. ZIENKIEWICZ, O.C., The Finite Element Method in Engineering Science, McGraw-Hill, 3rd Edition, 1978.

75. FORD, H., Advanced Mechanics of Materials, 1963, Longmans Green & Co Ltd, pp. 443 and 444.

76. ANDREWS, K.W., Physics in Tech., v.5, 1974, pp. 259-277.

77. BERANEK, L.L., Noise and Vibration Control, 1971, McGraw-Hill Inc., New York, p.23.

78. HAQUE, M.M. and HASHMI, M.S.J., Mechanics of Materials 3 (1984), pp. 245-256.

79. SHEWMON, P.G. and ZACKAY, V.F., Editors, Response of Metals to High Velocity Deformation; Interscience, New York (1961).

APPENDIX 1

Fortran Programme : Dynamic Results

Conversion of Strain Gauge Readings to Radial and Hoop Stress, Shear Stress and Angular Orientation

```
// JOB T  01AD 0001 1111                              1111

LOG DRIVE   CART SPEC   CART AVAIL  PHY DRIVE
  0000        01AD         01AD        0000
  0001        0001         0001        0001
  0002        1111         1111        0002

V2 M10  ACTUAL 16K  CONFIG 16K

// XEQ NC2
DATE  25.06.72
USER  22505/QUARTERMAIN B./STRESS
// *              JOB NO.      357

// FOR
*IOCS(CARD,1132PRINTER,KEYBOARD,TYPEWRITER,DISK)
*LIST SOURCE PROGRAM
      DIMENSIONG(3),E(3)
   99 WRITE(3,999)
  999 FORMAT(1HO,/// 8H NEW CUT)
    5 READ(2,10)G(1),G(2),G(3),GK,BV
   10 FORMAT(F6.3,F6.3,F6.3,F5.3,F5.3)
      IF(G(1)-30)14,99,99
   14 CONTINUE
      IF(G(2)-80)15,140,140
   15 DO20I=1,3
      E(I)=4.*G(I)/(GK*BV*1000.)
   20 CONTINUE
      P=(E(1)+E(3))/2.
      FEN=0.5*(E(1)-E(2))*(E(1)-E(2))
      FUN=(E(2)-E(3))*(E(2)-E(3))*0.5
      Q=SQRT(FEN+FUN)
      EX=P+Q
      EY=P-Q
      TIN=(2.*E(2)-E(1)-E(3))/(E(1)-E(3))
      TUN=(180./3.1416)*ATAN(SQRT(TIN*TIN))
      IF(TIN)30,100,40
   30 CONTINUE
      IF(E(1)-E(3))31,110,32
   31 CON=2.
      TUN=(180-TUN)/2
      GOTO120
   32 CON=4.
      TUN=(360-TUN)/2
      GOTO120
   40 CONTINUE
      IF(E(1)-E(3))41,105,42
   41 CON=3.
      TUN=(180+TUN)/2
      GOTO120
   42 CON=1.
      TUN=TUN/2
      GOTO120
  100 CON=10.
      GOTO120
  110 CON=20.
```

```
      GOTO120
  105 CON=30.
      GOTO120
  120 SHR=EX-EY
      WRITE(3,130)EX,EY,SHR,TUN,CON
  130 FORMAT(2X,F9.6,2X,F9.6,2X,F9.6,2X,F9.4,2X,F5.1)
      GOTO5
  140 CALL EXIT
      END

FEATURES SUPPORTED
 IOCS

CORE REQUIREMENTS FOR
 COMMON      0  VARIABLES     50  PROGRAM    446

END OF COMPILATION

// XEQ
```

APPENDIX 2

Fortran Programme : Dynamic Results

Experimental Stress Analysis : Turning Down/Boring Out Procedure and Specimen Print-out of Results

EXPERIMENTAL

```
10 DIM R(20),V(20),W(20),S(20),X(20),Y(20)
20 PRINT"EXPERIMENTAL DISC STRESS ANALYSIS"
30 PRINT"ENTER GAUGE RADIUS, INNER RADIUS, CM"
40 INPUT G,H
50 PRINT "ENTER NUMBER OF OUTER CUTS"
60 INPUT N
70 PRINT"ENTER RADIUS,VR,VH, FOR OUTER CUTS"
80 FOR I=1 TO N STEP 1
90 INPUT R(I),V(I),W(I)
100 NEXT I
 110 PRINT "ENTER NUMBER OF INNER CUTS"
120 INPUT M
130 PRINT"ENTER RADIUS, VR,VH FOR INNER CUTS"
135 FOR I=1 TO M STEP 1
140 INPUT S(I),X(I),Y(I)
150 NEXT I
160 A=1.31*H*H/(G*G)
170 PRINT"OUTER CUT"
175 PRINT"      RADIUS, RADIAL STRESS, HOOP STRESS"
190 FOR I=1 TO N STEP 1
200 F=(0.69-A)/(1-(H*H)/(R(I)*R(I)))
210 P=(-9.71E04)*V(I)/F
220 F=(0.69+A)/(1-(H*H)/(R(I)*R(I)))
230 Q=(-9.71E04)*W(I)/F
240 PRINT R(I),P,Q
250 NEXT I
260 PRINT"INNER CUT"
270 PRINT"      RADIUS,RADIAL STRESS, HOOP STRESS"
280 FOR I=1 TO M STEP 1
290 A=1.31*S(I)*S(I)/(G*G)
300 F=(0.69-A)/(1-S(I)*S(I)/(R(N)*R(N)))
310 T=((9.71E04)*X(I)+P*F)/(F-0.69)
320 F=(0.69+A)/(1-S(I)*S(I)/(R(N)*R(N)))
330 U=((9.71E04)*Y(I)+Q*F)/(F-0.69)
340 PRINT S(I),T,U
350 NEXT I
 360 END
```

B3 (EXPERIMENTAL PRINT-OUT)

```
EXPERIMENTAL DISC STRESS ANALYSIS
ENTER GAUGE RADIUS, INNER RADIUS, CM
  ?   10.66,3.79
ENTER NUMBER OF OUTER CUTS
  ?   3
ENTER RADIUS,VR,VH, FOR OUTER CUTS
  ?   17.53,113.8,148.8
  ?   16.24,-5.7,110
  ?   14.97,67.1,148.8
ENTER NUMBER OF INNER CUTS
  ?   5
ENTER RADIUS, VR,VH FOR INNER CUTS
  ?   5.11,161.4,131.25
  ?   6.45,41.4,-120
  ?   7.78,50,-231.25
  ?   9.2,41.6,-513.8
  ?   10.12,-36.7,-598.8
OUTER CUT
     RADIUS, RADIAL STRESS, HOOP STRESS
 17.53000          -2.008634E+07      -1.609779E+07
 16.23999          -997933.4          -1.180387E+07
 14.97000          -1.162792E+07      -1.580474E+07
INNER CUT
     RADIUS,RADIAL STRESS, HOOP STRESS
 5.110000          -4.225680E+07      -1.154480E+07
 6.450000          -2353079           -4.603354E+07
 7.780000          -7106045           -4.334494E+07
 9.200000          -8161100           -4.640610E+07
 10.12000          -4356952           -4.086765E+07
EDIT  RUN
```

APPENDIX 3

Basic (Apple-soft) : Static Results

Programme to obtain Equivalent Stress Values and Specimen Print-out

```
]
]POKE1657,96

]LIST                    PROGRAM TO OBTAIN EQUIVALENT STRESS VALUES

110  HOME : TEXT :D$ =  CHR$ (4)
120 :
130  GOSUB 10000: REM  SET UP SCREEN DISPLAY
140 :
150  REM  GET INITIAL INFORMATION
160  HOME : HTAB 1: VTAB 5: PRINT "PLEASE SUPPLY THE FOLLOWING DATA...."
170  HTAB 5: VTAB 10: INVERSE : PRINT "YOUNG'S MODULUS";: NORMAL : INPUT "      "
;YM$:YM =
      VAL (YM$)
180  HTAB 5: VTAB 11: INVERSE : PRINT "MU";: NORMAL : INPUT "                    "
;MU$:MU =
      VAL (MU$)
190  HTAB 5: VTAB 12: INVERSE : PRINT "EXCITATION VOLTAGE";: NORMAL : INPUT "   "
;EV$:EV =
      VAL (EV$)
200  HTAB 5: VTAB 13: INVERSE : PRINT "GAUGE FACTOR";: NORMAL : INPUT "         "
;GF$:GF =
      VAL (GF$)
205  HTAB 5: VTAB 14: INVERSE : PRINT "LOAD  IN KN)";: NORMAL : INPUT "         "
;LD$:LD =
      VAL (LD$)
210  HTAB 1: VTAB 20: PRINT "IF THESE ARE CORRECT PRESS <RETURN>"
220  HTAB 1: VTAB 21: PRINT "TO MAKE CORRECTIONS PRESS  <ESC>";
230  GET A$: IF A$ =  CHR$ (27) THEN 170
240  IF A$ <  > CHR$ (13) THEN 210
250 C = 0: REM   SET UP VOLTAGE COUNTER
260 :
270  REM  INPUT THREE VOLTAGES TO ASSESS
280 :
290  HOME :C = C + 1: HTAB 1: VTAB 5: PRINT "NOW ENTER 3 STRAIN GAUGE VOLTAGES..
."
300  HTAB 15: VTAB 8: INVERSE : PRINT "GAUGE  "; CHR$ (C + 64): NORMAL
310  HTAB 5: VTAB 10: INVERSE : PRINT "VOLTAGE 1";: NORMAL : INPUT "   ";V1$: VT
AB 10: HTAB
     24: INVERSE : PRINT "MILLIVOLTS":V1 =  VAL (V1$) * 1E - 3
320  HTAB 5: VTAB 12: INVERSE : PRINT "VOLTAGE 2";: NORMAL : INPUT "   ";V2$: VT
AB 12: HTAB
     24: INVERSE : PRINT "MILLIVOLTS":V2 =  VAL (V2$) * 1E - 3
330  HTAB 5: VTAB 14: INVERSE : PRINT "VOLTAGE 3";: NORMAL : INPUT "   ";V3$: VT
AB 14: HTAB
     24: INVERSE : PRINT "MILLIVOLTS": NORMAL :V3 =  VAL (V3$) * 1E - 3
340  HTAB 1: VTAB 20: PRINT "IF THESE ARE CORRECT PRESS <RETURN>"
350  HTAB 1: VTAB 21: PRINT "TO MAKE CORRECTIONS PRESS  <ESC>";
360  GET A$: IF A$ =  CHR$ (27) THEN 310
370  IF A$ <  > CHR$ (13) THEN 340
380 :
390  GOSUB 12000: REM  CALCULATIONS
400 :
410  REM  OUTPUT RESULTS
420 :
430  HOME
440  VTAB 6: HTAB 1: PRINT "DO YOU WANT A PRINTOUT OF THE RESULTS(Y/N)? ";: GET
A$: IF A$ =
     "Y" THEN  POKE 33,40: PRINT : GOSUB 14000: GOTO 460
450  IF A$ <  > "N" THEN 440
```

```
460  IF C< > 1 THEN 510
470  PRINT "YOUNG S MODULUS     = ";YM$
480  PRINT "MU                  = ";MU$
490  PRINT "EXCITATION VOLTAGE = ";EV$
500  PRINT "GAUGE FACTOR        = ";GF$
505  PRINT "LOAD                = ";LD$
510  PRINT : PRINT "GAUGE "; CHR$ (C + 64): PRINT
520  PRINT "STRAIN GAUGE VOLTAGE 1 = ";V1$;: HTAB 31: PRINT "MILLIVOLTS"
530  PRINT "STRAIN GAUGE VOLTAGE 2 = ";V2$;: HTAB 31: PRINT "MILLIVOLTS"
540  PRINT "STRAIN GAUGE VOLTAGE 3 = ";V3$;: HTAB 31: PRINT "MILLIVOLTS"
550  PRINT : PRINT
560  PRINT "EPSILON MAX    = ";EX
570  PRINT "EPSILON MIN    = ";EN
580  PRINT "ALPHA P        = ";AP
590  PRINT "BETA MAX       = ";BM
600  PRINT "SIGMA MAX      = ";SX
610  PRINT "SIGMA MIN      = ";SN
620  PRINT "TAU MAX        = ";TX
630  PRINT : PRINT : PRINT
640  PRINT : PRINT : PRINT "ELASTO-PLASTIC RESULTS": PRINT "----------------------
--"
650  PRINT : PRINT
660  PRINT "EQUIVALENT STRESS 1 IS    = ";Q1;" (EP)"
680  PRINT "EPSILON MAX IS NOW        = ";XX;" (EP)"
690  PRINT "EPSILON MIN IS NOW        = ";XN;" (EP)"
700  PRINT "SIGMA MAX IS NOW          = ";S2X;" (EP)"
710  PRINT "SIGMA MIN IS NOW          = ";S3N;" (EP)"
712  PRINT "EQUIVALENT STRESS 2 IS    = ";Q2;" (EP)"
715  PRINT : PRINT : FOR I = 1 TO 80: PRINT "*";: NEXT
716  PRINT
720  IF A$ = "Y" THEN  POKE 33,36: GOSUB 16000
730  PRINT "PRESS ANY KEY TO CONTINUE":: GET X$
740  GOSUB 10000
750 :
760  GOSUB 18000: REM  OPTION MENU
770  ON  VAL (A$) GOTO 160,290
780  REM


END OF PROGRAM DISPLAY


790  HOME
800  VTAB 10: HTAB 12: PRINT "**********";
810  VTAB 11: HTAB 12: PRINT "*";: HTAB 22: PRINT "*";
820  VTAB 12: HTAB 12: PRINT "*";: HTAB 22: PRINT "*";
830  VTAB 13: HTAB 12: PRINT "*";: HTAB 22: PRINT "*";
840  VTAB 14: HTAB 12: PRINT "**********";
850 TE$ = "THE END":L$ = ""
860  FOR I = 1 TO 7
870 L$ =  MID$ (TE$,1,I)
880  VTAB 12: HTAB 21 - I: PRINT  CHR$ (7);L$;
890  FOR K = 1 TO 500: NEXT
900  NEXT I
910 :
920 :
930 :
940  END ::::::::::::::::::::::::
950 :
960 :
970 :
980 :
9999  REM


SUBROUTINE FOR INITIALISING SCREEN SIZE AND BORDER DISPLAY


10000  POKE 32,0: POKE 33,39: POKE 34,0: POKE 35,24
```

```
10000  POKE 32,0: POKE 33,40: POKE 34,0: POKE 35,24
10010  INVERSE : HOME
10020  PRINT "         STRAIN GAUGE MEASUREMENT         ";
10030  FOR I = 1 TO 21
10040  PRINT "*";: HTAB 40: PRINT "*";
10050  NEXT
10060  PRINT " PROGRAM                --SEPTEMBER 1982 ";
10070  NORMAL
10080 :
10090  REM  SET UP SCREEN SIZE
10100  POKE 32,2: POKE 33,36: POKE 34,2: POKE 35,21
10110 :
10120  HOME : RETURN
10130 :
11999  REM
```

SUBROUTINE FOR CALCULATIONS

```
12000  REM
```

EX=E MAX
EN=E MIN
AP=ALPHA P
BM=BETA MAX
SX=SIGMA MAX
SN=SIGMA MIN
TX=TAU MAX

```
12010 E1 = (4 * V1) / (EV * GF)
12020 E2 = (4 * V2) / (EV * GF)
12030 E3 = (4 * V3) / (EV * GF)
12040 A = 2 * E2 - (E1 + E3)
12050 B = E1 - E3
12060 BM =  SQR (B * B + A * A)
12070 EX = ((E1 + E3) / 2) + BM / 2
12080 EN = ((E1 + E3) / 2) - BM / 2
12090 AP =  ATN (A / B) / 2 * 57.2957796
12100 SX = ((E1 + E3) / (1 - MU) + ((1 / (1 + MU)) * BM)) * YM / 2
12110 SN = ((E1 + E3) / (1 - MU) - ((1 / (1 + MU)) * BM)) * YM / 2
12120 Q1 =  SQR ((SX * SX) + (SN * SN) - SX * SN)
12130 EQ = Q1 / YM
12140  IF  ABS (EQ) >  = 1E - 3 THEN Q1 = 2E8 + 32.7E8 *  ABS (EQ) ^ 0.898
12150 XX = SX / YM:XN = SN / YM
12160  IF  ABS (XX) >  = 1E - 3 THEN S2X = 2E8 + 32.7E8 *  ABS (XX) ^ 0.898
12170  IF  ABS (XX) < 1E - 3 THEN S2X = SX
12180  IF  ABS (XN) >  = 1E - 3 THEN S3N = 2E8 + 32.7E8 *  ABS (XN) ^ 0.898
12190  IF  ABS (XN) < 1E - 3 THEN S3N = SN
12200 Q2 =  SQR ((S2X * S2X) + (S3N * S3N) -  ABS (S2X * S3N))
12205  IF SN < 0 THEN S3N =  -  SQR (S3N * S3N)
12210 TX = YM / (2 * (1 + MU)) * BM
12220  RETURN
13999  REM
```

SWITCH PRINTER ON

```
14000  TEXT : HOME
14001  PRINT D$;"PR#1": PRINT : RETURN
15999  REM
```

SWITCH PRINTER OFF

YOUNG'S MODULUS = 2E11
MU = 0.30
EXCITATION VOLTAGE = 5.04
GAUGE FACTOR = 2.10
LOAD = 2000

DISC D2 INCREASING LOAD

GAUGE A

STRAIN GAUGE VOLTAGE 1 = 0.76 MILLIVOLTS
STRAIN GAUGE VOLTAGE 2 = -.02 MILLIVOLTS
STRAIN GAUGE VOLTAGE 3 = -.16 MILLIVOLTS

EPSILON MAX = 3.25153828E-04
EPSILON MIN = -9.83964584E-05
ALPHA P = -17.4122446
BETA MAX = 4.23550286E-04
SIGMA MAX = 64974701.2
SIGMA MIN = -186881.304
TAU MAX = 32580791.2

ELASTO-PLASTIC RESULTS

EQUIVALENT STRESS 1 IS = 65068743.2 (EP)
EPSILON MAX IS NOW = 3.24873506E-04 (EP)
EPSILON MIN IS NOW = -9.34406521E-07 (EP)
SIGMA MAX IS NOW = 64974701.2 (EP)
SIGMA MIN IS NOW = -186881.304 (EP)
EQUIVALENT STRESS 2 IS = 64881462.4 (EP)

****

GAUGE B

STRAIN GAUGE VOLTAGE 1 = -.22 MILLIVOLTS
STRAIN GAUGE VOLTAGE 2 = 0.30 MILLIVOLTS
STRAIN GAUGE VOLTAGE 3 = 0.84 MILLIVOLTS

EPSILON MAX = 3.17495968E-04
EPSILON MIN = -8.31800194E-05
ALPHA P = .540462079
BETA MAX = 4.00675987E-04
SIGMA MAX = 64294936.7
SIGMA MIN = 2652477.15
TAU MAX = 30821229.8

ELASTO-PLASTIC RESULTS

****

GAUGE L

STRAIN GAUGE VOLTAGE 1 = 5.68 MILLIVOLTS
STRAIN GAUGE VOLTAGE 2 = 5.00 MILLIVOLTS
STRAIN GAUGE VOLTAGE 3 = 4.44 MILLIVOLTS

EPSILON MAX = 2.14773109E-03
EPSILON MIN = 1.67690988E-03
ALPHA P = -2.76377009
BETA MAX = 4.70821208E-04
SIGMA MAX = 582594297
SIGMA MIN = 510160265
TAU MAX = 36217016

ELASTO-PLASTIC RESULTS

EQUIVALENT STRESS 1 IS = 216407589 (EP)
EPSILON MAX IS NOW = 2.91297149E-03 (EP)
EPSILON MIN IS NOW = 2.55080133E-03 (EP)
SIGMA MAX IS NOW = 217279123 (EP)
SIGMA MIN IS NOW = 215337104 (EP)
EQUIVALENT STRESS 2 IS = 216314652 (EP)

****

GAUGE N

STRAIN GAUGE VOLTAGE 1 = 2.32 MILLIVOLTS
STRAIN GAUGE VOLTAGE 2 = 2.18 MILLIVOLTS
STRAIN GAUGE VOLTAGE 3 = -2.24MILLIVOLTS

EPSILON MAX = 1.19689319E-03
EPSILON MIN = -1.16665887E-03
ALPHA P = 21.5929041
BETA MAX = 2.36355206E-03
SIGMA MAX = 186130885
SIGMA MIN = -177492509
TAU MAX = 181811697

ELASTO-PLASTIC RESULTS

EQUIVALENT STRESS 1 IS = 209945516 (EP)
EPSILON MAX IS NOW = 9.30654423E-04 (EP)
EPSILON MIN IS NOW = -8.87462544E-04 (EP)
SIGMA MAX IS NOW = 186130885 (EP)
SIGMA MIN IS NOW = -177492509 (EP)
EQUIVALENT STRESS 2 IS = 181965544 (EP)

APPENDIX 4

Specimen Print-out Page from PAFEC Finite Element Analysis

PLASTIC STRAINS	0.941E-03		0.506E-03	
ELEMENT NO. 25 NODES	89	91	124	126
EQUIVALENT STRESSES	0.257E 03**	0.849E 02	0.217E 03**	0.145E 03
PLASTIC STRAINS	0.446E-02		0.310E-03	
ELEMENT NO. 36 NODES	122	124	158	160
EQUIVALENT STRESSES	0.277E 03**	0.227E 03**	0.278E 03**	0.208E 03**
PLASTIC STRAINS	0.133E-01	0.441E-02	0.125E-01	0.163E-02
ELEMENT NO. 24 NODES	87	89	122	124
EQUIVALENT STRESSES	0.259E 03**	0.259E 03**	0.282E 03**	0.228E 03**
PLASTIC STRAINS	0.928E-02	0.982E-02	0.138E-01	0.483E-02
ELEMENT NO. 35 NODES	120	122	156	158
EQUIVALENT STRESSES	0.297E 03**	0.279E 03**	0.311E 03**	0.271E 03**
PLASTIC STRAINS	0.156E-01	0.134E-01	0.184E-01	0.128E-01
ELEMENT NO. 23 NODES	85	87	120	122
EQUIVALENT STRESSES	0.250E 03**	0.255E 03**	0.297E 03**	0.282E 03**
PLASTIC STRAINS	0.818E-02	0.888E-02	0.161E-01	0.133E-01
ELEMENT NO. 34 NODES	118	120	154	156
EQUIVALENT STRESSES	0.278E 03**	0.296E 03**	0.275E 03**	0.314E 03**
PLASTIC STRAINS	0.135E-01	0.156E-01	0.133E-01	0.185E-01
ELEMENT NO. 22 NODES	83	85	118	120
EQUIVALENT STRESSES	0.256E 03**	0.250E 03**	0.283E 03**	0.297E 03**
PLASTIC STRAINS	0.891E-02	0.817E-02	0.135E-01	0.161E-01
ELEMENT NO. 33 NODES	116	118	152	154
EQUIVALENT STRESSES	0.230E 03**	0.279E 03**	0.207E 03**	0.279E 03**
PLASTIC STRAINS	0.471E-02	0.135E-01	0.157E-02	0.131E-01
ELEMENT NO. 21 NODES	81	83	116	118
EQUIVALENT STRESSES	0.262E 03**	0.258E 03**	0.230E 03**	0.284E 03**
PLASTIC STRAINS	0.103E-01	0.928E-02	0.521E-02	0.140E-01
ELEMENT NO. 32 NODES	114	116	150	152
EQUIVALENT STRESSES	0.922E 02	0.233E 03**	0.127E 03	0.219E 03**
PLASTIC STRAINS		0.712E-03		0.000E 01
ELEMENT NO. 20 NODES	79	81	114	116
EQUIVALENT STRESSES	0.121E 03	0.250E 03**	0.816E 02	0.234E 03**
PLASTIC STRAINS		0.497E-02		0.191E-03
ELEMENT NO. 31 NODES	112	114	148	150
EQUIVALENT STRESSES	0.430E 02	0.882E 02	0.490E 02	0.932E 02
ELEMENT NO. 19 NODES	77	79	112	114
EQUIVALENT STRESSES	0.215E 02	0.238E 02	0.214E 02	0.121E 03
ELEMENT NO. 30 NODES	110	112	146	148
EQUIVALENT STRESSES	0.333E 02	0.368E 02	0.324E 02	0.466E 02
ELEMENT NO. 18 NODES	75	77	110	112
EQUIVALENT STRESSES	0.348E 02	0.301E 02	0.336E 02	0.389E 02